# Optogenetic G Protein Coupled Receptors to Investigate Spatiotemporal Signalling

Laura Joyce Humphrys

MSci (Hons)

Thesis submitted to the University of Nottingham for the degree of Doctor of Philosophy

September 2019

## Abstract

Optogenetics describes the method of expressing a light-activated protein or compound in a biological system to investigate cellular and/or network signalling without the need for electrophysiological or pharmacological probes. Light sensitive G protein coupled receptors (GPCRs) are a powerful tool for investigating the spatiotemporal aspects of second messenger cell signalling as light can be targeted to single cells, or even subcellular domains, and allows for faster, less complex kinetics than ligand binding activation. Both the spatial and temporal aspects of optogenetic receptors can be fine-tuned for mimicking endogenous signals and investigating the physiology and pathophysiology of a specific signalling event. This technology is particularly interesting for investigation into cells with complex pharmacology and signalling, such as astrocytes – a neural cell type involved in supporting neuron function. The aim of this thesis was to manipulate optogenetic GPCR signalling by receptor mutagenesis and determine the consequences in primary astrocyte cultures. We also hypothesised the use of spatial targeting of a bioluminescent light stimulus by the subcellular targeting of active luciferase through complementation.

Two promising optogenetic $G_q$ coupled GPCRs, thus stimulating intracellular calcium release upon light activation, were investigated; the rhodopsin-$\alpha_{1A}$ adrenoceptor chimera, opto-$\alpha_{1A}$AR, and melanopsin. Fluorescent assays to monitor calcium signalling and receptor trafficking of opto-$\alpha_{1A}$AR and melanopsin post light activation were developed in HEK293 cells. C terminal truncation mutants were developed to decrease receptor desensitisation and endocytosis, promoted by C terminal phosphorylation of the receptor, and increase temporal control of receptor signalling with improved cell surface receptor expression. With truncation of the C terminus at $Ser^{371}$, calcium transients produced by continuous 470nm laser light stimulation of the opto-$\alpha_{1A}$AR increased. Receptor trafficking also decreased in the truncated $Ser^{371}$ mutant compared to wild type, indicating reduced receptor endocytosis as one mechanism behind the increased signal output.

Both opto-$\alpha_{1A}$AR and melanopsin were investigated in a more translational system using primary cortical rat astrocyte cultures. Melanopsin was recombinantly expressed at a higher level in the primary astrocytes, and light stimulation of

melanopsin using different temporal patterns induced astrocytic calcium signalling. The developed melanopsin C terminal truncation mutant at $Ser^{411}$ was utilised to increase the probability of a calcium transient produced by a repeated LED light stimulus, although this was to the detriment of maximal calcium production. Interestingly, when melanopsin transfected astrocytes were treated with pertussis toxin to block $G_{i/o}$ signalling, the number of light induced calcium transients increased, indicating a link between melanopsin activation and cAMP signalling in astrocytes.

Finally, opto-$\alpha_{1A}$AR and melanopsin were used in the development of a novel, complementation-based bioluminescence stimulation of optogenetic GPCRs for controlling subcellular activation. In this new system, one part of the fragmented luciferase NanoLuc (NanoBiT) was fused to the optogenetic GPCR, with the complementation fragment for a fully functional enzyme tagged to a compartmentalised target protein. Bioluminescence production from the furimazine substrate could only occur when the receptor was within a close proximity of the target protein, enabling spatially distinct bioluminescent light stimulation of the optogenetic receptor. Melanopsin fused to the high affinity, smaller fragment of NanoBiT produced calcium transients in HEK293 cells when co-transfected with the large NanoBiT fragment joined to the plasma membrane targeting sequence of Kras or the early endosome marker Rab5 and treated with furimazine. There was also an indication of a bioluminescence intensity-dependent internalisation of the melanopsin-NanoBiT, which was sensitive to endocytosis inhibitors Pitstop 2 and Dyngo 4a and differed between Kras or Rab5 localisation of the NanoBiT fragment.

Altogether, this thesis describes the development of cell signalling assays for optogenetic GPCRs, both in a model system and physiologically relevant cell cultures. Different light production techniques were utilised for constant, patterned or spatially defined stimulation of the light activated receptors, and C terminal receptor truncation mutants were created for increased temporal control of these tools. In future work, these optogenetic techniques have the potential for spatiotemporal investigations into potential GPCR treatment targets and their downstream responses.

## Acknowledgements

Although I think I've remembered most people, if you are reading this and find yourself missing, I can guarantee it's an error on my part and not yours.

Firstly, I would like to thank my supervisors, Dr Nicholas Holliday and Dr Tomas Bellamy, for all their input on the project and help with writing up this work. The guidance and support for these four years has been much appreciated. Special mention goes to Nick who has had to put up with the brunt of my organisational skills (which are still in development) and various non-work crises, and for the open door policy, always allowing me to pester when something in the lab has gone squiffy or a new idea has struck. Thank you both also for your trust in letting me supervise students and attend international conferences on my own, which have been invaluable experiences.

I would also like to thank the British Pharmacological Society for their funding of this project, and the University of Nottingham for the extra 6 months of spendies to write up this thing.

My direct lab buddies have been wonderful, and I shall miss working with you all. Thanks so much to the current fellow Holliday labbers who are always open for providing help and opinions and splitting flasks when Germany or London calls; to Jess Carpenter, for the BBQs and pub meets, Nikki Dijon, for the late evening office company and pharmacology nerd jokes, Desi Nesheva, for keeping me fit, socialised and in touch with my emotions, and James Farmer, for being a model undergraduate student with great taste in early music. Thank you also to the previous Holliday lab, including Laura Kilpatrick, Lisa Stott, Rachel Richardson and Penny Ensor, who all made me feel very welcome and helped me settle in. Thank you also to all the Bellamy lab for keeping me company in that tiny, hot cell culture room, especially Zoe Smith, for the prosecco related incidents, and Rawan Hareeri, for prepping the astrocytes week in week out, and yet always still having a lovely smile.

The entirety of the vast Cell Signalling, and now COMPARE, labs have all offered amazing help and advice towards this project, along with company and laughs, even when those experiments flatline. In no particular order, I'll name a bunch off the

top of my head, including my E floor based office; Birgit Caspar, Nick Groenewoud, Leigh Stoddart, the best desk buddies Matt Barron, Lydia Ogrodzinski and Rick Proudman, Mark Soave, Liz Rosethorne, Joelle Goulding, David Sykes, Chloe Peach, Maxine Roberts, Quynh Mai, Jack Lochray, Eddy Wragg, Charlie Lay, Carl White, Alessandra Bree, Rawan Al-Eidan, Diana Alcobia, Sam Cooper, Clare Harwood, Al Keen, and lastly Brad Hoare for keeping me sane (debatable) while writing over summer and printing this thing out.

The SLIM team, in particular Robert Markus, Tim Self and Seema Bagia were incredibly helpful in developing my light sensitive receptor-based fluorescence imaging assays, which proved to be as difficult as they sound. Finally, these labs would not run without the help of our great lab techs, Marleen Groenen and June McCulloch; thank you for all your assistance.

Outside of the office, I have had the best housemates in Lexy Fox and Astrid Delorme, who were always available for a good chat and glass of wine. My partner of all four years, Matt Freedman, was also very supportive when I needed an outlet. My parents, Ben and Sandra Humphrys, and sister, Liv, have been incredibly supportive during my PhD years - even if mum keeps telling me that I get weirder by the year.

Lastly, I'd like to dedicate this thesis to my grandma Gill, who inspired me so much in life and manged to fulfil her promise to see me graduate once, but unfortunately will miss out on any further potential celebrations.

## Abbreviations

| | | |
|---|---|---|
| AF | - | Alexa Fluor |
| AM | - | Acetoxymethyl ester |
| AP2 | - | Adaptor Protein 2 |
| ATP | - | Adenosine Triphosphate |
| bGH | - | bovine Growth Hormone |
| BSA | - | Bovine Serum Albumin |
| $Ca^{2+}$ | - | Calcium ion |
| cAMP | - | cyclic Adenosine Monophosphate |
| ChR2 | - | Channelrhodopsin 2 |
| CMV | - | Cytomegalovirus |
| CNO | - | Clozapine-*N*-Oxide |
| CNS | - | Central Nervous System |
| DAG | - | Diacylglycerol |
| $ddH_2O$ | - | double distilled water |
| DMEM | - | Dulbecco's Modified Eagle's Medium |
| DREADD | - | Designer Receptor Activated Exclusively by Designer Drug |
| Epacs | - | Exchange proteins directly activated by cAMP |
| ERK | - | Extracellular signal-Regulated Kinase |
| FastAP | - | shrimp Alkaline Phosphatase |
| GPCR | - | G Protein Coupled Receptor |
| G protein | - | GTP binding protein |
| GDP | - | Guanine Diphosphate |
| GFP | - | Green Fluorescent Protein |
| GIRK | - | G-Protein Gated Inwardly Rectifying $K^+$ |
| GRK | - | G protein coupled Receptor Kinases |
| GTP | - | Guanine Triphosphate |
| H33342 | - | Bisbenzimide H 33342, Hoechst 33342 |
| HBS | - | HEPES Buffered Saline solution |
| HEK | - | Human Embryonic Kidney |

| | | |
|---|---|---|
| $hM_3D$ | - | human Muscarinic 3 DREADD |
| ICL | - | Intracellular Loop |
| $IP_3$ | - | Inositol 1,4,5-trisphosphate |
| ipRGC | - | intrinsically photosensitive Retinal Ganglion Cell |
| KORD | - | κ Opioid Receptor DREADD |
| LB | - | Luria Bertani |
| LiGluR | - | Light activated ionotropic Glutamate Receptor 6 |
| NanoBiT | - | NanoLuc Binary Technology |
| Opn4 | - | Melanopsin |
| OptoXRs | - | Chimeric rhodopsin receptors |
| PCR | - | Polymerase Chain Reaction |
| $PIP_2$ | - | Phosphatidylinositol 4,5-bisphosphate |
| PKA | - | cAMP-dependent Protein Kinase |
| PKC | - | Protein Kinase C |
| PLC | - | Phospholipase C |
| PTX | - | Pertussis toxin |
| RASSL | - | Receptor Activated Solely by Synthetic Ligand |
| TBE | - | Tris-Borate-EDTA buffer |

# Contents


Abstract i

Acknowledgements iii

Abbreviations v

Contents vii

**Chapter One** Introduction 1

1.1 Mechanisms of the GPCR Pathway 2

1.1.1 The $G_q$ Proteins and Inositol Phospholipid Signalling Pathway 6

1.1.2 Cellular Calcium Signalling via $G_q$ Activation 7

1.1.3 The $G_i$ Proteins and Inhibition of Adenylyl Cyclase 9

1.1.4 Receptor Selectivity for G Protein Activation 10

1.1.5 Termination of GPCR Signalling: GRK and Arrestins 11

1.1.6 Compartmentalised GPCR Signalling 16

1.2 The Optogenetic Technique 19

1.2.1 Historical Perspective - Why Channelrhodopsin? 19

1.2.2 Rhodopsin Intracellular Signalling 21

1.2.3 Rhodopsin and Optogenetics 24

1.2.4 Animal GPCR Opsin-Based Pigments and their Optogenetic Potential 27

1.2.5 Chemogenetic GPCRs as an Alternative to Optogenetics 32

1.3 Astrocytes and GPCRs 36

1.3.1 Calcium Signalling in Astrocytes 36

1.3.2 Gq Coupled Receptors in Astrocytes 37

1.3.3 *In vitro* Astrocyte Cultures 38

1.3.4 *In vitro* Optogenetic Studies using Cultured Astrocytes 38

1.4 *In vitro* GPCR Assays 40

1.4.1 Chemical Calcium Indicators 40

1.4.2 Fluorescent Tagging of Receptors 41

1.4.3 Bioluminescence and its Practical Application 41

1.4.4 Inhibition of Key Subcellular Pathways 42

1.5 Aims of the Thesis 44

C**hapter Two** Materials and Methods 46

2.1 Animal Usage Ethics 47

2.2 Materials 47

2.2.1 Molecular Biology 47
2.2.2 Plasmids, Primers and Vectors 47
2.2.3 Cell Culture 50
2.2.4 Assay Chemicals 50
2.2.5 Imaging Buffers 51
2.3 Molecular Biology 52
2.3.1 Construction of SNAP tagged Optogenetic Receptors 52
2.3.2 NanoLuc Binary Technology cDNA Constructs 55
2.3.3 Polymerase Chain Reaction (PCR) 60
2.3.4 Restriction Digestion and Alkaline Phosphate Treatment 64
2.3.5 Agarose Gel Electrophoresis 64
2.3.6 Gel and Digest Purification 65
2.3.7 Ligation of Vector and Insert DNA 66
2.3.8 Transformation of Plasmids into Competent Cells 66
2.3.9 Purification of Plasmid DNA 67
2.4 Cell Culture 71
2.4.1 Astrocyte Collection 71
2.4.2 Passaging 72
2.4.3 Freezing and Defrosting 72
2.4.4 Transfection of Cells 73
2.5 Calcium Mobilisation Assays 75
2.5.1 Calcium Response in Primary Astrocyte Cultures to Ligand Addition 75
2.5.2 Calcium Mobilisation in Optogenetic Astrocyte Studies 76
2.5.3 Calcium Imaging in Optogenetic HEK Studies 77
2.6 Visualisation of SNAP-receptor Expression and Monitoring of Internalisation 82
2.6.1 Monitoring of SNAP-OptoR Trafficking in HEK Cells 82
2.6.2 Platereader Measurement of NanoBiT Bioluminescence and Receptor Internalisation 83
2.7 Bioluminescence Imaging 85
2.8 Data Analysis and Statistics 87
2.8.1 Analysis of Calcium Transients 87
2.8.2 Measuring SNAP-tagged Receptor Trafficking 90
2.8.3 Presentation and Statistics 92

**Chapter Three** Signalling and Internalisation of the Chimeric Rhodopsin-$\alpha_{1A}$-adrenergic Optogenetic Receptor 93

3.1 Introduction 94

3.1.1 Opto-$\alpha_{1A}$AR Chimeric Receptors 94

3.1.2 Altering Receptor Signalling and Regulation to Change Temporal Activation 96

3.1.3 Chapter Aims 98

3.2 Results 99

3.2.1 Preparation of SNAP-tagged Optogenetic Constructs 99

3.2.2 Sustained Laser Stimulus is Required for SNAP-opto-$\alpha_{1A}$AR Activation in HEK293T Cells 102

3.2.3 Calcium Mobilisation Dynamics in the HEK-SNAP-opto-$\alpha_{1A}$AR Stable Cell Line 107

3.2.4 SNAP-opto-$\alpha_{1A}$ARs Undergo Internalisation in Response to Light Stimulation and 9-*cis*-retinal Supplementation in Stably Transfected HEK Cells 111

3.2.5 Light-Stimulated Trafficking of Opto-$\alpha_{1A}$AR Receptors is Sensitive to Endocytosis Inhibitors 116

3.2.6 Internalisation of Opto-$\alpha_{1A}$AR under Retinal Supplementation is Dependent on Excitaiton Wavelength 120

3.2.7 Carboxyl Terminus Truncation of Opto-$\alpha_{1A}$AR Affects Receptor Internalisation 123

3.2.8 Endocytosis Inhibitors Insufficient for Blocking Opto-$\alpha_{1A}$AR-S371* Internalisation 129

3.2.9 Truncation of Opto-$\alpha_{1A}$AR at $Ser^{371}$ Internalises Independent to Light Stimulation 129

3.3 Discussion 134

3.3.1 SNAP-tagged Opto-$\alpha_{1A}$ARs are Functional 134

3.3.2 Single vs Continuous Laser Light Stimuli 134

3.3.3 Retinal Supplementation Improves Opto-$\alpha_{1A}$AR Responses 135

3.3.4 Calcium Oscillations Produced by HEK-opto-$\alpha_{1A}$AR Continuous Stimulation 136

3.3.5 Similarities in Internalisation Profile between the Opto-$\alpha_{1A}$AR and $\alpha_{1A}$-adrenoceptor 136

3.3.6 Internalisation of the Opto-$\alpha_{1A}$AR Requires Clathrin 137

3.3.7 Successive Truncation of the C Terminal Region Differentially Affects Light Stimulated Opto-$\alpha_{1A}$AR Internalisation and $Ca^{2+}$ Signalling 138

3.4 Conclusions 141

**Chapter Four** Melanopsin for Optogenetic Activation of Calcium Signalling in HEK293 Cells and Primary Astrocyte Cultures 142

4.1 Introduction 143

4.1.1 Calcium Indicators in Astrocytes 143

4.1.2 Transfection of Primary Cells 147

4.1.3 Chapter Aims 148

4.2 Results 149

4.2.1 Establishing Endogenous $G_q$ Related $Ca^{2+}$ Response in Primary Astrocyte Cultures via $\alpha_1$ adrenoceptor Activation 149

4.2.2 Optimised Transfection of Optogenetic GPCRs in Primary Astrocytes Requires Electroporation 152

4.2.3 External LED Light Stimulus Required for Melanopsin Activation in Rat Primary Cortical Astrocytes 158

4.2.4 Melanopsin Induces Calcium Transients in HEK 293T Cells Similar to the Chimeric Optogenetic Opto-$\alpha_{1A}$AR Receptor 164

4.2.5 Brightness of Stimulus Insufficient to Alter Melanopsin or Truncated Melanopsin Induced Calcium Transients 170

4.2.6 Melanopsin can Induce Calcium Transients to Multiple, Temporally Distinct Light Stimuli 172

4.2.7 Inhibition of $G_{i/o}$ Protein in Melanopsin Astrocytes Affects Calcium Response to Multiple Light Stimuli 179

4.3 Discussion 185

4.3.1 Primary Astrocytes Increase Complexity of Optogenetic Assays 185

4.3.2 Melanopsin vs Opto-$\alpha_{1A}$AR Activation 186

4.3.3 Potential Gliotransmission to Non-light sensitive Cultured Astrocytes 187

4.3.4 On-Off Light Stimulation of Melanopsin Produces Multiple Calcium Transients in Astrocytes 188

4.3.5 Truncation of the Melanopsin C terminus and the Effect on Receptor Expression and Function in Primary Astrocytes 189

4.3.6 Melanopsin $G_i$ Activation and the Effect on Calcium Signalling 190

4.4 Conclusions 192

**Chapter Five** Optogenetic Receptor Activation by Spatially Targeted Bioluminescence 193

5.1 Introduction 194

5.1.1 Spatially Localised Activation of Optogenetic Receptors in the Cell 194

5.1.2 Luminopsins 195

5.1.3 Subcellular Light Targeting and NanoBiT 197

5.1.4 Chapter Aims 200

5.2 Results 202

5.2.1 SNAP Tagged Optogenetic Opto-$\alpha_{1A}$AR-SmBiT Constructs Stably Express in HEK293T Cells and Produce Calcium Signals in Response to LED Stimulation 202

5.2.2 HEK-SNAP-Opto-$\alpha_{1A}$AR-SmBiT Cell Lines Produce Bioluminescence when Co-Transfected with LgBiT Marker Constructs and Treated with Furimazine 207

5.2.3 Luciferase complemented SNAP-Opto-$\alpha_{1A}$AR-SmBiT86 receptors do not Produce Calcium Transients in Response to Furimazine Addition 212

5.2.4 Investigation of SNAP-Opn4-SmBiT receptors as alternative OptoRs for luciferase complementation 216

5.2.5 The HEK-SNAP-Opn4-SmBiT86 Cell Line Co-Transfected with LgBiT Constructs can Produce Furimazine Induced Calcium Signalling 225

5.2.6 Furimazine Stimulated Opn4-sm86 Receptor Internalisation Following LgBiT Marker Complementation 232

5.2.7 Subcellular Localisation of Opn4-NanoBiT Bioluminescence Following Complementation with Different LgBiT Anchor Proteins 243

5.3 Discussion 246

5.3.1 NanoBiT Complementation using Compartmental Markers is Sufficient to Generate Robust Bioluminescence with SmBiT Tagged Optogenetic Receptors Opto-$\alpha_{1A}$AR and OP4 246

5.3.2 Bioluminescence from NanoBiT Complementation does not Induce Calcium Signalling in Opto-$\alpha_{1A}$AR 247

5.3.3 High Affinity SmBiT86 can Activate OP4 Calcium Mobilisation and Receptor Trafficking, but not Low Affinity SmBiT114 247

5.3.4 Evaluating the Potential for Split Complementation Luminopsins to Investigate Spatially Localised Signalling from Membrane and Endosomes. 249

5.3.5 Next Steps 250

5.4 Conclusions 252

**Chapter Six** General Discussion 253

6.1 Summary of Thesis Findings 254

6.2 Contribution of Work to the Research Field 255

6.3 Methodological Considerations 256

6.4 Future Steps 259

**Chapter Seven** References 262

# Chapter One
## Introduction

Neuroscience has been revolutionised by the development of optogenetic tools. The fine spatiotemporal control of individual neurons, or nervous tissue, provided by these methodologies has allowed researchers to assess the contribution of defined neural circuits to behaviour and physiology. Although noted for *in vivo* use, the precise nature of receptor activation has also inspired the application of optogenetic methods to investigate cellular signalling and intracellular cascades (Damez-Werno and Kenny, 2015; Rost *et al.*, 2017).

In the context of biological research, 'optogenetic tools' refer to biologically engineered proteins which respond to a light stimulus. Optogenetics uses light of a specific wavelength to cause activation or inhibition of a biological process, with the most widespread tools originating from channelrhodopsins, light-sensitive receptors originating from algae (Nagel *et al.*, 2002, 2003; Deisseroth, 2011). These tools allow control of a cell that has potential be more molecularly defined and spatiotemporally precise than exogenous neurotransmitter or invasive electrode stimulation.

Being able to fine-tune the spatiotemporal activation of cellular receptors is valuable in research into G protein coupled receptors (GPCRs), which are the interest of this current project. The superfamily of GPCRs are numerous, both in the number of different receptors and their physiological actions, and can be described as the most therapeutically important pharmacological targets (Armbruster and Roth, 2005; Sriram and Insel, 2018). They can be linked to several types of G proteins, including, but not exclusive to, the stimulatory $G_s$ and $G_q$ and inhibitory $G_i$ proteins. The $G_q$ proteins cause an increase in intracellular calcium to exert their cell signalling effects, and these downstream events have been linked to both pathophysiology and healthy physiology in many cells.

## 1.1 Mechanisms of the GPCR Pathway

The G protein coupled receptor family is a large group of membrane receptors with well-categorised intracellular actions in mammals. Different GPCR receptors can respond to different stimuli from the body, such as hormones and neurotransmitters, or external signals, for example light and olfaction cues. There are several subfamilies of GPCRs which can be based on structural similarity or DNA sequence homology. These include the class A rhodopsin-like receptors, class B secretin-like receptors, class C metabotropic receptors, and also the frizzled and adhesion receptor families (see *Figure 1.1*, Karchin *et al.*, 2002; Venkatakrishnan *et al.*, 2013). These families can be further divided by the different receptor stimuli - for example the widespread class A "rhodopsin" GPCRs include members responsive to monoamines, lipids, peptides and protein hormones, as well as the light sensitive opsins (Venkatakrishnan *et al.*, 2013, 2016). The interest for the current project resides with the class A GPCRs, which include adrenoceptors for noradrenaline and adrenaline, and rhodopsins.

Although there are many differences between and within subfamilies, GPCRs all share a similar 7 transmembrane (TM) polypeptide structure, in which the intracellular domains can bind to a membrane localised trimeric GTP binding protein (G protein) or other effectors, such as the signal-transduction regulating arrestin proteins (see *Figure 1.1*). GPCRs therefore, at the basic level, act as guanine nucleotide exchange factors for the cell. Current structures of the GPCRs rhodopsin and $\beta_2$ adrenoceptor have been investigated in great detail, with X-ray crystallography used to examine the structure (Palczewski *et al.*, 2000; Rasmussen *et al.*, 2007) and also any conformational changes when bound to ligands or effector proteins (Rasmussen *et al.*, 2012; X. E. Zhou *et al.*, 2016). The structures show arrangement of the transmembrane helices in a counterclockwise bundle around a central binding pocket (for small molecule ligands), with intracellular loops providing binding points for the heterotrimeric G proteins within the second and third intracellular loops (ICL2 and ICL3), and the promixal C terminus, including the juxtamembrane helix 8 (see *Figure 1.1*). In the class A family, highly conserved residues within each transmembrane domain provide the structural framework for helix organisation (Venkatakrishnan *et al.*, 2013). Agonist binding to the receptor

initiates conformational change through an inward movement of the upper ends of the transmembrane helices, with a corresponding outward movement and rotation of the inner transmembrane segments (particularly transmembrane helicies 3, 5 and 6). These conformational changes are transmitted to the ICLs and provide the binding surface for intracellular engagement of effectors such as G proteins, for example in the $\beta_2$ adrenoceptor (X. E. Zhou *et al.*, 2016).

The G protein heterotrimer consists of an αβγ complex, within which the α unit can bind guanine diphosphate (GDP) or guanine triphosphate (GTP), and the βγ subunit is a constitutive dimer. These two units (α and βγ) are both localised to the inner leaflet of the plasma membrane via lipid anchors (Magee and Newman, 1992). Activation of the bound receptor causes a conformational change, transferring to a further conformational change within the $G_\alpha$ protein which releases the bound GDP (Chung *et al.*, 2012). GTP then binds to the α subunit, resulting in the separation of α to the connected βγ subunits, both of which can activate various cellular effectors. The signal from the $G_\alpha$ subunit is terminated by its intrinsic GTPase activity, allowing reformation of the heterotrimeric $G_{\alpha\beta\gamma}$-GDP conformation (Chung *et al.*, 2012; Duc *et al.*, 2015).

G protein subunits have many genetic variants, with human DNA encoding for 16 $G_\alpha$, 5 $G_\beta$ and 12 $G_\gamma$ subunits (McIntire, 2009). G protein signalling of the GPCR of choice is usually named after the $G_\alpha$ subunit of the $G_{\alpha\beta\gamma}$ tetramer as the $G_\alpha$ subtype binding is selective for the receptor type. There are currently 4 accepted classes of $G_\alpha$ proteins found in humans, although more can be found in other organisms (Oka *et al.*, 2009). These classes are further divided into subgroups depending on their signalling pathways; $G_q$ proteins (including $G_{11}$, $G_{14}$, $G_{15}$ and $G_{16}$) act via the phospholipase C pathway, $G_i$ (including $G_z$, $G_o$ and $G_t$) and $G_s$ (also $G_{olf}$) proteins inhibit and stimulate, respectively, the enzyme adenylyl cyclase, and $G_{12/13}$ proteins signal using Rho guanine nucleotide exchange factors (Downes and Gautam, 1999; Siehler, 2009; Chakravorty and Assmann, 2018). In this thesis, there is a focus on the $G_{q/11}$ and $G_{i/o}$ classes of proteins due to their selective binding with the optogenetic receptors used in the studies.

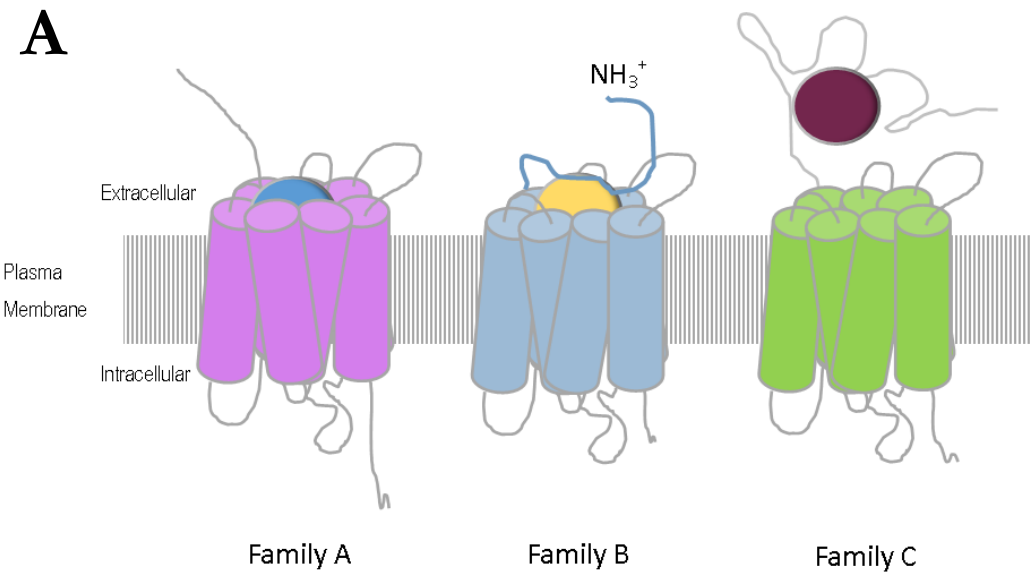
A
$NH_3^+$
Extracellular
Plasma
Membrane
Intracellular
Family A
Family B
Family C

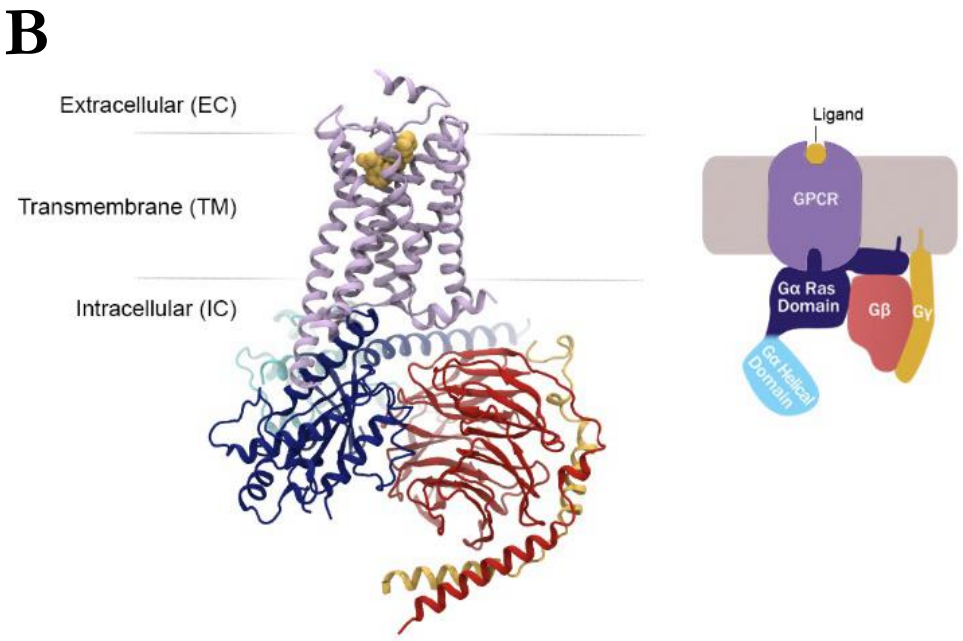
B
Extracellular (EC)
Transmembrane (TM)
Intracellular (IC)
Ligand
GPCR
Gα Ras Domain
Gβ
Gγ
Gα Helical Domain

***Figure 1.1* – GPCR general simplified structure with 7 transmembrane helices arranged in a bundle around a central binding pore.** A) Similar 7 transmembrane structure between the different sub-families of GPCRs, with the extracellular N terminus and intracellular C terminus. Family C is typically activated by amino acids such as glutamate or GABA, or ions such as calcium, using an N terminal venus fly trap domain. Family B receptors recognise peptides via a combination of the N terminal domain and upper transmembrane domain regions. Family A is a large group that have peptides, small molecules and glycoproteins as ligands. B) Transmembrane helices are visualised in a bundle with a central ligand binding site. ON the inner leaflet of the plasma membrane, a heterotrimeric G protein is bound to the intracellular domains of the receptor, made up of the αβγ subunits. Activation involves the replacement of bound GDP on the α subunit with GTP (taken from Sojka *et al.*, 2017).

### 1.1.1 The $G_q$ Proteins and Inositol Phospholipid Signalling Pathway

When a GPCR that can bind to $G_q$ proteins is activated, stimulation of the plasma-membrane bound enzyme phospholipase C-β (PLC) occurs. Upon GPCR stimulation, the $G_{\alpha q}$-GTP protein dissociates from the $G_{\beta\gamma}$ (Tewson *et al.*, 2014). Meanwhile, the $G_{\alpha q}$ protein stimulates PLC, activating the inositol phospholipid signalling pathway through cleavage of phosphorylated phosphatidylinositol 4,5-bisphosphate ($PIP_2$) into two components; inositol 1,4,5-trisphosphate ($IP_3$) and diacylglycerol (see *Figure 1.2*; Tewson *et al.*, 2012, 2014).

$IP_3$ is an intracellular mediator. After $IP_3$ is cleaved from $PIP_2$, the molecule leaves the membrane and binds to $IP_3$-gated $Ca^{2+}$-release channels on intracellular endoplasmic reticulum. Stored within the endoplasmic reticulum is a high concentration of calcium ions (1-5mM, dependent on cell type and location within the reticulum; Bygrave & Benedetti 1996), which are then released into the cytoplasm upon $IP_3$ receptor activation (Parekh, 2016). At the same time, the cleaved diacylglycerol remains in the plasma membrane where it is involved in cell signalling. One process allows diacylglyercol to be further broken down into arachadonic acid, a precursor for the synthesis of prostaglandins and related mediators involved in inflammation and pain. Another mechanism is the activation of protein kinase C (PKC) isoforms by diacylglycerol, $Ca^{2+}$ or phosphatidylserine (Tewson *et al.*, 2012). PKC is engaged in many intracellular phosphorylation mechanisms, and the target proteins vary depending on the cell type involved.

### 1.1.2 Cellular Calcium Signalling via $G_q$ Activation

The influx of $Ca^{2+}$ into the cytoplasm activated by $PIP_2$ causes a rapid increase in intracellular calcium concentration from around 10-100nM to micromolar concentrations, leading to many other calcium propagating responses within the cell (Clapham, 2007). Calcium signalling mechanisms exhibit great spatiotemporal complexity that vary between cell types. $Ca^{2+}$ signals can propagate between cells, using either connected gap junction channels or transmitter-gated $Ca^{2+}$ permeable ion channels (Shigetomi *et al.*, 2013, 2018; Harjes, 2019). In non-excitable cells, spikes of cytoplasmic $Ca^{2+}$ are formed from the regenerative discharge of stored $Ca^{2+}$, forming oscillations throughout the cell. Calcium also affects intracellular compartments. $IP_3$ receptors are the most widely expressed intracellular $Ca^{2+}$ release channels, and are predominantly found on endoplasmic reticulum. As $IP_3$ receptors only open when bound to $IP_3$, they are the link between GPCR PLC stimulation and release of $Ca^{2+}$ from the endoplasmic reticulum (Thillaiappan *et al.*, 2018). The efflux of $Ca^{2+}$ from the endoplasmic reticulum following $IP_3$ receptor activation causes a loss of $[Ca^{2+}]$ in the endoplasmic compartment. This mediates the activation of store-operated $Ca^{2+}$ entry through Orai $Ca^{2+}$ channels on the plasma membrane (Smyth *et al.*, 2010; Parekh, 2016). It is also unwise to view influx of $Ca^{2+}$ only on a whole-cell basis; $Ca^{2+}$ signalling can be localised to only a small segment of the cell, such as a single dendrite in a neuron or a defined area in the soma, causing calcium 'puffs' (Clapham, 2007; Croft *et al.*, 2016; Lock *et al.*, 2017). The subtle spatiotemporal aspects of calcium signalling are ripe for investigation, and methods studying the subcellular activation of $G_q$ coupled receptors will be useful in expanding the knowledge of these varied phenomena.

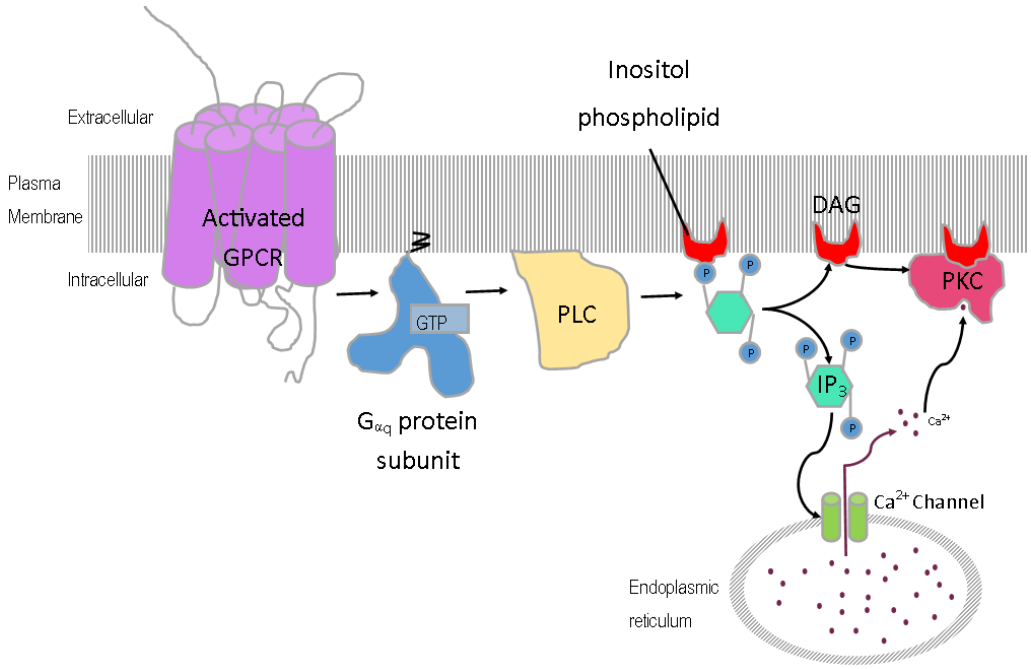


***Figure 1.2*** **– Intracellular signalling pathways from the $G_q$ coupled receptor, causing an increase in intracellular calcium ion concentration and activation of PKC.** The G protein is activated by its receptor, which separates the G protein subunits and starts the cascade. Phospholipase C (PLC) cleaves inositol phospholipids in the membrane, producing inositol 1,4,5-trisphosphate ($IP_3$) to release $Ca^{2+}$ from intracellular endoplasmic stores. Combined with the other cleaved product, diacylglycerol (DAG), the liberated intracellular $Ca^{2+}$ can then activate protein kinase C (PKC), leading to numerous cell signalling effects. Adapted from Alberts *et al.* 2008.

### 1.1.3 The $G_i$ Proteins and Inhibition of Adenylyl Cyclase

In common with the $G_{\alpha q}$ protein heterotrimers, $G_{\alpha i}$ is released from $G_{\beta\gamma}$ subunits by the binding of GTP upon GPCR activation. The rearrangement of the subunits may differ between $G_i$ and $G_q$, with several studies showing an increase in the spatial distance between the $G_{\alpha i}$-GTP and $G_{\beta\gamma}$ at activation without complete dissociation of the subunits, although the full extent of this potential molecular difference on cellular signalling is unknown (Bünemann *et al.*, 2003; Galés *et al.*, 2005, 2006; Tariqul Islam *et al.*, 2018). Once activated, the $G_{\alpha i}$-GTP subunit can associate with adenylyl cyclase, a transmembrane enzyme that catalyses the conversion of adenosine triphosphate (ATP) to cyclic adenosine monophosphate (cAMP), and inhibit the reaction, thereby reducing cAMP production (Wong *et al.*, 1991; Halls and Cooper, 2017). Decreased cAMP results in several downstream effects, predominantly mediated through lowered activity of cAMP-dependant protein kinase (PKA). Under normal activation, PKA catalytic units, released by cAMP binding to the regulatory subunits, phosphorylate serine and threonine residues of proteins in PKA-binding domains (Bieluszewska *et al.*, 2018). Phosphorylation by PKA is regulated by A kinase anchoring proteins to target PKA to its cellular substrates (Bauman *et al.*, 2006; Bieluszewska *et al.*, 2018). $G_{\alpha i}$ is therefore able to inhibit many different biological effects regulated by PKA phosphorylated proteins, dependant on cell type and PKA localisation. Alongside PKA, several other cAMP effectors, such as the exchange proteins directly activated by cAMP (Epacs), are also affected downstream of $G_{i/o}$ activation (Fujita *et al.*, 2017).

Although inhibition of cAMP accumulation and PKA is the main signalling pathway associated with $G_{i/o}$ protein activation, there are also non-canonical signalling cascades involved. Calcium signalling has been shown to be affected in different cell types with $G_{i/o}$ coupled receptor stimulation and sensitive to $G_{i/o}$ specific inhibitor pertussis toxin (Samways and Henderson, 2006; Stojilkovic *et al.*, 2009; Durkee *et al.*, 2019). The mechanism is likely cell specific and linked to activation of $G_{i/o}$-$\beta\gamma$ subunits, such as activation of PLC-$\delta_1$ causing intracellular calcium release, or interactions with PKC-$\beta_1$ and L-type calcium channels on the plasma membrane (Zeng *et al.*, 2003; Murthy *et al.*, 2004; Pérez-Garci *et al.*, 2013;

Zhang *et al.*, 2015). $G_{i/o}$ proteins also have the ability to regulate G protein gated inwardly rectifying potassium (GIRK) channels, which mediate inhibitory neurotransmission in the brain and heart, by direct binding of the $G_{\beta\gamma}$ subunits to the GIRK cytosolic domain, or $G_{\alpha i}$ directly binding to potentially cause selectivity of the signalling and regulate the basal activity (Dascal and Kahanovitch, 2015).

### 1.1.4 Receptor Selectivity for G Protein Activation

Most GPCRs are selective for one class or subclass of G protein. From biochemical studies, it has been determined that the C terminal α5 helix of the $G_\alpha$ subunit is required for binding to the intracellular domain of the activated receptor (Semack *et al.*, 2016). These amino acids differ between the main classes of $G_\alpha$ subunits, and swapping the C terminal 5 amino acids can swap G protein selectivity, for example the $G_{\alpha qi5}$ chimera couples $G_i$ receptors to $G_q$ pathways (Wood *et al.*, 2000). However, the primary amino acid sequence of the GPCR domain is not enough to determine coupling specificity (Flock *et al.*, 2017). G protein binding is therefore thought to be based on the 3D structure of the GPCR-G protein interaction. Suitable advances in single particle imaging using cryo-electron microscopy for structural investigations of GPCRs at high enough definition (<4 Å) have recently been developed (Liang *et al.*, 2017). Structural probing has concluded that there is no specific set of interactions with the GPCR-G protein interface that predicts coupling to the main subclasses of G proteins, $G_s$, $G_i$ and $G_q$ (García-Nafría and Tate, 2019). The dimensions formed by the side chains of α5 helix of the $G_\alpha$ protein are greater in $G_s$ compared to $G_{i/o}$, and this factor appears to be important for specificity of binding to the GPCR intracellular cleft for recognition, but the exact dynamics are unclear (García-Nafría *et al.*, 2018; García-Nafría and Tate, 2019).

Binding of multiple classes of G proteins to varying degrees can occur in some receptors. For example, the $\alpha_{2A}$ adrenergic receptor, endogenously activated by catecholamines adrenaline and noradrenaline, has been shown to activate pathways linked to $G_s$, $G_i$, and $G_q$, whereas the $\alpha_{2B}$ and $\alpha_{2C}$ adrenergic receptors are selective only for $G_{i/o}$ proteins (Eason and Liggett, 1996; Wong, 2003; Carpenter *et al.*, 2016). As GPCR native expression in cells is usually low, selectivity for G proteins can also be reduced in systems that express a high level of the receptor - for example

in transfected recombinant cells, a common methodology for pharmacological investigations.

There is some evidence in select receptors that agonist binding can lead to the receptor adopting different active conformations which is dependent on the ligand – referred to in the literature as "biased agonism", or functional selectivity. It is thought that these different conformations may in turn preferentially couple the receptor to different effectors (Tan *et al.*, 2018). For example, functional selectivity has been reported in the serotonin 5-$HT_2$ receptors, where different ligands have been shown to activate different signal transduction pathways, either PLC mediated IP accumulation ($G_{q/11}$ proteins) or phospholipase $A_2$ aracadonic acid release ($G_{i/o}$ protein activation of extracellular signal-regulated kinases (ERKs); Kurrasch-Orbaugh *et al.*, 2003), with different efficacies (Berg *et al.*, 1998). To investigate the potential molecular changes involved in 5-$HT_2$ receptor biased agonism, a crystal structure of the 5-$HT_{2B}$ receptor bound to lysergic acid diethylamide (LSD) was determined (Wacker *et al.*, 2017). LSD was shown to have an unexpected binding configuration in the orthosteric site that was dependent on LSD's diethylamide positioning, potentially indicating why LSD does not stimulate G protein signalling as readily as other agonists at the receptor (Wacker *et al.*, 2013, 2017).

### 1.1.5 Termination of GPCR Signalling: GRK and Arrestins

Termination of GPCR signalling can be through multiple mechanisms, including the degradation or removal of the agonist from the vicinity of the GPCR, the intrinsic GTP-ase activity inactivating the $G_\alpha$ subunit, and regulatory mechanisms restoring second messenger concentrations to the pre-stimulated levels, e.g. β-arresin binding to $Ca^{2+}$ transducer calmodulin (Wu *et al.*, 2006; Black *et al.*, 2016). However, a crucial part of regulation occurs at the level of the receptor, in which the activity of GPCRs is directly modified despite the continued presence of an agonist or stimulus, resulting in desensitisation. In homologous desensitisation, the activated receptors are selectively targeted for inactivation, and this process most typically involves G protein coupled receptor kinases (GRKs) and arrestins that compete for G protein binding (see *Figure 1.3*).

GRKs are kinases that selectively phosphorylate active conformations of GPCRs, usually at serine/threonine residues located within the carboxyl terminal and the

third intracellular loop of receptors (Gainetdinov *et al.*, 2004; Gurevich *et al.*, 2012). Phosphorylation of the GPCR does not directly prevent the G protein signalling, however this marks the receptor for arrestin binding. The arrestins are a family of scaffold proteins (including β-arrestins 1 and 2, together with visual arrestins) that bind exclusively to light-activated or agonist-occupied GPCRs phosphorylated by GRKs (Luttrell and Lefkowitz, 2002; Black *et al.*, 2016). Binding of arrestin blocks the G protein coupling to GPCRs, causing receptor desensitisation, and also readies the GPCR for sequestration (Black *et al.*, 2016). Once bound to the GPCR, arrestin promotes the translocation of the receptor to endocytic machinery which contain clathrin and adaptor protein-2 (Scarselli and Donaldson, 2009). These clathrin-coated pits remove the GPCR from the cell membrane and internalise the receptor to endosomes, removing the receptors from the vicinity of any agonists and reducing the number of receptors present at the cell surface. Arrestin affinity, often dependent on the pattern of GRK phosphorylation and conformational state of the phosphorylated receptor, determines whether the arrestin dissociates or continues to bind (Luttrell and Lefkowitz, 2002). Transient arrestin binding facilitates receptor recycling, with the endocytosed receptor returning quickly to the cell surface for further activation following agonist dissociation and dephosphorylation. Receptor degradation and delayed recycling can occur the arrestin remains bound to the GPCR, leading the receptor through further intracellular compartments and longer term downregulation of these responses (DeWire *et al.*, 2007). The decisions on receptor sorting to recycling or degradative compartments are also governed by other receptor post translational modifications (e.g. ubiquitination), and GPCR interactions with sorting proteins are involved in directing endosomal traffic (Marchese *et al.*, 2008; Rajagopal and Shenoy, 2018).

Alongside direct termination of GPCR signalling, arrestins can regulate activity through negative feedback mechanisms. For $G_s$ proteins associated with PKA activity, arrestins have been known to scaffold phosphodiesterases, which degrade cAMP, to the plasma membrane (Perry *et al.*, 2002). Similarly, in $G_q$ signalling, which is dependent on the DAG based second messenger system, arrestins can scaffold diacylglycerol kinases to degrade DAG and regulate the signal (Nelson *et al.*, 2007). Arrestins also have the capability to regulate the mitogen-activated protein kinase (MAPK) pathways, involved with proliferation and gene expression,

through Src kinase binding and activation (Luttrell *et al.*, 1999). β-arrestin also directly enhances activation of the ERK cascade by recruiting Raf, ERK and MAPK kinase to the activated receptor (DeFea *et al.*, 2000). This prevents the translocation of active ERK to the nucleus, only allowing for cytosolic catalysis (DeFea *et al.*, 2000).

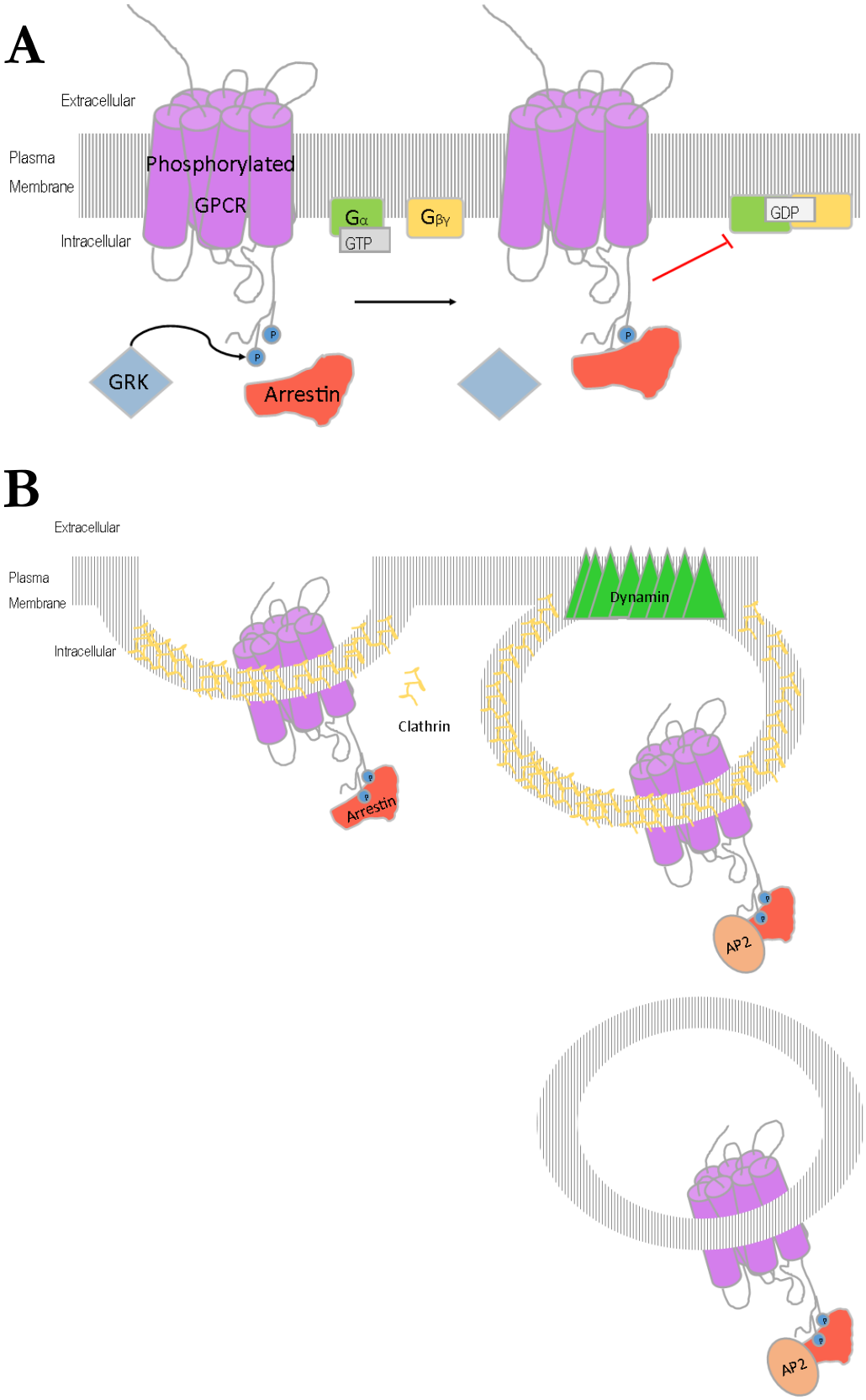
A
Extracellular
Plasma
Membrane
Intracellular
Phosphorylated
GPCR
Gα
GTP
Gβγ
GDP
GRK
Arrestin
B
Extracellular
Plasma
Membrane
Intracellular
Dynamin
Clathrin
Arrestin
AP2
AP2

***Figure 1.3* – Termination of GPCR signalling.** A) GPCR kinase (GRK) phosphorylates intracellular serine/threonine regions of the activated GPCR. Arrestin can then bind to the receptor, blocking G protein recruitment and desensitising the GPCR. B) Arrestin recruits endocytosis machinery to induce receptor sequestration. Clathrin forms a pit in the plasma membrane around the targeted receptor. Adaptor protein 2 (AP2) is recruited by arrestin to bind to the cargo (receptor) designated for internalisation to the clathrin coated membrane. Dynamin then cleaves the newly formed endosome from the plasma membrane, internalising the receptor away from further stimulation. Adapted from Black *et al.*, (2016).

### 1.1.6 Compartmentalised GPCR Signalling

Thus far, only GPCR signalling from the cell surface in the plasma membrane has been covered as the mechanism of transduction. This view is now regarded as oversimplified due to emerging studies that reveal the impact of some GPCRs signalling during trafficking in intracellular membranes, such as endosomes, Golgi apparatus, or the endoplasmic reticulum (Jong *et al.*, 2018; Lobingier and von Zastrow, 2019). Therapeutically, if the location of the receptor signalling in a pathogenic response is compartmentalised, this could provide opportunities in drug design (for example in considering membrane permeability), to promote plasma-membrane or intracellular targeting as required (Thomsen *et al.*, 2018). It is therefore important to understand the location and duration of GPCR activation. In fact, the spatiotemporal aspects of GPCR signalling are currently an intriguing and increasing body of work in the current pharmacological literature.

#### *1.1.6.1 Endosomal Signalling*

Current understanding of GPCR endosomal signalling is incomplete. It is generally accepted that there are G protein-independent pathways which are initiated by arrestin bound receptors in endosomes, for example the β-arrestin activation of extracellular signal-regulated kinases (ERKs) 1 and 2 by $\beta_2$ adrenoceptors (Shenoy *et al.*, 2006). There is also the hypothesis that GPCRs in endosomes still have the potential to signal through G protein pathways, although the evidence supporting this idea is not yet concrete (Lobingier and von Zastrow, 2019). Some early arguments for G protein signalling in endosomes utilise classic pharmacological methodology; sustained cAMP and PKA activation is observed from the vasopressin type 2 receptor post receptor stimulation and agonist washout, and endocytic inhibition of $D_1$ dopamine receptors reduced $G_s$ dependent cAMP accumulation (Kotowski *et al.*, 2011; Feinstein *et al.*, 2013). Two other notable GPCRs reported to generate intracellular cAMP increases when internalised are the parathyroid hormone receptor type 1 and the thyroid-stimulating hormone receptor (Ferrandon *et al.*, 2009; Calebiro, 2011). Although promising, there are limitations to these experiments. Agonist washout is not sufficient to prove complete removal of the ligand, and blocking endocytosis of receptors may produce other signalling effects not directly linked to the GPCR in question. Single-

domain antibodies (nanobodies) that bind specifically to a the active conformation of the $\beta_2$ adrenoreceptor also revealed that receptors in such a conformation are present in endosomes, although unfortunately these conformational biosensors do not relay any functional output (Irannejad *et al.*, 2013). Recent work has set out to show that receptors with strong arrestin binding have the potential to form a 'megacomplex' with both arrestins and G proteins and produce sustained endosomal signalling (Bahouth and Nooh, 2017). This complex has been visualised with the vasopressin type 2 receptor using both fluorescence co-localisation techniques and single particle electron microscopy, seen alongside sustained cAMP production (Thomsen *et al.*, 2016). Although the studies mentioned are not resolute in backing the hypothesis, results supporting endosomal G protein signalling are increasing, and development of compartmentally localised activators and sensors will aid in future studies. Most of the research on endosomal signalling currently focuses on $G_s$ protein responses, and less is known about these mechanisms in $G_i$ or $G_q$ coupled receptors. Endosomal $G_q$ signalling has been reported in calcitonin receptor-like receptor and neurokinin 1 receptor stimulation, with both receptors providing a target for the selective inhibition of pain signals (Jensen *et al.*, 2017; Yarwood *et al.*, 2017). There are still many unanswered questions about G protein endosomal signalling; for instance, how is the signal terminated, and is the mechanism different to cell surface activation? Further developments in methodology to elucidate the spatiotemporal characteristics of GPCR signalling are required to make advancements on answering such questions.

#### *1.1.6.2 Golgi and Endoplasmic Reticulum as Signalling Sites*

GPCR activation in the Golgi and/or the endoplasmic reticulum has also been observed and is thought to be induced via two different paths; either cotrafficking of the receptor and ligand from the cell surface, or ligand permeation/transportation into the intracellular compartments. A classic example involves the $G_q$ coupled metabotropic glutamate receptor 5 (mGluR5) which undergoes continual constitutive endocytosis to the Golgi and endoplasmic reticulum, as well as stable expression at the nuclear membrane (Sergin *et al.*, 2017). Antagonists that do not cross the plasma membrane are unable to completely block the calcium response initiated by glutamate at mGluR5, and inhibition of organic anion transporters, blocking intracellular sequestering of glutamate, also reduces

the signalling response (Jong *et al.*, 2005). Subcellular, compartmentalised activation of receptors is therefore a potential avenue of drug development that is yet untapped to its full potential.

## 1.2 The Optogenetic Technique

Historically, one of the limits to neuroscience research has been the inability to control a single type of cell within the central nervous system (CNS) (Banghart *et al.*, 2004; Boyden *et al.*, 2005). Electrodes cannot precisely target cellular subtypes accurately, relying on morphology and physiology, and drugs are difficult to control over time, with on and off binding kinetics affecting cell response. Controlling these cells with light offers a solution to this problem; light is fast to turn on and off, unlike washing a drug in and out, and can also be specific to a distinct subset of cellular receptors. The mammalian CNS does not contain light-sensitive receptors, apart from within the eye and the suprachiasmatic nucleus. Light dependent cellular activation was therefore a sought-after commodity which has serendipitously helped in developing methodology for increased spatiotemporal control of intracellular signalling *in vitro*.

### 1.2.1 Historical Perspective - Why Channelrhodopsin?

In order to use light as a stimulus, nature provides several different routes. Pioneering experimental methods to utilise light stimulation were derived from "caged" neurotransmitters (Marque, 1989; Callaway and Katz, 1993). One of the more successful experiments using caged neurotransmitters achieved laser activation of receptors in over 20,000 spatial locations within brain tissue (Shoham *et al.*, 2005). In these experiments, the neurotransmitter glutamate was caged within a biologically inert compound. Using ultraviolet light combined with a precise spatial excitation of a two-photon confocal microscope, the caged compound underwent photolysis, freeing glutamate to activate receptors (Shoham *et al.*, 2005). Although impressive spatial resolution was achieved, glutamate is the most common neurotransmitter in the brain, with a range of ionotropic ion channels and metabotropic GPCRs, and does not offer the ability to selectively activate a subset of neurons. Neither would the method be ideal for *in vivo* experiments, as laser activation cannot easily be used in freely moving animals. Several other caged neurotransmitters have proved useful to research, such as the use of caged ATP in *Drosophila* to analyse dopamine activation behaviour (Lima and Miesenböck, 2005). Specific targeting of the neurons activated was achieved through genetic

manipulation of the fly CNS to express the ATP gated ion channel $P2X_2$ on neurons which naturally did not code the receptor. This does allow targeting of specific neurons, unlike the methods used by Shoham *et al.* (2005), but was only performed in a simple fly nervous system, not the complexity of a mammalian brain. Ligands are also still used with caged neurotransmitters, so following release, ligand diffusion and receptor binding kinetics remain a potential influence on the signal (Lima and Miesenböck, 2005; Shoham *et al.*, 2005).

An alternative approach was established and coined 'optogenetics' by the Deisseroth lab using the algae receptor channelrhodopsin 2 (ChR2) to control cells using light (Boyden *et al.*, 2005). This receptor has a 7 transmembrane structure (though unrelated to GPCRs), and uses the photoisomerisable 11-*cis*-retinal as a covalently tethered ligand (Nagel *et al.*, 2003). Upon isomerisation of 11-*cis*-retinal to all-*trans*-retinal by light, ChR2 becomes cation permeable through a conformational change in the pore structure. Patch clamp techniques allowed the resulting cation conductance to be measured, and successful transfection of ChR2 in human embryonic kidney (HEK) 293 cell lines and oocytes demonstrated that blue light could activate the channel and cause a membrane potential response in animal cells (Nagel *et al.*, 2003). Boyden et al. (2005) saw a use for the rapid kinetics of the ChR2 and virally transfected the channel into a hippocampal culture. Through blue light stimulation, single spikes and precise spike trains could be evoked within the tissue on a millisecond timescale, allowing light control of nerve firing (Boyden *et al.*, 2005). ChR2 transfection produced minimal side effects and was reported to have no effect on nerve survival, demonstrating the potential for prolonged use. The fine spatiotemporal tuning and rapid induction of the ChR2 technique was exciting and reliable, promoting many more successful studies in culture and animals to investigate neural mechanisms and behaviours (see reviews Deisseroth, 2011b, 2015; Govorunova *et al.*, 2017). Although not without caveats, such as genetic alteration of tissue and invasive methods of light delivery to deep brain structures, channelrhodopsin activation of neuronal cells is now a powerful and widely used research method. Recent reviews have covered the wealth of other optogenetic tool that are currently available, for example inhibitory $Cl^-$ channels (halorhodopsins), other caged compounds, and photoswitchable ligands that can

activate the bound receptor using light (Rost *et al.*, 2017; Paoletti *et al.*, 2019). Here, the focus is on optogenetic receptors, with a key interest in GPCR opsins.

### 1.2.2 Rhodopsin Intracellular Signalling

Joining together the two streams of light-activation and GPCRs is the well-defined visual rhodopsin receptor – a phototransductor within the rods of the retina used for detecting low levels of light (Palczewski, 2006). These are distinct from the microbial rhodopsins, such as channelrhodopsin, which act as ion pumps and have been used often as optogenetic tools (Boyden *et al.*, 2005; Li *et al.*, 2013; Liske *et al.*, 2013; Govorunova *et al.*, 2017, 2019). Due to its light sensitive activation, structural stability and sensitivity for spectroscopy techniques, bovine rhodopsin was the first GPCR to have the crystal structure solved, and has therefore been studied intensely (Palczewski *et al.*, 2000; Olausson *et al.*, 2012; Kang *et al.*, 2015). Many of the activation and transduction events have been elucidated to great resolution, including the intermediate activated 'metarhodopsin' state (Van Eps *et al.*, 2017; Kang *et al.*, 2018) .

Rhodopsin is made up of a GPCR opsin motif, and a covalently bound retinal molecule to the protein $Lys^{296}$ via a Schiff-base linkage - the natural form of which is 11-*cis*-retinal, although other retinal analogues exist (Sekharan & Morokuma 2012). The lysine is found on transmembrane VII of rhodopsin and the retinal itself sits within a transmembrane binding pocket in the centre of the receptor (Kang *et al.*, 2018). To offset the positive charge of the base, a counterion in transmembrane helix 3 at $Glu^{113}$ (inactive) or $Glu^{181}$ (active) also interacts with the retinal binding pocket (Yan *et al.*, 2003). Structural investigations into the spatial binding of the chromophore have revealed that the N-terminal region of rhodopsin forms a 'cap' over the β-sheet lid to trap the retinal binding site (Kang *et al.*, 2015, 2018). Without light stimulus, the covalently bound 11-*cis*-retinal acts as an inverse agonist to stabilise the inactive receptor state, protecting against constitutive activation (Maeda *et al.*, 2018). Two other important motifs for the stabilised inactive 'dark' form of rhodopsin are the NPIVY and ERY domains – highly conserved regions found in most GPCRs (Fritze *et al.*, 2003; Favre *et al.*, 2005). NPIVY contributes to a network of stabilising interactions at the bottom of the transmembrane domains I, II and VII (Fritze *et al.*, 2003). ERY is part of the "ionic lock", an interhelical

hydrogen-bond network formed in family A GPCRs, where $E^{134}$ (glutamate, negatively charged) and $R^{135}$ (arginine, positively charged) form salt bridges in transmembrane III, but also with another glutamate residue in transmembrane VI (Palczewski *et al.*, 2000; Vogel *et al.*, 2008).

For activation, maximal absorption of rhodopsin is at 500nm, which differs from the trichromatic cone opsin pigments at blue (414nm), green (533nm) and red (560nm) wavelengths (Janz and Farrens, 2001). The spectral tuning, i.e. the maximal wavelength and colour absorption, of these opsins is achieved by interactions of residues in the chromophore binding pocket with the Schiff base (Lin *et al.*, 1998; Janz and Farrens, 2001). In rhodopsin transduction, the retinal undergoes isomerisation from the inactive 11-*cis*-retinal to all-*trans*-retinal when stimulated by photons, causing a conformational change and activation of the opsin receptor (Palczewski, 2006; Saari, 2012). There are several transient stages involved in the receptor conformational change as photoisomerisation of retinal is faster than the protein movements (Tian *et al.*, 2017). First identified through spectrophotometry experiments, it was found that rhodopsin relaxes through several distinct states upon full activation with light until it enters the active conformational state named metarhodopsin II (Frederiksen *et al.*, 2016; Tian *et al.*, 2017). Proton uptake by rhodopsin during activation causes protonation of the E based ionic bonds in the ERY motif, disrupting the ionic lock (Vogel *et al.*, 2008). The recently revealed cryo-EM structure has shown an outwards rocker switch movement of the inner ends of transmembrane III and VI away from each other upon activation, which opens up the intracellular binding site for the G protein (Kang *et al.*, 2018).

Metarhodopsin II activates the $G_{i/o}$-like $G_t$ protein, also known as transducin. The second messenger functional effectors from $G_t$ activation are unique where, instead of inhibition of adenylyl cyclase, $G_{\alpha t}$-GTP activates cGMP phosphodiesterase, an enzyme that hydrolyses cGMP to 5'-GMP (Spiegel, 1987; König *et al.*, 1989). As cGMP activates cGMP-gated cation channels, reduction in intracellular cGMP leads to hyperpolarisation of the membrane potential, which, in its native environment, regulates electrical activity and therefore synaptic transmission in rod cells (Cukkemane *et al.*, 2011).

Rhodopsin saturates rapidly, but regenerates the visual pigment slowly, typically taking 40min to recover sensitivity in humans (Cideciyan *et al.*, 1998; Saari, 2012). Desensitisation and recycling of rhodopsin following activation is important for this regeneration of signalling as the receptor itself cannot photoisomerise the all-*trans* form of retinal back to the inert *cis*-retinal, instead relying on external enzymes in separate cells for the process (Choe *et al.*, 2011). Prevention of back isomerisation in the receptor is thought to have developed to increase the sensitivity and decrease dark noise of rhodopsin, and the placement of retinoid processing machinery outside of the rod cells is due to the inherent toxicity of retinoids (Lamb, 2009; Choe *et al.*, 2011). In rhodopsin desensitisation, Ser/Thr residues on the C terminus are phosphorylated by rhodopsin kinase (GRK1), allowing for binding of visual arrestin which blocks $G_t$ protein activation (Frederiksen *et al.*, 2016). Although some visual arrestins do recruit AP2 for clathrin-mediated endocytosis of rhodopsin (notably, splice variant p44 does not), the affinity is weak and rhodopsin expression in rod cells remains constant in vertebrates with little trafficking (Satoh and Ready, 2005; Moaven *et al.*, 2013). All-*trans*-retinal is released from the binding pocket through hydrolysis of the Schiff base linkage, where, in the native rod cell environment, it diffuses to the cytoplasmic leaflet of the intraluminal discs for conversion to all-*trans*-retinol by dehydrogenases (Kiser *et al.*, 2012). The retinol form is chaperoned to retinal pigment epithelial cells where it can be isomerohydrolased and then oxidised back to 11-*cis*-retinal for reuse in opsin binding, and regeneration of rhodopsin formation (Kiser *et al.*, 2012).

Correct rhodopsin processing is crucial in retaining rhodopsin functional output. Retinal is required for activation and recycling of the receptor, and loss of this ligand can lead to receptor degradation and retinal disease (Park, 2014; Maeda *et al.*, 2018). Also, the congenital Oguchi disease, which causes night blindness, is characterised by mutations in GRK1 or visual arrestin, accounting for a loss of dark adaption and leading to eventual degradation of rod cells (Yamamoto *et al.*, 1997; Alloway *et al.*, 2000; Moaven *et al.*, 2013). On the other hand, loss of the C terminal phosphorylation sites in mouse rhodopsin has been shown to prolong photoresponses (Chen *et al.*, 1995). It is therefore important to consider the retinoid and receptor processing machinery if utilising rhodopsin as an optogenetic tool.

### 1.2.3 Rhodopsin and Optogenetics

As rhodopsin is selective for the visual $G_t$ protein, the receptor has limited use as an optogenetic tool in other cell types or for investigations with other cell signalling cascades. Similarities in structure within the class A rhodopsin-like GPCR family stimulated the idea that chimeric GPCRs between rhodopsin and the intracellular domains of the other receptors could be used to couple light activation to signalling mechanisms initiated by $G_s$, $G_{i/o}$ or $G_{q/11}$ (Karnik *et al.*, 2003; Kim *et al.*, 2005). The concept of using chimeric rhodopsin receptors (optoXRs) *in vivo* was validated by a study using rhodopsin and adrenoceptor fusion proteins (Airan *et al.*, 2009). Extracellular loops and transmembrane helices were taken from the rhodopsin, whereas the $\beta_2$ and $\alpha_1$ adrenoceptor (although not specified by the authors, subtype $\alpha_{1A}$-AR) intracellular loops, with predominant coupling to the $G_s$ and $G_q$ protein respectively, were used for the cytoplasmic part of the membrane receptor (see *Figure 1.*). When opto-$\alpha_{1A}$AR was transfected into HEK cells, 60s of exposure to green light caused an increase in calcium within the cell, detected by the calcium indicator Fura-2, and a significant increase in $IP_1$ (a product of $IP_3$) (Airan *et al.*, 2009). Building on this success, the optoXRs were transfected into the nucleus accumbens of adult mice using lentivirus techniques. Due to the need for retinoids as a chemical cofactor, *in vivo* activation of the optoXRs could have been a problem. However, studies into ChR2 and optogenetics revealed that there were enough of the cofactors present in the mammalian brain without supplementation (F. Zhang *et al.*, 2006). Indeed, the cortical tissue revealed neuronal spiking activity when exposed to light, demonstrating activation of the opto-$\alpha_{1A}$AR, without addition of any cofactors (Airan *et al.*, 2009). Spatiotemporal activation of $G_q$ intracellular signalling was thus shown to be effective both *in vitro* and *in vivo*. Opto-$\beta_2$AR produced an inhibitory effect in these tissues, also demonstrating a functional response. In another study, the opto-$\beta_2$AR was compared to the wild type $\beta_2$ adrenoceptor, where it was found that the two receptors produced similar intracellular responses in terms of cyclic adenosine monophosphate generation, MAP kinase activation and receptor internalisation, demonstrating retention of wild type adrenoceptor properties in the chimera (Siuda *et al.*, 2015). Both of the adrenoceptor optoXRs have also been successfully transfected and activated in astrocytes, a neural cell type that will be of interest to the current study and outlined

in further detail in section 1.3 (Figueiredo *et al.*, 2014). Further to the success of utilising the adrenoceptors for $G_s$ and $G_q$ downstream signalling upon light stimulation, several chimeric rhodopsin constructs have been made using the intracellular regions of $G_{i/o}$ coupled receptors; opto-5-HT 1A, which also leads to an increase in intracellular potassium, PA-$CXCR_4$ and opto-MOR, using rat rhodopsin and the μ-opioid receptor (Oh *et al.*, 2010; Xu *et al.*, 2014; Siuda *et al.*, 2015). The main downside of the use of rhodopsin as an optogenetic tool is the natural bleaching process of the photopigment, which causes the dissipation of intracellular responses over repeated stimulations, and the reliance of rhodopsin signalling on retinal recycling machinery being present in the cell model of choice. Other opsin based GPCRs may instead be a viable option for experiments requiring high temporal control.

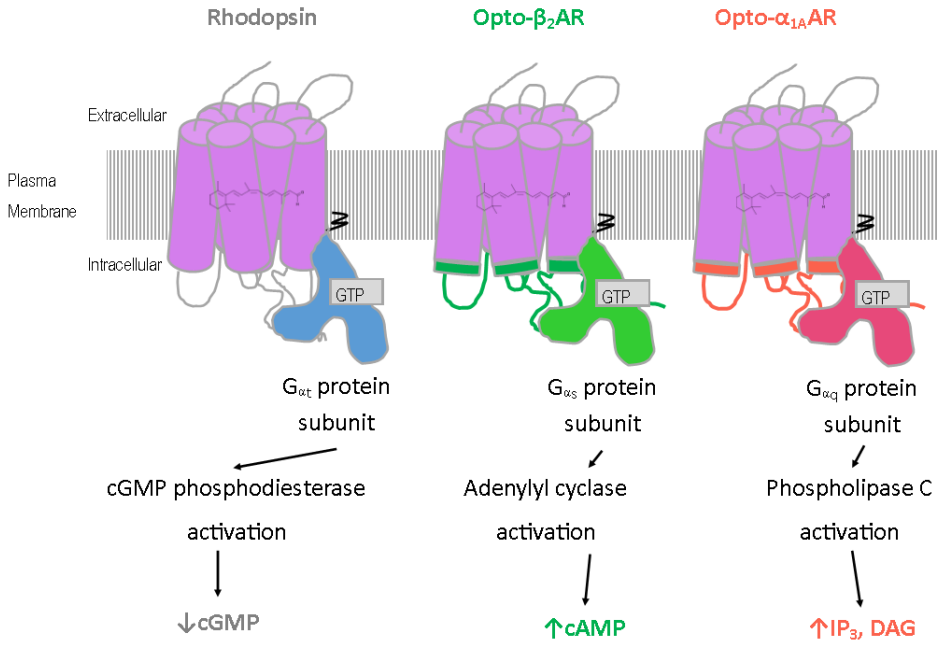


***Figure 1.4* – Chimeric optogenetic receptors made from rhodopsin and adrenoceptors.** Originally, rhodopsin and its intracellular loops activate the coupled $G_t$ protein and, through activation of the rod phosphodiesterase, cause a decrease in cyclic guanine monophosphate (cGMP). Other transduction cascades from light activation via $G_s$ and $G_q$ proteins are achieved by using the intracellular loops of the $\beta_2$ and $\alpha_1$ adrenoceptors, respectfully. Adapted from Airan *et al.* (2009).

### 1.2.4 Animal GPCR Opsin-Based Pigments and their Optogenetic Potential

There are a large variety of GPCR opsin-based pigments found in the animal kingdom which can act as photoreceptors for various functions, such as vision, circadian rhythm and pupillary response. As with the related rhodopsin, these photosensitive receptors contain an opsin protein moiety and use a non-protein moiety in the form of retinal (commonly 11-*cis*-retinal) as the activating chromophore (Terakita, 2005; Tsukamoto and Terakita, 2010). There are thousands of identified opsins that can be grouped into eight genomic classifications, which tends to correspond to the receptor functionality (Terakita *et al.*, 2012). Five of these groups inhibit cyclic nucleotide signalling via their G protein cascades; the $G_{i/o/t}$ coupled vertebrate visual pigments and vertebrate non-visual pigments, $G_{i/o}$ coupled Opn3 (encephalopsin) and invertebrate opsin, and $G_i$ coupled Opn5 (neuropsin). Cnidarian $G_s$ coupled opsins, $G_q$ coupled visual pigment and the $G_q$ coupled Opn4 (melanopsin) make up the other three groups of animal opsins (Tsukamoto and Terakita, 2010; Koyanagi and Terakita, 2014). GPCR opsins are therefore very diverse in the phototransduction cascades available, making them good targets for use as optogenetic tools investigating G protein activation.

The photochemical properties of opsin-based pigments can affect the efficiency and duration of the phototransduction. Vertebrate visual opsins, including rhodopsin, are monostable, often named "bleaching pigments", as they are thermally unstable and release the retinal post light activation (Koyanagi and Terakita, 2014; Berry *et al.*, 2016). Most other animal opsins form bistable pigments that revert back to their stable dark, inactive state from the photo-activated state following sufficient light absorption (Tsukamoto and Terakita, 2010; Sexton *et al.*, 2012; Díaz *et al.*, 2016).

Of the many light-sensitive receptors available, several opsin-based pigments have been singled out for optogenetic use due to their unique photochemical properties and transduction cascades.

#### 1.2.4.1 Melanopsin

Melanopsin, also known by its genetic name Opn4, is a photosensitive receptor found in intrinsically photosensitive retinal ganglion cells (ipRGCs). Light activation of melanopsin is non-image producing and instead linked to regulation of the circadian pacemaker in the hypothalamus, which synchronises light-dark cycles of the day with physiological and behavioural responses (Newman *et al.*, 2003; Melyan *et al.*, 2005). Other functions include input on pupillary light reflexes, melatonin synthesis suppression in the pineal gland for sleep regulation, and light inhibition of activity (Díaz *et al.*, 2016). The transduction cascade of melanopsin is prolonged compared to that of rhodopsin or cone receptors; in ipRGCs, the integration time was found to be 8s, 100 fold greater than in mammalian cones and 20 fold longer than rods (Do *et al.*, 2009). A longer period for transduction is consistent with the physiological function of melanopsin cells to integrate sensory information, rather than discriminate details of a light stimulus with high temporal resolution. Indeed, although expressed in vertebrates, melanopsin is most homologous to rhabdomeric pigments found in invertebrates which have a reduced complexity in visual systems (Shichida and Matsuyama, 2009; Terakita *et al.*, 2012).

Molecular understanding of melanopsin structure, photochemistry and signalling is limited and not yet on par with that of rhodopsin. Part of the reason for this is due the naturally low cellular expression of melanopsin in ipRGCs, around 100 fold less than rhodopsin in the retina, although current methods of protein purification are addressing this issue (Walker *et al.*, 2008; Shirzad-Wasei *et al.*, 2013). Isoforms appear to affect functional response of the receptor, perhaps indicating a photochemical difference useful for optogenetics; for example, the gene for melanopsin, Opn4, has shown to have two different functions in the mouse retina, with pupillary response attributed to the short C terminus isoform (Opn4S) and long (Opn4L) to negative masking (Pires *et al.*, 2009; Jagannath *et al.*, 2015). Also of interest to optogenetic studies, melanopsin was first recognised as a bistable pigment where 11-*cis*-retinal is photoisomerised to all-*trans*-retinal reversibility under blue-green wavelengths of light, allowing for switching of retinal between the light-activated and dark states once sufficient light absorption is reached (Mure *et al.*, 2007; Sexton *et al.*, 2012). This is perhaps useful for neuronal studies which require better temporal precision than, for example, the 40min recovery needed by

rhodopsin. The maximum absorbance of melanopsin has no exact figure in the literature. Mouse melanopsin, with its longer C terminal tail, has been reported to have a maximum absorbance between 520-540nm, whereas human melanopsin has been reported to have maximal light sensitivity anywhere between 420-480nm (Walker *et al.*, 2008; Bailes and Lucas, 2013; Emanuel and Do, 2015). Further investigation into the photochemical properties of melanopsin have revealed a potential third state that may explain the broad wavelength ranges of maximal sensitivity (Matsuyama *et al.*, 2012; Emanuel and Do, 2015). In one study, the third state was proposed to be induced by switching of all-*trans*-retinal in the active "meta" state to 7-*cis*-retinal, which was promoted by a red-shifted excitation wavelength (leading to a second dark state with 446nm maximal absorption). This contrasted to the standard dark state (467nm maximal absorption) bound to 11-*cis*-retinal (Matsuyama *et al.*, 2012). Although convincing as a mathematical model, the study was performed with restricted conditions, such as the model being performed at 0ºC, and 7-*cis*-retinal is yet to be observed in nature. Under a more physiologically relevant system of retinal tissue, Emanuel and Do (2015) also reported maximal electrophysiological responses that differed from stimulating melanopsin in a dark state (471nm maximal response, named the 'cyan' state) and stimulating the receptor with 600nm background light (454nm maximal response, named the 'violet' state), again indicating tristability of the receptor between the 'meta' activated states and the cyan and violet silent states. Short wavelengths are therefore thought to shift the photoequilibrium to meta states (longest wavelength of absorption at 471nm); long excitation wavelengths favour the violet state (shortest wavelength of absorption at 453nm), which is thought to be silent as this decreases ipRGC activity (Emanuel and Do, 2015). This dual-sensitivity difference of 20nm (the difference between green and red visual cone opsins) has yet to be shown in any other opsin, making melanopsin unique in its photochemistry.

In phototransduction, melanopsin is selective for the $G_q$ family of G proteins, with the functional output being a rise in intracellular calcium (Graham *et al.*, 2008; Hughes *et al.*, 2014). It is however interesting that abolishment of $G_{q/11}$ in mice was not able to completely block light-induced calcium responses in ipRGCs (Chew *et al.*, 2014). There could be an unwanted upregulation of the two other $G_q$ proteins in this model ($G_{14/15}$), although these are not thought to be expressed in ipRGCs.

There is also evidence that some isoforms of melanopsin have the ability to bind $G_{i./o}$ proteins which could be activating the $Ca^{2+}$ response (Chew *et al.*, 2014). In one such study, Bailes and Lucas (2013) found a small PTX-dependent reduction in forskolin induced cAMP production when HEK293T cells expressing either human or mouse melanopsin were stimulated with a range of light wavelengths (420-600nm). The response was more transient and less marked than rhodopsin activation, which itself is more selective for $G_t$ than $G_{i/o}$, and as the experiment was only performed in HEK cells, may be cell specific as such responses have not been seen in the native ipRGCs (Bailes and Lucas, 2013; Tsunematsu *et al.*, 2013). Another study investigated the ability of both human and mouse melanopsin to activate GIRK channels, a downstream signal attributed to $G_{i/o}$ activation, as outlined in section 1.1.3 (Spoida *et al.*, 2016). In HEK cells, 470nm light caused activation of these channels and 560nm light deactivated the response for both receptors (reflecting the tristable model of melanopsin), though the human variant showed greater desensitisation of GIRK activation over multiple light pulses than the mouse melanopsin (Spoida *et al.*, 2016). In neural cells, however, it appears that $G_q$ proteins are the main transducers of melanopsin activation, indicating that cell type is crucial to melanopsin signalling, requiring characterisation of the receptor in the cell of choice before any optogenetic experiments are carried out (Tsunematsu *et al.*, 2013; Spoida *et al.*, 2014, 2016). It is also interesting to note that the mouse melanopsin has the ability to cause an extracellular influx of calcium, which the human melanopsin does not, again highlighting the versatility of melanopsin signalling and different avenues useful for optogenetic innervation (Spoida *et al.*, 2016).

Due to the interesting photochemistry of melanopsin allowing for good temporal control of activation, and its link to $G_q$ protein activation, several recent studies have promoted the use of the receptor as an optogenetic tool. Perhaps surprisingly, optogenetic melanopsin activation was not pioneered in neuroscience or GPCR research, but was first used to drive expression of a transgene to express glucagon-like peptide 1 through activation of calmodulin (from $Ca^{2+}$ increase under blue light) and the NFAT transcription factor pathway, attenuating glycaemic excursions in type II diabetic mice (Ye *et al.*, 2011). This is also one of the first suggestions of potential optogenetic therapy for a disease, although the ethical debate of genetic

treatments still remains. The inherent $G_q$ signalling of melanopsin was also utilised in cardiomyocytes to control the beating rate and pacemaker activity of the cells with high spatiotemporal precision, demonstrating that melanopsin could be useful as a tool to control local $G_q$ activation in cardiac tissue (Beiert *et al.*, 2014). In neuroscience, melanopsin has been used to study astrocyte-neuron networks by mimicking endogenous $G_q$ activation, where the researchers found evidence of increased $G_q$ astrocyte innervation enhancing episodic-like memory *in vivo* (Mederos *et al.*, 2018).

For future research, studies with different isoforms of melanopsin show that its light activation can be adaptable to mimic different temporal signalling events, as seen in comparisons between mouse and human melanopsin (Spoida *et al.*, 2016). Using structural homology models as a design base, a mutant Y211F mouse melanopsin (targeting the chromophore binding pocket) has also been developed with a blue-shifted activation and on/off kinetics which are twice as fast as the wild type melanopsin, allowing for better temporal control of the optogenetic tool (Tennigkeit *et al.*, 2019). Two melanopsin chimeras have also been created in a similar manner to the rhodopsin variants – one using the intracellular loops of 5-$HT_{2A}$ for activation of CNS neurons, and the other successfully combining melanopsin with the metabotropic glutamate receptor 6 (mGlu6) (van Wyk *et al.*, 2015; Mcgregor *et al.*, 2016). In particular, mGlu6 light activation is an interesting prospect for therapy as endogenous mGlu6 is expressed in the retina and mutations in the mGlu6 coding gene are associated with congenital stationary night blindness (van Wyk *et al.*, 2015). In less than a decade, melanopsin has proven to be a versatile and viable G protein optogenetic tool with far reaching potential.

#### *1.2.4.2 Jellyfish Opsin*

An interesting recent addition to the optogenetic GPCR toolbox is a bistable opsin discovered in box jellyfish, known as JellyOp. JellyOp is the only reported opsin that naturally activates $G_s$ signalling, and is therefore useful for light stimulation of intracellular cAMP (Koyanagi *et al.*, 2008; Koyanagi and Terakita, 2014). Unlike typical bistable pigments, JellyOp does not revert back to its original dark state under light irradiation in experimental conditions, although there is still the possibility that the bistability of JellyOp is more typical when natively expressed, perhaps due to a different temperature in the organism (Koyanagi *et al.*, 2008). Very

little is currently known about the photochemistry and molecular nature of JellyOp, however this has not hindered its use as an optogenetic tool. JellOp use was verified by Bailes *et al.* (2012) when JellyOp was expressed in HEK 293 cells and stimulated with light to produce a reversible, sustained increase in cAMP that was more robust under repeated stimulation than the $G_s$ coupled opto-$\beta_2$AR. Following this success, JellyOp and its F112A G protein-impaired signalling mutant was used to investigate the impact of $G_s$ and arrestin on the circadian clock in fibroblasts (Bailes *et al.*, 2017). Although both receptors induced light-dependent shifts in the circadian rhythm, there was a difference in the generation of circadian phases, suggesting that the two receptors can be used to selectively manipulate $G_s$ and β-arrestin signalling in cells (Bailes *et al.*, 2017). The latest study using JellyOp was a proof of concept for optogenetic stimulation of $G_s$ signalling in the whole heart (Makowka *et al.*, 2019). Spatial (left vs right $G_s$ signalling in the atria) and temporal (delay between receptor activation and contractility) aspects of $G_s$ signalling were elucidated using light activation, as well as a lack of adverse dark activity of the JellyOp (Makowka *et al.*, 2019). Summarised, JellyOp is an up and coming optogenetic tool that may have further applications in the near future.

### 1.2.5 Chemogenetic GPCRs as an Alternative to Optogenetics

Although a powerful tool for selective spatiotemporal activation of GPCRs, the optogenetic method has several disadvantages. For example, the results obtained with receptors activated by light may not translate well back to endogenous ligand activated receptors, with different activation kinetics and receptor recycling. Light can also be difficult to control in a laboratory setting, particularly with fluorescent/bioluminescent assays, and contamination of the experiment with ambient light is possible. GPCR chemogenetics is an alternative to optogenetics that allows for increased selectivity of the receptor of interest over endogenous receptors, allowing for investigations into specific receptor activation pathways, while retaining ligand binding and similar activation kinetics. The principle behind receptor chemogenetics is to find a mutation that stops the receptor binding to its endogenous ligand/s, but can still be activated by a synthetic compound (Bishop *et al.*, 2000). Such receptors have been coined as either RASSLs (Receptors Activated Solely by Synthetic Ligands) or DREADDs (Designer Receptors Exclusively

Activated by Designer Drugs)(Redfern *et al.*, 1999; Armbruster *et al.*, 2007). DREADDs are usually preferred as the synthetic compound used to activate the mutated receptor does not bind to the endogenous receptor, in principle only binding to the chemogenetic receptor in a biological system.

The first described chemogenetic GPCRs were the Ro1 and Ro2 RASSLs, both $G_{i./o}$ coupled $\kappa$ opioid receptors that were mutated to no longer activate with the endogenous ligands (Redfern *et al.*, 1999). Ro1 was further used to induce bradycardia when expressed in the heart and activated with spiradoline in mice, investigate opioid receptor temporal signalling events, and to activate sweet and umami taste receptors (Coward *et al.*, 1998; Zhao *et al.*, 2003; Scearce-Levie *et al.*, 2005). Rho1s success lead to the development of RASSLs for the $\beta_2$ adrenoceptor (termed 'TREC', therapeutic receptor-effector complex, with a bound $G_s$ protein), serotonin 5-$HT_4$, and melaocortin-4 receptors, all $G_s$ coupled (Small *et al.*, 2001; Claeysen *et al.*, 2003; Srinivasan *et al.* 2003). Unfortunately, the lack of specificity for the synthetic ligand to the RASSLs has limited their use to tissues and cells that do not contain the wild type receptor, and there were no developments for the other G protein subtypes (Pauwels and Colpaert, 2000).

The latest form of RASSL to be developed are the DREADD based chemogenetic receptors. These differ from the first RASSLs as the activating ligand does not activate the wild type receptor at physiological concentrations. The first DREADDs developed were based on the $M_3$ and $M_4$ muscarinic GPCRs; $G_q$ and $G_{i/o}$ coupled receptors, respectively. Two point mutations in both the $M_3$ and $M_4$ stop the native muscarinic ligand acetylcholine from binding to the receptor, but drastically increase its affinity for the synthetic compound clozapine-*N*-oxide (CNO) (Armbruster *et al.*, 2007). The $M_3$ DREADD ($hM_3D$) receptor was then successfully used *in vivo* to selectively activate $hM_sD$ expressing forebrain neurons (Alexander *et al.*, 2009). Alongside the $G_q$ and $G_i$ proteins, the $G_s$ pathway can also be stimulated by muscarinic DREADDs. This tool was created using a mutated rat $M_3$ receptor that incorporates the $\beta_1$ adrenoceptor ECL2 and 3, allowing $G_s$ coupling (Conklin *et al.*, 2008). Of particular interest to the study of GPCR signalling pathways, two further $hM_3D$ receptors were created that display pathway bias. One does not bind to G proteins, allowing for investigations into $\beta$ arrestins and associated pathways without G protein activation (Nakajima and Wess, 2012).

The other $hM_3D$ mutation cannot interact with β arrestins, creating a tool that preferentially activates the $G_{q/11}$ proteins (Hu *et al.*, 2016). Aside from the muscarinic DREADDs, there is also a κ opioid receptor DREADD (KORD). KORD was developed using several point mutations which drastically decrease the binding of endogenous ligand dynorphin A and increase affinity for the pharmacologically inert salvinorin B (Vardy *et al.*, 2015). When expressed in mice and stimulated with salvinorin B, KORD inhibited of dopamine neuron tonic firing and decreased locomotor activity, showing its potential as a chemogenetic tool (Marchant *et al.*, 2016).

DREADD use has been seen throughout the literature since the receptors' conceptions. For example, the $G_q$ and $G_s$ coupled $M_3$ DREADDs were first used *in vivo* in β cells to study the effects of the two G proteins on cell metabolism (Guettier *et al.*, 2009). Systemic application of CNO allowed the researchers to selectively activate the $hM_3D$ receptors expressed in the pancreatic β cells and found that $G_q$ or $G_s$ activation lead to increased insulin release and glucose tolerance. The $hM_3D$ has also been used in molecular investigations, such as in muscarinic dimers where the activation of $M_2$ altered heterodimer interactions, but activation of $hM_3D$ did not (Aslanoglou *et al.*, 2015).

The selectivity and low biological activity of designer drugs allows for a similar comparison to the use of light in optogenetics, if not quite as selective, and the ease of drug administration vs. light administration allows for less invasive or light sensitive investigations. Pathway selectivity with the two $hM_3D$ mutants is also very useful for signalling research, although this theoretically could also be developed in the optogenetic GPCRs. Although a powerful tool for selective cell stimulation and inhibition, the use of chemogenetics does present a unique disadvantage. Muscarinic DREADDs appear to be the most frequently used in the literature, normally activated by CNO. An investigation into the DREADD occupancy of clozapine revealed a high affinity for the receptors, whereas the binding of CNO was low (Gomez *et al.*, 2017). With their labelled compounds, only clozapine crossed the blood-brain barrier through systemic admission (Gomez *et al.*, 2017). This is further complicated by the metabolism of CNO by the body, where it is converted to clozapine or *N*-desmethylclozapine, ligands which are biologically active and not receptor selective (MacLaren *et al.*, 2016). Suitable CNO controls

without the DREADD receptor are therefore required in these experiments. New compounds are also being tested at DREADD receptors to develop a better tool with less potential for offsite actions, and some could even have translation into the clinic, such as the atypical antipsychotic olanzapine (Chen *et al.*, 2015; Weston *et al.*, 2019).

## 1.3 Astrocytes and GPCRs

Astrocytes belong to a subset of neural cells called glia. The main function of glia remained a mystery for decades as, unlike neurons, they are electrically nonexcitable. Instead, glia support neuron function, and the cellular signalling by astrocytes is associated with intracellular ions and second messengers, not action potentials. Some physiological roles assigned to astrocytes include extracellular ion and neurotransmitter buffering, energy supply, and homeostatic regulation (Agulhon *et al.*, 2013). One of the crucial intracellular processes that regulate astrocyte function is calcium signalling.

### 1.3.1 Calcium Signalling in Astrocytes

First found in astrocyte cultures by Cornell-Bell *et al.* (1990), intercellular calcium waves are known to arise through mechanical or neurotransmitter stimulation. The coding and functionality of calcium waves within the astrocyte population is complex, and many neuroprotective and neurotoxic roles are associated with the phenomenon (Nedergaard *et al.*, 2010). Like many cells, astrocytes also have intrinsic intracellular $Ca^{2+}$ fluctuations that do not require a signalling response (Nett *et al.*, 2002). $IP_3$ receptors on the endoplasmic reticulum can be activated by a high density expression of $G_q$ coupled receptors and the intrinsic activity that generates $IP_3$ signals, or focal points of high [$Ca^{2+}$] which act as an $IP_3$ receptor coagonist (Khakh and McCarthy, 2015). Spatial aspects of calcium responses, such as IP3 receptor expression and $Ca^{2+}$ location, are therefore of interest when studying astrocytes. Calcium signalling within astrocytes can also be confined within single cells to subcellular microdomains. It is these underlying subcellular puffs caused by intracellular signals (such as $G_q$ protein signalling) which amount to calcium induced calcium release, and thus global calcium signalling (Croft *et al.*, 2016). Calcium waves can propagate quickly through astrocyte syncytia via gap junction channels and purinoceptors (Kuga *et al.*, 2011; Giaume *et al.*, 2013). Astrocytes are thought to release neurotransmitters in response to calcium signalling methods, although the physiological importance of so called "gliotransmitters" is controversial with debated links to neuron and vascular function (Bazargani and Attwell, 2016).

### 1.3.2 $G_q$ Coupled Receptors in Astrocytes

Astrocytes use elevated intracellular calcium as a signalling mechanism for many of their various functions. Astrocytes therefore endogenously express many GPCRs which couple to the $G_q$ protein and associated pathways for $IP_3$ release of intracellular calcium stores.

#### *1.3.2.1 $\alpha_1$ Adrenoceptors in Astrocytes*

The $G_q$ GPCR $\alpha_1$ adrenoceptor is endogenously expressed in a range of astrocytes. Functions of the receptor include regulation of gap junctions, glycogen breakdown and secretion of neurotrophins (Kötter and Klein, 1999). These receptors are also thought to be involved in the coordinated signalling of cortical astrocytes (Bekar *et al.*, 2008; Ding *et al.*, 2013). When electrically stimulating the locus coeruleus, the sole source of noradrenaline to the cortex, astrocytes were found to have a rapid increase in $Ca^{2+}$ (Bekar *et al.*, 2008). This was found to be modulated by $\alpha$ adrenoceptor agonists and antagonists. Cortical injections of adrenergic agonists also caused robust astrocytic calcium responses in awake mice, and blocking $\alpha_1$ adrenoceptor actions from the locus coeruleus blocked spontaneous astrocytic signals (Ding *et al.*, 2013). Pathophysiologically, the links of $\alpha_1$ adrenoceptors to neurogenesis and gliogenesis are of interest when looking into the lack of neural regrowth in CNS injuries (Gupta *et al.*, 2009). A better understanding of the $\alpha_1$ adrenoceptor endogenous response would therefore be useful in many fields for the understanding of astrocyte development and physiology.

#### *1.3.2.2 Muscarinic $M_1$, $M_3$ and $M_5$ Receptors*

Astrocytes can express any of the muscarinic acetylcholine receptors, and the $M_1$, $M_3$ and $M_5$ receptors are all $G_q$ coupled (Elhusseiny *et al.*, 1999; Oda *et al.*, 2018). Acetylcholine action at these receptors is important for various processes in the CNS, such as cerebral blood flow, eye accommodation, long term potentiation and memory (Abrams *et al.*, 2006; Sugihara *et al.*, 2016). Specifically in hippocampal astrocytes, several studies have shown responses to acetylcholine, and that these astrocytes may be involved in synaptic potentiation (Perea and Araque, 2007; Henneberger *et al.*, 2010). It has also been shown through whole cell patch-clamping and calcium imaging that astrocyte response to muscarinic innervation is important for cortical plasticity (Chen *et al.*, 2012). Pathophysiologically, there are hopes that positive allosteric modulators of the muscarinic $M_5$ receptor will be

effective treatment for cognitive decline in diseases such as Alzheimer's or schizophrenia, which could potentially be acting at astrocytes in the CNS (Cieślik *et al.*, 2019; Gould *et al.*, 2019). There is also the possibility of using muscarinic antagonists in the CNS to help control the inflammatory response of multiple sclerosis (Di Bari *et al.* 2017).

### 1.3.3 *In vitro* Astrocyte Cultures

Primary astrocyte cultures from animals, both in whole tissue and culture, can be used to provide a more translational biological system than immortalised cell lines. Although *in vivo* and *ex vivo* work provide good translation from cell to organism function, *in vitro* cultures allow for an environment that is easier to control, providing a good preliminary basis of biological mechanisms before setting up animal experiments, and therefore decreasing the number of animals required for a study. Indeed, many important astrocytic physiology discoveries have been attributed to work in primary cultured astrocytes, such as the activation of calcium waves under glutamate stimulation (Cornell-Bell *et al.*, 1990; Araque *et al.*, 1998, 1999). The key to *in vitro* work is the ability for translation of the findings into an endogenous system. Current developments in stem cell differentiation (allowing for human astrocyte lineages), 3D culture and microfluidics are all decreasing the translational deficits of cultured astrocytes (Pa ca *et al.*, 2015; Renault *et al.*, 2015; Gonçalves-pimentel *et al.*, 2018).

### 1.3.4 *In vitro* Optogenetic Studies using Cultured Astrocytes

Pioneering optogenetic *in vitro* astrocyte research involved the characterisation of ChR2. The light activated ion channel induced an intracellular increase of $Ca^{2+}$ after blue light stimulation, attributed to release from intracellular stores through cation influx from the membrane (Figueiredo *et al.*, 2014; Ono *et al.*, 2014). Studies using ChR2 in primary astrocyte cultures also show that ChR2 stimulation of intracellular $Ca^{2+}$ causes $Ca^{2+}$ increase and electrophysiological responses in cells not expressing ChR2 (Berlinguer-Palmini *et al.*, 2014; Ono *et al.*, 2014). The described response was found to be inhibited using antagonists for ion channel glutamate receptors, suggesting that light activated cells release glutamate as a gliotransmitter to activate nearby cells (Berlinguer-Palmini *et al.*, 2014). Another physiological response has been investigated *in vitro* using ChR2 in bipotential glial progenitor cell lines, named

OS3 cells (Ono *et al.*, 2017). When expressing ChR2 and activated with light, the OS3 cells were more likely to differentiate into oligodendrocytic lineages, rather than astrocytic cell types, with a decrease in GFAP expression and increased myelination functions.

In addition to the standard ChR2, other ion channel optogenetic tools with greater $Ca^{2+}$ activity have been designed. One such receptor is the light activated ionotropic glutamate receptor 6 (LiGluR) whereby a bound photoswitchable ligand allows for receptor control via light (Volgraf *et al.*, 2006). This has successfully been used in astrocyte cultures to demonstrate the same instance of glutamate transmission via light activation as shown with ChR2 (Li *et al.*, 2012). Inhibiting gap junctions and extracellular ATP did not reduce $Ca^{2+}$ transients, again providing evidence that extracellular glutamate is a principal gliotransmitter. Another receptor for $Ca^{2+}$ investigation is a ChR2 mutation named the calcium translocating ChR2, where mutations in transmembrane 3 of ChR2 increases $Ca^{2+}$ permeability (Kleinlogel *et al.*, 2011). Mager *et al.* (2017)designed an optogenetic tool using the calcium translocating ChR2 and voltage-dependent large conductance potassium channels to enable localised $Ca^{2+}$ transients at the membrane, rather than the entire cytosol, in a concentration that could be varied using voltage and light stimulation. When used in human astrocyte cultures, the receptors allowed for control of endogenous potassium channels (Mager *et al.*, 2017). This is an exciting tool of localised signalling with future applications in co-cultures to study astrocyte-neuron interaction via potassium channels.

Although useful for the general stimulation of astrocytes, these ion channel based, light-activated receptors are not specific for one ion, and lack the ability to activate other important second messenger systems which are crucial in the physiological responses of astrocyte calcium signalling. The rhodopsin-adrenoceptor chimeras (optoXRs) were therefore investigated for use in astrocytes as a potential optogenetic activator of GPCR function, where they could produce good $Ca^{2+}$ signalling profiles in cultured astrocytes (Figueiredo *et al.*, 2014). Interestingly, they found that the bulk of $Ca^{2+}$ responses could be blocked with an ATP degrading enzyme, potentially linking an autocrine action of ATP.

## 1.4 *In vitro* GPCR Assays

To investigate the intracellular activation of GPCRs, there are many cell assays that are widely accepted and commonly used by the scientific community. Here, the most relevant assays for the study will be briefly outlined, including the monitoring of intracellular calcium, receptor trafficking and effector recruitment, with a focus on the use of different bioluminescent and fluorescent compounds as means to visualise and/or measure these responses. When designing a study, it is important to note that many cell types can express a variety of receptor subtypes, even cell lines that have been purposefully engineered for research. The contribution of the particular receptor subtype of interest to the response profile can consequently be difficult to determine. It is therefore advantageous to selectively activate a single type of receptor in a cell by other means, thus increasing the power of the cell assay.

### 1.4.1 Chemical Calcium Indicators

Using fluorescent calcium sensitive dyes, the amount of calcium ions ($Ca^{2+}$) in the cell can be measured. Chemical calcium indicators are made up of a calcium chelator and a fluorophore. Upon binding $Ca^{2+}$, there is a conformational change that causes the fluorescent molecule to undergo an increase in quantum yield or a shift in the excitation and emission wavelength (Grienberger and Konnerth, 2012). The change in the fluorescence intensity can be visualised and/or quantified through imaging techniques (Paredes *et al.*, 2008). Several chemical $Ca^{2+}$ indicators are available, allowing different fluorescent wavelengths and $Ca^{2+}$ affinities to tune the assay towards the desired dynamic range and sensitivity (Paredes *et al.*, 2008; Oheim *et al.*, 2014). Dyes can be injected into a cell or are made cell-permeable by addition of an acetoxymethyl ester linkage, which is then cleaved by cytoplasmic esterases in the intracellular compartments, leaving the dye to accumulate in the cytosol. Calcium mobilisation enables insight into the stimulation of GPCR $G_q$ proteins via intracellular [$Ca^{2+}$] and provides some quantification of the receptor stimulation by the intensity of signal. The different calcium signalling methodologies will be covered in greater detail in section 4.1.1.

### 1.4.2 Fluorescent Tagging of Receptors

Another method of measuring receptor activation is via the endocytosis and recycling of receptors post-stimulation, and this may be achieved through imaging labelled receptors via fluorescence imaging. A common approach is to fuse the receptor to a fluorescent protein, such as green fluorescent protein (GFP; Zhang *et al.*, 2002) but a more recent system is to use the SNAP-tag enzyme protein, with associated stable fluorophore substrates that may be cell permeable or not (Keppler *et al.*, 2003). The 180 amino acid SNAP sequence can be fused to the chosen receptor using molecular biology methods, thereby allowing a fluorescently labelled substrate to covalently bind to the receptor. SNAPsurface fluorophores cannot enter the cell, and label only extracellular SNAPtags (for example, fused to the N terminus of a GPCR at the cell surface). Thus redistribution of this fluorescence to intracellular compartments reflects endocytosis of the labelled receptor to intracellular endosomes. Agonist-stimulated endocytosis can then be quantified, using imaging platereaders and analysis, to provide information on concentration dependent effects and ligand pharmacology.

### 1.4.3 Bioluminescence and its Practical Application

Bioluminescence refers to light which is produced from a biochemical reaction and, unlike fluorescence or phosphorescence, does not require absorption of electromagnetic radiation. These bioluminescent systems all use a luciferase enzyme to oxygenate a luciferin substrate, which then emits photons when returning to its ground state. Bioluminescence systems are found in many different organisms, including bacteria, insects and marine creatures, and show diversity in their biochemistry. Some bioluminescence production requires cofactors, such as ATP, or other enzymes and intermediate steps, and a subset of luciferases (photoproteins) can bind and stabilise the substrate, only releasing light under the presence of cations, such as $Mg^{2+}$ (Kahlke and Umbers, 2016).

For practical application, several different luciferases derived from nature have been utilised in cell assays, each with their own biochemical characteristics. The first bioluminescence assays were developed using firefly luciferase (FLuc), with a popular analysis utilising the linear increase in light production with ATP, a required

participant of the FLuc reaction (Marques and Esteves Da Silva, 2009). FLuc as a biological tool is however not optimal due to its reliance on ATP and $Mg^{2+}$ and the large size of the protein (61kDa). *Renilla* luciferase (RLuc) was recognised as a more appropriate luciferase for application as a bioluminescent tag; RLuc substrate (coelenterazine; CTZ) only requires oxygen for luminescence production, and the 36kDa size is also preferable, although stability of RLuc output required optimisation through mutagenesis (Loening *et al.*, 2006). Further developing on the success of RLuc, another CTZ luciferase was discovered in the marine copepod *Gaussia princeps* (GLuc) that is both brighter (2,000 fold more sensitive than RLuc) and smaller (18kDa), allowing for the successful use of GLuc in high throughput systems (Maguire *et al.*, 2009). More recently, the development of an engineered luciferase NanoLuc (NLuc) using the catalytic subunit from the deep sea shrimp *Oplophorus gracilirostris* luciferase and its synthetic substrate furimazine has allowed for even brighter bioluminescence production with a much longer, sustained signal, lower background autoluminescence and good tolerance to pH and temperature changes (Hall *et al.*, 2012). Luciferase bioluminescence has a broad range of application, for example, direct measuring biological responses, such as metabolism, use as genetic reporters or intracellular biosensors, or monitoring of protein-protein interactions. For protein-protein interactions, this can be quantified using a fragmented luciferase; the two parts of the enzyme can be fused to the different proteins of interest, with bioluminescence output only being produced when the two fragments are in close enough proximity to catalyse the substrate. RLuc, GLuc and NLuc all have their own split reporters for studies of this nature, with their use depending on the study design and assay of choice (Paulmurugant and Gambhir, 2003; Remy and Michnick, 2006; Dixon *et al.*, 2016).

### 1.4.4 Inhibition of Key Subcellular Pathways

Inhibitors can be used to block specific intracellular pathways and analyse which molecules are required in signalling cascades. For G protein inhibition, of which $G_q$ and $G_{i/o}$ are the focus in this study, several compounds are available. FR900359 and YM-254890 are cyclic peptides that show good potential for selective inhibition of $G_{q/11}$ signalling without affecting other GPCR pathways, even though their use is not yet common across the literature (Schrage *et al.*, 2015). Instead, inhibition of

PLC by U73122 has historically been used to target the downstream signalling of a $G_q$ coupled receptor, with the main caveat that U73122 may lead to alkylation of several other proteins (Horowitz *et al.*, 2005). Although it is currently difficult to target and inhibit $G_q$ proteins, $G_{i/o/t}$ are the only pertussis toxin (PTX) sensitive G proteins and can therefore be inhibited selectively in a cell (Mangmool and Kurose, 2011). Unfortunately, $G_z$ is not PTX sensitive, and this should be taken into account when analysing PTX data (Wong *et al.*, 1992). Also of interest is the function of β-arrestin in GPCR signalling pathways. Clathrin dependent endocytosis inhibitor Pitstop 2 and dynamin inhibitor Dyngo 4a can be used downstream targets of β-arrestin binding (Mccluskey *et al.*, 2013; Willox *et al.*, 2014). There is also a recently developed inhibitor of the β-arrestin/AP2 complex, named Barbadin, which shows promising signs as a cellular tool for targeting β-arrestin function directly (Beautrait *et al.*, 2017).

## 1.5 Aims of the Thesis

Optogenetic GPCRs are a powerful tool for investigating the spatiotemporal aspects of cell signalling through their use of light as an activator of intracellular cascades. Light as an agonist offers unrivalled specificity over electrode or drug cell stimulation. Spatially, light can also be targeted to single cells, or even subcellular domains, easier than electrodes or ligands. Temporally, light activated GPCRs offer faster, less complex kinetics than typical ligand binding. Current optoXRs, once activated by the 11-*cis*-retinal isomerisation, rely on receptor regulation events to define the timecourse of their de-activation. This provides the opportunity to manipulate the spatial and temporal aspects of optogenetic receptor responses in order to better mimic physiologically relevant endogenous signals – for example, of varied duration. This technology is particularly interesting for investigation into complex cell types, such as the heterogeneous astrocytes which express a wide variety of endogenous GPCRs and multifaceted calcium signalling. In this thesis, the aim is to develop and engineer $G_q$ coupled optogenetic receptors with greater control over spatial activation and temporal signalling for their use in elucidating astrocytic calcium signalling events and consequences.

**Chapter Three** focuses on the development of fluorescent cell signalling assays to monitor calcium signalling and receptor trafficking of light activated, $G_q$ coupled opto-$\alpha_{1A}$AR. The HEK293 cell line is utilised as a model system for receptor expression and activation in order to develop suitable methodologies for further *in vitro* work. Temporal characteristics of the opto-$\alpha_{1A}$AR signalling are also tuned through use of C terminal truncation mutants, potentially altering receptor desensitisation and trafficking post activation and increasing signal output.

The application of $G_q$ coupled optogenetic receptors in a more translational system is investigated in **Chapter Four**. Primary cortical rat astrocyte cultures are optimised for transfection with melanopsin (Opn4). Light stimulation of different patterns is used to induce astrocytic calcium signalling, and C terminal truncations are again utilised to try and alter temporal activation.

Finally, **Chapter Five** covers the development of a novel, complementation-based bioluminescence stimulation of optogenetic GPCRs for controlling subcellular activation. Bioluminescence systems have been used to activate optogenetic

receptors previously, but only using channelrhodopsins and full luciferase constructs (Birkner *et al.*, 2014; Berglund *et al.*, 2016). In this new system, one part of the fragmented luciferase NanoLuc (NanoBiT) is fused to the optogenetic GPCR, with the complementation fragment for a fully functional enzyme tagged to a compartmentalised target protein (Kras for the plasma membrane, and Rab5 for early endosomes). Bioluminescence production from the furimazine substrate can only occur when the receptor is within a close proximity of the target protein, for example on the plasma membrane, potentially enabling spatially distinct bioluminescence stimulation of the optogenetic receptor.

Chapter Two

# Materials and Methods

## 2.1 Animal Usage Ethics

Animals were sacrificed in accordance with guidelines outlined in the code of practice for humane killing under Schedule 1 of the UK Home Office Animals (Scientific Procedures) Act 1986. Experiments were performed according to policies on the care and use of laboratory animals of British Home Office and European Community laws and were approved by The University of Nottingham Animal Welfare and Ethical Review Body.

## 2.2 Materials

### 2.2.1 Molecular Biology

Kits were used to perform basic molecular biology techniques. The PCR Cleanup Kit, Gel Extraction Kit and Miniprep Kit were all provided by Sigma-Aldrich Ltd. (Poole, UK). The Maxiprep Kit was supplied by Qiagen (Hilden, Germany). Buffers were created using compounds from Sigma-Aldrich, unless otherwise stated. Bacterial growth media, Luria Bertani (LB) Broth (used at 20mg.mL$^{-1}$) and LB Agar (used at 35mg.mL$^{-1}$, containing 1% peptone, 0.5% yeast extract and 1% NaCl), were also supplied by Sigma-Aldrich, and were made up in dd$H_2O$ to final concentration, before autoclaving to sterilise. Ampicillin (50mg.mL$^{-1}$; Sigma-Aldrich) was made up to final concentration using double distilled water (dd$H_2O$). Thermo Fisher Scientific (Waltham, MA, USA) provided the FastDigest enzymes, shrimp alkaline phosphatase (FastAP) and the T4 DNA Ligase, all with associated buffers.

### 2.2.2 Plasmids, Primers and Vectors

pcDNA3.1(+) neo or zeo vectors containing an N terminal 5HT3 signal sequence and SNAPtag (located between Kpn1 and BamH1 sites) were made by the Holliday lab prior to this project (Watson *et al.*, 2012).

The rhodopsin-$\alpha_{1A}$ adrenoceptor chimera plasmid, pcDNA3.1-opto-$\alpha_{1A}$AR-EYFP-v5his, was supplied by the Deisseroth lab (Stanford, CA, USA; see *Figure 2.1*). The human melanopsin receptor cDNA (Opn4; Genbank Ref NM_033282) was supplied as an IMAGE clone by Source Bioscience (Nottingham, UK). LgBiT and

SmBiT constructs of the NanoBiT were made in-house using sequences provided by Promega (Southampton, UK). SmBiT was created via synthesis and annealing of a double stranded primer with RE overhangs into the pcDNA3.1$_{ZEO}$ vector. N terminal LgBiT with the 5 or 10 Gly/Ser linker region, and flanked by HindIII and BamH1 sites, was synthesised by GeneArt (Invitrogen; Regensburg, Germany). Human Rab5 was also synthesised by GeneArt with flanking EcoR1 and XbaI sites. All primers were designed in-house and produced by Sigma-Aldrich.

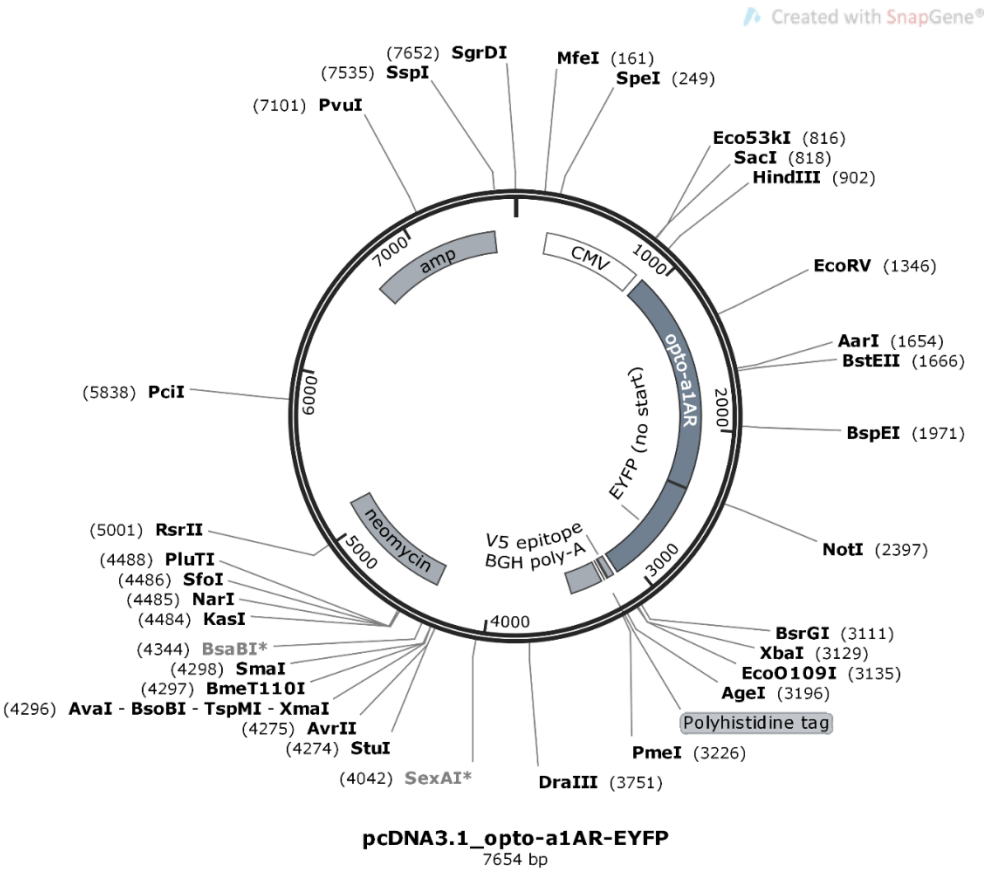


***Figure 2.1*– The opto-$\alpha_{1A}$AR vector from the Deisseroth lab.** Opto-$\alpha_{1A}$AR was provided in a pCMV vector with flanking restriction sites HindIII and NotI (Airan *et al.* 2009).

### 2.2.3 Cell Culture

Dulbecco's Modified Eagle's Medium (DMEM) with high glucose (4500mg.$L^{-1}$) was purchased from Sigma-Aldrich. The solution differs from the original DMEM by containing a more stable glutamine derivative, L-alanyl-L-glutamine dipeptide. Media supplement L-proline was provided by Sigma-Aldrich, and Foetal Bovine Serum (FBS) and Foetal Calf Serum (FCS) were provided by GE Healthcare Life Sciences, Buckinghamshire, UK. FCS originates from 3-10 day old calves and provides a higher content of proteins and immunoglobulins, but lower concentrations of growth factor compared to FBS. Antibiotics penicillin and streptomycin (10,000U.$mL^{-1}$ penicillin, 10,000µg.$mL^{-1}$ streptomycin; Thermo Fisher Scientific) were provided in solution and stored at 4°C. Geneticin (G418, used at 0.2mg/mL; Invitrogen, San Diego, CA, USA) and zeocin (used at 20µg/mL; Thermo Fisher Scientific) were made up to 10x concentration in DMEM and stored at -20°C for future use. Black 96 well flat bottom plates were ordered from Greiner Bio-One (Frickenhausen, Germany; model 655090). Chemotransfection agents Lipofectamine and Lipofectamine 3000 were supplied by Invitrogen, and electroporation was performed using the Nucleofector device with the Amaxa Basic Nucelofector Kit for Primary Mammalian Glial Cells from Lonza (Basel, Switzerland).

### 2.2.4 Assay Chemicals

All ligands (phenylephrine, ATP, carbachol) were ordered from Tocris Bioscience (Poole, UK), and stored in 10mM aliquots of 10-20µL at -20°C in dimethyl sulphoxide (DMSO). Supplements 9-*cis*-retinal and all-*trans*-retinal (both Sigma-Aldrich) were aliquoted out in 20µL at -20°C in DMSO. As they are light sensitive, both retinals were stored in brown Eppendorf tubes and foil covered to protect them from light. Endocytosis inhibitors Pitstop 2 and Dyngo 4a were provided by Abcam (Cambridge, UK) and SNAP-Surface Alexa Fluor (AF) compounds from New England Biolabs (Hitchen, UK). Calcium indicator dyes Fluo-5F AM, Fura Red AM, XRhodI AM and Rhod 2 AM, along with Pluronic F-127 surfactant (20% solution in DMSO), were all ordered from Thermo Fisher, whereas Cal6-30 AM was purchased from AAT Bioquest (Sunnyvale, CA, USA). Pertussis toxin (PTX) in lyophilized format was ordered from Enzo Life Sciences (Farmingdale, NY,

USA). Probenecid, an inhibitor of the canalicular multispecific organic anion transporter, was purchased from Sigma-Aldrich. Furimazine, the substrate for NanoLuc Luciferase bioluminescence production, was purchased from Promega, named as Nano-Glo Substrate. Bovine serum albumin (BSA; Sigma-Aldrich, 4°C) was used in the dilution of proteins prior to cellular application. BSA limits non-specific binding of other reagents by competing for non-specific sites on plastic, while also binding and increasing solubility of chemicals, such as retinal and furimazine.

### 2.2.5 Imaging Buffers

Two different HEPES based imaging buffers were used in this thesis. One HEPES Buffered Saline Solution (HBS) was used exclusively in HEK cell experiments, which was autoclaved and stored long term in 10x concentrate at 4 ºC. The working solution contained 10mM HEPES, 145mM NaCl, 5mM KCl, 10mM D-glucose, 1.3mM $CaCl_2$, 1.0mM $MgSO_4$, 1.5mM sodium bicarbonate ($NaHCO_3$), and 2mM sodium pyruvate, and buffered using NaOH to pH 7.45. Glucose was added last to a fully diluted, autoclaved and pH buffered solution. The other HBS was used for primary astrocyte studies, of which the stock contained 10mM HEPES, 135mM NaCl, 3mM KCl, and 15mM D-glucose, and buffered using NaOH to pH 7.4. On the day of the experiment, 2mM $CaCl_2$ and 1mM $MgSO_4$ were added to the buffer, avoiding any bacterial growth over time in storage at 4ºC. Pyruvate was avoided due to the potential complications with the complex astrocytic metabolism (Bouzier-Sore and Pellerin, 2013).

## 2.3 Molecular Biology

### 2.3.1 Construction of SNAP tagged Optogenetic Receptors

Both the opto-$\alpha_{1A}$AR and Opn4 receptors were fused to an N terminal SNAPtag. Briefly, the desired receptor cDNA sequence was amplified from the DNA vectors provided (pcDNA3.1-opto-$\alpha_{1A}$AR-EYFP provided the opto-$\alpha_{1A}$ARAR, and the cDNA for Opn4 was provided as an IMAGE clone plasmid) using the polymerase chain reaction (PCR). This was performed using forward and reverse primers to remove the start methionine amino acid and add both a STOP codon and flanking restriction sites (BamH1 and XhoI). The PCR product produced was then purified and digested with the enzymes matching the inserted restriction sites (BamH1 and XhoI). This enabled the receptor sequence to be ligated into a similarly digested $p3.1_{NEO}$-SNAP vector. Following transformation, the colonies were screened for the ligated plasmid using miniprep cultures, before the amplification of plasmids in a maxiprep and double stranded sequencing (see *Figure 2.2* for complete plasmid maps).

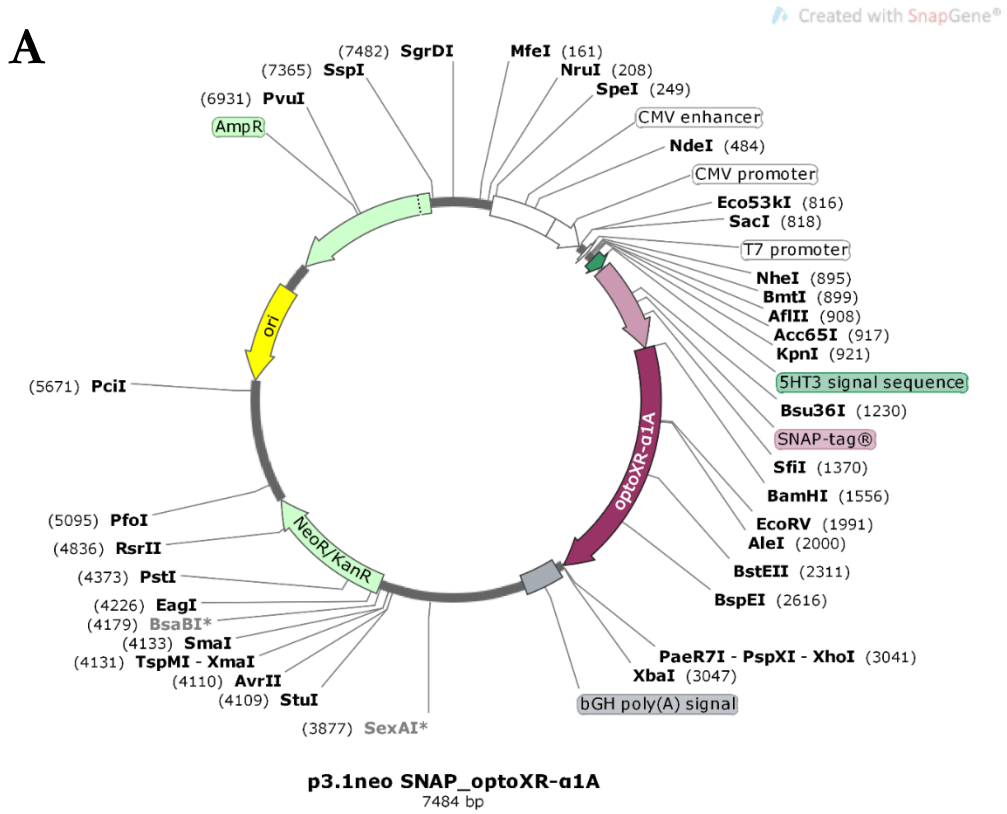


**p3.1neo SNAP_optoXR-α1A**
7484 bp

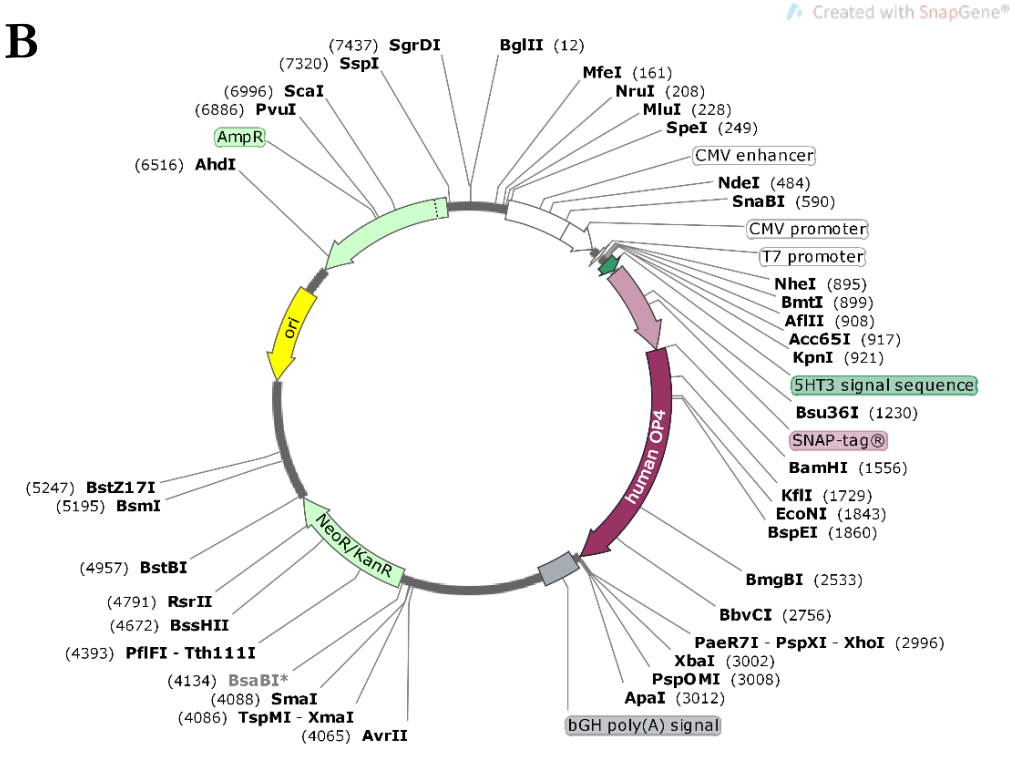


**p3.1neo SNAP_Opn4**
7439 bp

***Figure 2.2*** **– Vector maps of A) pcDNA3.1$_{NEO}$-SNAP-opto-$\alpha_{1A}$AR and B) pcDNA3.1$_{NEO}$-SNAP-Opn4 plasmids.** Mammalian expression of the receptor cDNA is controlled by a cytomegalovirus (CMV) enhancer and promotor region, flanked at the 3' end by bovine Growth Hormone (bGH) poly(A) site. A Kozak site followed by the 5HT3 receptor signal sequence and SNAP tag sequence is fused to the N terminus end of the receptor via a BamH1 site (linker Gly-Ser). Neomycin (mammalian) and ampicillin (bacterial) resistance genes are also coded in the cDNA, while sequencing primer sites are provided by T7 promoter and BGHrev sequencing.

### 2.3.2 NanoLuc Binary Technology cDNA Constructs

NanoLuc Binary Technology (NanoBiT) refers to the structural complementation bioluminescence reporter designed from the NanoLuc protein which comes in two subunits; the Small BiT (smBiT) and Large BiT (LgBiT). Bioluminescence is produced by furimazine addition when the two separate proteins of the divided NanoLuc are close enough structurally complement (Dixon *et al.*, 2016). The 11 amino acid smBiT comes in two forms; the low affinity NanoBit (smBiT114) and the high affinity HiBiT (smBiT86), referring to the affinity of the smBiT for the LgBiT 18kD protein. In this assay, the smBiT was attached to the intracellular C terminus of the optogenetic receptor and the LgBiT was attached to two different target sites; the plasma membrane Kras targeting sequence or the early endosome protein Rab5.

SNAP-receptor-smBiT plasmids were created using the SNAP-Opn4 and opto-$\alpha_{1A}$AR constructs. First, reverse primers for the opto-$\alpha_{1A}$AR and Opn4 receptors without STOP codons and with flanking BamH1 and XhoI restriction sites were amplified in the PCR to create insert DNA for the optogenetic receptors without a STOP codon. This DNA was then inserted into the pcDNA3.1$_{NEO}$-SNAP vector plasmid using restriction digestion of vector and insert with BamH1/XhoI, DNA purification steps, ligation, transformation and plasmid purification to create pcDNA3.1$_{NEO}$-SNAP-receptor$^{-}$* plasmids, where $^{-}$* denotes loss of the STOP codon. The SNAP-opto-$\alpha_{1A}$AR$^{-}$* and SNAP-Opn4$^{-}$* constructs from these plasmids were then used as insert DNA into pcDNA3.1$_{ZEO}$-smBiT114 and pcDNA3.1$_{ZEO}$-smBiT86 vectors (prepared previously by the Holliday group). These vectors contain a short 4 amino acid linker before the smBiT sequence, followed by a STOP codon between restriction sites XhoI and XbaI. The flanking restriction sites for the vector and insert digest were KpnI and XhoI, placing the smBiT on the C terminus of the receptors (see *Figure 2.3* for final plasmid map). Ligation, transformation and plasmid purification were then performed to create four different constructs; pcDNA3.1$_{ZEO}$-SNAP-Opn4-smBiT114, pcDNA3.1$_{ZEO}$-SNAP-Opn4-smBiT86, pcDNA3.1$_{ZEO}$-SNAP-opto-$\alpha_{1A}$AR-smBiT114 and pcDNA3.1$_{ZEO}$-SNAP-opto-$\alpha_{1A}$AR–smBiT86.

LgBiT constructs were created with the help of Nicola Dijon and James Farmer (University of Nottingham, UK). LgBiT sequences with a Kozak sequence, start codon and no STOP codon, between HindIII and EcoR1, were synthesised by GeneArt. Two alternative sequences were used for different sized Gly/Ser linkers between the LgBiT and 3' EcoR1 site (one with a short EF due to the EcoR1 site, see *Figure 2.5* for the longer linker). The LgBiT sequence was then used to replace GFP (between HindIII and EcoR1) in pcDNA3.1$_{ZEO}$-GFP-Kras. This vector contains the prenylation sequence for Kras between EcoR1 and XbaI (a polybasic KKKK motif followed by prenylation motif CVIM). The human Rab5a sequence (Genbank NM_004162) was also synthesised by GeneArt, this time with flanking EcoR1 and XbaI sites, a STOP codon and no start codon. This was cloned into the EcoR1 and XbaI sites of the LgBiT vectors to generate fused Rab5 constructs. Altogether, the LgBiT constructs cloned were pcDNA3.1$_{ZEO}$-LgBiT-Kras, pcDNA3.1$_{ZEO}$-LgBiT-Rab5, pcDNA3.1$_{ZEO}$-LgBiT-LL-Kras and pcDNA3.1$_{ZEO}$-LgBiT-LL-Rab5 constructs (see *Figure 2.4* and *Figure 2.5*).

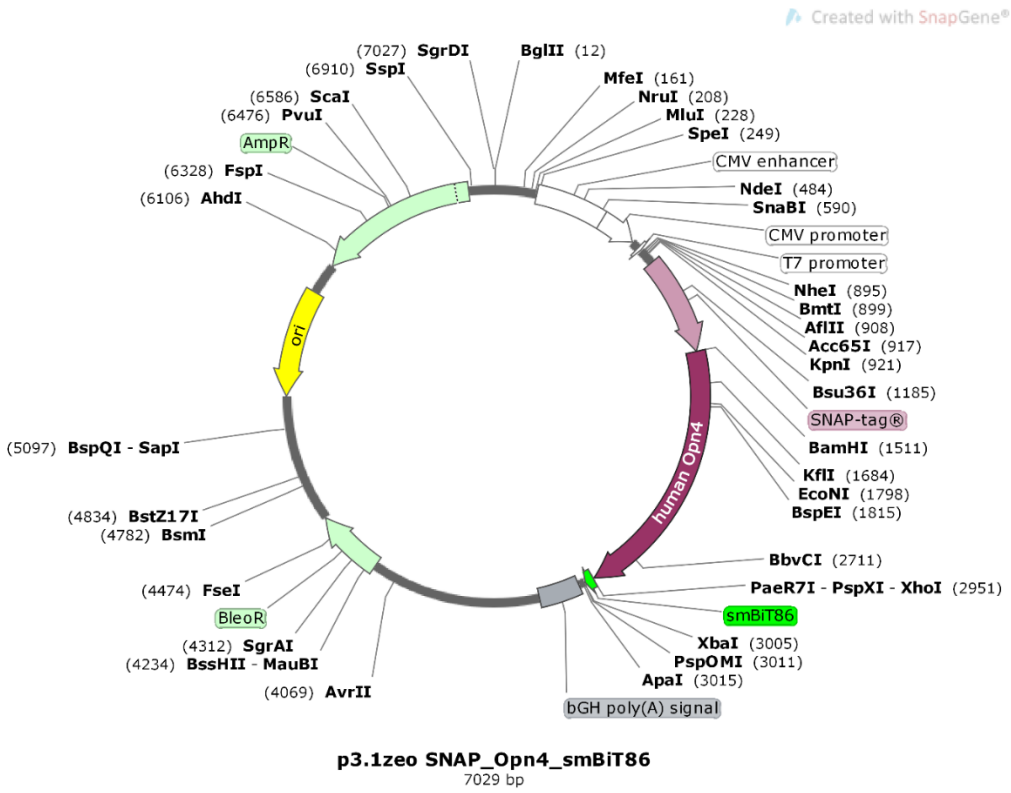


**Gly/Ser Linker – post XhoI, pre smBiT**

ggg agt tct ggc

G S S G

**smBiT 86 sequence**

gtg agc ggc tgg cgg ctg ttc aag aag att agc

V S G **W** R L F **K** **K** I **S**

**smBiT 114 sequence**

gtg agc ggc tac cgg ttg ttc gag gag att ctc

V S G **Y** R L F **E** **E** I **L**

***Figure 2.3*** **– Vector map of pcDNA3.1$_{ZEO}$-SNAP-Opn4-smBiT86, representative of all SNAP-receptor-smBiT constructs.** Following the CMV promotor is the SNAP tag protein, attached to the N terminus of the optogenetic Opn4 receptor. The smBiT 11 amino acid sequence is then bound to the C terminus of the receptor, after a 4 amino acid linker of Gly/Ser following the XhoI site. Below, the difference between the high affinity smBiT86 and low affinity smBiT114 sequence.

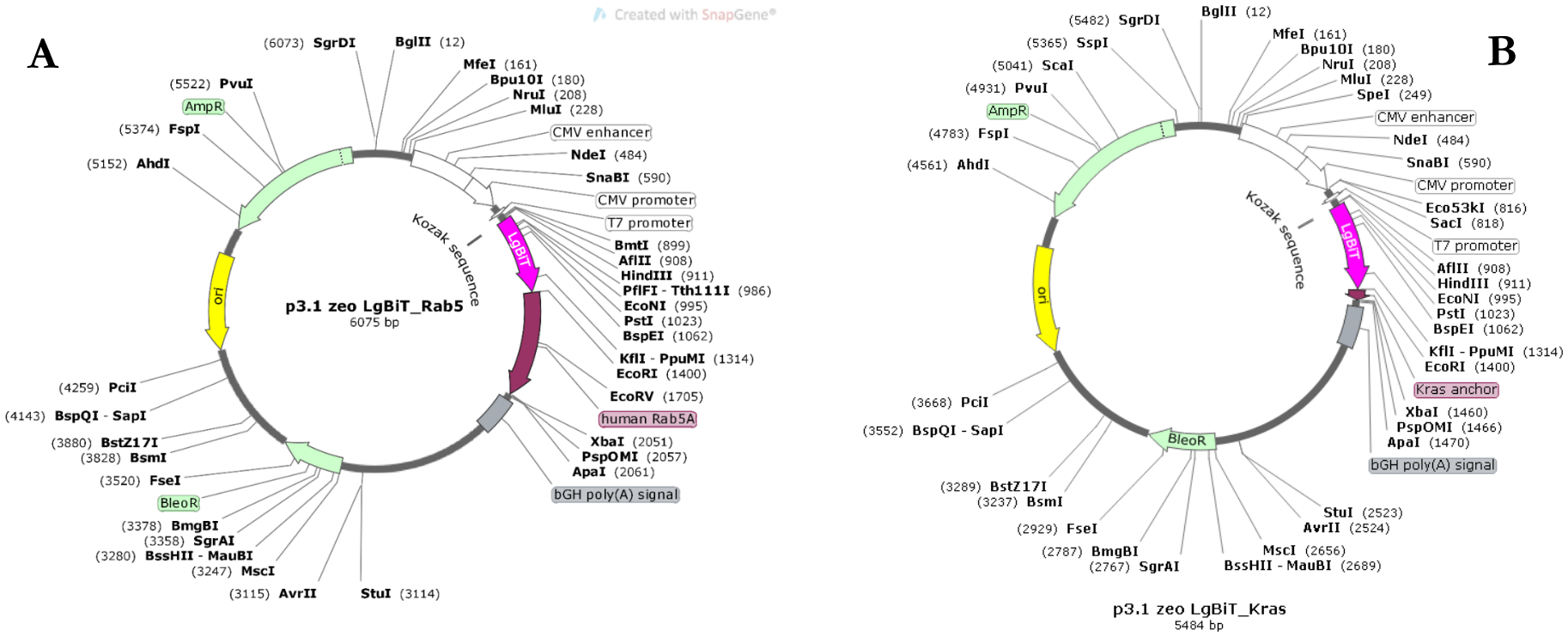


***Figure 2.4* – Plasmid maps for the two pcDNA3.1$_{ZEO}$-LgBiT-protein constructs.** A) LgBiT-Rab5 and B) LgBiT-Kras. Both use a CMV promotor with the LgBiT attached to the N terminus of the target protein and BleoR provides zeocin resistance. The Kozak sequence (GCCACCATG) is present to enhance translation in mammalian cells (Kozak, 1987)

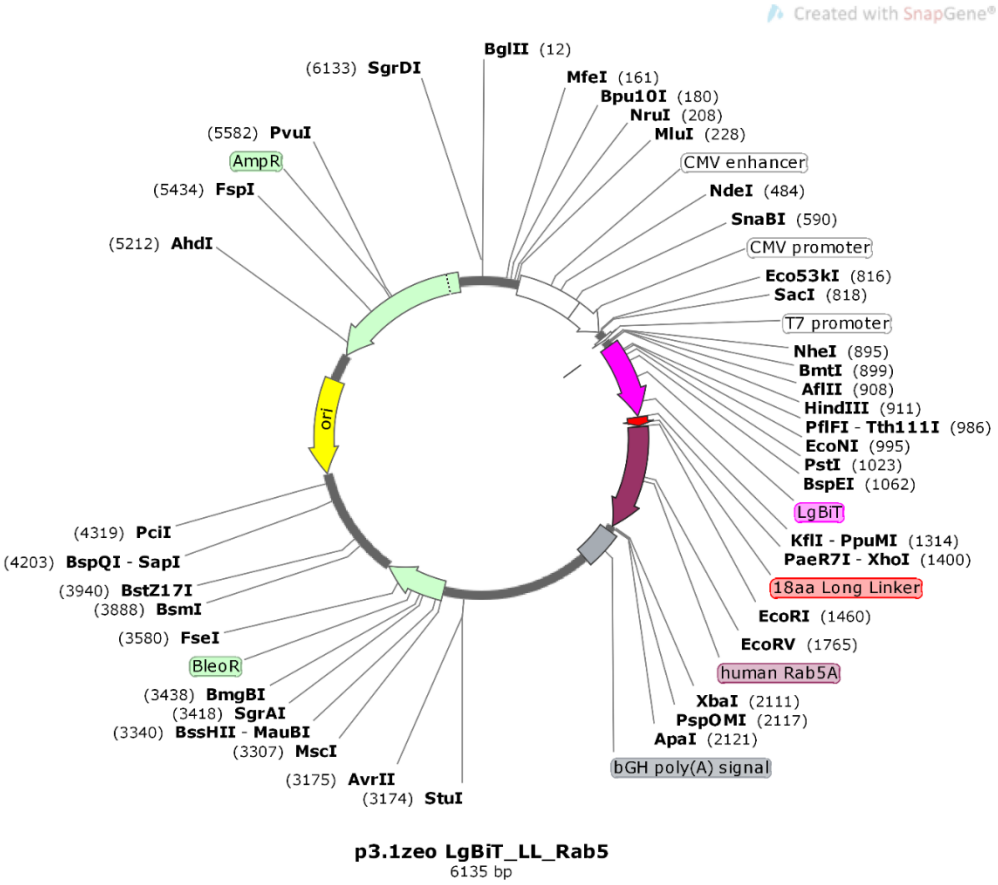


## Gly/Ser 18aa Long Linker Sequence

agc ggc gga tct ggt gga aca ggt gga agt ggc gga agc gga gga aca ggc gga

S G G S G G T G G S G G S G G T G G

***Figure 2.5* – Plasmid map of the pcDNA3.1$_{ZEO}$-LgBiT-LL-Rab5.** An 18 amino acid long linker (*red*) has been inserted between the LgBiT sequence and target protein (see below map for sequence). This also represents the plasmid using a long linker between the LgBiT and Kras anchor protein target.

### 2.3.3 Polymerase Chain Reaction (PCR)

Through the PCR technique, the sequence of DNA for the receptor was amplified from the vectors. Using the appropriate 5' and 3' primer, this allows the position of the start and stop codons to be altered, and the correct flanking restriction enzyme sites to be added for cloning into a vector of choice.

Forward and reverse primers were designed to complement the beginning and end of the receptor DNA sequence within the plasmid (see *Table 2.1*). Also incorporated into the design were the flanking restriction sites, added to the beginning and end of the receptor sequence. A STOP codon was also required at the end of the receptor coding DNA for receptors without further C terminal modification, and the start methionine from the original vector was removed to enable N terminal fusion of the SNAP tag. Mutation cleavage sites were chosen by targeting groups of serine and threonine residues which make up phosphorylation sites for protein kinases (see *Figure 2.6*).

PCRs were carried out using the Mastercycler Gradient (Eppendorf, Stevenage, UK) PCR machine. The PCR protocol involved cycles of; denaturation of the double stranded DNA template; annealing, where primers bound to DNA; and extension, which amplified the DNA template between the primers. For all receptors, Pwo DNA polymerase (2.5U; Roche Life Science, Penzberg, Germany), a proof reading polymerase with exonuclease activity to reduce the error:fidelity ratio, with respective 10x buffer containing a final concentration of 1.5mM magnesium sulphate (5µl), was used in a final reaction volume of 50µl. The PCR reaction also contained the forward and reverse primers (600nM each), DNA template (50ng) and deoxyribose nucleoside triphosphates (200µM). An initial "Hot Start" step (to limit non-specific amplification) consisted of denaturation at 95°C for 2min, annealing the primers at 58°C before addition of the Pwo enzyme, then heating to 72°C for 1.5min (appropriate for 1.2kbp product). For the first ten cycles, denaturation was carried out at 95°C for 30s, annealing at 58°C for 1min, and extension at 72°C for 1.5min. The last fifteen cycles were performed at the same temperatures and timings, only with a 5s per cycle increase to the extension time, applied to allow for decreased polymerase activity during the PCR. Finally, the reaction was subjected to 72°C for 7min to complete extension of remaining

DNA. The PCR products were then resolved by agarose gel electrophoresis and purified using the Gel Purification kit.

| Receptor | Primer Direction | Sequence |
|---|---|---|
| Opto-$\alpha_{1A}$AR | Forward | 5'- TAAGTA **GGATCC** AATGGGACCGAGGGTCCAAAT |
| | Reverse, STOP Insert | 5'- CCATCT **CTCGAG** CTA AACTTCCTCGCCGTTTTCGC |
| | Reverse, no STOP codon | 5'- CCATCT **CTCGAG** AACTTCCTCGCCGTTTTCGC |
| Opto-$\alpha_{1A}$AR-T471* | Reverse, STOP insert | 5'- TGTGAG **CTCGAG** CTA GGGAACCTGATGGTTCTTATCG |
| Opto-$\alpha_{1A}$AR-S421* | Reverse, STOP insert | 5'- CCATCC **CTCGAG** CTA GAAAAACTTCCACTCGCAGACTCC |
| Opto-$\alpha_{1A}$AR-S371* | Reverse, STOP insert | 5'- TTCGAG **CTCGAG** CTA CTGCTTCCGACAGAGGCATTGG |
| Opn4 | Forward | 5'- TATGTA **GGATCC** AACCCTCCTTCGGGGCCAAGAGTC |
| | Reverse, STOP Insert | 5'-TTAATT **CTCGAG** CTA CATCCTGGGGTCCTGGCTGGGGAT |
| | Reverse, sans STOP codon | 5'-TTAATT **CTCGAG** CATCCTGGGGTCCTGGCTGGGGAT |
| Opn4-T463* | Reverse, STOP Insert | 5'-TTATTG **CTCGAG** CTA TGCTTCGTGTCCCTGGGGTCTGGG |
| Opn4-S411* | Reverse, STOP Insert | 5'-TTCTAA **CTCGAG** CTA CTGGCGCCTCCGTATGGAGATCC |
| Opn4-S375* | Reverse, STOP Insert | 5'-AAT CAA **CTCGAG** CTA ACCCAGCAGCACCCCCAGGCAGGG |

***Table 2.1* – Primers designed and used for PCR to generate optogenetic receptor constructs.** The receptor cDNA templates were provided in their original vector for use in PCR. TAG STOP codon (reversed and complimented as CTA) is underlined, whereas the restriction enzyme sequences are in bold, GGATCC for BamH1, CTCGAG for XhoI.

**A) Opto-$\alpha_{1A}$AR**

N[341]PVIYIMMNKQFRKAFQNVLRIQCLCRKQS[3]
[71]SKHALGYTLHPPSQAVEGQHKDMVRIPVGS
RETFYRISKTDGVCEWKFFS[421]SMPRGSARIT
VSKDQSSCTTARVRSKSFLQVCCCVGPSTPS
LDKNHQVPT[471]IKVHTISLSENGEEVETSQVAP
A

**B) Melanopsin**

N[346]PIIYAITHPKYRVAIAQHLPCLGVLLGVS[375]
RRHSRPYPSYRSTHRSTLTSHTSNLSWISIRR
RQES[411]LGSESEVGWTHMEAAAVWGAAQQA
NGRSLYGQGLEDLEAKAPPRPQGHEAET[463]P
GKTKGLIPSQDPRM

***Figure 2.6* – The end of transmembrane helix 7, helix 8 and C-terminal residues of opto-$\alpha_{1A}$AR and melanopsin.** The conserved NPxxY domain (red) is crucial for conformational changes between inactivation and activation, and the Cys residues (green) are palmitoylation sites which promote the juxtamembrane formation of helix 8 by fatty acid modification and plasma membrane association. This region was preserved in all mutant receptors. Ser and Thr residues after these regions (yellow) show potential sites of receptor kinase phosphorylation, including both GRKs and PKC (red letters, 3aa consensus site S/T, x, R/K). For opto-$\alpha_{1A}$AR, Ser[375], Ser[411] and Thr[463] were the sites used for the truncation mutants (A, removing 4, 3 and 1 PKC consensus sites respectively), replaced with a STOP codon, which was reflected in melanopsin at Ser[375], Ser[411] and Thr[463] (B, removing 3, 0 and 0 PKC consensus sites respectively).

### 2.3.4 Restriction Digestion and Alkaline Phosphate Treatment

PCR products or selected DNA were next inserted within a vector. When cloning and developing the plasmid, two different restriction enzyme sites were used for the beginning and end of the sequence. This has a significant advantage to single digests as the inserted sequence can only be ligated into the vector in one, correct orientation. It was important when digesting the plasmids that the enzymes did not cut within the receptor sequence, but also match sites within the vector for correct placement in frame. For example, BamH1 was chosen for the start, and XhoI for the end of the DNA sequence for insertion into the $p3.1_{NEO}$-SNAP vector. Once digested, the PCR products were classed as 'insert' DNA. The vector was also digested with the same enzymes to allow combining with the receptor DNA in later stages of plasmid creation.

Restriction digests were performed in a reaction volume of 20μL. The solution included 2μg DNA vector plasmid, or 16μL PCR product, in $ddH_2O$ and 2μL 10x Fast Digest Green buffer, with 1μL of each FastDigest restriction enzyme. Incubation lasted 1hr at 37°C, before heat inactivating the enzymes, followed by 5min at 80°C, and 20min at 65°C.

Vector digests were then treated with shrimp alkaline phosphate to prevent self-ligation of the DNA by removing the terminal 5'-phosphates. This was done by adding 2μL 10x FastAP Buffer and 2μL FastAP to the finished digest. The solution was incubated for 30min at 37°C, followed by heat activation of the phosphatase for 10min at 75°C.

### 2.3.5 Agarose Gel Electrophoresis

In an electric field, negatively charged DNA migrates towards an anode. When run across an agarose gel, the migration is restricted by the size of the pores in the agarose, dependent on the percentage of agarose in the gel. Smaller fragments are therefore transported faster, and move further, and the DNA is separated according to molecular weight. Intercalating the DNA, in this case with ethidium bromide, makes the DNA bands visible through ultraviolet light.

The gel was made up of agarose (1% w/v) in Tris-Borate-EDTA buffer (TBE, 89mM Tris HCl, 89mM Boric acid, 2mM EDTA, pH 7.6). This solution was microwaved to dissolve the agrose and then cooled before adding 0.1μg.mL$^{-1}$ ethidium bromide. After setting in a tray, with a comb in place to form wells, the gel was moved to an electrophoresis chamber and covered in TBE buffer. Each digested DNA was loaded into a separate well, with a DNA ladder (1kB, associated with 6x Gel Loading Dye; both New England BioLabs) as a molecular mass marker in the final well. Gels were run at 80V, monitoring progress visually using dyes contained within the ladder and loading buffers (e.g. bromophenol blue, running at the position of a 500bp fragment). DNA bands were visualised under UV irradiation using the GeneFlash gel documentation system (Syngene Bioimaging, Cambridge, UK) and a PULNiX TM-300 CCD camera.

### 2.3.6 Gel and Digest Purification

Following digestion and alkaline phosphatase treatment (vector) or gel electrophoresis (insert), the DNA was purified by a PCR Cleanup Kit or Gel Purification Kit. Both kits used silica gel based column purification to purify the DNA from solution, performed as per the manufacturer's instructions (Sigma-Aldrich).

For gel purification, a 100mg section of DNA gel was added to 300μL Gel Solubilisation Solution, and heated at 57°C until the gel was completely dissolved. Before loading into the column, 100μL isopropanol was added to the dissolved gel. When using DNA straight from digestion, such as the vector DNA, the solution was made up to 100μL with dd$H_2O$. Binding Solution was added at 5x the volume (500μL). Both kits contain a chaotropic salt in the preparation solution to promote DNA binding to silica in the subsequent steps.

The column provided in each kit was put into a collection tube with 500μL Column Preparation Solution. This was centrifuged at 14,000rpm for 1min and the flow through was discarded. The dissolved gel or the vector DNA solution were then added to the column and centrifuged at 14,000rpm for 1min. The elute was castoff before addition of 500μL Wash Solution with ethanol. Tubes were then span at 14,000rpm for 30s, elute discarded, and then centrifuged at 14,000rpm for 2min to eradicate any leftover ethanol in the column. To elute the DNA, the column was

moved to a fresh collection tube and 50µL $ddH_2O$ (gel purification, giving 10-20ng.µL$^{-1}$ DNA product for a typical PCR product) or 40µL $ddH_2O$ (PCR purification, approximately 40ng.µL$^{-1}$ for a standard vector digestion) was added. This was incubated for 1min at room temperature, and then centrifuged at 14,000rpm for 1min.

### 2.3.7 Ligation of Vector and Insert DNA

Vector and insert DNA were ligated using T4 DNA ligase to join the fragments into a full plasmid. Digestion by the restriction enzymes left the ends of the fragments with overhanging 'sticky' sequences. These sequences complemented each other on the vector and insert.

Two ligation reactions were set up for each plasmid, one with the insert DNA (positive), and one without (negative). Both required 50ng of digested and purified vector DNA. In the positive reaction, insert was added in a 3:1 ratio with the vector. The volume of DNA product to be added was calculated with an assumed 80% yield from the previous processing and an initial DNA quantity of 2µg for the vector (*Equation 1*). For PCR products an approximate yield was estimated from the intensity of the stained band on the agarose gel.

$$2{,}000 \times \left(\frac{vector\ or\ insert\ size}{total\ size}\right) \times 0.8 = \boldsymbol{a}\ ng.\mu l^{-1} \qquad \textit{Equation 1}$$

Both reactions then had 1µL 10x T4 DNA Ligase Buffer and 1µL T4 DNA Ligase added, before being made up to a final volume of 10µL with $ddH_2O$. The reactions were incubated either at 16°C for 16hr, or 21°C for 2hr.

### 2.3.8 Transformation of Plasmids into Competent Cells

Plasmids were transformed into competent *Escherichia coli* bacterial cells to increase yield through bacterial replication. The competent cells used were either XL-1-Blue, a strain of *Escherichia coli* which contains several mutations to restrict bacterial growth only to culture media, and the *hsd*R17 mutation to prevent restriction digestion of the plasmid DNA and improve the quality of the preparation, or One

Shot™ TOP10F' cells, where the F'-episome carries a tetracycline resistance. The choice of bacterial cells was made based on lab availability at the time of the experiment. XL-1-Blue chemically competent cells were produced by Marleen Groenen (University of Nottingham, UK).

Before transformation of the ligated plasmids, competent cells were defrosted on ice. Each ligation reaction required 100µL (XL-1) or 25µL (TOP10F') competent cells. To increase the efficiency of transformation for the XL-1-Blue, 1.5µL β-mercaptoethanol (1.4M in dd$H_2O$, Sigma-Aldrich) was added to the competent cells and left to incubate for 10min on ice. After activation, 4µL (XL-1) or 2.5µL (TOP10F') of the relevant ligation was combined in the tube and incubated on ice for 30min. The bacteria then underwent heat shock at 42°C for 45s, a process which changed the fluidity of the bacterial membrane and allowed the DNA to enter. The cells were immediately returned to the ice for a further 2min, before addition of 400µL LB Broth, using sterile technique. Incubation at 37°C on a shaking plate (250rpm) for 1hr was then used to stimulate antibiotic resistance expression in the bacteria with the pcDNA3.1 plasmids (ampicillin). Agar plates were prepared prior to transformation with the relevant antibiotic (autoclaved LB Agar, to which 75µg.mL$^{-1}$ ampicillin was added on cooling to <55°C) and left to dry at 37 °C to remove excess moisture. Under sterile conditions, 50µL of each reaction was streaked over the agar plates. The plates were incubated at 37°C overnight. Successful ligation and transformation was deemed to have occurred when less bacterial colonies were present on the negative reaction than the positive plates.

### 2.3.9 Purification of Plasmid DNA

#### *2.3.9.1 Miniprep*

To purify a smaller amount of DNA for insert and sequence testing, minipreps were prepared from bacterial colonies by the Miniprep Kit (Sigma-Aldrich). Single bacterial colonies were picked from the agar plates the day before cDNA extraction. The colony was then expelled into 5mL LB Broth (75µg.mL$^{-1}$ ampicillin). Colonies were left incubating on a shaking plate (250rpm) at 37°C overnight.

The next day, 3mL of broth was centrifuged at 4,000rpm for 5min, and supernatant discarded. The alkaline lysis method was then used to extract plasmid DNA. Cells were resuspended in 200µL Resuspension Solution containing hypo-osmotic

sucrose to make the bacterial cells swell and burst, with RNAase to degrade any RNA present. To break up the cells, 200µL Lysis solution containing NaOH and sodium dodecyl sulphate was mixed in for up to 5min. This process causes lysis of the cell wall and denaturation of proteins and genomic DNA. Plasmid DNA was not irreversibly denatured because it is small compared to the bacterial chromosome. Meanwhile, 500µL Column Preparation Solution was added to a silica column and spun at 14,000rpm for 1min, with the elute discarded. After lysis of the cells, 350µL Neutralisation Solution was added and centrifuged at 14,000rpm for 10min. Neutralisation Solution (containing potassium acetate) causes the denatures genomic DNA, proteins and cell wall components to precipitate out, leaving plasmid DNA in the supernatant. The solution also contains the crucial chaotropic salt required for binding of the plasmid DNA to silica columns. The lysate from the cells was then added to the prepared column and spun at 14,000rpm for 1min. To wash the DNA in the column, 500µL Wash solution with ethanol was added to the column and centrifuged at 14,000rpm for 30min, elute discarded, and span for a further 2min. The column was then transferred to a new collection tube, and 100µL dd$H_2O$ used to elute the miniprep DNA via centrifugation at 14,000 for 1min.

Miniprep DNA was used to test colonies for insert DNA via electrophoresis. The miniprep DNA was first digested with the same restriction enzymes noted previously, before being run on an agarose gel to check for digested insert DNA. The miniprep DNA was then sequenced by University of Nottingham sequencing facility using the T7 and BGHrev primers to verify the construction of the full length receptor fusion protein cDNA and make sure no spontaneous mutations have arisen during the PCR or subsequent cloning.

#### *2.3.9.2 Maxiprep*

For further use of the DNA, such as transfecting into various cell types, transformed bacterial preparations were grown from screened minipreps in a larger volume and purified. The day before maxiprep processing of the cells, 100µL of miniprep culture was added to 5mL LB Broth and incubated at 37°C on a shaking plate (250rpm) for ~2hr to stimulate bacterial growth. The bacteria were then added to 120mL autoclaved LB Broth with appropriate antibiotic and grown overnight on a shaking plate (250rpm).

The bacterial growth was centrifuged at 4,000rpm for 15min, and supernatant discarded. Pellets were then resuspended in 10mL Buffer P1 solution (4°C) from the Qiagen Maxiprep Kit. Alkaline lysis of the cells was performed using 10mL Buffer P2, incubating at room temperature for up to 5min. To neutralise the preparation, 10mL Buffer P3 (4°C) was added and poured into the supplied QIA cartridge, and left to incubate at room temperature for 10min. During cell incubation, the Qiagen Tip was equilibrated with 10mL Buffer QBT and allowed to empty via gravity flow. The cell lysate was then transferred into the Qiagen tip and allowed to empty. Two washes with 30mL Buffer QC were then used to clean the DNA within the filter. The DNA was eluted from the column using 15mL Buffer QF, and then precipitated with 10.5mL isopropanalol (Sigma-Aldrich), before centrifugation at 4,000rpm for 1hr. Pellets from the spin were resuspended in 300μL Tris-EDTA buffer (10mM Tris-HCl, 1mM disodium EDTA, pH 8.0), before ethanol precipitation of the DNA. Ethanol precipitation was performed by adding 1/10 volume 3M NaOAC (pH5.2, 30μL) and 2 volumes 100% ethanol (660μL) to the DNA, which was centrifuged at 14,000rpm for 10min. To wash the DNA pellet, 200μL 70% ethanol in $ddH_2O$ was added and span at 14,000rpm for 5min. Supernatant was discarded and the pellet was allowed to dry, before resuspension in an appropriate volume of Tris-EDTA, dependant on pellet size. The purity and concentration of DNA was measured using a UV spectrophotometer (Eppendorf Biophotometer; Eppendorf UK). This was calculated using an algorithm for double stranded DNA where the concentration of DNA, was based on $50\mu g.mL^{-1}$ DNA preparation having an absorbance of 1 unit at a wavelength (A260) of 260 nm. The A260/A280 ratio was then calculated to determine DNA purity (optimal 1.8 ratio), with ratios >1.9 indicating RNA contamination and <1.7 protein contamination. Receptor constructs from the maxiprep plasmids were fully sequenced using the T7 and BGHrev primers, as with the minipreps, prior to use in cell transfection. This ensured there were no mutations of the receptor, and that the receptor was correctly cloned in frame with the SNAP tag to generate the appropriate fusion protein. All maxipreped cDNA plasmids produced for this thesis are listed in *Table 2.2*.

| Chimeric opto-$\alpha_{1A}$AR | Melanopsin – Opn4 | SmBiT Constructs | LgBiT Constructs |
|---|---|---|---|
| pcDNA3.1$_{NEO}$-SNAP-opto-$\alpha_{1A}$AR | pcDNA3.1$_{NEO}$-SNAP-Opn4 | pcDNA3.1$_{ZEO}$-SNAP-opto-$\alpha_{1A}$AR-smBiT114 | pcDNA3.1$_{ZEO}$-LgBiT-Rab5 |
| pcDNA3.1$_{NEO}$-SNAP-opto-$\alpha_{1A}$AR-T471* | pcDNA3.1$_{NEO}$-SNAP-Opn4-S411* | pcDNA3.1$_{ZEO}$-SNAP-opto-$\alpha_{1A}$AR-smBiT86 | pcDNA3.1$_{ZEO}$-LgBiT-Kras |
| pcDNA3.1$_{NEO}$-SNAP-opto-$\alpha_{1A}$AR-S421* | pcDNA3.1$_{NEO}$-SNAP-Opn4-S375* | pcDNA3.1$_{ZEO}$-SNAP-Opn4-smBiT114 | pcDNA3.1$_{ZEO}$-LgBiT-LL-Kras |
| pcDNA3.1$_{NEO}$-SNAP-opto-$\alpha_{1A}$AR-S371* | | pcDNA3.1$_{ZEO}$-SNAP-Opn4-smBiT86 | pcDNA3.1$_{ZEO}$-LgBiT-LL-Rab5 |

***Table 2.2*** **– Outline of created cDNA constructs for experiments for both optogenetic receptors and the NanoBiT SmBiT-LgBiT constructs.**

## 2.4 Cell Culture

All primary and cultured cell lines were maintained in a sterile environment within a fume hood, using sterile techniques to eliminate exposure to contaminants. Cultured cells were incubated at 37°C in 5% $CO_2$ environment. HEK 293T cells were used for transfections, a cell line expressing the SV40 large T antigen to increase recombinant protein production (DuBridge *et al.*, 1987). Primary astrocytes were collected from Wistar rats.

### 2.4.1 Astrocyte Collection

Primary astrocyte cells were taken from postnatal (P4 days post birth) or embryonic (E18 days) rat cortices. Dissection of the animals was carried out in a flow hood under sterile conditions, after undergoing cervical dislocation and decapitation. Skin was removed from the cranium, before cutting of the skull to reveal the cortex. This was then collected in dissection buffer (DMEM high glucose, 10% FBS), kept ice cold. In a sterile hood, the dissection media was drawn off and replaced with papain (20U/mL) in glial media (DMEM high glucose, 10% FBS, 50ng/mL L-proline, 1.5mL pen-strep antibiotic), a cysteine protease to help break down the connective tissues. The tissue was triturated several times with a 1mL blue pipette tip, before incubation for 40min at 37°C with 5% $CO_2$. After incubation, 0.5mL DNAse solution was added to degrade the excess DNA, before centrifugation at 2,000rpm for 6min. Supernatant was removed and replaced with 2mL glial media with 0.5mL DNAse to resuspend the pellet. This was spun at a lower 700rpm for 3min. The supernatant was kept, and replaced with 10mL media before 20x trituration with a 1mL pipette. Centrifugation was carried out again at 700rpm for 3min, with the supernatant retained. This step was repeated, yielding 25mL of supernatant altogether. All supernatant was centrifuged at 2,000rpm for 6min, before removal of the new supernatant. To resuspend the pellet, 10mL media was used, before filtering through a cell strainer. The cells could then be transferred into a culture T75 flask, or directly onto coverslips, before their use after 7 days incubation.

### 2.4.2 Passaging

Routine culture of HEK293 cells required media containing DMEM high glucose with 10% FCS. Primary astrocytes were cultured in glial media (DMEM high glucose, 10% FBS, 50ng/mL L-proline, 1.5mL pen-strep antibiotic). From their culture flasks, cells could be passaged into new flasks when too confluent, or to encourage growth, or grown on plates or coverslips for imaging. Old media was aspirated and 1mL of PBS was used to wash the cells, before dissociation from the flask with 1mL trypsin/EDTA. To collect the cells from the flask, 10mL of relevant media was added and the solution was centrifuged for 3-5min at 1,000rpm. Supernatant was then removed, before resuspension of the pellet in 5 or 10mL relevant media. The cells could then be added to a new flask to continue growth, or cultured onto an imaging plate or coverslip. Poly-D-lysine P6407 (HEKs, $10\mu g.mL^{-1}$; Mr=70-150kD, Sigma-Aldrich) or poly-L-lysine (astrocytes, $10\mu g.mL^{-1}$) was applied to plates or coverslips for 30min, and washed with media, prior to cell seeding.

### 2.4.3 Freezing and Defrosting

HEK cell lines could be frozen in liquid nitrogen for long term storage and reuse. To freeze cells, the flasks were split (as above) and the cells resuspended in freezing media (FCS with 10% DMSO). These were quickly transferred into cryovials (1mL/vial) and put into a Mr Frosty freezing container (Thermo Scientific) containing isopropanol. In this container, the cells were frozen slowly in a -80°C environment, minimising cell damage. After 24hr, the vials could then be safely transferred to liquid nitrogen for long time storage.

Defrosting of cells was carried out at room temperature. Cells in freezing media were added 10min relevant media, then centrifuged at 1,000rpm for 4min. The cells were then be resuspended in fresh media and added to culture flasks. The media in these flasks were replaced after 24hr to encourage growth.

### 2.4.4 Transfection of Cells

#### *2.4.4.1 Generation of Stable Transfected HEK 293T Cell Lines*

Lipofectamine (Thermo Fisher Scientific) was used as the transfection reagent in Opti-MEM Reduced Serum Media (Thermo Fisher Scientific) to generate stable HEK293 cell lines. To transfect, 2µg plasmid DNA was added to 200µl Opti-MEM and 18µl lipofectamine was added to another 200µl Opti-MEM. The mixtures were combined, before incubation for 30min at room temperature. Meanwhile, the media in the cultured cell flasks (25cm$^2$, 70-80% confluency) was replaced with 1.2mL Opti-MEM and incubated at 37°C for the same timeframe. After incubation, 800µl Opti-MEM was added to the DNA-lipofectamine mix, with all 1.2mL then added to the incubated flask. The solution was left overnight. After 24hr, the Opti-MEM was aspirated and replaced with fresh relevant media and high concentration of the relevant antibiotic (G418, 0.8mg.mL$^{-1}$; Zeocin, 0.25mg.mL$^{-1}$), for which the transfected plasmid provided resistance (pcDNA3.1$_{NEO}$=G418, pcDNA3.1$_{ZEO}$=zeocin). The selection period lasted 7-14 days, to generate resistant colonies which were then expanded as mixed population stable transfected cell lines. These cells were cultured in a reduced antibiotic concentration (0.2mg.mL$^{-1}$ G418, or 50µg.mL$^{-1}$ zeocin) to maintain the selection pressure.

#### *2.4.4.2 Transient Transfection of HEK293 Cells*

HEK-SNAP-optogenetic receptor-smBiT cell lines were transiently co-transfected with LgBiT-marker cDNA for NanoBiT bioluminescence experiments. Lipofectamine 3000 was used in transients to increase transfection efficiency as this reagent has been shown to have a lower toxicity and result in increased DNA expression in recombinant cells. Optimisation of transient transfections (e.g. DNA:Lipofectamine 3000 ratio) led to development of the protocol outlined here. HEK-SNAP-optogenetic receptor-smBiT cell lines were seeded onto 6 well plates the day before tranfection in 2mL of HEK media/well, with an aim of 70-90% confluency at the point of transfection. On the day of transfection, the media was aspirated, and the cells washed with PBS before replacement with 1mL of Opti-MEM 30min prior to transfection. For each well on the 6 well plate, 3.75µL of Lipofectamine 3000 reagent was diluted in 125µL Opti-MEM. DNA for the relevant LgBiT marker protein was prepared using 2.5µg in 125µL Opti-MEM and 5µL P3000 reagent, another part of the Lipofectamine 3000 nanolipid complex to

increase transfection efficiency. The diluted Lipofectamine 3000 and DNA were then combined at a 1:1 ratio and incubated for 10-15min at room temperature, before being added to the relevant well. Cells were then plated 24hr post transfection onto poly-D-lysine coated black 96 well Greiner 655090 plates in normal HEK media, or 35mm glass bottomed Petri dishes. Transfected cells were then used 24hr to 48hr for cell imaging and luminescence studies.

#### *2.4.4.3 Transient Transfection of Primary Astrocytes by Cationic Lipid Transfection or Electroporation*

Lipofectamine mediated transfection of astrocytes (in 96 well black walled plates) was tested with a variety of conditions to assess optimal ratios of Lipofectamine to DNA, also comparing the use of full astrocyte media and Opti-MEM. Otherwise, the protocol followed the same directions as for the HEK cells in section 2.4.4.2. Primary astrocytes transfected by this route were analysed up to 72hr post transfection.

Electroporation was used for primary cortical astrocyte transfection to improve its efficiency in some experiments, in comparison to the Lipofectamine method. In this method, a brief electrical field applied across the cell is suggested to cause formation of hydrophilic pores in the plasma membrane, allowing cDNA to pass through into the cytosol ready for cellular uptake, although this is still debated (Mellott *et al.*, 2013). Primary astrocytes were used 14-21 days post collection when fully confluent. Cells were then split as defined above but with a cell count before centrifugation. 2-3million cells diluted in 10mL media were then added to a tube for centrifugation at 1,500rpm for 10min. The supernatant was completely removed with a pipette and the pellet was resuspended in 100µL room temperature Basic Nucleofector Solution for Mammalian Glial Cells (Lonza). This was then combined with 3.5µg of relevant cDNA, before transfer of the entire solution to an electroporation cuvette. The cuvette was inserted into the Nucleofector I device and the T-20 program (optimised from similarly labelled programs) applied to the cells. Astrocytes were then immediately added to 500µL astrocyte media, before being plated onto poly-L-lysine coated 22mm coverslips in 6 well format containing 1.5mL astrocyte media. Transfected primary astrocytes were used 24-48hr post electroporation.

## 2.5 Calcium Mobilisation Assays

Calcium intracellular transients were measured using fluorescent calcium dye indicators (see *Table 2.3* for summary). Several different calcium sensors were used across the different experiments, depending on the required fluorescence wavelength and affinity for calcium (determined using the dissociation constant, $K_d$, where a smaller $K_d$ represents a greater binding affinity). All dyes used were bulk loaded, and so contained an acetoxymethyl (AM) ester group to make the compound cell permeable. AM esters modify the negative carboxylate of the indicator, making it uncharged and hydrophobic for permeability. Intracellular esterases, which can be found in almost every cell type, hydrolyse the AM group upon entry to the cell, causing intracellular accumulation of the indicator (Lavis *et al.*, 2011). Combined fluorescence excitation and optogenetic stimulation was avoided by using red-shifted calcium indicators with excitation wavelengths outside of rhodopsin and melanopsin activation wavelengths (see *Figure 2.7*).

### 2.5.1 Calcium Response in Primary Astrocyte Cultures to Ligand Addition

Wildtype cultured astrocytes were seeded onto 22mm round glass coverslips coated with poly-L-lysine in a 6 well plate at a $5x10^4$ density for use 24hr post seeding at 40-50% confluency. Fluo5F AM was used as a green calcium sensor for investigations in non-optogenetic astrocytes with excitation/emission peaks of 494/516nm, a fold fluorescence change of >100, and a high $K_d$ for calcium at 2.3μM. X-Rhod-1 AM was used as a red shifted calcium dye comparison, with excitation/emission peaks at 580/602nm, a similar fold fluorescence fold change, and a slightly lower $K_d$ of 700nM.

The astrocyte imaging solution HBS (see section 2.2.5 for composition) was used in conjunction with 1μM Fluo5F AM/X-Rhod-1 AM (from 100μM, 30μL aliquot stock diluted in Pluronic F-127, 20% solution in DMSO) to load the cells with indicator for 30min at room temperature. Coverslips were then transferred to HBS without indicator for 30min in order to remove non-loaded dye and fluorescent debris. Using a bespoke mounting system, coverslips were then sandwiched between a round plastic holder and metal cylinder, with silicone grease around the

outside to keep the chamber watertight. 1mL HBS was then pipetted into the chamber, before moving to the microscope stage at room temperature (Nikon Eclipse Ti-E; Nikon Ltd., Surrey, UK) and vacuum tube attached. Micromanager on ImageJ with an Andor Zyla 4.1 camera was used to capture widefield fluorescence images for a 20min period at 1 frame per second, 512x512 pixel and 16 bit resolution, unless otherwise stated. Manual solution exchange was performed after a 2min baseline recording using a disposable Pasteur pipette using the final concentration of ligand, diluted in HBS. During this period, the LED light of set wavelength for fluorescence excitation (470nm for Fluo5F AM, 565nm for X-Rhod-1; CoolLED PE-2; CoolLED Ltd., Andover, UK), was controlled by a Micromanager algorithm to flash only when image was being captured to minimise fluorescent photobleaching. The FITC (BP 470-525nm; Fluo5F) and Cy3 (BP 535-590nm; X-Rhod-1) filters (both Nikon) were manually selected before imaging. A 10x air objective (Nikon CFI Plan 10x/0.25NA 10.5mm WD Objective) was used to capture all images.

### 2.5.2 Calcium Mobilisation in Optogenetic Astrocyte Studies

Astrocytes were transiently transfected using electroporation (see section 2.4.4.3) and seeded onto 22mm round glass coverslips coated with poly-L-lysine in a 6 well plate at a $5x10^4$ density for use 24-48hr post transfection at 40-50% confluency. X-Rhod-1 AM (ex/em 580/602nm) was the calcium indicator used for all primary astrocyte optogenetic calcium experiments. SNAP-Surface AF488 to check for transfected SNAP-receptor expression. For calcium dye loading and labelling of the SNAPtag, the loading solution was made using astrocyte HBS (see section 2.2.5 for composition) with 1μM X-Rhod-1 AM (from 100μM, 30μL aliquot stock diluted in Pluronic F-127, 20% solution in DMSO), 0.2μM SNAP-Surface AF488, and 1μM 9-*cis*-retinal. Cells were loaded in the dark for 30min at room temperature, before coverslips were then transferred to HBS with 1μM 9-*cis*-retinal and without indicator for 30min in order to remove non-loaded dye and fluorescent debris. When used, PTX ($100ng.mL^{-1}$) was added to cells 24hr post transfection, and then incubated with cells for 24hr in astrocyte media before calcium experiments.

Optogenetic calcium studies were performed on a scanning laser confocal (ZEISS 710, inverted with temperature control box; Carl Zeiss Ltd., Cambridge, UK) as the

widefield microscope did not have sufficient filter capabilities to block stimulus light (470-500nm) from the fluorescent dye read (always red-shifted). After the HBS wash, the coverslip was transferred to a metal imaging cylinder and loaded with 1mL HBS with 1µ 9-*cis*-retinal. The cells were left on the microscope stage (set at 37ºC) for 15min before imaging to minimise drift as the temperature equilibrated. The z distance was adjusted to focus on the cytoplasmic region of the cells using a red widefield light to minimise optogenetic receptor stimulation. Cells were imaged at 1 frame per second, for 5-15min where the scan time was 900ms (561nm, 1.58µs pixel dwell) across the coverslip using a EC Plan-Neofluar 10x/0.45 M27 (Zeiss) air immersion lens, with a pinhole of 1.64 Airy Units (AU), 512x512 pixels, 12 bit resolution and red Cy5 filter, BP 570-692nm. An external LED of 470nm (CoolLED PE-2) was used to stimulate cells by being positioned at a 2cm distance above the imaging chamber. As the LED was external, the on/off procedure was performed manually using a timer after a 2min baseline fluorescent read. Post X-Rhod-1 fluorescent timecourse, astrocytes were imaged using a 488nm laser (BP 495-550nm filter) to visualise SNAP-Surface fluorescence, and therefore optogenetic receptor cell surface expression. Image acquisition settings (including the gain and offset) were kept the same within an experiment, and were optimised to avoid image saturation.

### 2.5.3 Calcium Imaging in Optogenetic HEK Studies

Optogenetic stable HEK cell lines were seeded onto 22mm round glass coverslips coated with poly-D-lysine in a 6 well plate at a $5x10^4$ density for use 24-48hr post seeding at 70-80% confluency. From this point onwards, cells were kept as far as possible in the dark. On the day of the experiment, the media was first replaced with retinal supplements in DMEM (either 9-*cis*-retinal or all-*trans*-retinal, both 1µM; Sigma-Aldrich) for 1hr at 37°C, 5% $CO_2$, if required. The appropriate retinal was also included in all subsequent steps in DMEM and HBS imaging solutions. First, each coverslip was transferred to a Petridish on parafilm to localise incubating media and ease coverslip removal. Cells were stained with SNAP-Surface AF488 (0.5µM), used to check receptor expression, applied in 400µL DMEM (10% FCS) for 30min at 37°C, 5% $CO_2$. After labelling of the SNAPtag, cells were then loaded with 1µM calcium indicator with probenecid (250nM), an anion transporter

inhibitor added to prevent the export of cleaved negatively charged calcium indicator compounds from the cytoplasm, in 400µL DMEM (10% FCS) for 45min (Fura Red) or 1hr (Cal-630) at 37°C, 5% $CO_2$. For experiments with a continuous laser stimulation, Fura Red AM calcium indicator (ex/em, 458/597nm) was used, whereas experiments with an external LED or bioluminescence light stimulus were performed using Cal-630-AM (ex/em, 608/626nm). Fura Red AM allowed cells to be imaged in the green spectra for the SNAP labelling at the same time as the calcium indicator in the red spectra with good time resolution, which was useful in experiments with a continuous stimulation. This was not prudent to use with a single/bioluminescence stimulus; Cal-630 AM was used in these experiments due to the red-shifted excitation wavelength allowing no interference with light stimulation. HEK cells were then transferred to a new Petridish and washed for 5min in HEK HBS (see section 2.2.5 for composition) at 37 ºC in order to remove non-loaded dye and fluorescent debris. After the HBS wash, the coverslip was transferred to a metal imaging cylinder and coated with 1mL HBS.

Optogenetic calcium studies were performed on a laser scanning confocal (ZEISS 710, inverted with environmental control; Carl Zeiss Ltd.). HEK cells were left on the microscope stage (set at 37ºC) for 15min before imaging to minimise drift as the temperature equilibrated. The z distance was adjusted to focus on the cytoplasmic region of the cells using a red widefield light to minimise optogenetic receptor stimulation. Cells were imaged at 1 frame per second, for 5-15min where each coverslip took 900ms (1.58µs pixel dwell) to scan with 512x512 pixels, 12 bit resolution. For Fura Red/SNAP-Surface AF488 imaging, a 488nm laser was used in conjunction with the C-Apochromat 40x/1.20 W Korr M27 (Zeiss) water immersion lens with a pinhole of 1.79 AU, and FITC (BP 493-584, SNAP-Surface AF488) and Cy5 (BP 605-759 nm, Fura Red) filters. For Cal-630, the 633nm laser was used with an EC Plan-Neofluar 20x/0.50 Ph2 M27 (Zeiss) air immersion lens with a pinhole of 1.53 AU, and red longpass filter, BP 638-756nm. The 20x air lens was used for Cal-630 experiments to include more cells – the water immersion of the 40x lens was not required to increase light availability as these cells were not simulated with the 488nm laser.

The 488nm laser used to take the Fura Red and SNAP-Surface AF488 images was used as continuous receptor stimulation, set at a consistent 10% laser power. For

single stimulations using Cal-630 AM as the calcium indicator, an external LED of 470nm (CoolLED PE-2) was used to stimulate cells by being positioned at a 2cm distance above the imaging chamber. As the LED was external, the on/off procedure was performed manually using a timer after a 2min baseline fluorescent read. When NanoBiT bioluminescence was used as a light stimulus, cells were not activated by microscope lasers or external LED light. Instead, 100μM furimazine (varied concentration, made up in HBS to 10x final concentration) was added to a reduced imaging HBS volume of 900μL after a 2min baseline using a mechanical pipette to the side of the imaging cylinder. Post Cal-630 fluorescent timecourse, HEKs were imaged using a 488nm laser (BP 495-550nm filter) to visualise SNAP-Surface AF488 fluorescence, and therefore optogenetic receptor cell surface expression. Image acquisition settings (including the gain and offset) were kept the same within an experiment, and were optimised to avoid image saturation.

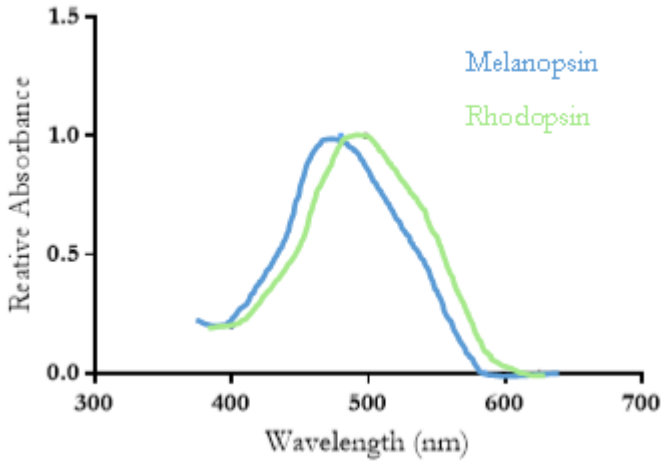


***Figure 2.7*** **- Respective excitation wavelengths of melanopsin and rhodopsin.** Reported excitation wavelengths show activation of both receptors in blue/green visible light spectra. Wavelengths above 600nm, known as the red-shifted range, do not activate either receptor. Approximate values taken from Kandori, Shichida and Yoshizawa (2001) and Hankins, Peirson and Foster (2008).

| Calcium Dye | Ex/Em | Fluorescence Intensity Change on $Ca^{2+}$ Binding (at Peak Emission) | $K_d$ $Ca^{2+}$ | Other notes | Reference |
|---|---|---|---|---|---|
| Fluo-5F | 494/516nm | >100 fold increase | 2.3μM | Lowest affinity used | (Loughrey et al., 2003) |
| Fura Red | Excitation shift 458 to 597nm | >100 fold decrease | 0.4μM | Highest affinity used | (Kurebayashi *et al.*, 1993) |
| X-Rhod-1 | 580/602nm | >100 fold increase | 0.7μM | Mitochondrial and cytoplasmic localisation | (Li et al., 2009) |
| Cal-630 | 608/626nm | >100 fold increase | 1.2μM | Furthest red shifted emission | (Miyazaki *et al.*, 2019) |

***Table 2.3*** **- Summary of the four different calcium indicator dyes used in calcium mobilisation experiments.** All dyes were bulk loaded into cultured cells using an AM ester. Ex/Em represents the excitation and emission wavelengths of the calcium bound indicator. Most calcium indicators show fluorescent enhancement after $Ca^{2+}$ binding with a small wavelength shift, apart from Fura Red which displays an excitation shift upon binding calcium.

## 2.6 Visualisation of SNAP-receptor Expression and Monitoring of Internalisation

### 2.6.1 Monitoring of SNAP-OptoR Trafficking in HEK Cells

For single cell observations, HEK cells were seeded at $1x10^5$ cells/well onto poly-D-lysine coated 22mm coverslips in a 6 well plate. From this point onwards, cells were kept as far as possible in the dark. On the day of the experiment (24-48hr post seeding), if required, the media was first replaced with retinal supplements in DMEM (either 9-*cis*-retinal or all-*trans*-retinal, both 1μM; Sigma-Aldrich) for 1hr at 37°C, 5% $CO_2$. The appropriate retinal was also included in all subsequent steps in DMEM and HBS imaging solutions. First, each coverslip was transferred to a Petridish on parafilm to localise incubating media and ease coverslip removal. To SNAP label the receptors, cells were covered in 400μl membrane impermeant SNAP-Surface fluorophore (SNAP-Surface AF647 or AF488, 0.5μM) in DMEM, containing retinal and 10% FCS, for 30min at 37°C and 5% $CO_2$. If required, endocytosis inhibitors Pitstop 2 or Dyngo 4a (final concentration 30μM) were also added to the media at this point. Coverslips were then transferred to a petridish containing 1mL HBS to remove unbound SNAPtag, before being sandwiched into a round, metal, hollow cylinder and sealed with vacuum grease. The cylinder was filled with 1mL HBS (plus retinal, if required) and fixed to a laser scanning confocal microscope (LSM 710, ZEISS), with a temperature regulated 37°C stage. The bottom of the coverslip was immersed in $ddH_2O$ on a C-Apochromat 40x/1.20 W Korr M27 (Zeiss) objective. The z distance was adjusted to focus on the cytoplasmic region of the cells using a red widefield light to minimise optogenetic receptor stimulation. Cells were imaged at 0.1 frames a second for 30min (controlled using Zeiss Zen Black software) at 512x512 pixels, 12 bit resolution. Experiments using SNAP-Surface AF488 required the 488nm laser at 10% power, 1.89 AU pinhole size, and a BP 493-630nm filter to both stimulate and image the optogenetic cells. When using SNAP-Surface AF647, the 633nm laser was used at 20% power, 1.53 AU pinhole size, in combination with a longpass filter, BP 638-756nm. Image acquisition settings (including the gain and offset) were kept the same within an experiment, and were optimised to avoid image saturation.

### 2.6.2 Platereader Measurement of NanoBiT Bioluminescence and Receptor Internalisation

NanoBiT bioluminescence was used as a stimulus for the optogenetic receptors (see *Figure 2.8*). Bioluminescence intensity was recorded in all HEK-SNAP-optoR-smBiT cell lines co-transfected with LgBiT-Kras or LgBiT-Rab5 and stimulated with furimazine, before bioluminescence-mediated receptor internalisation was measured in the same cells. Following transient transfection (see section 2.4.4.2), cells were seeded at a density to achieve around 70% confluency on the day of the experiment in the central 60 wells of a black 96 well Greiner 655090 plate, coated with poly-D-lysine. All plates were kept in the dark throughout experimental setup, until cell fixing.

First, cells were incubated with SNAP-Surface fluorophore (SNAP-Surface AF647, 0.2μM; New England BioLabs, Hitchin, UK) and 9-*cis*-retinal (1μM) for 30min at 37°C and 5% $CO_2$ with 50μl DMEM in each well. If required, endocytosis inhibitors Pitstop 2 or Dyngo 4a (both 30μM) were added to the media at this point, also incubating for 30min. After SNAP-Surface AF647 labelling, cells were washed in HBS and the HEK media was replaced with 100μL HBS with 0.1% BSA containing AF546-conjugated transferrin (1:1000 dilution) and 1μM 9-*cis*-retinal. Labelling of transferrin allows detection of early and recycling endosomes as the bound transferrin receptor undergoes constitutive trafficking through these endosomes. Furimazine, 10μL diluted in HBS with 0.1% BSA to x10 final concentration, was added in increasing concentrations across the wells before the plate was quickly placed in the PHERAstar plate reader (BMG Labtech, Aylesbury, UK). Luminescence was detected using the 230-750nm filter and photomultiplier tubes on the PHERAstar, selected by Reader Control software (BMG Labtech). Intensity of bioluminescence for every well was measured at 2min intervals for 26min, also simultaneously allowing for 30min stimulation of the optogenetic receptors (4min of recording lost between furimazine addition and movement between lab areas). Data were extracted using MARS Data Analysis software (BMG Labtech).

After bioluminescence experiments, cells were fixed and prepared for imaging on the ImageXpress Ultra (confocal). Cells were incubated in 100μl/well of 3%

paraformaldehyde for 10min, before washing with PBS. A nuclear stain was added using Hoechst 33342 (H33342; 355/465nm), applied for 15min before replacement with PBS for imaging. Images of each well were taken using a Nikon x40 extra long working distance NA0.6 objective for 4 different sites on the Image Express Ultra. Fluorescence excitation and image capture was performed with the relevant combination of laser wavelength and filter cube (Nikon TE2000). The following laser-filter (ex/em) pairs were utilised; DAPI 405nm laser-405/447nm filter (H33342), Texas Red 561nm laser-561/593nm filter (AF546-transferrin) and Cy5 635nm laser-635/685nm filter (SNAP-Surface AF647).

## 2.7 Bioluminescence Imaging

Bioluminescence was visualised in HEK-SNAP-Opn4-smBiT114 and HEK-SNAP-Opn4-smBiT86 cell lines transfected with LgBiT-Kras or LgBiT-Rab5 to determine the spatial localisation of the signal. Following transient transfection (section 2.4.4.2), cells were seeded into glass bottomed 35mm Petridishes the day before imaging to 70% confluency and the media was replaced with 1mL HBS prior to experiments. The Petridishes were then placed into the Olympus Lumiview (LV200) inverted microscope (Olympus, Southend-on-Sea, UK) in a 37°C heated stage with a x40 (1.3NA) oil immersion objective (Nikon). They were left for 1hr to settle before addition of substrate to minimise microscope z drift. Furimazine was diluted in HBS with 0.1% BSA 1:25 from the manufacturer's stock, in a final assay volume of 1mL, making the final concentration ratio 1:250 when added to the cells. Cells were imaged using 10s (smBiT114) or 5s (smBiT86) exposure images for 2hr at 1 frame every 20s using cellSens software to control acquisition at 512x512 pixel and 16 bit depth. The LV200 is kept within a light-tight dark box and uses an EM-CCD camera at minimal distance to maximise light acquisition from the sample, allowing for imaging of low-level bioluminescence. Both before and after acquisition, a widefield image was also taken alongside the bioluminescence image.

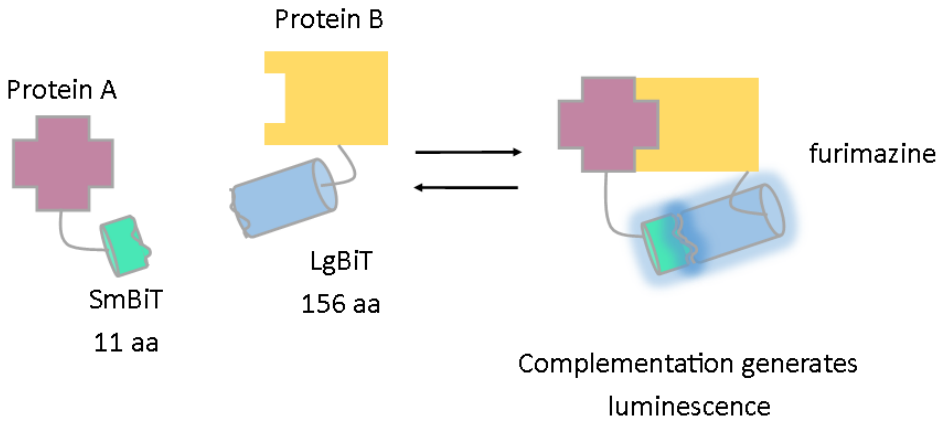


***Figure 2.8* - Production of NanoBiT bioluminescence.** The SmBiT and LgBiT fragments of the NanoBiT are fused to two proteins of interest via peptide linkers. Upon complementation of the NanoBiT fragments once the two target proteins are in close enough proximity, NanoBiT can catalyse furimazine to produce a bioluminescent signal.

## 2.8 Data Analysis and Statistics

### 2.8.1 Analysis of Calcium Transients

ImageJ and the plugin Micromanager (both open source) were used to collect image frames for single cell calcium analysis. To analyse the data, the plugin Time Series Analyzer [sic] for ImageJ was used to place uniform regions of interest (ROI) near cell nuclei throughout the image stack, from which a cytosolic fluorescence read could be determined over time (see *Figure 2.9*). An algorithm set up by Dr Wayne Croft was used in MATLAB vR2015b (MathWorks, Cambridge, UK) to then analyse measured data from the timeseries (Croft *et al.*, 2016).

The percentage of astrocytes responding to a ligand was calculated by setting a threshold of fluorescence change (ΔF) and counting the number of cells with ΔF over the threshold after 5s of solution exchange. The time 5s was chosen to minimise false positives from spontaneous calcium mobilisation within the astrocytes at other times during the recording. The threshold fold change was independently determined for each experiment due to variation between astrocyte cultures, based on manual inspection of the transient recordings (~1.4 ΔF).

The percentage of astrocytes or HEK cells responding to light stimulation was calculated by setting a threshold of fluorescence change (ΔF) and counting the number of cells with ΔF over the threshold over the time period of recording (2-15min). The fold change threshold was chosen based on manual inspection of the frames due to variation between cultures (~1.3 ΔF X-Rhod-1, ~1.5 ΔF Cal-630). Under continuous laser stimulation, the whole timecourse was analysed. For LED stimulation patterns, timecourses for analysis were divided into the duration of each LED on/off cycle (e.g. 20s on/20s off – 40s total).

For those cell responses which were over the threshold, addition parameters were used to quantify the transients obtained - the maximum fold change in fluorescence over the threshold, the area under the curve of the response transient and time taken to the first peak (see *Figure 2.10* for a representation of these measurements). In calcium transients recorded using the Fura Red indicator, thresholds and transient parameters were defined on the basis of a calcium-dependent decrease, rather than increase in the fluorescent signal.

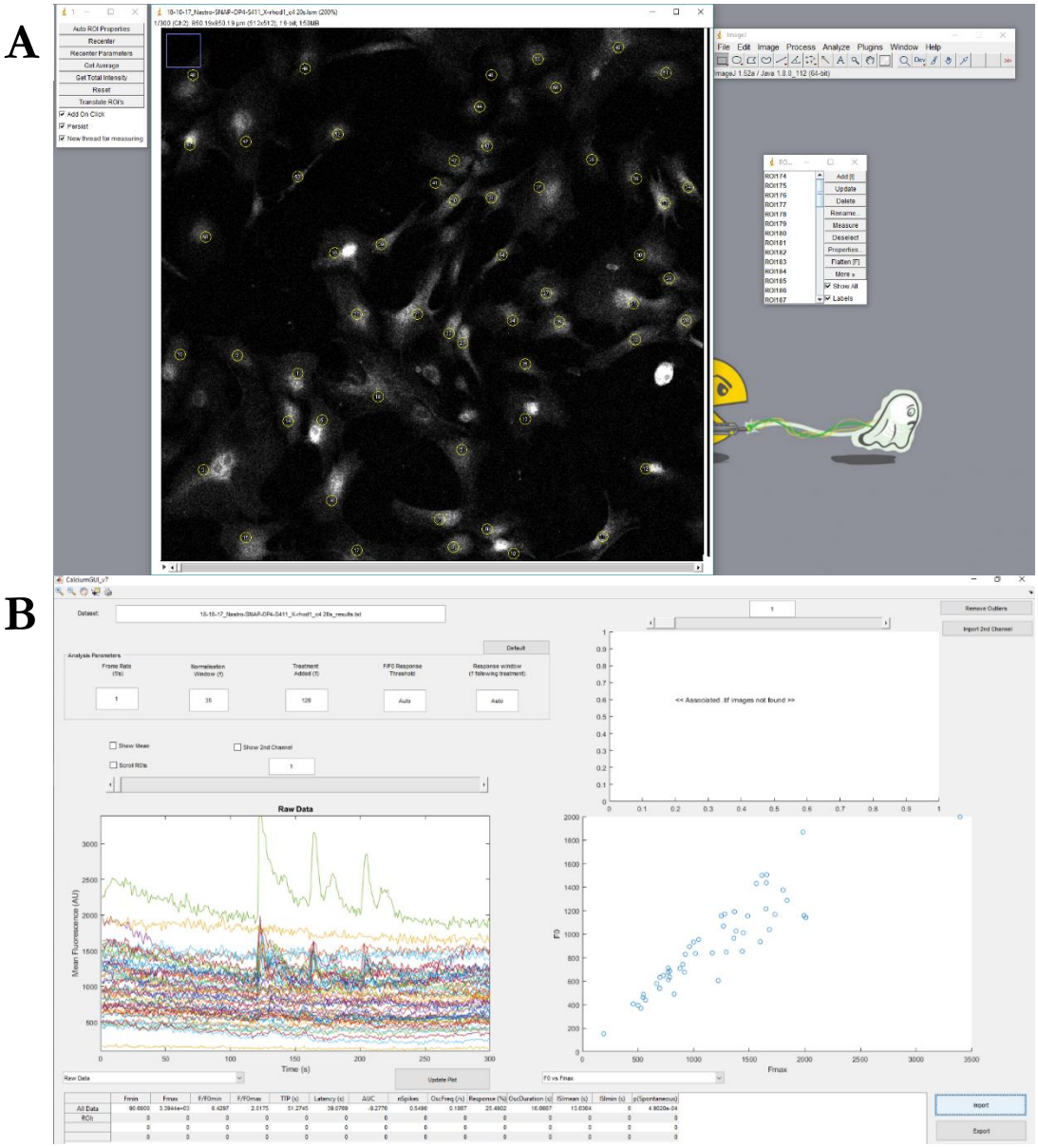


***Figure 2.9*** **- Image analysis process for single cell calcium response.** Microscope image timecourses were opened in ImageJ and uniform ROIs were applied manually near the brighter nucleus region of each cell throughout the entire stack (A). Results from these ROIs were then imported into the MATLAB user interface for calcium response measurements (B). Any measurements by the algorithm could then be exported for use. Here shown with melanopsin transfected primary cortical astrocytes, *n*=1 coverslip with X-Rhod-1 AM where the LED was used in a 20s on/off pattern.

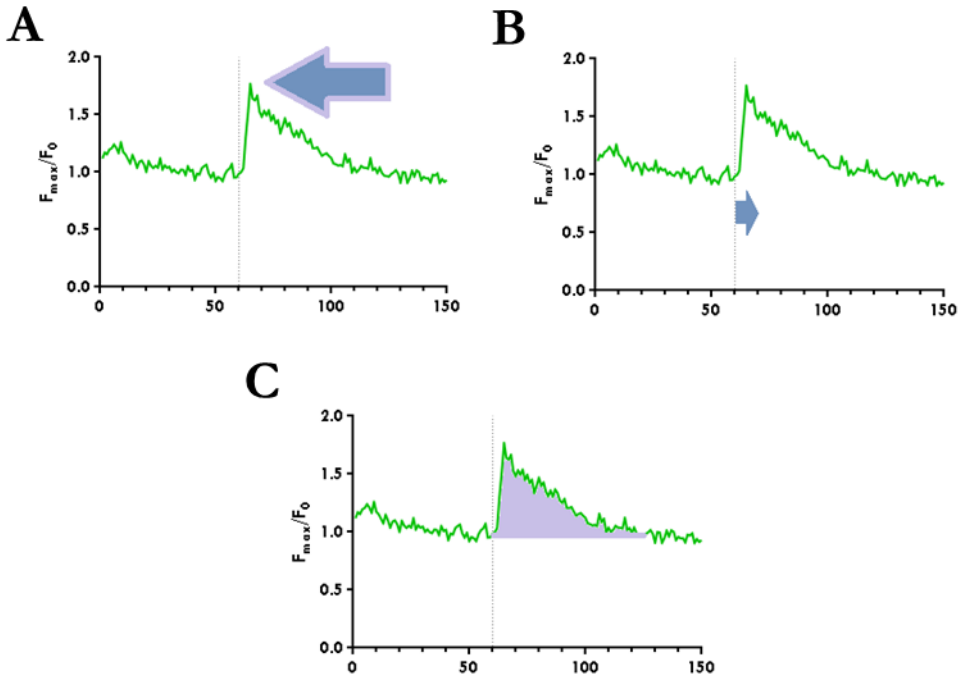


***Figure 2.10*** **- Representation of the different measurements taken from fluorescent traces of calcium transients.** A) The peak fold change value taken after cell stimulation, B) arrow demonstrating the time taken to peak measurement on the x axis and C) demonstrates the area under the curve that was measured post stimulation for 120s with a 60s stimulation.

### 2.8.2 Measuring SNAP-tagged Receptor Trafficking

Single cell analysis of SNAP-tagged receptor trafficking was performed using Volocity (x64; Quorum Technologies, ON, Canada) and Excel (Office 365, Microsoft, Reading, UK). First, microscope image stacks (512x512 pixels, 12 bit) of fluorescently labelled receptors were loaded into Volocity. Single cross-section profiles were drawn across the centre of the cell and covering the cellular membrane both sides for 10< random cells (see *Figure 2.11*). The placement of the cross-section required checking the profile across the entire timeseries due to cellular movement. The gray scale fluorescence intensity of each pixel in the cross-section was then obtained across the timeseries for all cells. In Excel, each cell was analysed individually to determine the position of the first peak in fluorescence intensity, representing the plasma membrane. This position was different for each individual cell, depending on membrane movement across the experiment. The intensities at this position were then identified across the time-series and were plotted against time (as individual cell records or pooled data), following normalisation to the intensity at time 0, and subtraction of background baseline.

Bioluminescence stimulated internalisation was analysed using the translocation algorithm in MetaXpress 5.3 software (high content image analysis software, Molecular Devices; Johnston *et al.*, 2010). Images of transferrin labelling (Texas Red channel) were used to identify labelled compartments of 3μm diameter based on a threshold intensity which was set independently by manual inspection for each experiment. In the translocation algorithm, this compartment mask was then applied to the receptor image (Cy5) to calculate the mean receptor intensity colocalised within each compartment, as a measure of receptor internalisation. Average cell mean intensities were calculated from the 4 individual site images taken for each well. Data were then normalised to the highest furimazine concentration (100% response) and average HBS vehicle control (0% response).

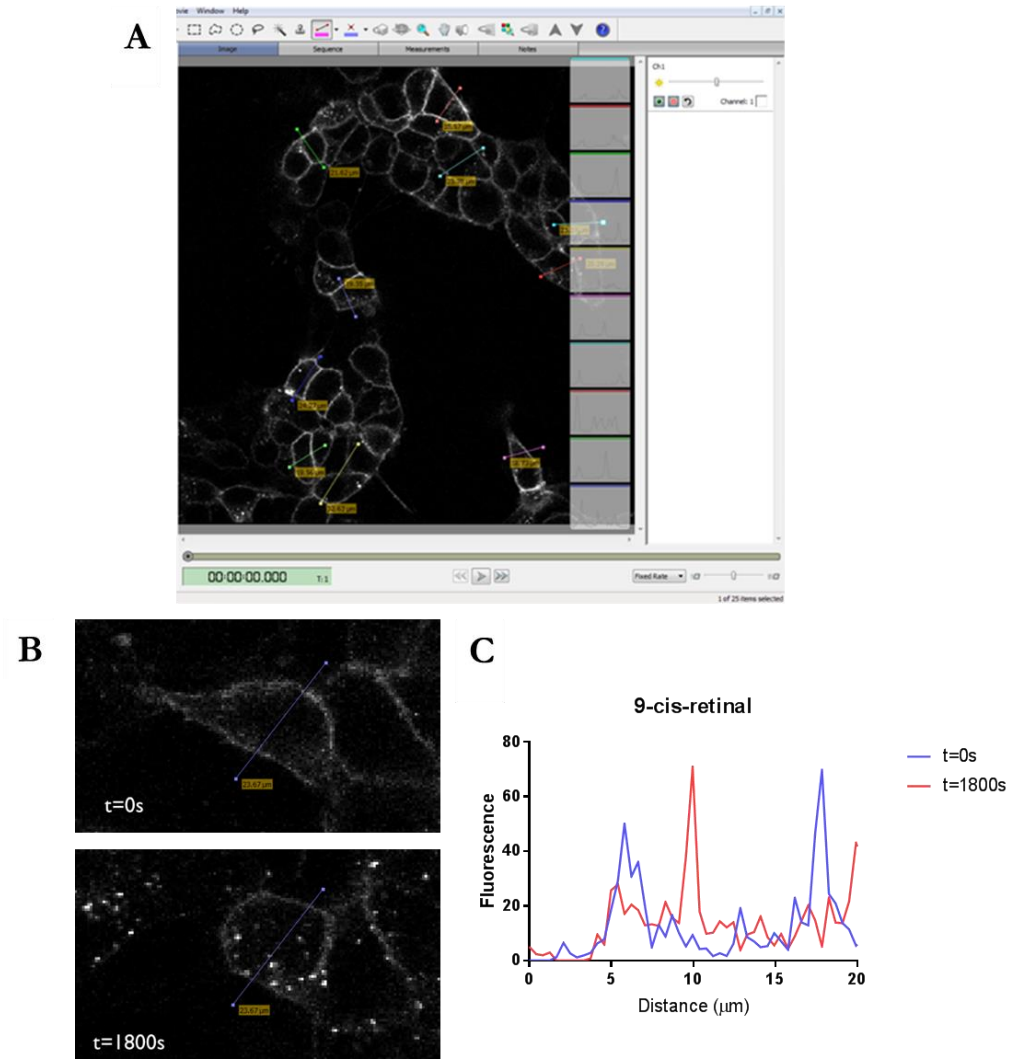


***Figure 2.11*** **- Processing of single cell receptor trafficking of SNAP tagged receptors.** A) Random allocation of cross-sections of cells. B) The two images represent a single cell across the timeseries. At t=0s, the receptors are distributed evenly at the cell surface, however at t=1800s there are visible differences in receptor distribution with brighter spots appearing in the cell. C) The graph shows the two profiles of the different time frames. The peaks at the start and end of the distance measured shows the bright plasma membrane. The first peak, representing the cell surface, decreases in the later time point. There is also an increase in the fluorescence reading between the membrane peaks in the later timepoint. Taken from $n$=1 coverslip of the stable HEK-SNAP-opto-$\alpha_{1A}$AR cell line with 0.5μM SNAP-Surface AF488 and 1μM 9-*cis*-retinal, and 30min stimulation with a 488nm laser at 10% power.

### 2.8.3 Presentation and Statistics

Graphpad Prism v7.0 (Graphpad Software, San Diego, CA) was used to normalise data, create the graphs and calculate statistical tests, such as *t* tests and Analysis of Variance (ANOVA). The 95% confidence level was used to prove statistical significance

Data are displayed as mean±S.E.M and *n* represents the number of plates or coverslips used, unless otherwise stated.

# Chapter Three

## Signalling and Internalisation of the Chimeric Rhodopsin-$\alpha_{1A}$-adrenergic Optogenetic Receptor

## 3.1 Introduction

### 3.1.1 Opto-$\alpha_{1A}$AR Chimeric Receptors

The concept of using bovine rhodopsin and the human $\alpha_{1A}$-adrenoceptor to create the opto-$\alpha_{1A}$AR construct has been outlined in section 1.2.3 (Airan *et al.*, 2009). The predicted 2D structure of the chimeric receptor is shown in *Figure 3.1* where the intracellular loops, known for their involvement in the activation of G proteins and phosphorylation by kinases for arresting signalling, are swapped from rhodopsin residues to those of the $\alpha_{1A}$ adrenoceptor protein sequence. The $\alpha_{1A}$ adrenoceptor is one of three highly homologus subtypes, with $\alpha_{1B}$ and $\alpha_{1D}$ the other two. The $\alpha_1$ adrenoceptors are expressed in many tissues, including but not exclusive to smooth muscle vasoconstriction, cortical neural cells associated with appetite and memory, and the liver (Piascik and Perez, 2001; Chalothorn *et al.*, 2002)t. The $\alpha_1$ adrenoceptors are selective for noradrenaline, one of the main catecholamines released by sympathetic nervous innervation (Piascik and Perez, 2001). Coupled to the $G_{q/11}$ proteins, the opto-$\alpha_{1A}$AR chimeric receptor has the potential to study $\alpha_{1A}$ adrenoceptor intracellular signalling and the known functional endpoints with fine spatial resolution, such as inositol 1,4,5- trisphosphate ($IP_3$) and $Ca^{2+}$ production, independent of the influence of agonist binding kinetics and avoiding off-site actions of ligand addition.

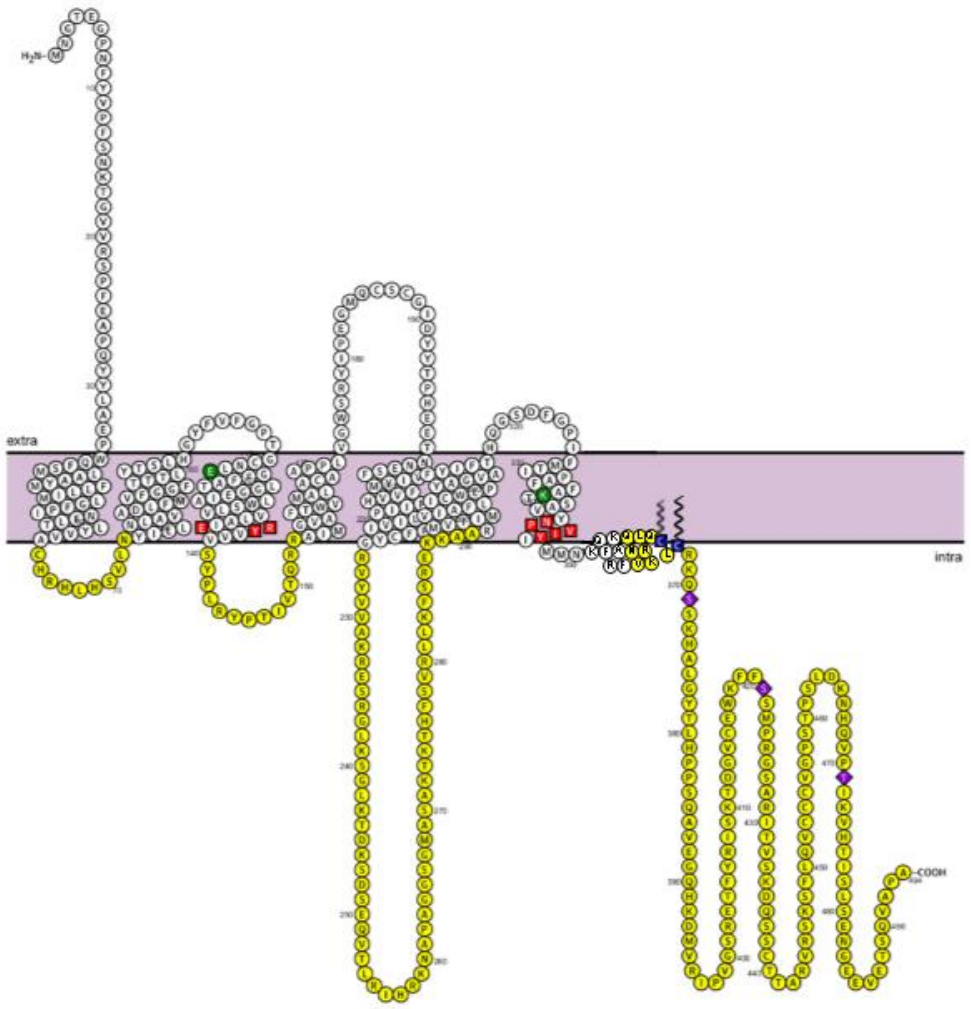


***Figure 3.1* – Predicted structure of the opto-$\alpha_{1A}$AR receptor.** Bovine rhodopsin transmembrane and extracellular amino acids (*white*) form the core 7 transmembrane helix structure and the juxta membrane helix 8. Intracellular residues have been replaced with the $\alpha_{1A}$ adrenoceptor protein sequence (*yellow*). The highly conserved class A GPCR motifs NPxxY (NPVIY for bovine rhodopsin) and D(E)RY (*red*) are important regulators of the rhodopsin conformational state, as discussed in text. Two Cys in helix 8 form parmytiolation sites (*blue*), now part of the $\alpha_{1A}$ C terminal region. 11-*cis*-retinal binds to the $Lys^{336}$ in helix 6 via a protonated Schiff base, and the positive charge of the base is neutralised by counter ion $Glu^{113}$ (both in green, potentially $Glu^{181}$ in the active formation, Yan *et al.*, 2003). Truncations of the receptor were made at $Ser^{371}$, $Ser^{421}$ and $Thr^{471}$ for this study (purple). Created using Protter (Omasits *et al.*, 2014).

### 3.1.2 Altering Receptor Signalling and Regulation to Change Temporal Activation

The simple kinetics of the opto-$\alpha_{1A}$AR activation allows for a fast stimulation time, however rhodopsin based GPCR optogenetic receptors are often used with a single stimulus due to slow regeneration of the inactivated all-*trans*-retinal metarhodopsin II formation back into the inactive *cis*-retinal state, required for re-activation (Saari, 2012; Frederiksen *et al.*, 2016). Rhodopsin also undergoes rapid desensitisation, which limits its signalling duration at the surface of the cell, and slow recycling, as the full rhodopsin requires rebinding with 11-*cis*-retinal before restimulation (Saari, 2012). Thus, the chimeric rhodopsin is not a perfect model for temporal activation of the receptor.

Instead of altering the delicate activation kinetics of rhodopsin, it was decided that changing the desensitisation of the opto-$\alpha_{1A}$AR could create a receptor with more applicable cellular signalling to ligand binding GPCRs. The main pathway for GPCR internalisation and recycling is through phosphorylation of the receptor, leading to β-arrestin binding and clathrin endocytosis (see section 1.1.5). There are several sites on the C terminus of GPCRs that can be phosphorylated, forming what can be described as a "barcode" to mediate effector binding and therefore receptor signalling (Reiter *et al.*, 2012). An X-ray crystal structure of rhodopsin bound to arrestin was used to determine several codes and binding conformations of arrestin (Inoshima *et al.*, 2017). Only full phosphorylation with a pattern of Px(x)PxxP (where P = Ser/Thr) residues in the C terminus was sufficient for high-affinity arrestin binding, with other partial codes allowing for different binding and therefore downstream signalling, for example of β-arrestin and ERK, or Jun kinase (Inoshima *et al.*, 2017). At these sites, GRK is one of the main kinases for GPCR phosphorylation (Bahouth and Nooh, 2017). Another phosphorylation route could involve casein kinase 1α, which has been reported to regulate agonist-mediated phosphorylation of the $M_3$ muscarinic receptor (Budd *et al.*, 2000). PKC is also thought to contribute to receptor phosphprylation and arrestin binding, with the PKC target sites involving PxR/K residue patterns (Freeley *et al.*, 2011). A good summary of phosphorylation sites at different receptors and the kinase involved has been reviewed in Tobin *et al.* (2008).

Binding of β-arrestin blocks the $G_q$ coupling to all subtypes of $\alpha_1$ adrenoceptors, causing receptor desensitisation and allowing endocytosis (Luttrell and Lefkowitz, 2002; Perez-Aso *et al.*, 2013). Investigations into internalisation and desensitisation of the $\alpha_{1A}$-adrenoceptor have shown clear roles for β-arrestin binding, linked to receptor kinase phosphorylation (Chalothorn *et al.*, 2002; Price *et al.*, 2002). There are four PKC sites that can be found on the $\alpha_{1A}$AR C tail (*Figure 3.1*) at $Ser^{371}$ (SSK), $Ser^{427}$ (SAR), $Thr^{441}$ (TAR) and $Thr^{471}$ (TIK). It was then hypothesised that removing phosphorylation sites in the C terminus could potentially restrict desensitisation. Without kinase interaction with the receptor at the terminus, some ligand activated GPCRs can no longer recruit β-arrestin which can affect cell trafficking and desensitisation, an interaction seen with the $\alpha_{1B}$ and $\beta_1$ adrenoceptors, for example (Stanasila *et al.*, 2008; Hinz *et al.*, 2017).

### 3.1.3 Chapter Aims

The aims of this chapter are three fold;

i. To assess the calcium signalling profile and requirements for activation of the opto-$\alpha_{1A}$AR expressed in a model cell line (HEK293).
ii. To monitor opto-$\alpha_{1A}$AR trafficking in HEK293 cells in response to light activation.
iii. To use C terminal truncation mutants to develop opto-$\alpha_{1A}$AR constructs with tuned temporal signalling characteristics.

In this chapter, opto-$\alpha_{1A}$AR responses will be assessed via calcium mobilisation assays. These fluorescent-based assays utilise cell permeable $Ca^{2+}$-sensitive dyes which change their fluorescence output when bound to $Ca^{2+}$ (see section 2.5). Increases in intracellular $Ca^{2+}$ are a major activation response of both the endogenous $\alpha_{1A}$ adrenoceptor and opto-$\alpha_{1A}$AR. SNAPtag opto-$\alpha_{1A}$AR constructs will also be developed and characterised to allow the covalent labelling of the receptor with fluorescent substrates, which have the potential to be cell impermeable or permeable, as required by the assay (Keppler *et al.*, 2003). Through labelling with a range of SNAP fluorophores, the receptor can be visualised and monitored over time using fluorescence microscopy (see section 2.6). Redistribution of non-permeable SNAP surface fluorescence to intracellular compartments reflects endocytosis of the labelled receptor to intracellular endosomes, and will thus been used to measure opto-$\alpha_{1A}$AR internalisation. In order to alter receptor trafficking, mutations can be made in the C terminus to change phosphorylation sites, thereby changing the activation and desensitisation cycle. Here, C terminal truncation mutants of the opto-$\alpha_{1A}$AR will be made to remove these phosphorylation sites, which could change the temporal signalling characteristics.

## 3.2 Results

### 3.2.1 Preparation of SNAP-tagged Optogenetic Constructs

The opto-$\alpha_{1A}$AR receptors and the truncation mutants at residues Thr471, Ser421 and $Ser^{371}$ were successfully ligated into the $p3.1_{NEO}$-SNAP vector via PCR amplification of the receptor cDNA (in pcDNA3.1-opto-$\alpha_{1A}$AR-EYFP-v5his vector) and subcloning using the flanking restriction sites (BamH1/XhoI) introduced by the PCR primers. Successful insertion of the receptor DNA in the new constructs was detected by restriction digestion using the flanking restriction enzymes (BamH1, Xho I) and agarose gel electrophoresis of maxiprep samples, where an additional band was shown when the receptor is present compared to the vector backbone (6.0kbp alone) – predicted sizes for the insert were 1.48kbp for opto-$\alpha_{1A}$AR, 1.41kbp for opto-$\alpha_{1A}$AR-T471*, 1.26kpb for opto-$\alpha_{1A}$AR-S421* and 1.11kbp for optoXR-$\alpha_{1A}$-S371* (*Figure 3.2*). The sequence was verified in the maxiprep DNA preparation by sequencing with T7 and BGHrev to confirm no PCR errors and that an in frame fusion protein (N terminal signal sequence, followed by SNAP tag, followed by receptor cDNA and STOP codon) was correctly encoded.

Post transfection, cell lines with the opto-$\alpha_{1A}$AR were visualised by labelling the SNAP receptor protein with the appropriate SNAP fluorophore. HEK293 cells stably expressing full length or C-terminal truncated SNAP- opto-$\alpha_{1A}$AR showed a clear membrane expression and high transfection rate of the receptor following membrane impermeant SNAP-Surface AF488 labelling (*Figure 3.3*).

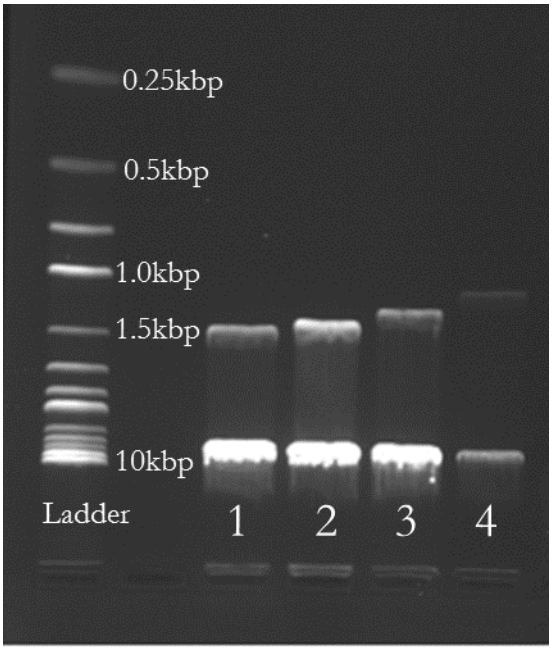


***Figure 3.2* – Agarose gel electrophoresis of the p3.1$_{NEO}$-SNAP-opto-$\alpha_{1A}$AR, mutant constructs and vector plasmids (numbered lanes 1-4) using a double restriction digestion of BamH1 and XhoI**. The left lane contains a diagnostic DNA ladder of known molecular weight bands. Lane 1 is the wild type receptor opto-$\alpha_{1A}$AR with a band at 1.5kbp and the vector at the 6kbp range, with lane 2 displaying the opto-$\alpha_{1A}$AR-T471* truncation at slightly reduced size, lane 3 showing the band at around 1.25kbp for the opto-$\alpha_{1A}$AR-S421* truncation, and lane 4 showing a band of the opto-$\alpha_{1A}$AR-S371* mutant at around 1.1kbp.

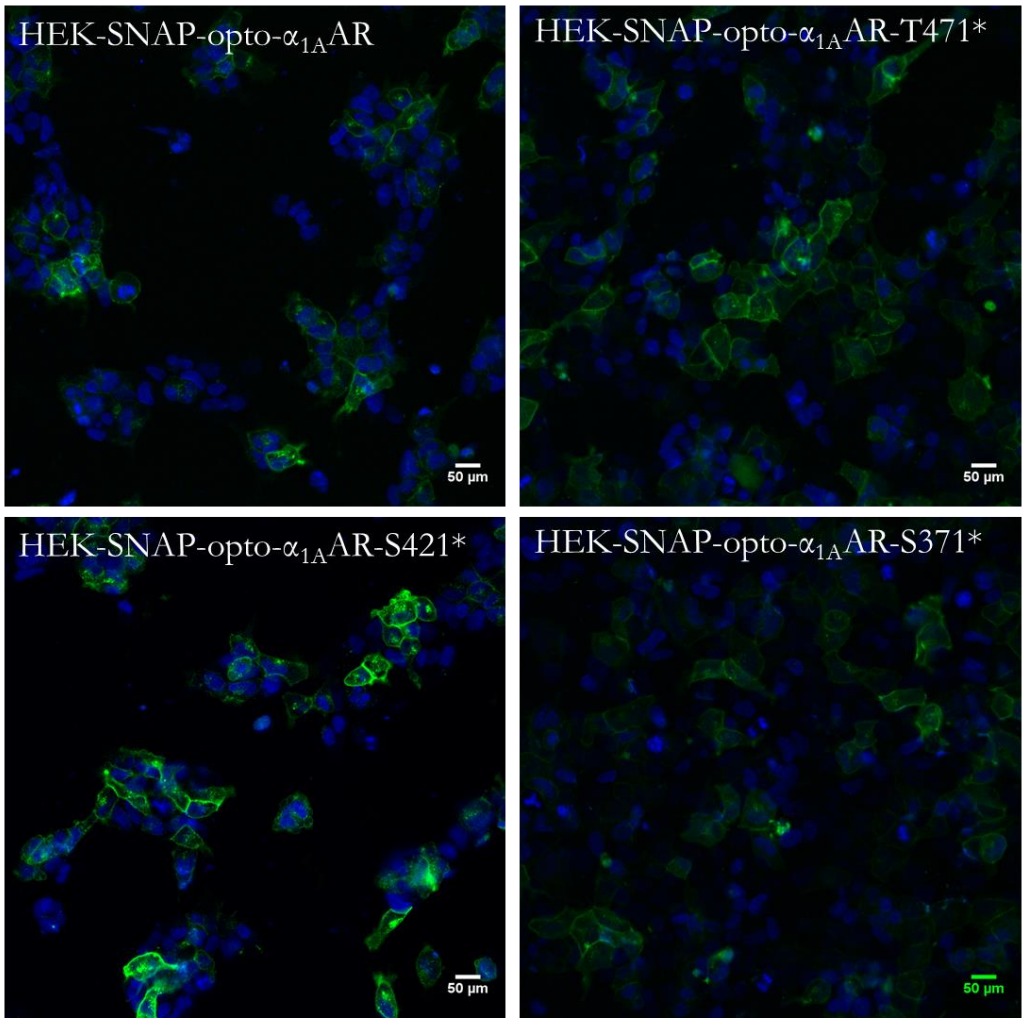


***Figure 3.3*** **– SNAP-opto-$\alpha_{1A}$AR and truncated mutants' expression in stable HEK293 cell lines.** Cells were stained with H33342 (blue) to identify cells and SNAP-Surface AF488 (0.2µM, green) to visualise receptor expression. All receptors show clear membrane expression and high transfection rate.

### 3.2.2 Sustained Laser Stimulus is Required for SNAP-opto-$\alpha_{1A}$AR Activation in HEK293T Cells

Coupled to the $G_q$ protein, opto-$\alpha_{1A}$AR activation is linked to downstream $Ca^{2+}$ influx and release in cells, increasing intracellular [$Ca^{2+}$]. Receptor function for the opto-$\alpha_{1A}$AR was therefore detected by imaging $Ca^{2+}$ concentration via intracellular fluorescent $Ca^{2+}$ indicators in transfected cells. Peak excitation of rhodopsin is at around 500nm wavelength, and wavelengths between 470-510nm have been used in previous studies to initiate opto-$\alpha_{1A}$AR signalling cascades (Airan *et al.*, 2009). As rhodopsin requires covalently bound retinal to function, 9-*cis*-retinal (1μM), was used to supplement the cells. Optimisation of receptor stimulation was first trialled as a short, high-power (70%) 488nm laser stimulus to a specific area using a fluorescence recovery after photobleaching (FRAP) technique. Using the HEK-SNAP-opto-$\alpha_{1A}$AR stable cell line, cells were loaded with calcium indicator X-Rhod-1 (1μM; ex/em, 580/602 nm), which increases in fluorescence upon binding to $Ca^{2+}$, and imaged on a line scanning confocal microscope. FRAP was used to bleach for 1s over a short 12s timecourse in a defined ROI of 40$\mu m^2$ area using Zeiss' Zen Black Software at 70% power. Neither the cells inside the FRAP area or those around produced calcium transients in response to 488nm laser stimulus suggesting that a high dose of photons for a short time was not adequate for opto-$\alpha_{1A}$AR receptor function under these conditions (*n*=3, *Figure 3.4*).

Instead of a short burst of high intensity laser stimulus, a sustained 488nm laser stimulus was applied to the cells in an alternating line scan protocol with the 561nm laser, used to image the X-Rhod-1, for 30s at 20% laser power. First, the cells were imaged without the green 488nm laser, then imaged again including 488nm excitation applied to the whole field, and then imaged for a third time to test cell viability after stimulation with a known agonist for HEK $G_q$ activation and $Ca^{2+}$ influx (10μM carbachol, *n*=3, *Figure 3.5*). The HEK-SNAP-opto-$\alpha_{1A}$AR cell line did not produce $Ca^{2+}$ transients when stimulated with the 561nm laser, but did show fluorescent peaks when stimulated with the green laser, indicating that 30s with the 488nm laser was sufficient to activate the opto-$\alpha_{1A}$AR receptor. Cells were then stimulated again with carbachol to show that viable $G_q$ calcium responses could still be obtained after a sustained laser stimulus. To validate that the calcium response by the SNAP-opto-$\alpha_{1A}$AR was not phototoxic in nature, wild type HEK293 cells

were also subjected to the same protocol. These cells did not produce a calcium response to the green 488nm laser, indicating that the calcium transients produced were dependent on SNAP- opto-$\alpha_{1A}$AR expression (*Figure 3.6*).

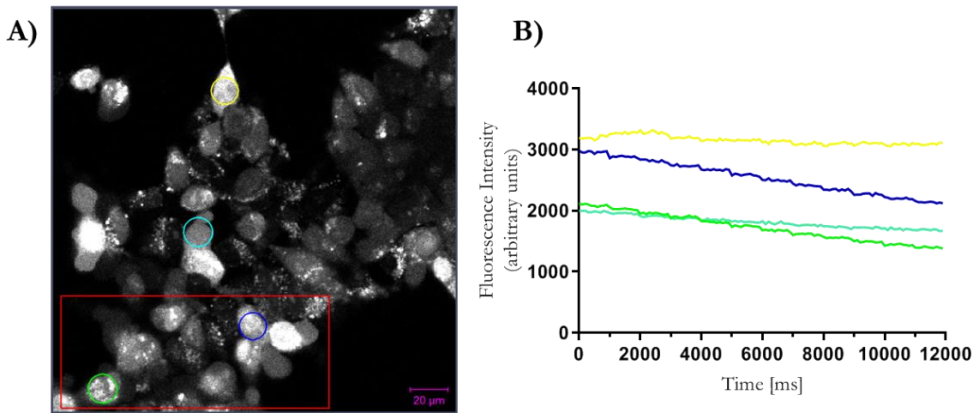


***Figure 3.4* – HEK SNAP-opto-$\alpha_{1A}$AR cells do not respond to a single, high power scanning laser stimulus.** Cells were loaded with 1µM X-Rhod-1 and 1µM 9-*cis*-retinal and images taken for 12s at 10 frames per second using a 561nm laser and filter BP 570-692nm. A) The image shows the area selected to be stimulated with a 70% power 488nm scanning laser for 1s under FRAP bleaching (red box) while X-Rhod-1 fluorescence is monitored, and ROIs of different cells. B) Fluorescence traces from the stimulated area (*green*, *dark blue* ROIs representative) show a decrease in fluorescence, possibly due to bleaching, and no fluorescence peaks to indicate calcium transients. Non-stimulated cells (*yellow*, *light blue* ROIs representative) have no change in fluorescence with decreased bleaching ($n$=1, representative of $n$=3 coverslips).

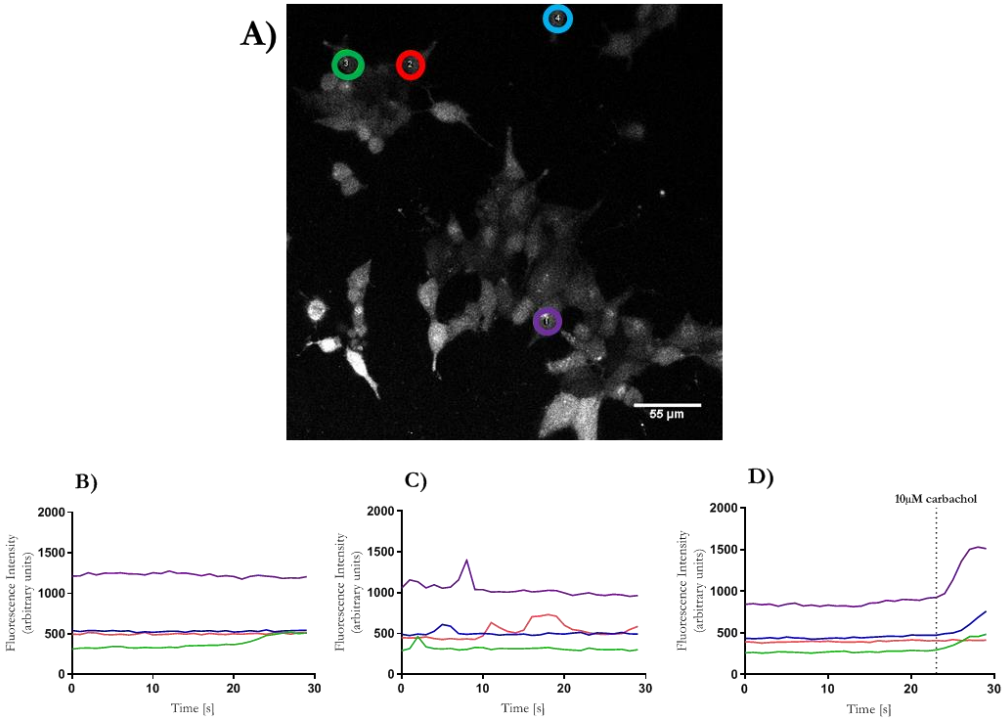


***Figure 3.5* – HEK SNAP-opto-$\alpha_{1A}$AR cells produce calcium transients in response to sustained 488nm laser excitation.** A) Image depicts cells subjected to three different laser stimuli, loaded with 1µM X-Rhod-1 and 1µM 9-*cis*-retinal and imaged using a 561nm laser and filter BP 570-692nm. B-D) from left to right, each graph depicts the same 4 representative cells, identified by their ROI colour, in sequential experiments, and performed 2.5min apart. B) Lack of fluorescence change in response to 30s 561nm laser excitation, followed by C) the production of $Ca^{2+}$ transients with 30s 488nm laser excitation at 20% power, and finally D) cells are still viable after laser stimulation – fluorescence increase showing $Ca^{2+}$ response to known agonist carbachol (10µM; $n$=1, representative of $n$=3 coverslips).

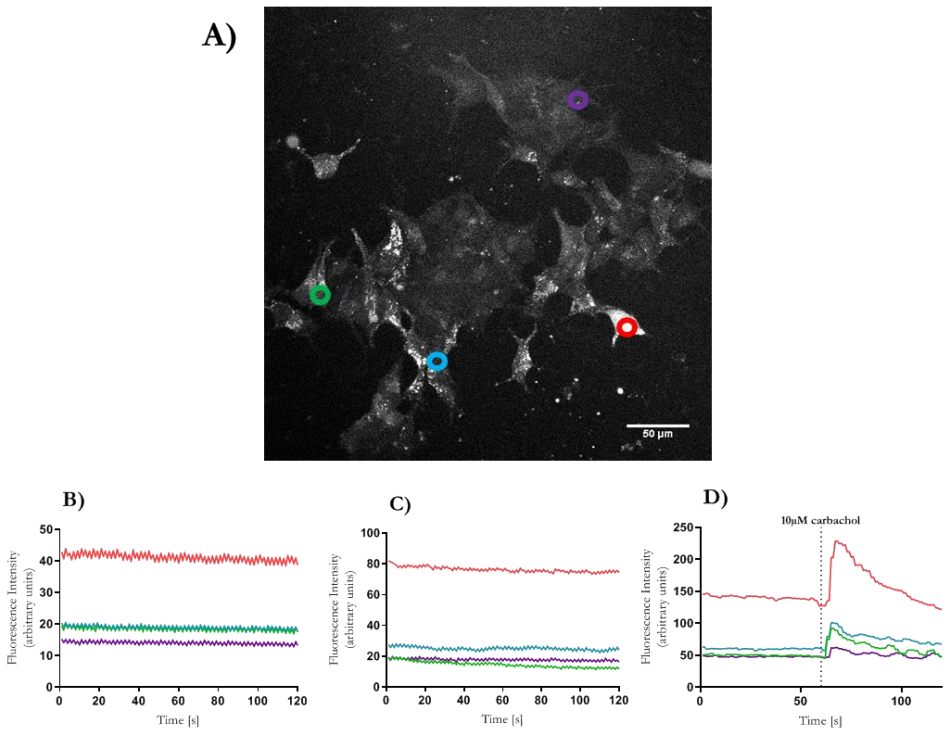


***Figure 3.6* – HEK293 wild type cells do not respond to a sustained 488nm laser stimulus.** A) Image depicts cells subjected to three different laser stimuli conditions, loaded with 1µM X-Rhod-1 and 1µM 9-*cis*-retinal and imaged using a 561nm laser, filter BP 570-692nm. B-D) from left to right, each graph depicts the same 4 representative cells, identified by their ROI colour, in sequential experiments, and performed 5min apart. B) Lack of fluorescence change in response to 120s 561nm laser excitation, followed by C) 488nm laser excitation at 20% power failing to elicit fluorescence changes, and finally D) cells are still viable after laser stimulation – fluorescence increase showing $Ca^{2+}$ response to known agonist carbachol (10µM; *n*=1, representative of *n*=3 coverslips).

### 3.2.3 Calcium Mobilisation Dynamics in the HEK-SNAP-opto-$\alpha_{1A}$AR Stable Cell Line

Fura Red is a calcium indicator dye whose peak fluorescence excitation when bound to $Ca^{2+}$ ions shifts from 458nm to 597nm, therefore decreasing the 458nm intensity in the presence of calcium. Using the sustained laser stimulation method shown in section 3.2.2, Fura Red can be excited with the same green 488nm laser used to stimulate the opto-$\alpha_{1A}$AR, but crucially its fluorescence can be monitored simultaneously with a second 488nm fluorophore with emission in the 515–535nm range. For example, this might include SNAP-Surface AF488 labelled SNAP tagged receptors to monitor localisation. The single wavelength excitation for rhodopsin stimulation, Fura Red and SNAP label fluorescence enables imaging at increased temporal resolution, for example compared to X-Rhod-1 experiments. As discussed below, several parameters of the calcium transients in individual HEK-SNAP-opto-$\alpha_{1A}$AR cells were investigated to compare native and truncated mutant receptors as follows; percentage cell response, average latency, number of $Ca^{2+}$ spikes and peak fold change in fluorescence (defined in section 2.8.1). Furthermore the responses in the absence and presence of 9-*cis*-retinal or all-*trans*-retinal (both 1μM) supplementation were investigated. 9-*cis*-retinal is not the native retinal that binds to rhodopsin (11-*cis*-retinal) but is the more stable form of the molecule, useful for exogenous supplementation, and studies have demonstrated 9-*cis*-retinal conjugated rhodopsin (isorhodopsin) is functional (Nakamichi *et al.*, 2007; Sekharan and Morokuma, 2012). Supplementation of retinal was performed 1hr prior to experiments to allow for binding with rhodopsin.

The presence of 9-*cis*-retinal led to multiple calcium transients being observed over the light stimulation period in many cells (see *Figure 3.7* for individual transient examples). These responses were much more evident than in cells without supplementation or with all-*trans*-retinal supplementation, although the temporal changes in $Ca^{2+}$ signalling were heterogeneous and collation of the individual cell timecourses as pooled transients was not useful in determining signalling parameters. These observations were supported by the pooled data analysis (see *Figure 3.8*). In experiments using full length SNAP-labelled opto-$\alpha_{1A}$ARs stably expressed in HEK cells, the presence of 9-*cis*-retinal led to a two-fold increase in the number of calcium peaks over the 20min stimulation period (one way ANOVA,

Tukey's post test; p=0.0098); other parameters (latency, percent responders and peak change) were not significantly changed. This suggests that 9-*cis*-retinal supplementation is required for receptor stimulation.

In calcium assays using 9-*cis*-retinal supplemented HEK cells, there were no significant differences in the behaviour of opto-$\alpha_{1A}$AR -T471* and opto-$\alpha_{1A}$A-S421* mutant receptors compared to the opto-$\alpha_{1A}$AR wild type (see *Figure 3.8*). However, expression and stimulation of the opto-$\alpha_{1A}$AR-S371* mutant led to the following significant differences in calcium responses to the wild type receptor; there was a 30% increase in the percentage of cells to respond, a 0.5 fold increase in fluorescence change, and a 30% increase in the number of $Ca^{2+}$ responses (one way ANOVA, Tukey's post test; p=0.028, 0.016, 0.005, respectively). As confirmation, the S371* mutant calcium responses were also highly dependent on 9-*cis*-retinal supplementation, with a reduction in its absence (one way ANOVA, Tukey's post test; p=0.0001 percentage response, <0.0001 number of calcium transients, <0.0001 response magnitude). Overall, these data provided evidence that the S371 truncation mutant produced a more robust $Ca^{2+}$ response under stimulus compared to the wild type opto-$\alpha_{1A}$AR and the shorter T471 and S421 truncations.

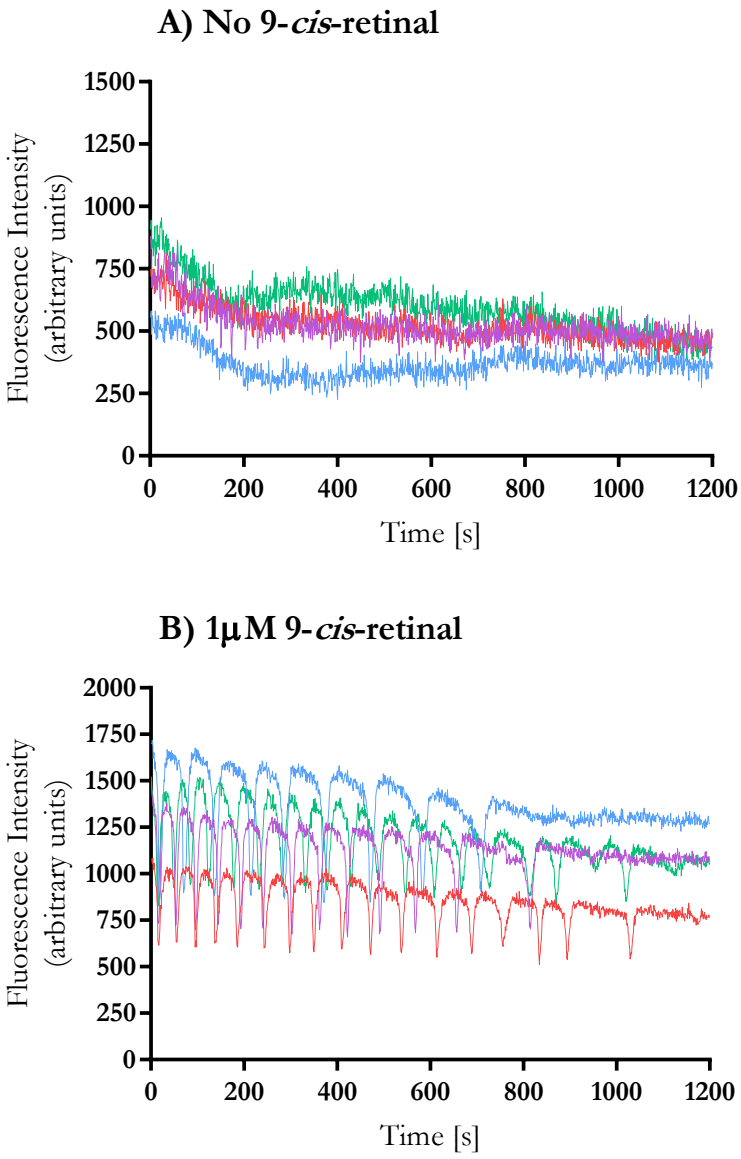


***Figure 3.7* – Representative HEK-SNAP-opto-$\alpha_{1A}$AR (wild type) responses to light stimulation measured using Fura Red $Ca^{2+}$ fluorescence.** Cells were stimulated with 488nm, 10% power laser light for 30min at 37°C. A) Cells not supplemented with retinal show no calcium responses (above, *n*=4 cells, representative of 28 cells on a single coverslip from 3 experiments). B) Supplementation with 1µM 9-*cis*-retinal (preincubated for 1hr) produces calcium peaks (*n*=4 cells, representative of 42 cells on a single coverslip from 3 experiments).

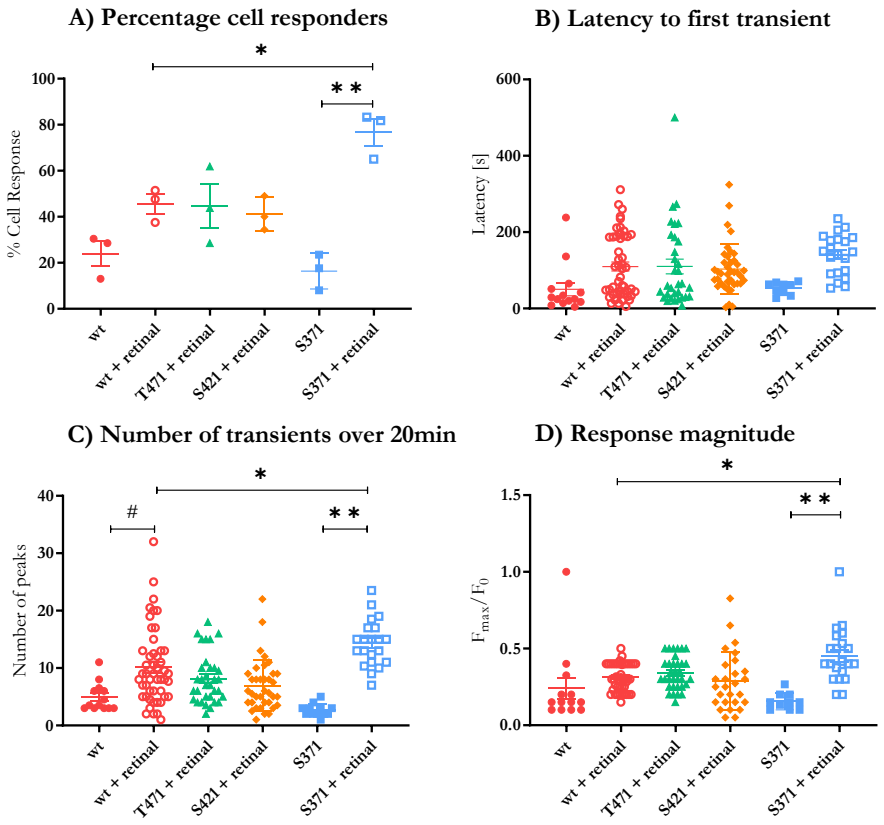


***Figure 3.8* – Different parameters of the calcium response profiles in the HEK-SNAP-opto-$\alpha_{1A}$AR cell lines measured using Fura Red.** Cells were simulated and recorded using the 488nm laser at 1 frame per second, over a 20min period. Retinal = 1μM 9-*cis*-retinal with a 1hr preincubation. A) Percentage of cells per experiment displaying Fura Red response above threshold as an indication of stimulated $Ca^{2+}$ signalling ($n$=3, with at least 16 cells per coverslip, and coverslip measurements performed in duplicate). Supplemented mutant opto-$\alpha_{1A}$AR-S371* has a significantly higher response rate per experiment than the wild type receptor, *p=0.028, and unsupplemented cells, **p=0.0001 (one way ANOVA, Tukey's post hoc). Individual cell responses (total cells, $n$≥16 from 3 experiments, showing only cells responding above threshold as described in A) can be seen in B), latency to first peak, C) number of $Ca^{2+}$ spikes, S371 mutant*p=0.0145 compared to the wild type with retinal, **p<0.0001 compared to unsupplemented cells (one way ANOVA, Tukey's post hoc); wild type #p=0.010 compared to control cells in the absence of retinal (one way ANOVA, Tukey's post hoc), and D), peak fluorescent change, S371 mutant *p=0.029 compared to the wild type with retinal, **p<0.0001 compared to unsupplemented cells (one way ANOVA, Tukey's post hoc)..

### 3.2.4 SNAP-opto-$\alpha_{1A}$ARs Undergo Internalisation in Response to Light Stimulation and 9-*cis*-retinal Supplementation in Stably Transfected HEK Cells

In order to investigate the effects of C terminal truncation on SNAP-opto-$\alpha_{1A}$AR function further, the kinetics of receptor internalisation after stimulation were monitored by confocal microscopy. Internalisation of the $\alpha_{1A}$ adrenoceptor has been shown to be dependent on β-arrestin recruitment in HEK293 cells (Chalothorn *et al.*, 2002). On this basis, an effect of the mutations on receptor internalisation might infer inhibition of β-arrestin binding to the truncated receptor, and a lack of receptor desensitisation by this process.

High light intensity (10% laser power) and constant stimulation with a 488nm laser was used on a scanning confocal microscope to activate the opto-$\alpha_{1A}$ARs in HEK cells, while simultaneously recording the intracellular trafficking of SNAP-Surface AF488 pre-labelled receptors. As the SNAP label is cell impermeant, only those receptors present at the cell surface during the labelling period are subsequently localised by fluorescence during the internalisation assay. In the absence of retinal supplementation, or when using all-*trans*-retinal for the retinoid supplementation, the majority of SNAP labelled receptor remained at the cell surface over the 30min period (see *Figure 3.9*). However, once the cell media was supplemented with 1μM 9-*cis*-retinal, the SNAP-opto-$\alpha_{1A}$AR receptors underwent internalisation to compartments within the 30min recording period, with cells showing a decrease in membrane fluorescence and an increase in punctate intracellular fluorescence.

To quantify the internalisation, analysis was carried out by measuring plasma membrane SNAP receptor fluorescence on each cell across the time period, normalised to the initial time point (see *Figure 3.11*). These traces indicated a stable membrane fluorescence intensity in the unsupplemented HEK cells for 30min; a limited reduction over this period might reflect low level internalisation of the receptor, but might also be explained by photobleaching of the AF488 fluorophore. However supplementing cells with 9-*cis*-retinal in the 1hr preincubation step led to a marked increase in the level of receptor internalisation observed (*Figure 3.9*and *Figure 3.10*). Over the 30 min period, plasma membrane intensity dropped to approximately half the initial value, a significantly greater effect than in non-supplemented cells (two-way ANOVA followed by Sidak post-test; p=0.0301

where $n$=5, $F_{(1, 4)}$=10.85). Change between the two treatments was statistically analysed using the post hoc test, and the point at which membrane fluorescence started to differ was after 12.6min (p=0.0009, t=4.60, DF=716), thus providing a potential latency for opto-$\alpha_{1A}$AR receptor internalisation. This indicates that the full length SNAP-tagged opto-$\alpha_{1A}$AR internalises in HEK cells, and this is dependent on the provision of the *cis*-retinal ligand.

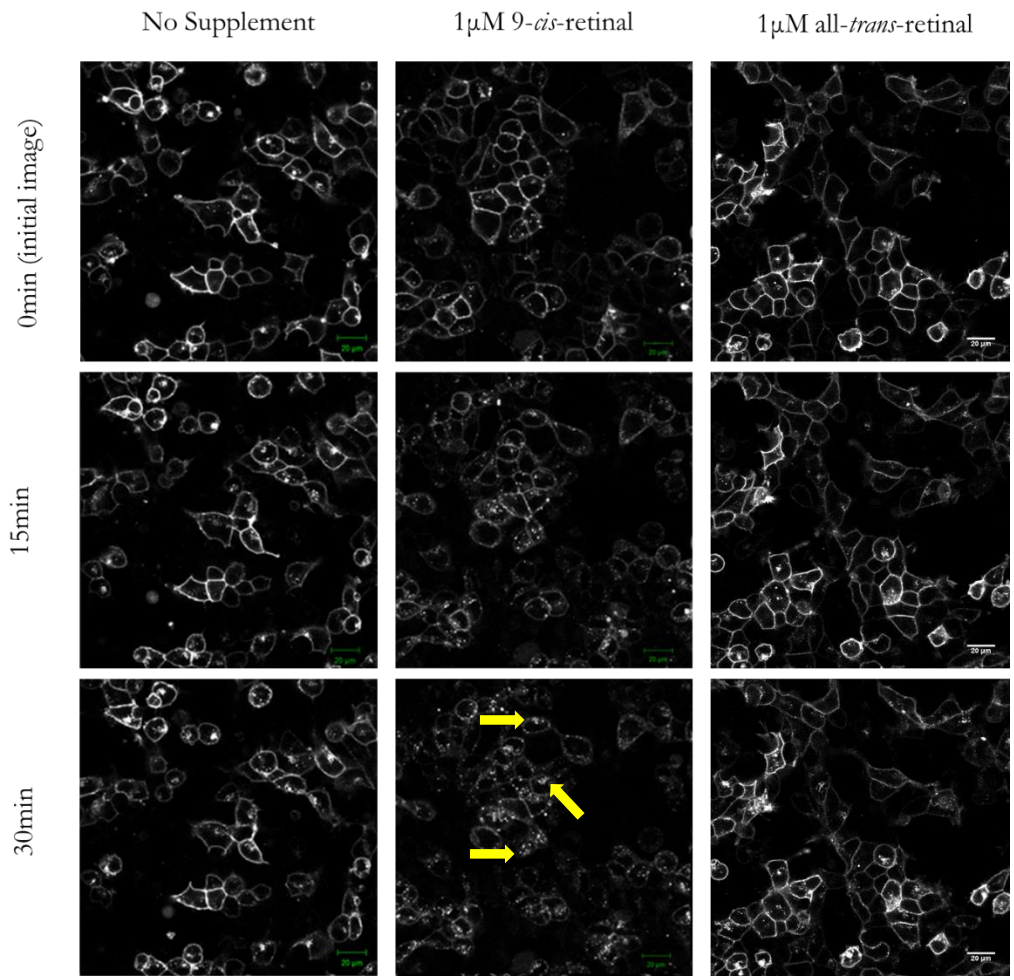


***Figure 3.9*** **– HEK-opto-$\alpha_{1A}$AR stable cell line requires 9-*cis*-retinal for receptor internalisation.** Confocal images at 0, 15 and 30min in a 30min timeseries of SNAP-Surface AF488 tagged cells. Cells were stimulated with 488nm, 10% power laser light for 30min. With no retinal supplement or supplementation with 1μM all-*trans*-retinal, there is little change in labelled receptor localisation across the time period. Supplementing with 1μM 9-*cis*-retinal shows an increase in fluorescence in intracellular compartments, a few example cells as indicated by the yellow arrows ($n$=1 for each condition, taken on the same day, representative of $n$=5 in duplicate).

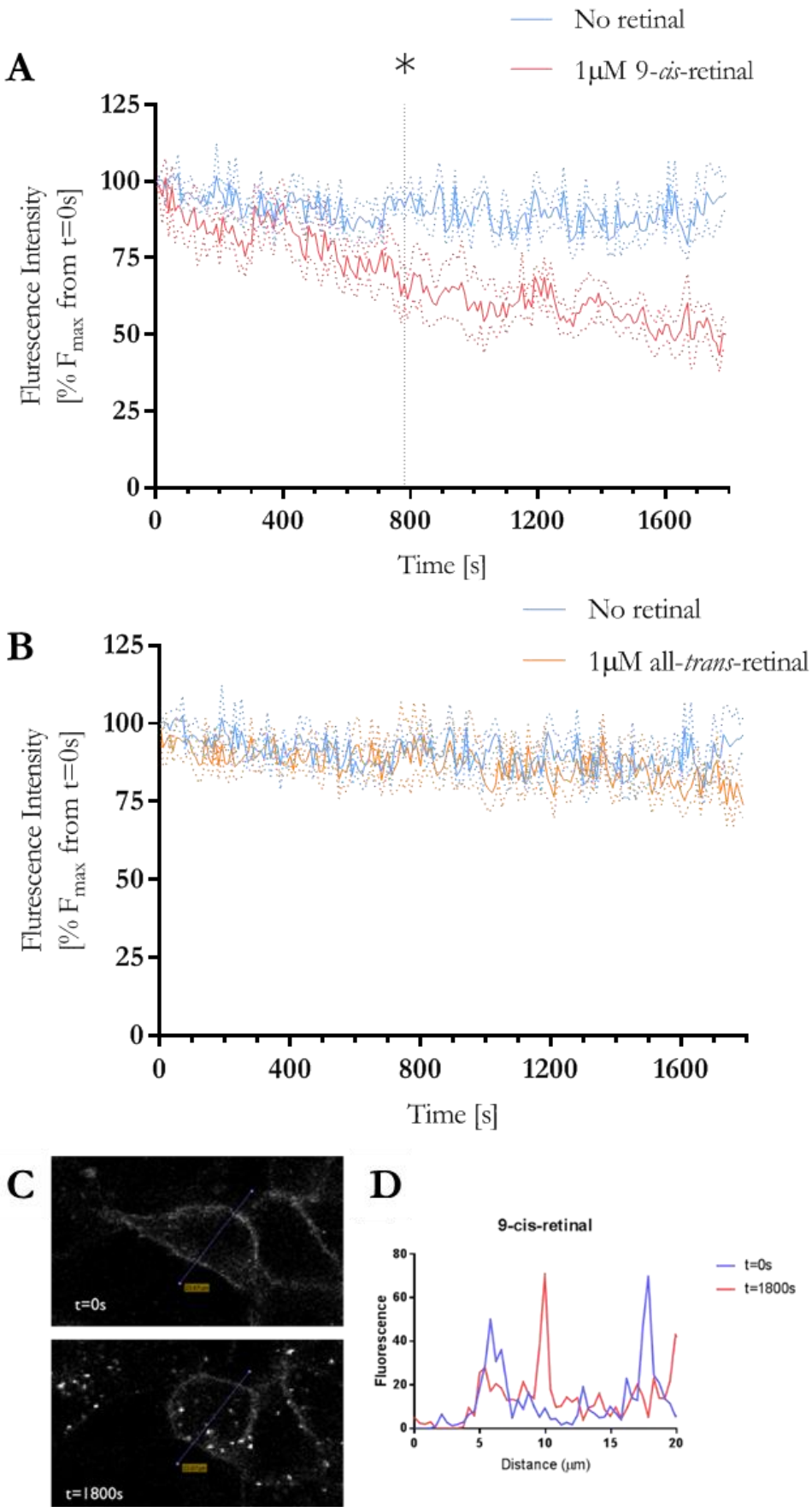
A
No retinal
1µM 9-cis-retinal
*
Flurescence Intensity
[% F max from t=0s]
125
100
75
50
25
0
0
400
800
1200
1600
Time [s]
B
No retinal
1µM all-trans-retinal
Flurescence Intensity
[% F max from t=0s]
125
100
75
50
25
0
0
400
800
1200
1600
Time [s]
C
τ=0s
τ=1800s
D
9-cis-retinal
t=0s
t=1800s
Fluorescence
80
60
40
20
0
0
5
10
15
20
Distance (µm)

***Figure 3.10* – Quantification of light stimulated opto-$\alpha_{1A}$AR internalisation using analysis of changes in plasma membrane fluorescence intensity.** HEK-SNAP-opto-$\alpha_{1A}$AR receptors were labelled with 0.5μM SNAP-Surface AF488 and stimulated with 488nm laser excitation for 30min. Receptor internalisation was measured by selecting the first plasma membrane peak in a cross section profile and measuring fluorescence over time (normalised to initial intensity), whereby reduced fluorescence was interpreted as loss of receptor at the membrane. Data are presented as the mean plasma membrane fluorescence intensity (solid line) ±SEM (dotted line). A) A 50±8% reduction in membrane fluorescence was observed with the supplementation of 1μM 9-*cis*-retinal (two way ANOVA, $p$=0.0301, $F_{(1, 4)}$=10.85, $n$=5 with each experiment performed on duplicate coverslips, and 10 cells analysed per image). The vertical line represents the timepoint where a significant difference between the supplemented and non-supplemented cells was first detected (*$p$=0.0009, t=4.60, DF=716). B) Membrane fluorescence intensity of 1μM all-*trans*-retinal supplemented cells ($n$=5 with each experiment performed on duplicate coverslips, and 10 cells analysed per image). C) and D) depict the analysis process where a line profile is drawn across the cell (C) and the first peak fluorescence is taken as the measurement of plasma membrane fluorescence.

### 3.2.5 Light-Stimulated Trafficking of Opto-$\alpha_{1A}$AR Receptors is Sensitive to Endocytosis Inhibitors

Small molecule inhibitors of internalisation machinery, Pitstop 2 and Dyngo 4a, were utilised to scrutinise the pathways involved in opto-$\alpha_{1A}$AR trafficking from the membrane. Dyngo 4a is an inhibitor of dynamin, a GTPase enzyme which cuts clathrin-coated vesicles from the plasma membrane (Mccluskey *et al.*, 2013; Jimenez-Vargasa *et al.*, 2018). Pitstop 2 is another potent inhibitor of clathrin-dependent endocytosis which interrupts internalisation dynamics by binding to the N-terminal domain of clathrin (von Kleist *et al.*, 2011; Yarwood *et al.*, 2017). There is also a potential for Pitstop 2 to block clathrin-independent endocytosis through inhibition of other cargo proteins, making it less specific in determining the endocytosis mechanism (Dutta *et al.*, 2012; Willox *et al.*, 2014).

Both Pitstop 2 and Dyngo 4a were used at a concentration of 30μM. This concentration was chosen by using previous cell based microscopy research as a reference (Jensen *et al.*, 2017; Yarwood *et al.*, 2017). Higher concentrations have been shown to be toxic to the cells, whereas a decreased concentration is ineffectual to endocytosis inhibition (Dutta *et al.*, 2012). The SNAP-tagged opto-$\alpha_{1A}$AR wild type internalisation assay (10% 488nm 30min laser excitation, 1μM 9-cis-retinal supplementation and 0.5μM SNAP-Surface AF488) produced reduced opto-$\alpha_{1A}$AR trafficking in the HEK cells treated either with Pitstop 2 or Dyngo 4a (*Figure 3.11*). Quantification of the maximum fluorescence intensity of the membrane over time revealed that Pitstop 2 treatment caused a decrease in receptor trafficking, with membrane fluorescence intensity only falling by 12±8% after 30min stimulation (*Figure 3.12*). This was significantly different to control cells, which displayed a 50±4% drop in membrane fluorescence after 30min stimulation (two-way ANOVA followed by Sidak post-test, p=0.0040 where $n$=5, $F_{(1, 4)}$=35.45), with the first timepoint to show a reduction compared to control cells at 13min (p=0.0454, t=3.7, DF=716), similar to the response seen in cells not treated with 9-*cis*-retinal. Dyngo 4a also produced a reduction in receptor trafficking, with membrane fluorescence decreasing 18±2% after 30min sitmulation, which was significant when compared to controls (two-way ANOVA followed by Sidak post-test, p=0.2280 where n=5, $F_{(1,4)}$=13.57).

Sensitivity to both Dyngo 4a and Pitstop 2 indicates that opto-$\alpha_{1A}$AR trafficking in this assay is dynamin and clathrin mediated. Increased inhibition of receptor endocytosis by Pitstop 2 over Dyngo 4a suggests there may also be clathrin independent factors to the receptor trafficking.

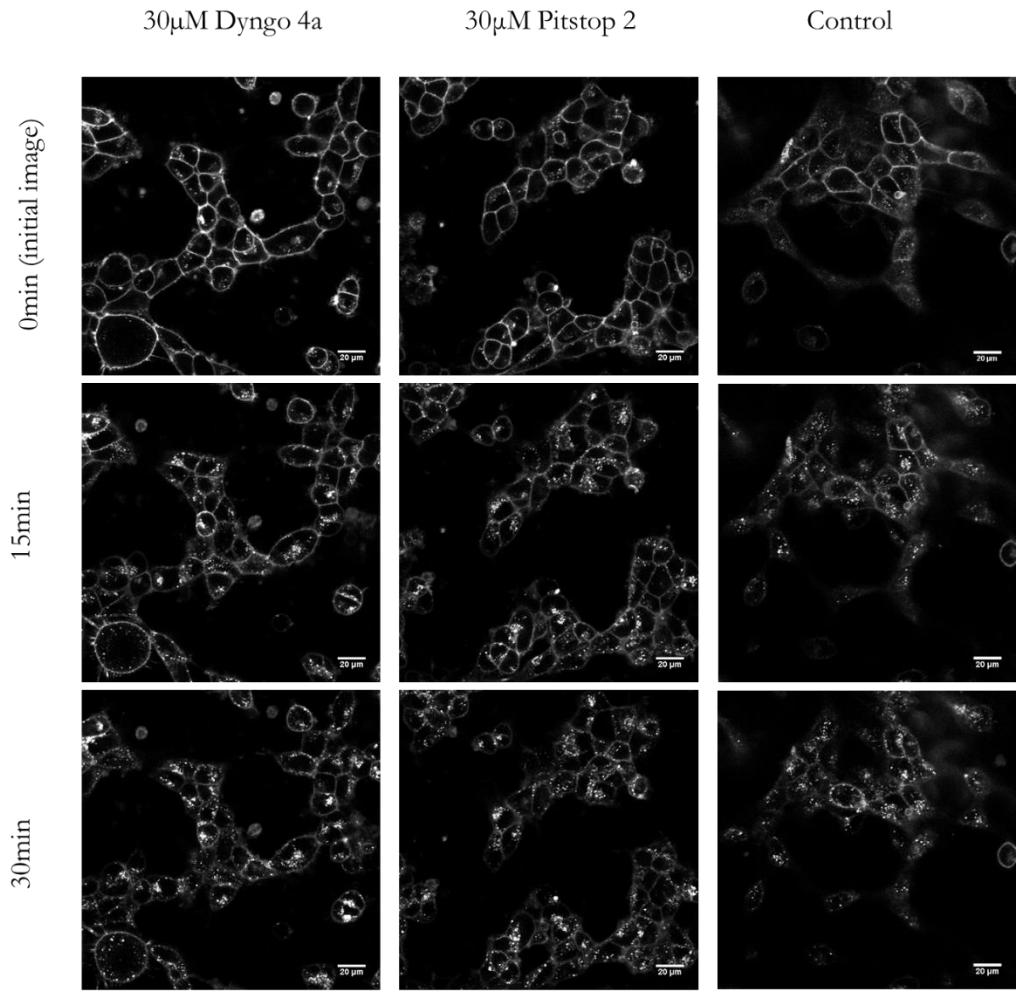


***Figure 3.11* – The effect of clathrin and dynamin inhibitors on SNAP-opto-$\alpha_{1A}$AR internalisation.** Confocal images at 0, 15 and 30min in a 30min timeseries of SNAP-Surface AF488 (0.5μM) tagged cells. Cells were stimulated with 488nm, 10% power laser light for 30min. There is more plasma membrane expression of the SNAP-tagged receptors when the cells were preincubated with Dyngo 4a or Pitstop 2 endocytosis inhibitors (both 30μM, 30min) ($n$=1 for each condition, representative of $n$=5 in duplicate).

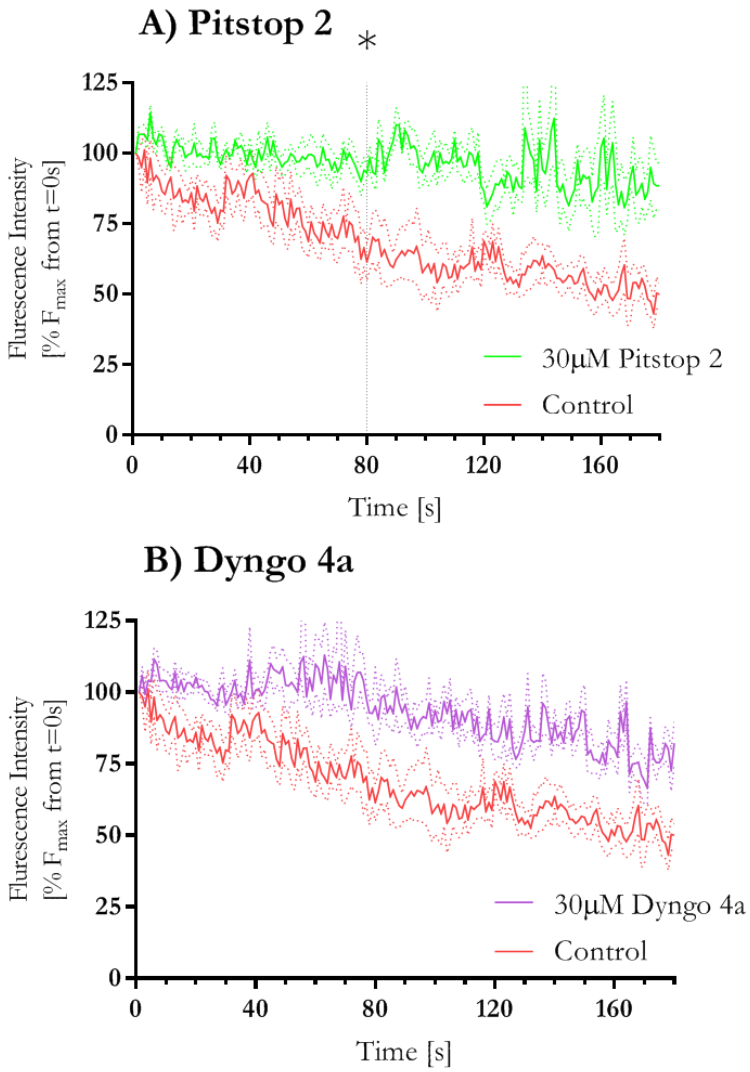


***Figure 3.12*** **– Analysis of changes in plasma membrane fluorescence intensity of SNAP tagged opto-$\alpha_{1A}$AR following light stimulation, in the absence and presence of endocytosis inhibitors.** HEK-SNAP-opto-$\alpha_{1A}$AR receptors supplemented with 9-*cis*-retinal (1µM) were labelled with SNAP-Surface AF488 (0.5µM, 30min incubation) and stimulated with 488nm, 10% power laser excitation for 30min in the presence of either Pitstop 2 (A) or Dyngo 4a (B) (both 30µM). The vertical line in A) represents the timepoint where a significant difference between the Pitstop 2 treated and non-treated cells is first detected, *$p$=0.0040 (two way ANOVA, , Sidak post hoc, $F_{(1, 4)}$=35.45). Dyngo 4a treated cells show increased membrane trafficking compared to Pistop 2 treated cells. For all conditions, $n$=5 with each experiment performed on duplicate coverslips, and 10 cells analysed per image.

### 3.2.6 Internalisation of Opto-$\alpha_{1A}$AR under Retinal Supplementation is Dependent on Excitaiton Wavelength

One disadvantage of the experimental protocol in section 3.2.4 is that the 488nm excitation used to stimulate rhodopsin activation is the same as that to image the receptor localisation, and consequently the response. Thus excitation parameters for rhodopsin stimulation (e.g. time, dynamics, magnitude) cannot be independently controlled from those needed to image receptor internalisation over time. As a consequence, SNAP-Surface AF647 labelling and imaging of SNAP-opto-$\alpha_{1A}$AR cells, at 647nm excitation, was investigated as a means of deconvolving activation and imaging protocols. Here it was used to determine whether internalisation of the retinal supplemented opto-$\alpha_{1A}$AR receptor was an active process through blue-green light activation, based on the peak excitation range of rhodopsin (peak 500nm, tails off at 600nm; see Tsukamoto and Terakita, 2010).

Stimulation with 647nm laser excitation (10 % laser power) did not produce trafficking of the opto-$\alpha_{1A}$AR receptor away from the plasma membrane, even with 1μM 9-*cis*-retinal supplementation (*Figure 3.13*). When the membrane fluorescence intensity was quantified over the 30min, there was no significant difference between absence and supplementation of retinal (two-way ANOVA with Sidak post hoc, $p=0.5899$, $F_{(1, 2)}=0.40$, $n=3$) and there was only a small decrease in membrane fluorescence (*Figure 3.14*). This small decrease under both conditions was likely attributed to fluorophore bleaching, as shown in the images where the fluorophore loses brightness over time regardless of spatial orientation in the cell (*Figure 3.13*). Thus wavelengths of light stimulation within the excitation range of rhodopsin are required to cause membrane trafficking of the opto-$\alpha_{1A}$AR receptor, indicating that previous receptor trafficking under 488nm laser stimulation is likely to be associated with light-stimulated opto-$\alpha_{1A}$AR activation.

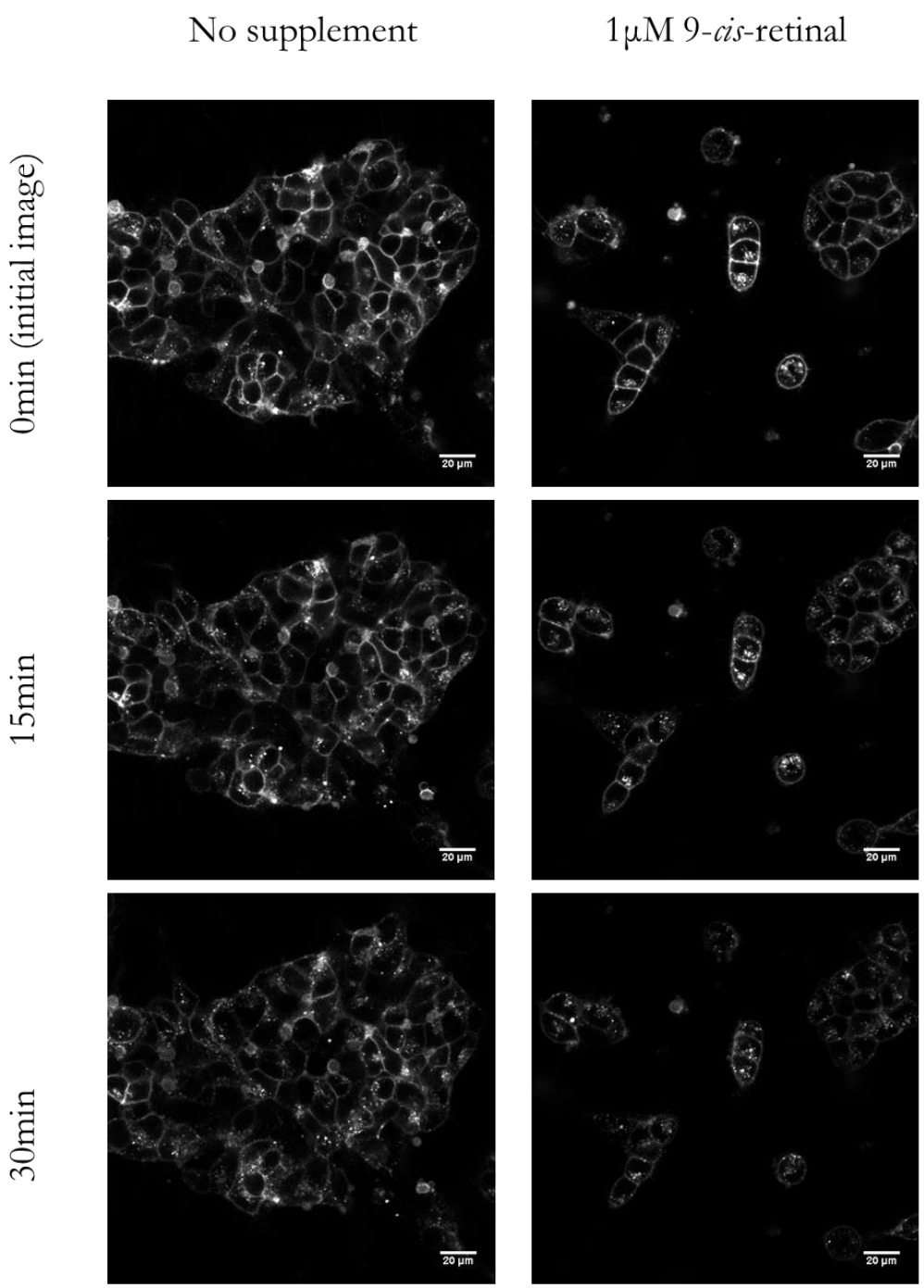


***Figure 3.13* – SNAP-opto-$\alpha_{1A}$AR receptor internalisation is dependent on the wavelength of laser excitation.** Confocal images are illustrated at 0, 15 and 30min in a 30min timeseries of SNAP-Surface AF647 tagged cells (0.5μM, 30min incubation). Cells were stimulated with 647nm, 20% power laser light for 30min. (*n*=1 for each condition, representative of *n*=3 in duplicate).

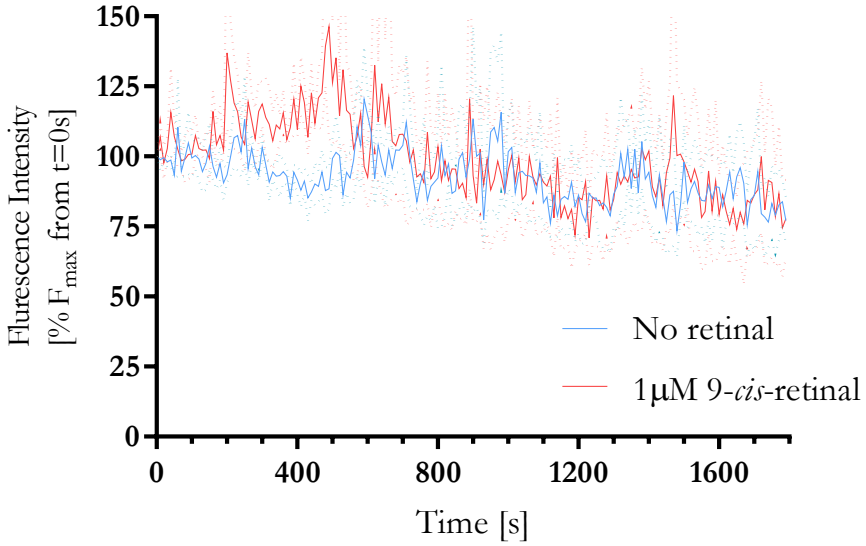


***Figure 3.14* – Quantification of changes in plasma membrane fluorescence intensity of SNAP tagged opto-$\alpha_{1A}$AR under red light stimulation.** HEK-SNAP-opto-$\alpha_{1A}$AR cells were labelled with SNAP-Surface AF647 and stimulated with 647nm laser excitation for 30min in the presence and absence of 9-cis-retinal (1µM). There was no difference between the two conditions and there was no detection of a decrease in membrane fluorescence in the retinal-supplemented cells compared to no retinal (two way ANOVA, p=0.5899, $F_{(1, 2)}$=0.40, n=3 with each experiment performed on duplicate coverslips, and 10 cells analysed per image).

### 3.2.7 Carboxyl Terminus Truncation of Opto-$\alpha_{1A}$AR Affects Receptor Internalisation

Using the combined 488nm imaging and excitation protocol as described for the full length opto-$\alpha_{1A}$AR receptor, the localisation and light stimulated intracellular trafficking of the three C tail truncation mutants were investigated. These displayed different internalisation properties depending on the location of the truncation.

Using SNAP-Surface AF488 labelling, SNAP-opto-$\alpha_{1A}$AR-T471* receptors were predominantly localised to the HEK293 cell surface, as for the full length construct, and also underwent a similar degree of light stimulated internalisation only in the presence of 9-*cis*-retinal (*Figure 3.15*). However further truncation at S421 and S371 residues led a differing internalisation profiles from full length receptors. Both mutants in unstimulated cells were expressed at the cell surface, but there was evidence of somewhat greater constitutive internalisation compared to the full length SNAP-opto-$\alpha_{1A}$AR (*Figure 3.16* and *Figure 3.17* compared to *Figure 3.15*), in the absence or presence of 1μM 9-*cis*-retinal. Moreover, both mutants appeared resistant to further light stimulated endocytosis over a 30 min period.

These differences between the truncation mutants were confirmed in the quantified data (*Figure 3.18*). A similar sized reduction in membrane fluorescence intensity was observed for T471 compared to the full length receptor over 30 min, demonstrating that this mutant internalised effectively on exposure to light (two-way ANOVA followed by Sidak post-test; $p<0.0001$ where $n=5$, $F_{(1, 4)}=2.06$). Following post hoc analysis, the point at which the membrane fluorescence significantly changes between the two treatment groups was after 8.0min ($p=0.002$, $t=2.53$, $DF=358$). In contrast, no significant difference was detected between untreated and retinal-treated conditions for the S421 or the S371 truncation (two-way ANOVA followed by Sidak post-test; $p=0.992$ where $n=3$, $F_{(179, 358)}=0.727$). For both S421 and S371 mutants, the decline in the membrane fluorescence intensity over time in the absence of retinal was more rapid than for the full length or T471 receptors, with a statistically significant reduction at 30 min compared to the initial time point opto-$\alpha_{1A}$AR, suggesting that these receptors may undergo more constitutive internalisation. In contrast to full length and T471 experiments, retinal supplementation did not significantly enhance the rate of internalisation over the

light stimulation period. In light of these findings, it appears different regions of the carboxyl terminus may have roles in agonist-stimulated and constitutive internalisation of the opto-$\alpha_{1A}$AR.

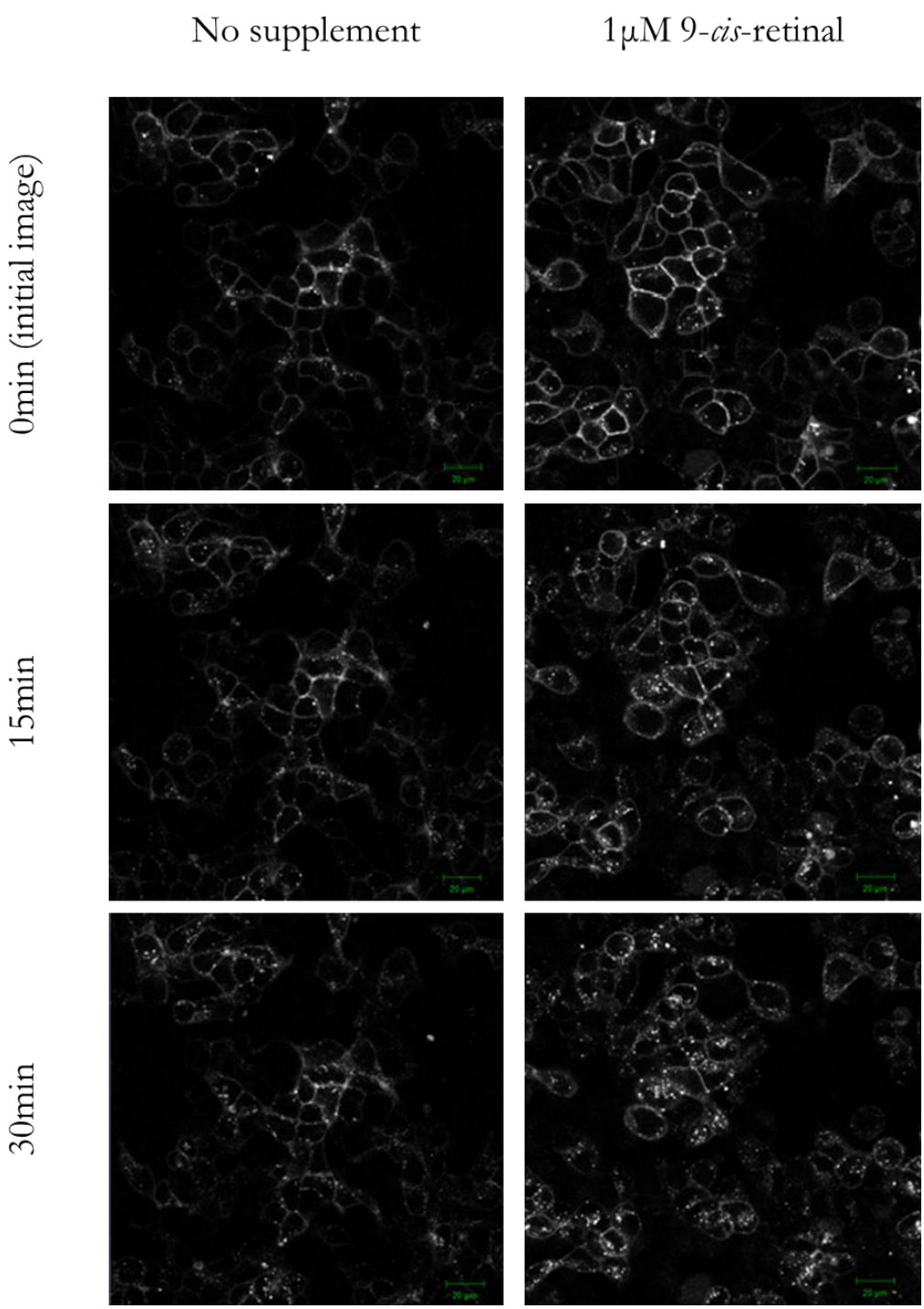


***Figure 3.15* – HEK-opto-$\alpha_{1A}$AR-T471* internalises under light stimulation, requiring 9-*cis*-retinal.** Confocal images at 0, 15 and 30min in a 30min timeseries in SNAP-Surface AF488 tagged (0.5μM, 30 min incubation) cells. Cells were stimulated with 488nm laser at 10% power (*n*=1 for each condition, representative of *n*=3 in duplicate).

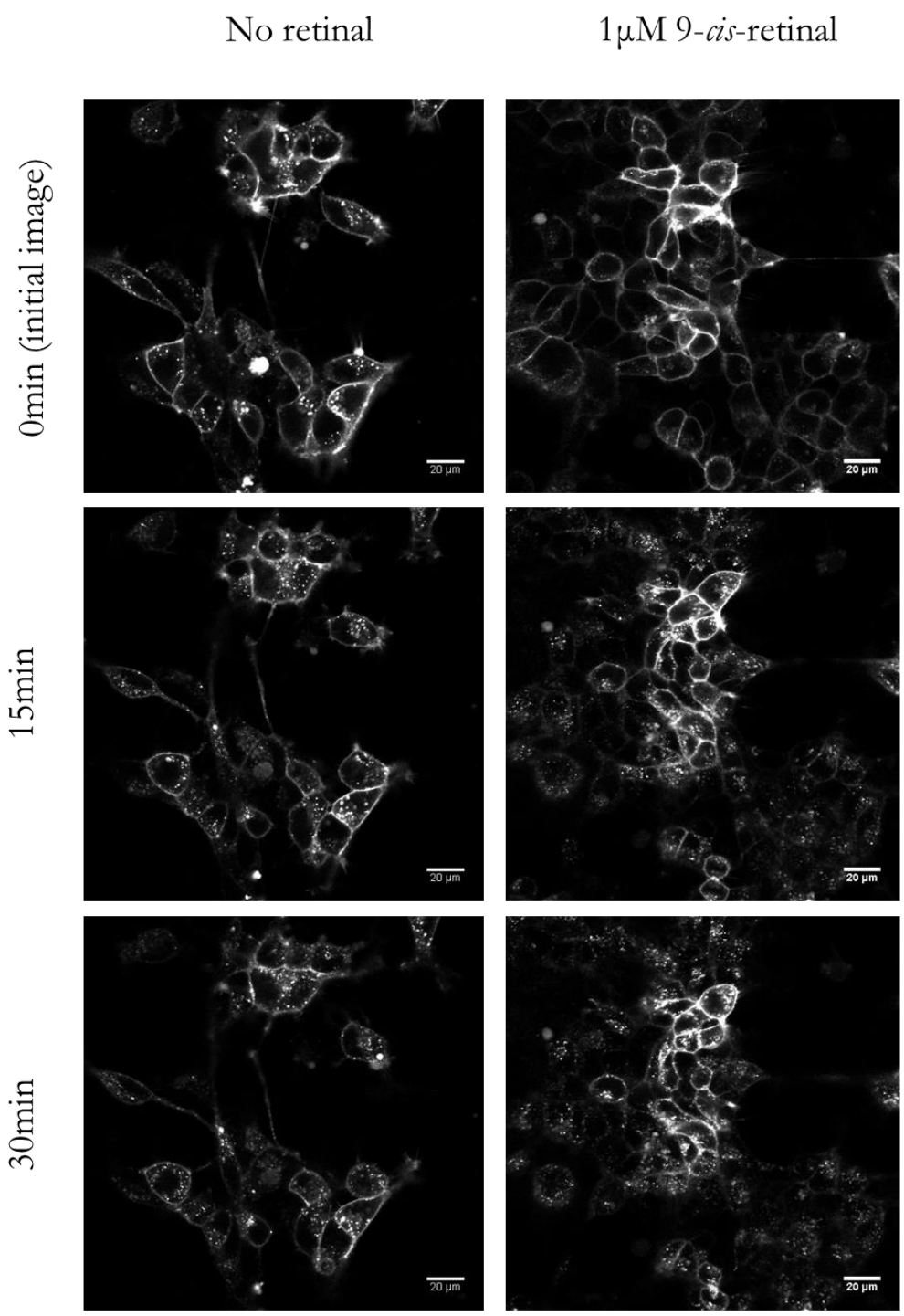


***Figure 3.16* – Equivalent trafficking of the opto-$\alpha_{1A}$AR-S421* mutant with or without 9-*cis*-retinal and light stimulation.** Confocal images at 0, 15 and 30min in a 30min timeseries in SNAP-Surface AF488 tagged (0.5μM, 30 min incubation) cells show increased internalisation of labelled receptors away from the membrane. Cells were stimulated with 488nm laser at 10% power ($n$=1 for each condition, representative of $n$=3 in duplicate).

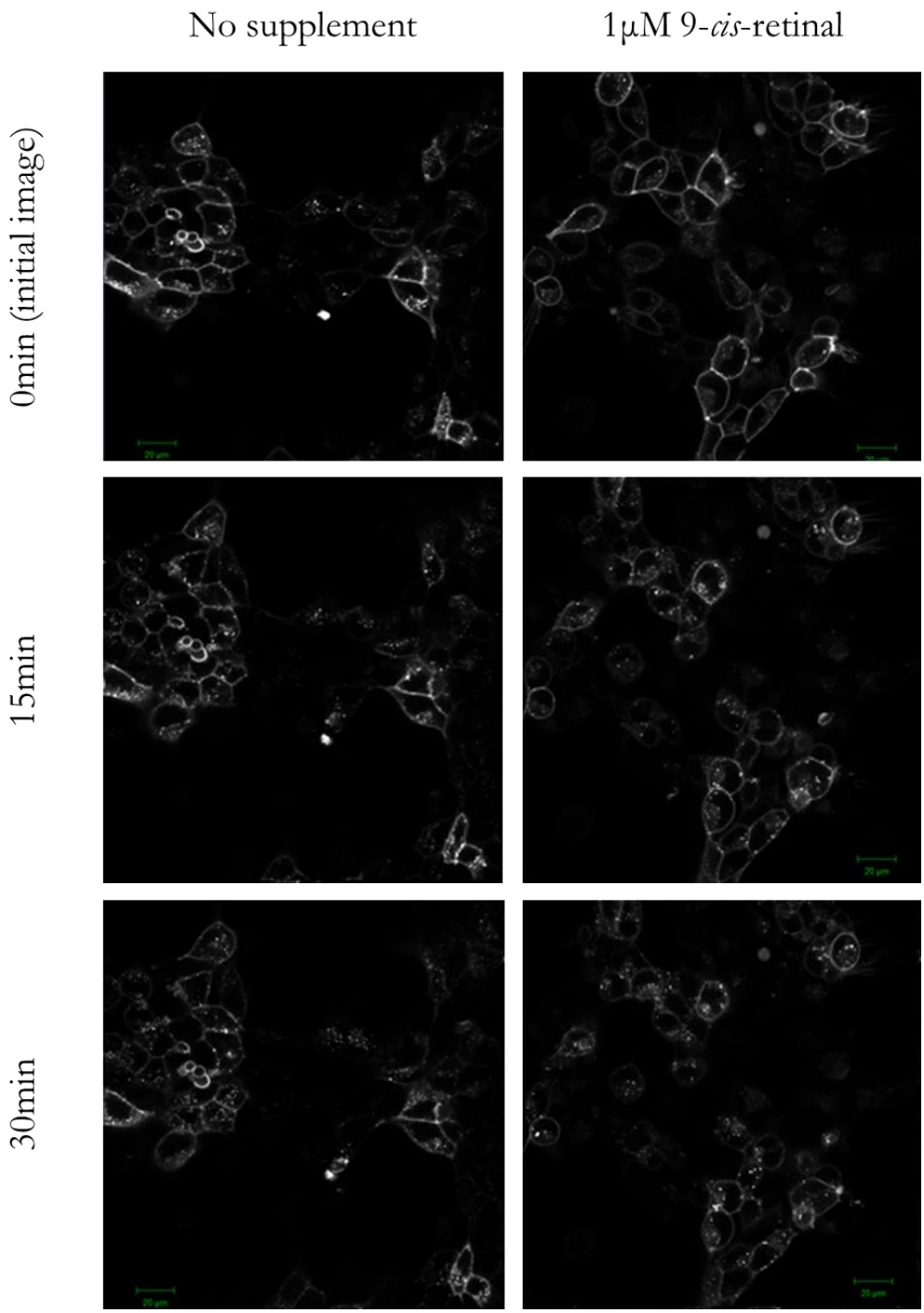


***Figure 3.17*** **– Opto-$\alpha_{1A}$AR-S371* receptors undergo a similar degree of internalisation, with or without 9-*cis*-retinal, after 488 nm light stimulation.** Confocal images at 0, 15 and 30min in a 30min timeseries in SNAP-Surface AF488 tagged HEK-SNAP-**o**pto-$\alpha_{1A}$AR-S371* cells (0.5μM, 30 min incubation). Constitutive internalisation of cell surface receptors is evident in the absence and presence of 1μM 9-*cis*-retinal supplement. Cells were stimulated with 488nm laser at 10% power ($n$=1 for each condition, representative of $n$=3 in duplicate).

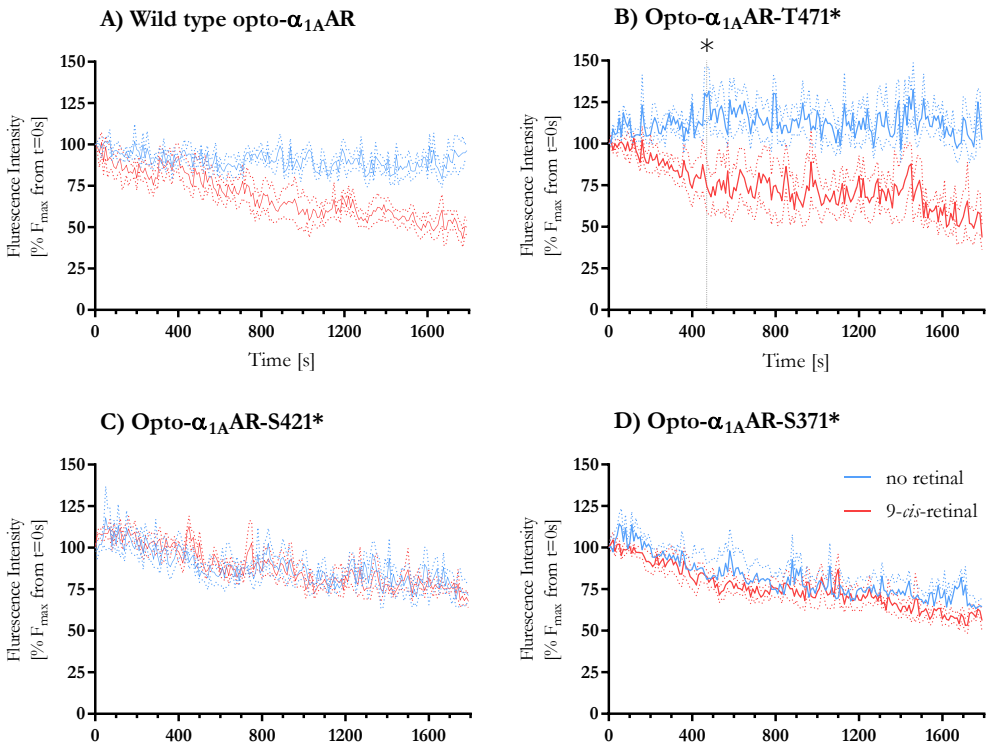


***Figure 3.18* – Analysis of changes in plasma membrane fluorescence intensity of SNAP tagged opto-α$_{1A}$AR truncated mutants in HEK293 cells.** Receptors were labelled with SNAP-Surface AF488 (0.5μM, 30 minute incubation) and stimulated with 488nm 10% power laser excitation for 30min with or without 1μM 9-*cis*-retinal supplementation. A) Recap of wild type opto-α$_{1A}$AR internalisation upon laser stimulus and 9-*cis*-retinal supplementation, as seen in *Figure 3.11*. B) SNAP-opto-α$_{1A}$AR-T471* mutant showed a 50% decrease in membrane fluorescence over 30min with 1μM 9-*cis*-retinal compared to non-supplemented cells *$p$=0.0053 (two way ANOVA, $F_{(1, 4)}$=30.47). C) SNAP-opto-α$_{1A}$AR-S421* and S371* (D) mutants show trafficking away from the membrane independent of retinal ($n$=3-5 with experiments performed in duplicate, 10 cells per image).

### 3.2.8 Endocytosis Inhibitors Insufficient for Blocking Opto-$\alpha_{1A}$AR-S371* Internalisation

To help determine the mechanism of opto-$\alpha_{1A}$AR-S371* receptor constitutive internalisation, endocytosis inhibitors Pitstop 2 and Dyngo 4a were used to see if mutant receptor trafficking was dependent on clathrin or dynamin (*Figure 3.19*). Inspection of the images indicated that endocytosis might be inhibited in some cells, but not in others. However the quantified data did not demonstrate a significant effect on constitutive internalisation of the opto-$\alpha_{1A}$AR-S371* (*Figure 3.20*). These data suggest that there may be more than one mechanism in action for the receptor trafficking seen in the mutant.

### 3.2.9 Truncation of Opto-$\alpha_{1A}$AR at $Ser^{371}$ Internalises Independent to Light Stimulation

As with the wild type opto-$\alpha_{1A}$AR, the S371 mutant was also labelled with SNAP-Surface AF647, supplemented with 9-*cis*-retinal and tracked under 647nm red light stimulus to determine if internalisation depended on effective stimulation of the chimeric receptor (see section 3.2.6 for wild type opto-$\alpha_{1A}$AR response). *Figure 3.21* demonstrates that under these conditions internalisation of the receptor was still detected. When the membrane fluorescence intensity was quantified over the 30min time series, there was no significant difference between absence and supplementation of retinal (two-way ANOVA with Sidak post hoc, $p=0.5899$, $F_{(1, 2)}=0.40$, $n=3$) and still a $46\pm6\%$ decrease in membrane fluorescence compared to time 0 (*Figure 3.22*). Internalisation independent of a 488nm stimulus indicated that the opto-$\alpha_{1A}$AR-S371* receptor may undergo constitutive internalisation without receptor activation.

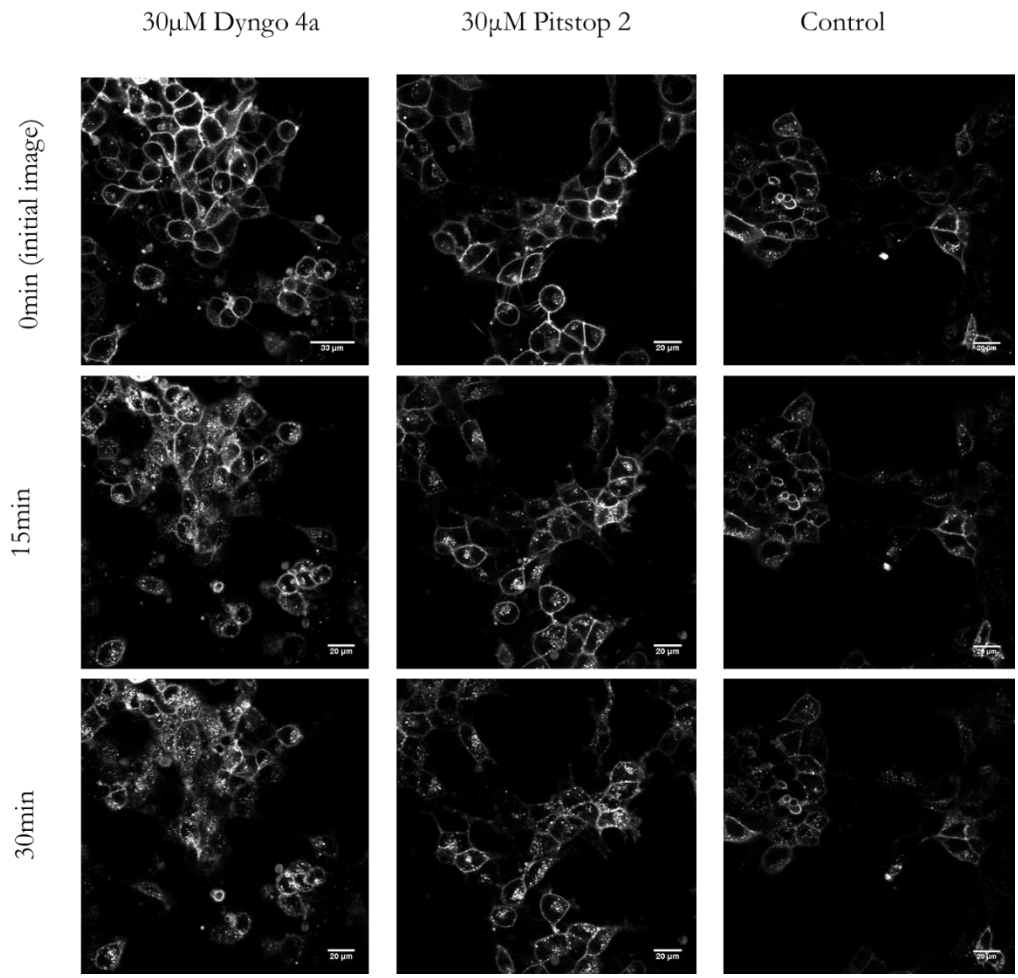


***Figure 3.19*** **– Opto-$\alpha_{1A}$AR-S371* receptors continue to show constitutive trafficking from the membrane in the presence of clathrin or dynamin inhibitors.** Confocal images at 0, 15 and 30min in a 30min timeseries in SNAP-Surface AF488 tagged cells (0.5μM with 30min preincubation) stimulated with 488nm 10% laser in the presence of 1μM 9-*cis*-retinal with 30μM Dyngo 4a or Pitstop 2 (*n*=1 for each condition, representative of *n*=3 in duplicate).

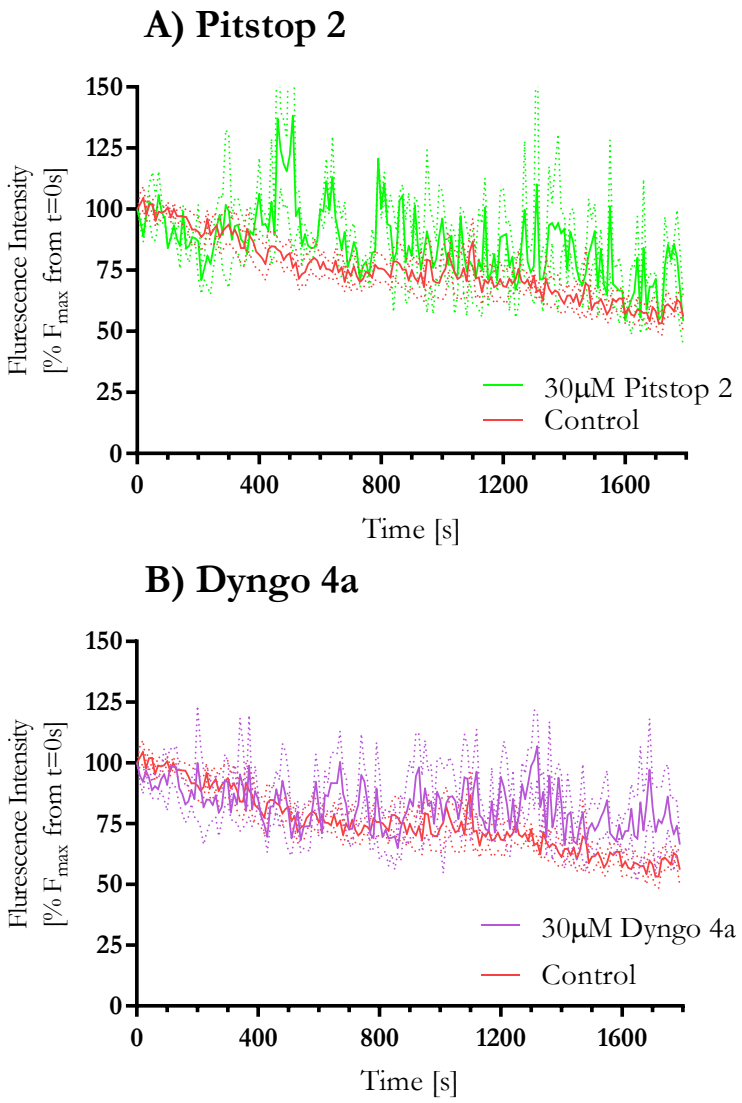


***Figure 3.20*** **– Analysis of changes in plasma membrane fluorescence intensity of SNAP tagged opto-$\alpha_{1A}$AR-S371 mutant with endocytosis inhibitors.** HEK-SNAP-opto-$\alpha_{1A}$AR-S371 cells were labelled with SNAP-Surface AF488 (0.5μM 30min preincubation), supplemented with 1μM 9-*cis*-retinal and stimulated with 488nm laser at 10% power for 30minin in the presence of either Pitstop 2 or Dyngo 4a (both 30μM). Neither Pitstop 2 nor Dyngo 4a completely ablate receptor trafficking from the membrane ($n$=3 with each experiment performed on duplicate coverslips, and 10 cells analysed per image).

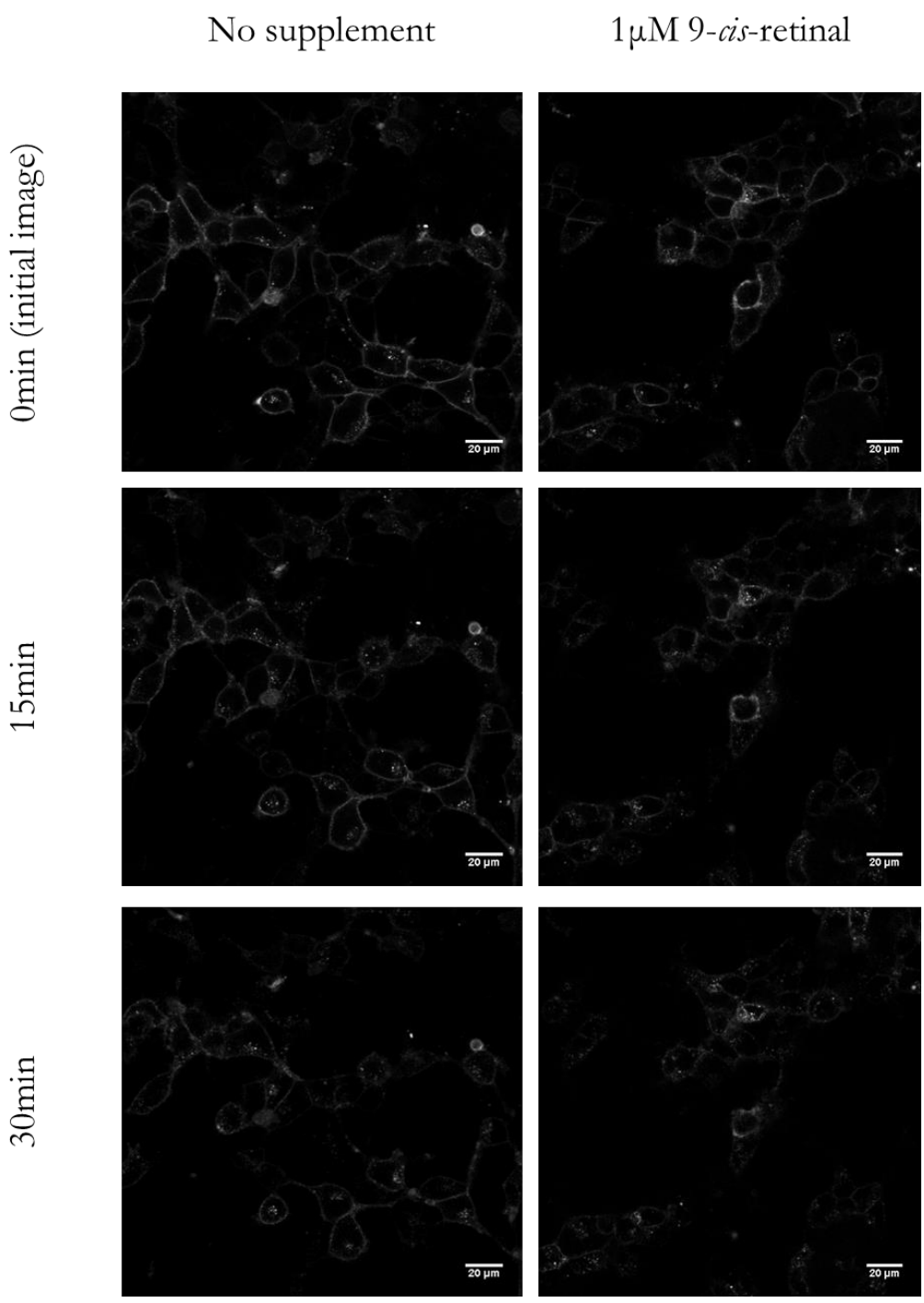


***Figure 3.21* – HEK-opto-$\alpha_{1A}$AR-S371* cell line shows receptor trafficking from the membrane without green 488nm laser stimulus.** Confocal images at 0, 15 and 30min in a 30min timeseries in SNAP-Surface AF647 tagged cells (0.5μM, 30min incubation) stimulated with a 647nm 20% power laser. Labelled receptors show trafficking away from the membrane to intracellular compartments regardless of 1μM 9-*cis*-retinal supplementation. (*n*=1, representative of *n*=3 coverslips in duplicate).

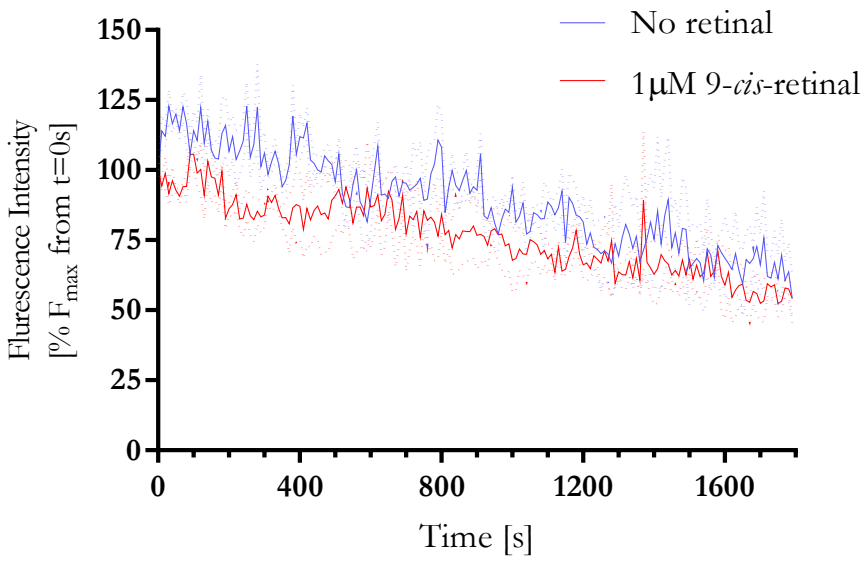


***Figure 3.22* – Quantification of changes in plasma membrane fluorescence intensity of SNAP tagged truncated opto-$\alpha_{1A}$AR-S371* under red light stimulation.** HEK-SNAP-opto-$\alpha_{1A}$AR-S371* cells were labelled with SNAP-Surface AF647 and stimulated with 647nm laser excitation for 30min in the presence and absence of 9-*cis*-retinal (1μM). Under both conditions, the membrane localised fluorescence declines with no difference between retinal supplementation and its absence ($n$=5 with each experiment performed on duplicate coverslips, and 10 cells analysed per image).

## 3.3 Discussion

In this chapter SNAP-tagged versions of the opto-$\alpha_{1A}$AR were successfully generated. These receptor constructs produced calcium signalling responses to light activation and allowed for monitoring of light stimulated internalisation by confocal microscopy of the opto-$\alpha_{1A}$AR for the first time. The characteristics for effective stimulation of the opto-$\alpha_{1A}$AR in HEK293 cells were established which included the need for a high intensity laser stimulation and 9-*cis*-retinal supplementation. Calcium signalling and internalisation dynamics were successfully manipulated by C tail truncation mutants, generating an opto-$\alpha_{1A}$AR construct with an extended calcium stimulus profile (truncation mutant at $Ser^{371}$) and a mutant with differential actions on calcium and internalisation endpoints (truncation mutant at $Ser^{421}$). Future studies should explore the molecular basis of these findings, for example the PKC versus GRK phosphorylation and arrestin mechanisms.

### 3.3.1 SNAP-tagged Opto-$\alpha_{1A}$ARs are Functional

The N terminal modification of the SNAP tag is based on acyl guanine transferase, of which the substrate is benzyl guanine linked to fluorophore, leading to irreresible labelling with the fluorophore linker of the enzyme active site Ser (Maurel *et al.*, 2008). This is a large 180 amino acid addition which could affect receptor function. This was not the case with the opto-$\alpha_{1A}$AR, consistent with other studies where the SNAP-receptor is functional. One major advantage of the SNAPtag as a receptor label instead of an intrinsically fluorescent protein, such as GFP, is the versatility, as substituting different fluorophores or other functions, such as biotin or blocking agents, requires no new cloning or expression.

### 3.3.2 Single vs Continuous Laser Light Stimuli

Although the SNAP-opto-$\alpha_{1A}$AR constructs were functional, light activation in these experiments required a high intensity laser stimulus. The optogenetic $\alpha_{1A}$ adrenoceptor was designed and tested by Airan et al. (2009) in which they demonstrated $G_q$ associated endpoints including an increase in IP1 (a degradation product of IP3), calcium ions and neuron firing rate when stimulated by light in various systems, using 60s of 500nm light ($7mW.mm^{-2}$) to achieve their results. In

this chapter, a SNAP labelled version of the opto-$\alpha_{1A}$AR was used to investigate signalling and changes in receptor localisation. The SNAP construct was capable of functional calcium and internalisation responses in response to continual 488nm light stimulation across the field of view, however any experiments utilising only a single localised laser stimulus, for a limited duration proved ineffective. It is unclear as to why the single light stimulus does not work in the new construct as it seems unlikely that the N-terminal SNAP protein would by itself affect light induced isomerisation of the rhodopsin and activation. Difference in experimental setup may mean that the SNAP-opto-$\alpha_{1A}$AR is not being stimulated as effectively under the protocols used. For instance, in the Airan et al. (2009) study an external 500nm xenon light was used with a spinning disk confocal microscope for the *in vitro* work, potentially allowing more powerful stimulation and quicker recordings. Constant lower power stimulation throughout the time course has still proved fruitful in this study, without evidence of phototoxicity, and notably calcium responses and internalisation was observed within early timepoints (<5 min) after the onset of this stimulation. The protocol also replicates a continued agonist exposure across a time frame in typical pharmacological assays.

### 3.3.3 Retinal Supplementation Improves Opto-$\alpha_{1A}$AR Responses

For both calcium and internalisation assays, supplementation with 9-*cis*-retinal was crucial in enhancing the light stimulated responses. When using in vitro cell lines as the model recombinant system, such as HEKs, several studies using native or chimeric opsins have chosen to supplement the media with 9-*cis*-retinal (Cao *et al.*, 2012; Siuda *et al.*, 2015), 11-*cis*-retinal (Karunarathne *et al.*, 2013), or all-*trans*-retinal (Airan *et al.* 2009, supplementary). Although 11-*cis*-retinal is the most abundant isomer found endogenously, 9-*cis*-retinal was selected for supplementation as the more stably stored molecule that displays a very similar excitation energy and photoisomeration profile, and arguably could also be used in physiology or pathophysiological states, such as a lack of 11-*cis*-retinal synthesis machinary (Fan *et al.*, 2003; Sekharan and Morokuma, 2012). Isorhodopsin, the analog of rhodopsin bound with 9-cis-retinal, is functional but does display slower photoisomerisation dynamics (600fs isorhodopsin vs 200fs rhodopsin), meaning slower activation

(Schoenlein *et al.*, 1993). Airan et al. (2009) used all-*trans*-retinal to characterise the optoXR chimeras in HEK cells, which seems an unwise choice as in the *trans* conformation the molecule is already in the 'active' formation and might directly stimulate the apo-receptors without the need for light, whereas any *cis*-retinal labelled receptors would only be activated under light stimulation. Here, supplementing with all-*trans*-retinal was not sufficient to produce a receptor response. Indeed, Cao *et al.* (2012) used both the *cis* and *trans* retinals in their *Caenorhabditis elegans* assay to study rhodopsin and melanopsin activation, and only found compelling evidence for enhanced activation using the *cis* conformation.

### 3.3.4 Calcium Oscillations Produced by HEK-opto-$\alpha_{1A}$AR Continuous Stimulation

In the full length opto-$\alpha_{1A}$AR, calcium oscillations were generated by a sustained light stimulus, although this still allows for an on/off pattern using a laser scan, rather than a simple continual light. Previous studies have not utilised a continual laser stimulation before, but several studies have used a repeated stimulation of opto-$\alpha_{1A}$AR between long dark periods to generate multiple calcium transients (Airan *et al.*, 2009; Figueiredo *et al.*, 2014). Using extracellular $Ca^{2+}$ to drive calcium oscillations in a calcium-sensing receptor HEK293 cell line, Szekely *et al.* (2009) found that the frequency of oscillations were around $4min^{-1}$ under normal conditions and required a critical $Ca^{2+}$ concentration of 2mM. This is slower than the observed oscillations seen in the HEK-SNAP-opto-$\alpha_{1A}$AR cell line, though this could be receptor/activator dependent. Indeed, $Ca^{2+}$ oscillations as fast as the ones seen in this study have been reported (Dupont *et al.*, 2011). It is thought that the mechanism is release from $Ca^{2+}$ from intracellular stores and from the extracellular environment, although not always needed. Store-operated $Ca^{2+}$ channels drive the response, creating a calcium-release-activated calcium current (Dupont *et al.*, 2011).

### 3.3.5 Similarities in Internalisation Profile between the Opto-$\alpha_{1A}$AR and $\alpha_{1A}$-adrenoceptor

The subcellular localisation of the full length SNAP-tagged opto-$\alpha_{1A}$AR was broadly similar to that reported for the endogenous $\alpha_{1A}$ adrenoceptor, with mostly plasma membrane expression but some intracellular presence (Chalothorn *et al.*,

2002). Compared to the $\alpha_{1B}$ adrenoceptor subtype, the $\alpha_{1A}$ subtype is reported to undergo a lower level of agonist stimulated internalisation and desensitisation, and studies with up to 60min required for complete internalisation of the receptor following agonist stimulation (Chalothorn *et al.*, 2002; Morris *et al.*, 2004), and even the absence of significant internalisation under some conditions (Stanasila *et al.*, 2008). The opto-$\alpha_{1A}$AR also required 30min stimulation at 37ºC in the SNAP internalisation assay, with no significant decrease in receptor membrane presence until 12min of stimulation, and the retention of some receptor on the plasma membrane even at the final timepoint of 30 min. It is therefore unclear as to whether the opto-$\alpha_{1A}$AR internalisation profile is related to a potential delay in light activation of the receptor, or is showing a low rate of internalisation as the endogenous $\alpha_{1A}$ adrenoceptor. It would therefore be of interest to use an opto-$\alpha_{1A}$AR construct with the $\alpha_{1B}$ carboxyl terminal to see if this would change the internalisation profile.

### 3.3.6 Internalisation of the Opto-$\alpha_{1A}$AR Requires Clathrin

Inhibition of endocytosis via Dyngo 4a and Pitstop 2 stopped internalisation of the light activated opto-$\alpha_{1A}$AR receptor. The two inhibitors revealed different receptor trafficking movements, where Dyngo 4a treated cells were observed to internalise light activated receptors after a 10min delay, but the trafficking profile of Pitstop 2 treated cells looked similar to those without 9-*cis*-retinal. This could be due to a difference in mechanism between the two inhibitors. Dyngo 4a blocks dynamin and is thought to be specific for clathrin-dependent endocytosis (Mccluskey *et al.*, 2013). The inhibition of receptor trafficking of the opto-$\alpha_{1A}$AR at first is therefore most probably due to clathrin-dependent endocytosis, however the loss of receptor at the cell surface later into the 30min timecourse indicates that there could also be clathrin-independent factors for receptor internalisation which happen in a different temporal pattern. Pitstop 2 is known to inhibit clathrin-independent processes as well as clathrin-mediated endocytosis (Dutta *et al.*, 2012). The continued inhibition of receptor trafficking by Pitstop 2 treated cells for the duration of the 30mins therefore suggests a clathrin-independent means of internalisation is also important in the receptor recycling. In other studies utilising both Dyngo 4a and Pitstop 2, it is common that both small molecules produce an

internalisation inhibition of similar magnitudes *in vitro*, for example blocking chloride release from internal stores in chick retinal cultures, and inhibiting transferrin internalisation and clathrin mediated endocytosis dependent virus entry in HeLa cells (Krzyzaniak *et al.*, 2013; Dunn and Gleason, 2018). However, these studies do not look at the temporal differences between the two inhibitors and focused on a specific endpoint. For a more time-dependent study, Merriam *et al.* (2013) investigated the difference between dynamin inhibition and Pitstop 2 action in synaptic vesicle release in primary neural cultures. Although no temporal differences were seen in the functional response of dynamin inhibition vs Pitstop 2 (measured as an increase in neural depression following stimulus), there was an observed acidification of vesicles and mitochondria when using Pitstop 2 (Merriam *et al.*, 2013). Although not directly related to endocytosis, a change in pH could potentially affect receptor recycling over the measured time. Further studies could investigate this pathway further, perhaps utilising arrestin knockout CRISPR HEK cell lines, or even pharmacological inhibition of GRKs (Alvarez-Curto *et al.*, 2016).

### 3.3.7 Successive Truncation of the C Terminal Region Differentially Affects Light Stimulated Opto-$\alpha_{1A}$AR Internalisation and $Ca^{2+}$ Signalling

Mutant receptor C terminal truncations of the opto-$\alpha_{1A}$AR were designed to remove potential phosphorylation sites for GRK and PKC at groups of serine and threonine residues. Cleavage of the opto-$\alpha_{1A}$AR receptor protein at site $Ser^{371}$ successfully removed all 4 PKC phosphorylation sites downstream of the important cysteine residues in helix 8 that act as potential palmitoylation sites, whereas $Ser^{421}$ removes 3 and $Thr^{471}$ just the last site (Olausson *et al.*, 2012).

Truncation at T471 had no effect on either assay, producing wild type responses. This indicated the final PKC site on the C terminus of the receptor is not required for either of the two downstream signals (endocytosis and calcium production).
The S421 truncation had no effect on calcium properties compared to wild type. This mutant did however display an increased level of (retinal-independent) constitutive internalisation, without light-stimulated trafficking. This is consistent with previous reports where deletion of the C terminus results in enhanced agonist independent GPCR endocytosis either by removing a plasma membrane retention

motif, or exposing a motif necessary to drive internalisation (Holliday *et al.*, 2005). The lack of effect on calcium profiles compared to the wild type receptor suggests that mechanism regulating the dynamics – e.g. GRK/arrestin or PKC mediated desensitisation – remain intact. Of these, the PKC route may be more likely as arrestin recruitment to the truncated receptor should be expected to still support light-stimulated internalisation.

Removing all the PKC sites and most of the C tail in the S371 truncation improved the trigger for calcium responses and produced sustained calcium oscillations compared to wild type. This demonstrates an improvement in the stimulus-response properties compared to the original full length opto-$\alpha_{1A}$AR. Internalisation profiles of the S371* receptor were similar to the S421* receptor, which indicates that the S421 – T471 region may be important for receptor endocytosis. As a hypothesis to why an increase in constitutive internalisation of the S371 and S421 C terminal truncations was observed, there may be a loss of sequences that aid in retaining the receptor at the membrane. For example, the PDZ binding motif GEEV in the $\alpha_{1A}$, identified by its binding with nitric oxide synthase (Pupo and Minneman, 2002). However, this motif would also be removed in the truncation at T471 which did not display a loss of plasma membrane expression, or 9-*cis*-retinal supported light stimulated internalisation. It is a possibility that a combination of constitutive recruitment of other internalisation-promoting proteins and loss of the PDZ domain would produce constitutive internalisation of the S371 and S421 truncation mutants. S371* may also lack negative feedback or regulatory elements for calcium as a lack of desensitisation which would allow for a longer duration of receptor activation and increase $Ca^{2+}$ generation. Different studies have looked at the effect of PKC at the $\alpha_{1A}$ adrenoceptor, showing that PKC activated with phorbol 12-myristate 13-acetate desensitises $\alpha_{1A}$ receptors (Price *et al.*, 2002) and the PKC inhibitor Ro 31-8425 reduced ERK1/2 phosphorylation, another pathway of desensitisation (Perez-Aso *et al.*, 2013).

In other research, the $\alpha_{1A}$ receptor's slow agonist stimulated internalisation and desensitisation has been suggested to be linked to a low affinity of β-arrestin for the carboxyl tail (Stanasila *et al.*, 2008). The binding of different known $\alpha_1$

adrenoceptor ligands, within the transmembrane domains, has also been shown to be crucial in mediating different patterns of $\alpha_{1A}$ adrenoceptor phosphorylation following activation (Alcántara-hernández *et al.*, 2017). This implies that in the chimeric opto-$\alpha_{1A}$AR, using transmembrane regions from rhodopsin, the active receptor conformation may support different interactions with various downstream kinases, and this may then alter the phosphorylation bar code in an unpredictable fashion (Tobin *et al.*, 2008). Another intriguing insight is a study by Price *et al.* (2002) in which carboxyl tail cleavage suggested that $\alpha_{1A}$ receptor internalisation is independent of C-terminal binding. The truncation point used for the $\alpha_{1A}$ receptor, T348, is equivalent to T379 in the opto-$\alpha_{1A}$AR, slightly distal to the S371 mutant used in this study. Price *et al.* (2002) measured the internalisation of the $\alpha_{1A}$ wild type and T348 receptors by changes in the plasma membrane expression and observed no change of agonist induced internalisation rate. However, we observed that the S371 truncation removed the effect of *cis*-retinal in light-promoted internalisation and appeared to stimulate constitutive internalisation that was independent of both light stimulation and clathrin binding. This view would be supported by a study where Morris *et al.* (2004) found a high degree of constitutive internalisation of the $\alpha_{1A}$ adrenoceptor to allow for continuous recycling and agonist stimulation of the receptor via clathrin pits. This mechanism could potentially be increased in the C terminus truncation mutant by exposing other intracellular motifs for protein binding, such as for the AP2 adaptor protein which is also linked to clathrin pit endocytosis (Zimmerman *et al.*, 2009), and could be an explanation as to why a decrease in internalisation was not observed by Price *et al.* (2002).

For further insight into these truncated receptors, direct arrestin binding could be investigated using arrestin assays, such as bioluminescence resonance transfer, or direct β-arrestin labelling (Gundry *et al.*, 2017). It would also be interesting to investigate the extent to which internalisation is required to recycle the chimeric receptor for sustained signalling over the long term, and the destinations of the receptors once they are endocytosed. Colocalisation with transferrin recycling could be used as a potential assay to determine endosomal presence of the receptors (Mccluskey *et al.*, 2013).

## 3.4 Conclusions

In this chapter, a new SNAP construct of the optogenetic opto-$\alpha_{1A}$AR receptor has been successfully used to investigate $Ca^{2+}$ signalling and, for the first time, receptor trafficking within stably transfected HEK cells. Furthermore, studies on a range of C terminal truncations of the opto-$\alpha_{1A}$AR construct identified a mutant receptor (opto-$\alpha_{1A}$AR-S371*) in which light-stimulated internalisation was limited, and which could maintain more sustained calcium dynamics compared to wild type. In common with previous reports, these studies also identified a requirement for retinal supplementation for effective responses in the HEK293 cell system, and the need for sustained patterns of laser light excitation, both of which provide some limitations (e.g. in terms of sensitivity, or applying dynamic patterns of stimulation) in the use of such chimeras as GPCR optogenetic tools. In the next chapter, the opto-$\alpha_{1A}$AR signalling profile will be compared with another $G_q$ coupled opsin, melanopsin, and its use in a primary cell system.

# Chapter Four

## Melanopsin for Optogenetic Activation of Calcium Signalling in HEK293 Cells and Primary Astrocyte Cultures

## 4.1 Introduction

Having characterised the optogenetic tools in a model HEK293 cell line, the next step was to investigate the application of calcium mobilisation in a more physiologically relevant system. As discussed in section 1.3, astrocytes express many $G_q$ coupled GPCRs and have several physiological and pathophysiological mechanisms linked to these receptors. The $G_q$ coupled optogenetic GPCRs are therefore a relevant tool to investigate the intracellular signalling of astrocytes in a more translational environment of primary cells.

### 4.1.1 Calcium Indicators in Astrocytes

Calcium fluorescent indicators allow functional imaging of astrocytic calcium signalling via the change of fluorescence of the dye upon binding of calcium. The main factors that determine utility of a calcium indicator are; method of introduction of the dye, fluorescent excitation and emission properties, affinity for calcium, and cell distribution of the dye once loaded. Each of these parameters need to be optimised for use in primary cell cultures, such as the rat cortical astrocytes required in this study.

There are three viable options of dye loading for astrocyte cultures; 1) injection of a single cell with a non-permeable dye for looking at calcium transients of a single cell 2) general loading of all cells in an area using cell permeable dyes, and 3) transfection of cells with a genetically expressed calcium indicator protein (GECIs). Injection of non-permeable dyes have been useful for looking at single patch-clamped astrocytes in a tissue environment using dyes, such as Fluo-3, to look at ionic calcium permeant receptors, such as the NMDA receptor (Palygin *et al.*, 2011; Navarrete *et al.*, 2013). For the purposes of *in vitro* investigation of primary astrocytes on a coverslip with broad stimulation, non-permeable dyes for looking at a single cell are less useful. Instead, bulk loading can be achieved using cell-permeable versions of calcium indicators, usually incorporating acetoxymethyl (AM) groups through esterfications which make the dye neural and hydrophobic, enabling it to cross the cell membrane. These AM esters are naturally cleaved by intracellular esterases, leaving the calcium indicator intact and trapped within the cell (Gee *et al.*, 2000). Another option for primary astrocyte monitoring of calcium

is the use of GECIs, such as the GCaMPs, which can be specifically targeted for transfection into astrocytes in an animal to monitor calcium binding through fluorescence (Pologruto *et al.*, 2004; Ohkura *et al.*, 2012). Although GCaMPs allow selective targeting of astrocytes over other cell types, there is the potential for loss of resolution of calcium transients with this method in astrocytes. This was investigated by Lock and colleagues (2017) who directly compared the parameters of single calcium puffs released via $IP_3$ uncaging measured with chemical calcium indicators and GCaMPs in neuroblastoma cells. In all cases, the chemical indicators outperformed the GCaMPs as they were able to detect calcium transients faster with better signal-to-noise ratio and a better dynamic range (Lock *et al.*, 2017). Bulk loading of primary astrocyte preparations with small molecule calcium indicators was therefore used in this study to enable easier loading and optimal calcium detection.

There is a large range of fluorescent excitation and emission variants for calcium indicators. Historically, green fluorescence has been widely used in astrocyte calcium experiments due to wide availability of instrumentation for green fluorescent imaging and the downside of aggregation of red-emitting fluorescent proteins (Oheim *et al.*, 2014). This is, however, not an option for use in experiments which require the shorter wavelengths for other fluorescent readings or, as in this case with optogenetic receptors, where cells are activated by the same wavelength as the dye. X-Rhod-1 (ex/em 580/600nm) and Rhod-2 (ex/em 557/581nm) are the two best characterised red-shifted calcium indicators for use in astrocytes (Paredes *et al.*, 2008). They both exhibit similar, relatively low affinities for calcium ($K_d$ 570nM for Rhod-2 and 700nM for X-Rhod-1, compared to 345nM of Fluo-4), with X-Rhod-1 edging Rhod-2 in preference due to its longer wavelength of emission and excitation and slightly lower calcium affinity. When it comes to selecting optimum calcium affinity of the dye, the goal is to balance sensitivity of the dye against response kinetics. Small, low amplitude transients are better detected by a high affinity dye with a low $K_d$ for calcium as high affinity dyes buffer more strongly, saturating the response at relatively low concentrations (i.e. large scale responses will be blunted) and distorting the kinetics of the response by buffering the rise and fall of $Ca^{2+}$ in the cytoplasm. X-Rhod-1 is a good compromise for picking up low amplitude responses without saturating during high amplitude

responses. The largest downside for using X-Rhod-1 or Rhod-2-AM is the fact that the AM ester creates a net positive charge of these molecules, promoting the loading of mitochondria in astrocytes rather than the cytosol, although this can be useful in mitochondrial studies (B.-X. Zhang *et al.*, 2006; Dubouskaya *et al.*, 2018). Cal-630 has been developed to address the problems of X-Rhod-1, with similar excitation and emission wavelengths (ex/em 608/6286nm) and a lower affinity for calcium ($K_d$ 1.2μM), while simultaneously also being negatively charged to stop cell leaking and mitochondrial sequestering of the dye (Liang *et al.*, 2019). Unfortunately, this dye was not available at the start of the project and therefore was not used in the astrocyte studies, however the potential was realised in HEK293 cells in a partnering investigation into the optogenetic stimulation of melanopsin (*Figure 4.1*).

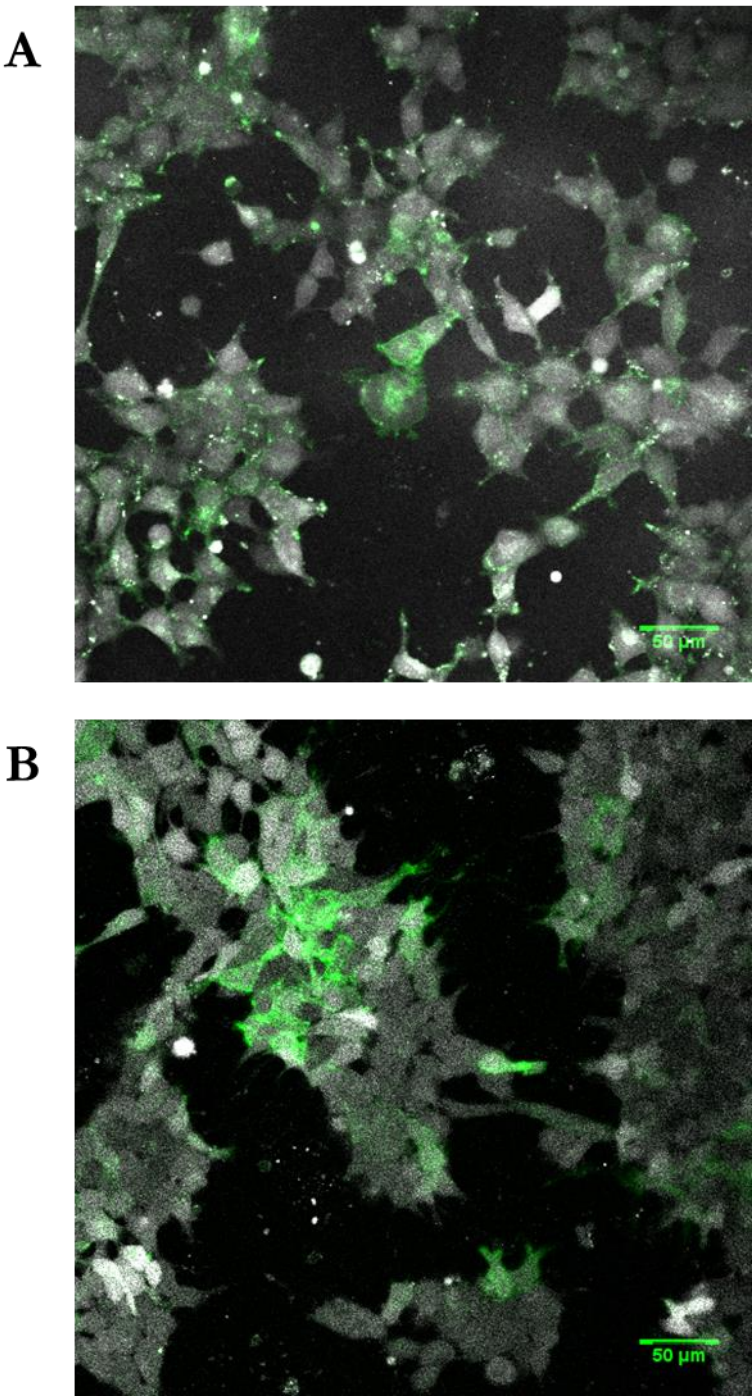


***Figure 4.1*** **– Difference between X-Rhod-1 and Cal-630 calcium dye loading in the HEK-Opn4 stable cell line.** Images taken on a confocal with 20x dry lens. Calcium indicators are shown in grey, imaged using 631nm laser, with the SNAP-Surface AF488 (0.2µM, 30min incubation) in green to show receptor expression. A) X-Rhod-1 (1µM, 45min incubation) suitably labels cell cytosol with fluorescent dye but has more intracellular spots and extracellular conjugates with a lower signal to noise ratio than B) Cal-630 (1µM, 1hr incubation).

### 4.1.2 Transfection of Primary Cells

Transfection of primary cells presents a new challenge compared to stably transfected cell lines, such at the HEK293 cell line. This is usually attributed to several factors, such as poor cellular or nuclear uptake of the DNA or RNA, release of nucleic acids into the cytoplasm, or sub-optimal metabolism and division rates (Kumar *et al.*, 2019). To optimise primary astrocyte transfection of optogenetic complexes, there are three broad classes of techniques; biological, chemical and physical (Kim and Eberwine, 2010).

Biological methods utilise viral transduction to integrate the desired genetic code into the host genome and is known for its high transfection efficiency in cells which usually prove difficult to transfect (Gerits *et al.*, 2015). There are, however, several downsides of the technique, such as increased chance of insertional mutagenesis, immunogenicity and inflammation responses (Keriel *et al.*, 2006). The inflammatory response is of particular note for primary astrocytes as induction of inflammatory pathways is usually a desired endpoint of investigations, and response to infection and inflammation is a key physiological role of astrocytes.

Chemical transfection provides an alternative to viral vectors, with cationic lipid reagents usually preferred. The reagent of choice for this study was the lipid-based lipofectamine, although there are several reagents available commercially (Kumar *et al.*, 2019). The cationic chemical transfection reagents take up negatively charged DNA into a positively charged complex, allowing permeation through the negatively charged cellular membrane. Compared to viral methods, the transfection efficiency can be sub-optimal in primary cells and depends on several factors, such as pH and ratio of DNA to chemical transfection reagent. If a desired transfection percentage can be achieved, however, the chemical transfection technique is more desirable due to lower cytotoxicity, fewer inflammatory responses and no mutagenesis of the DNA (Trentin *et al.*, 2005).

The final option for DNA transfection involves physical methods of insertion which can be broadly covered by six different methods; micro injection, biolistics, laser stimulation, electroporation, sonoporation and magnetofection (Mellott *et al.*, 2013; Hamann *et al.*, 2019). Out of these six, electroporation is the most widely used method as the process easy and reliably transfects large batches of cells in a

short period of time. Although the exact mechanism of electroporation is not yet understood, it is hypothesised that electrical pulses create small holes in the cellular membrane which the DNA can pass through (Mellott *et al.*, 2013). When chemical transfection does not yield high enough transfection efficiency, the electroporation method is a viable alternative for both ease of use and none of the disadvantages of viral transfection.

### 4.1.3 Chapter Aims

The aim of this chapter is to investigate light activated GPCR signalling in astrocytes through calcium imaging using primary astrocyte cultures. This will be achieved by;

i. Investigating $\alpha_1$ adrenoceptor $G_q$ stimulation in primary rat astrocyte cultures with several different calcium indicators to characterise the *in vitro* ligand activated GPCR calcium signalling in astrocytes.
ii. Optimising optogenetic GPCRs for $G_q$ protein activation for transfection and light activation in primary rat cortical astrocytes.
iii. Altering stimulation patterns of light activation to mimic endogenous signals.
iv. Mutating the optimised optogenetic GPCR to potentially alter temporal receptor activation responses for a varied, useful optogenetic activation, as shown in Chapter 3.

## 4.2 Results

### 4.2.1 Establishing Endogenous $G_q$ Related $Ca^{2+}$ Response in Primary Astrocyte Cultures via $\alpha_1$ adrenoceptor Activation

Due to the endogenous expression of the $\alpha_1$ adrenoceptor in cortical primary astrocytes and its potential link to the opto-α1AAR receptor signalling seen in the Chapter 3, phenylephrine $Ca^{2+}$ response was investigated in astrocytes as a robust, selective agonist for the $\alpha_1$ adrenoceptor (Kurita *et al.*, 2018). Functional output of endogenous $\alpha_1$ activation was measured as $Ca^{2+}$ responses, detected by two different $Ca^{2+}$ indicators, Fluo-5F (ex/em 494/506nm) and X-Rhod-1 (ex/em 580/602nm). Fluo-5F AM is a robust green shifted fluorescent indicator commonly used for detecting intracellular $Ca^{2+}$ in astrocytes. Unfortunately, this cannot be used in assays with the optogenetic receptors required for later experiments as the excitation is a similar wavelength to the receptor activation. X-Rhod-1 was then used as a red-shifted indicator, allowing comparison between the two.

Primary cortical astrocytes (neonatal P3; DIV 14-18) were loaded with 1μM fluorescent indicator and imaged on a widefield microscope for 20min at 1 frame per second with agonist addition of phenylephrine after a 2min baseline (see *Figure 4.2*). Astrocytes produced calcium transients upon agonist addition with different temporal profiles and fold fluorescence increases independent of phenylephrine concentration (*Figure 4.3*). The percentage of cells that responded were taken as an end point to determine functional response, determined by fold fluorescence increase in the ROI increasing above a predetermined threshold (*Figures 4.4*). X-Rhod-1 AM produced a different response profile to Fluo-5F AM with a 30% decrease in the amount of cells responding to the highest concentration of phenylephrine (100μM). This could be due to the low number of coverslips used, not allowing for a large enough sample size of the heterogeneous astrocytes.

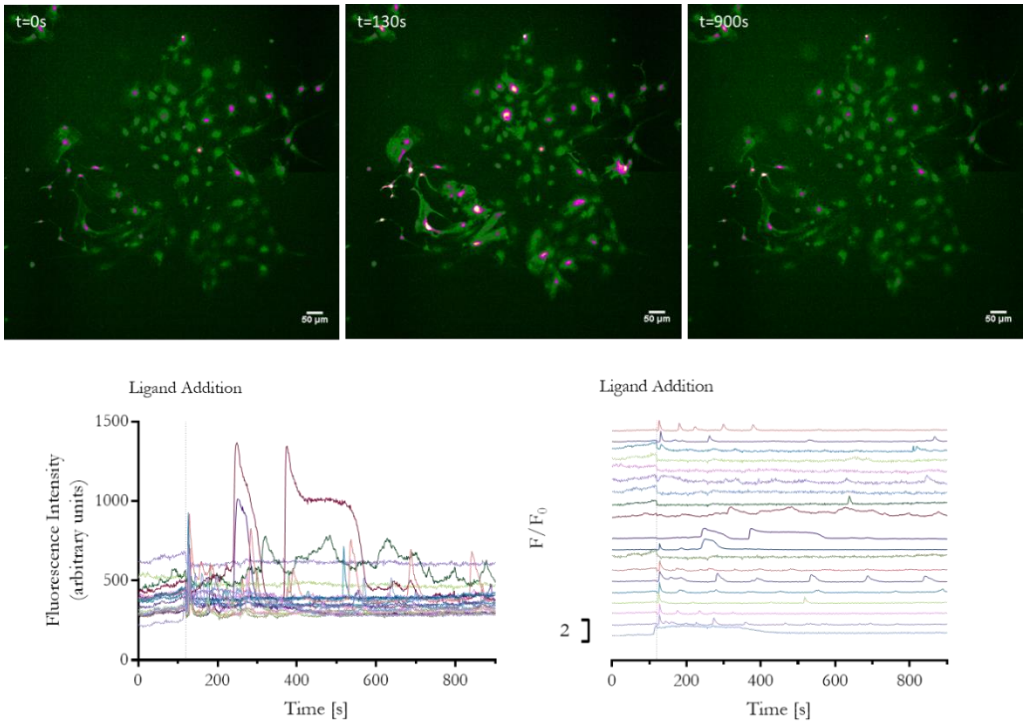


***Figure 4.2* – Calcium response to phenylephrine in primary cortical astrocytes (neonatal P3)**. Fluo-5F AM fluorescence response to phenylephrine (1µM). Images taken from a widefield timecourse (1 frame per second) where phenylephrine was added at 120s. Cells increase in fluorescence at ligand addition and decrease back to baseline after 15min. Fluorescence was measured by pixel intensity and plotted below for 20 randomly selected cells. There is a general peak around ligand addition at 120s and other calcium waves during the trace while phenylephrine is present.

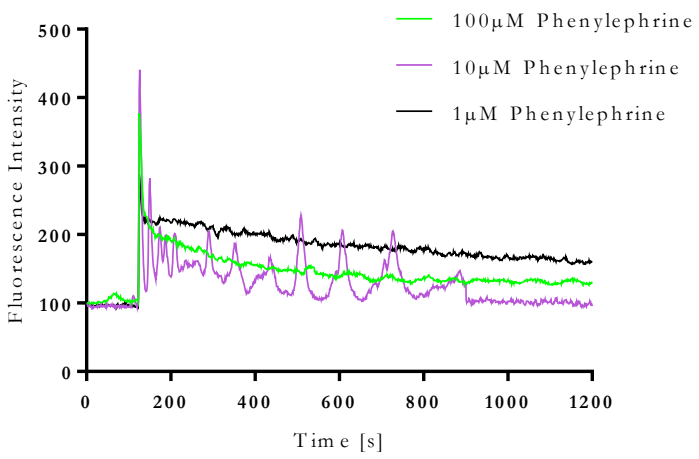


***Figure 4.3* – Single astrocyte $Ca^{2+}$ transients induced by different concentrations of phenylephrine**. Primary rat cortical astrocytes (DIV 14-18) were loaded with calcium indicator Fluo-4 (1µM) and imaged for 20min every 1s on a widefield microscope at 470nM LED excitation. Phenylephrine was added after 2min via solution exchange and the raw fluorescence intensity of the dye from a static ROI is shown. For all three concentrations of phenylephrine, astrocytes can produce transients with different temporal responses (cells represent different temporal patterns where 1 cell is taken from *n*=4 coverslips for each concentration).

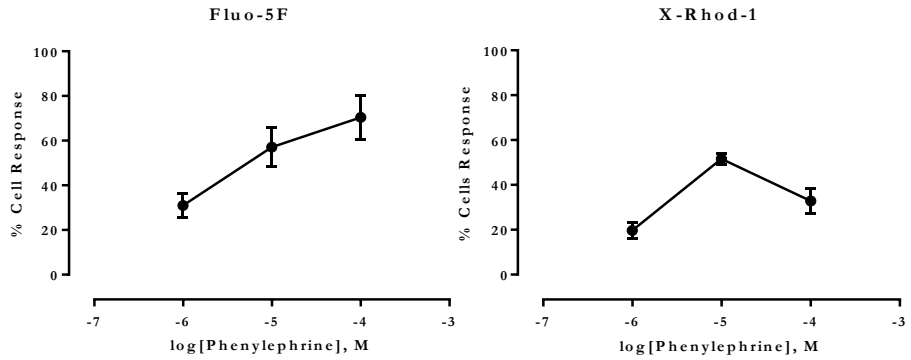


***Figure 4.4* – Percentage of astrocytes on a coverslip responding to phenylephrine of varied concentrations using different calcium indicators.** When detected using Fluo-5F (1µM), the percentage of cells on a coverslip producing calcium transients to phenylephrine follows a concentration response relationship. X-Rhod-1 (1µM) shows similar percentage of cells until 100µM phenylephrine, where the percentage of cells drops by 45% compared to those measured with Fluo-4 ($n \geq 4$ coverslips with at least 20 cells per coverslip).

### 4.2.2 Optimised Transfection of Optogenetic GPCRs in Primary Astrocytes Requires Electroporation

The primary candidate for investigating $G_q$ activation by optogenetic GPCRs in astrocytes was the chimeric opto-α1AAR receptor characterised in Chapter 3, enabling comparison between the endogenous $\alpha_1$ adrenoceptor response and light-activated signalling. Unlike recombinant HEK cells, primary cells present a difficulty in transfection efficiency. Several different chemotransfection reagents were therefore tried for optimisation. Primary rat cortical embryonic astrocytes (E18) were transfected using Lipofectamine 2000, Lipofectamine LTX and Lipofectamine 3000 with suggested protocols for primary cells from Thermo Fisher in a 96 well plate with varied transfection times (5hr, 24hr and 48hr) and two concentrations of Lipofectamine and cDNA plasmids. Cells transfected with SNAP tagged receptors were labelled with SNAP-Surface AF488 and imaged on the Ultra confocal plate reader. Unfortunately, neither the SNAP-opto-$\alpha_{1A}$AR plasmid nor the eYFP tagged derivative were found at a suitable surface expression when transfected into rat cortical primary astrocytes using Lipofectamine, and the control transfection using a GFP tagged membrane-bound Kras anchor protein was also unsatisfactory (see *Figure 4.5* for summary of the best results using 3μL Lipofectamine 3000 over 24hr).

As an alternative to chemotransfection, electroporation using Nucleofection was investigated. Primary astrocytes were transfected, labelled with SNAP-Surface AF488 and imaged on a confocal microscope. Although GFP expression from transfection of GFP-Kras increased under this methodology, there was still a lack of surface expression of SNAP-opto-α1AAR (see *Figure 4.6*). It was therefore hypothesised that the opto-α1AAR receptor complex used is not stable enough for transfection into these astrocytic primary cells, potentially being broken down by cell machinery before expression or because the cDNA plasmid prepared contained too many endotoxins for primary cell transfection.

For the reasons mentioned in section 1.2.4.1, melanopsin was perceived as a good alternative candidate receptor for optogenetic stimulation of calcium transients. Naturally coupled to $G_q$ and endogenously expressed in mammals, melanopsin had a greater potential for successful expression in hard to transfect primary cells.

Under Nucleofection, melanopsin was successfully transfected into primary cortical rat astrocytes with good expression rates and a high amount of labelled receptor at the cell surface (see *Figure 4.7*).

As performed with the opto-$\alpha_{1A}$AR in section 3.2.1, 3 C terminus truncations of the Opn4 receptor were created at $Ser^{375}$, $Ser^{411}$ and $Thr^{471}$ (similarly close to Thr/Ser phosphorylation groups as with the opto-$\alpha_{1A}$AR $Ser^{371}$ and $Ser^{421}$, respectfully) to potentially alter temporal signalling of the receptor. Although successful in transfection via Nucleofection for both truncations, only the Opn4-$Ser^{411}$ truncation expressed at a high enough rate to allow for experimental results (see *Figure 4.8*). The Opn4-$Ser^{375}$ receptor created may not be stable enough to express at the membrane in primary astrocyte cells, potentially due to membrane anchoring issues, limiting its usefulness.

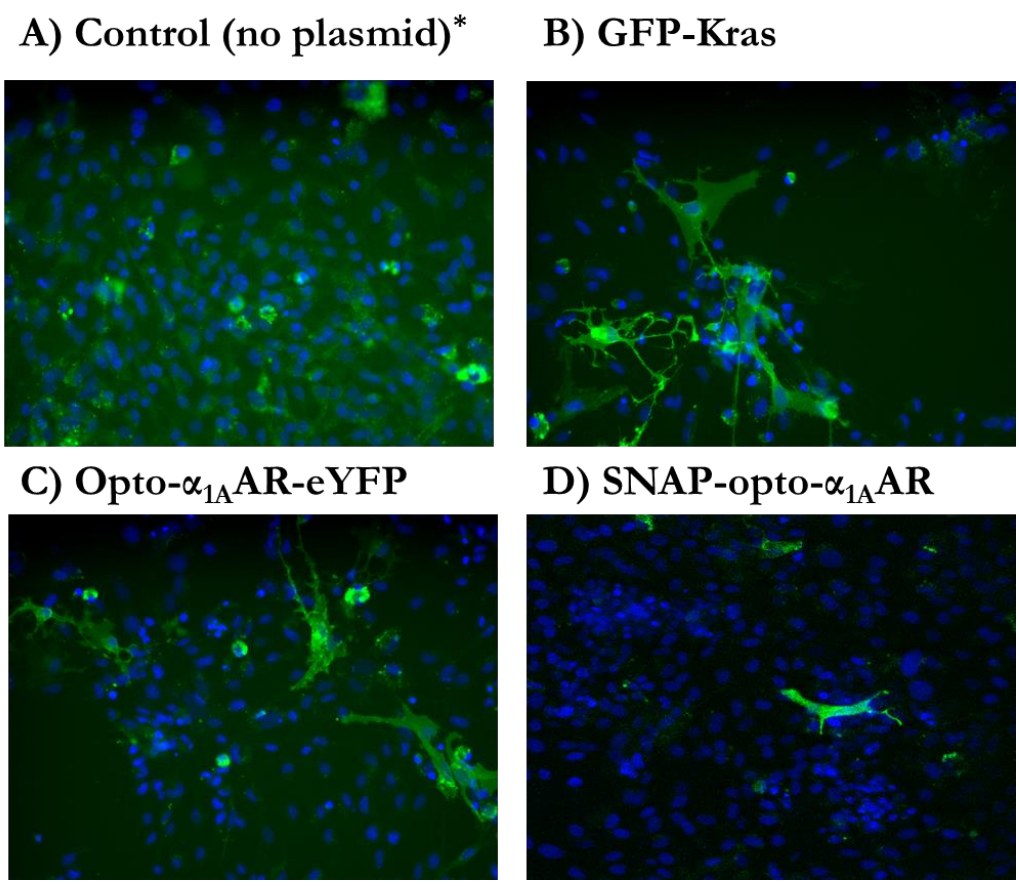


***Figure 4.5* – Best Lipofectamine 3000 transfection rates of various plasmids in embryonic, cortical rat astrocytes (E18).** Images captured using IX Ultra confocal plate reader 24hr or *72hr post transfection. Receptors are shown in *green* (GFP, eYFP or 0.5μM SNAP-Surface AF488, as stated) and nuclei in *blue* (H33342). A) Adding Lipofectamine 3000 by itself does not hinder cell growth or viability, as shown by the confluency of the nuclei after 72hr. Green background noise has been picked up by the high stimulus light. B) GFP-tagged membrane anchor of the membrane-bound Kras protein was successfully transfected using Lipofectamine into some primary astrocytes, although not always successfully (average 3/12 wells transfected). C) Opto-$\alpha_{1A}$AR-eYFP sometimes transfected, but only in 3 wells from the 3 experiments. D) None of the wells for the SNAP-opto-$\alpha_{1A}$AR transfection showed signs of receptor expression, except for one well. All images show the best transfection rates from 12 transfected wells per plate, 4 images taken per well where $n$=3 96 well plates.

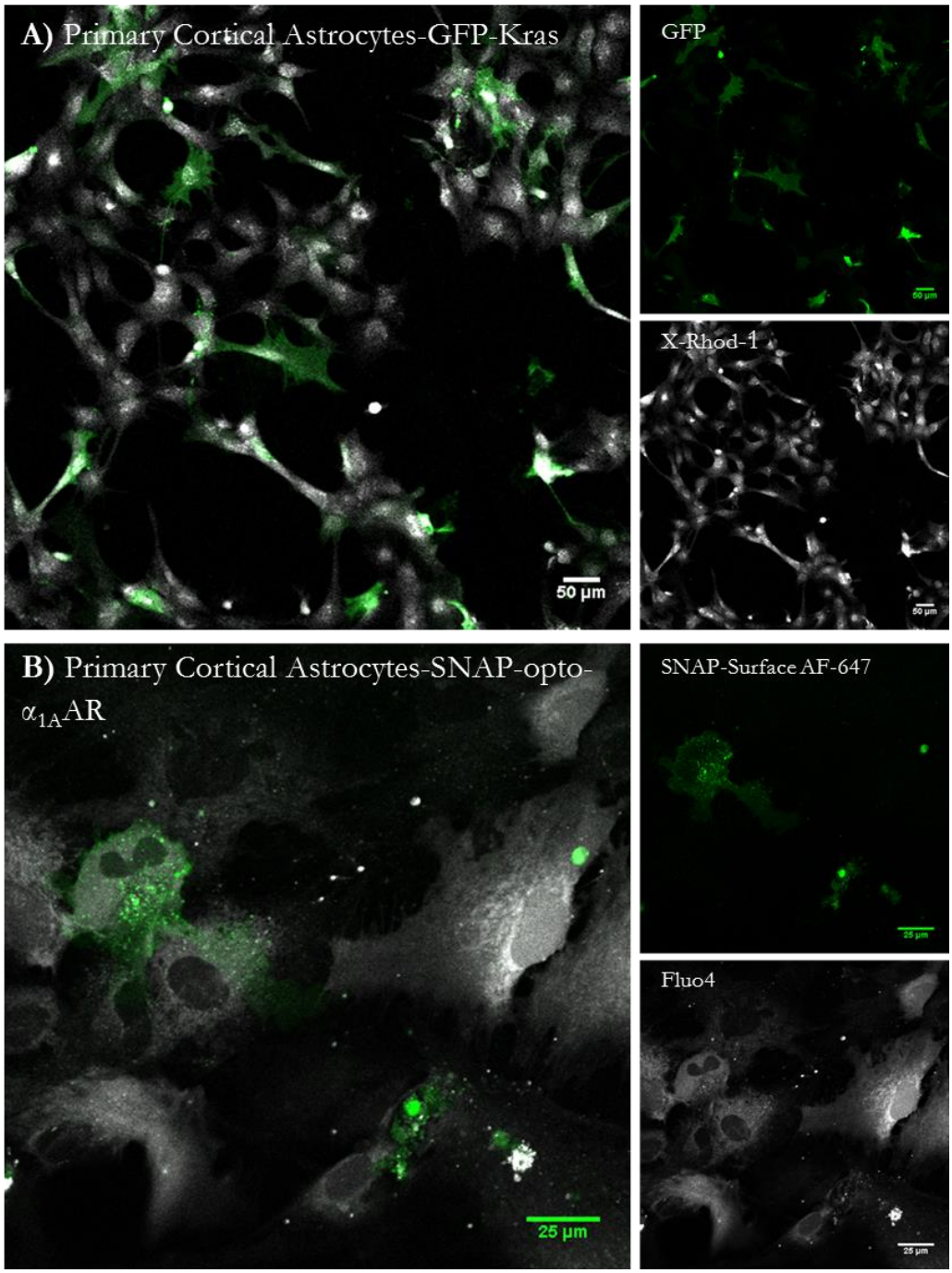


***Figure 4.6*** **– Expression of tagged proteins in primary cortical astrocytes following nucleofection.** Embryonic rat cortical astrocytes (DIV 14-21) were electroporated and seeded 24hr before expression check, performed on a confocal microscope on coverslips. A) The GFP tagged Kras anchor protein is transfected efficiently. B) The SNAP tagged opto-$\alpha_{1A}$AR chimeric optogenetic receptor does not transfect well, with only 2 cells detected on a coverslip. Where $n$=1, representative of 3 coverslips. Calcium studies were also performed in these cells.

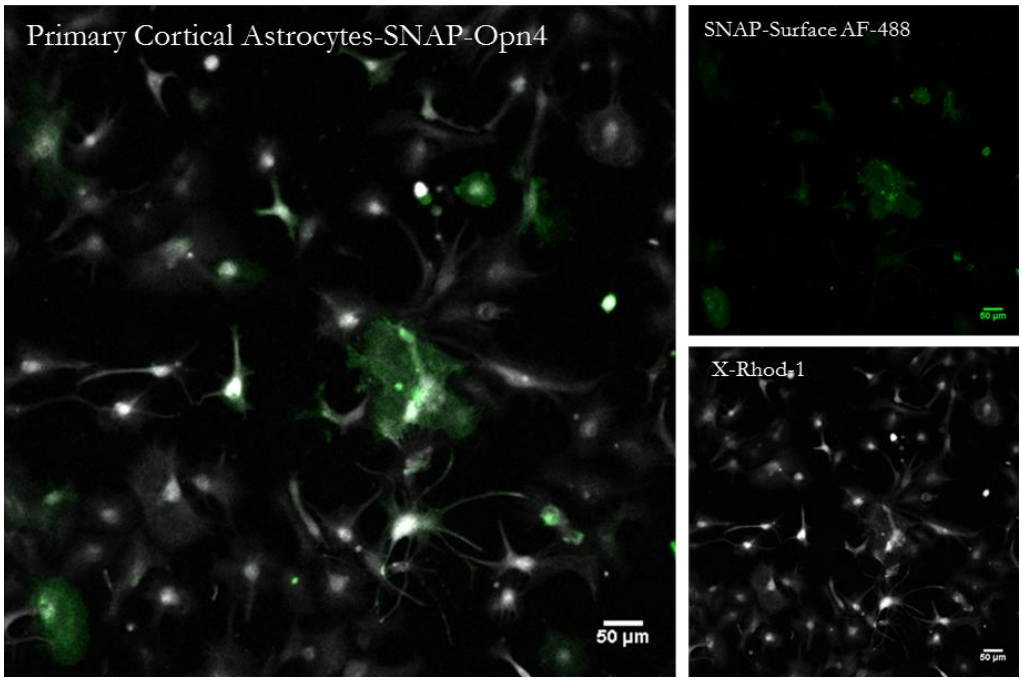


***Figure 4.7*** **– Nucleofection of melanopsin, Opn4, in primary cortical astrocytes.** Embryonic rat cortical astrocytes (DIV 14-21) were electroporated and seeded onto coverslips 24hr before expression check, performed on a confocal microscope using X-Rhod-1 AM (1µM) to stain cells and SNAP-Surface AF488 (0.2µM) to label receptors. The SNAP tagged melanopsin receptors express on the cell surface to a high percentage. Where $n$=1, representative of 3 coverslips. Calcium studies were also performed in these cells.

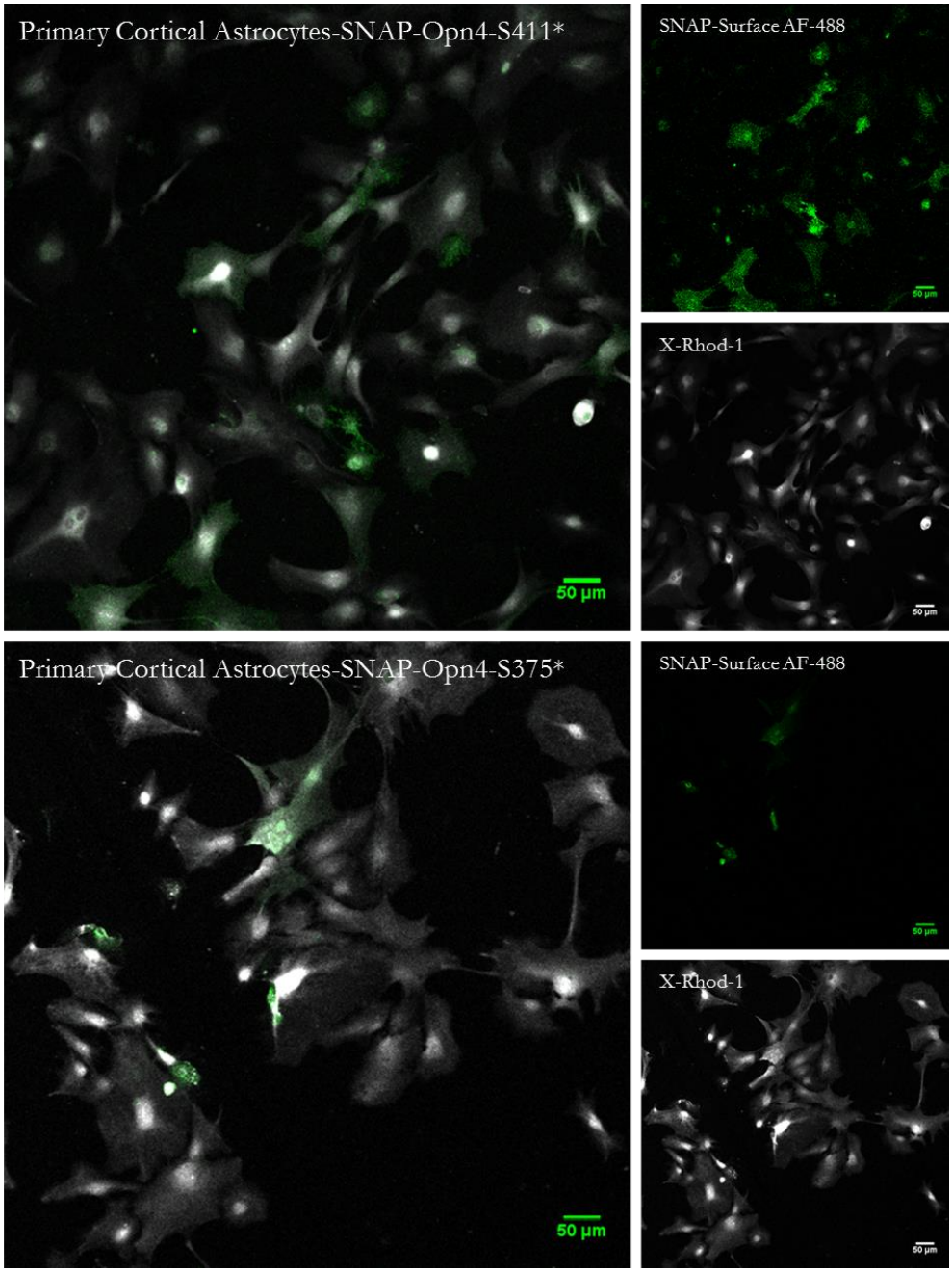


***Figure 4.8* – Nucleofection of Opn4 C terminus truncation mutants S411* and S375* in primary cortical astrocytes.** Embryonic rat cortical astrocytes (DIV 14-21) were electroporated and seeded onto coverslips 24hr before expression check, performed on a confocal microscope using X-Rhod-1 AM (1µM) to stain cells and SNAP-Surface AF488 (0.2µM) to label receptors. The SNAP tagged Opn4-S411* receptors express on the cell surface to a high percentage, similar to wild type receptors, whereas the Opn4-S375* does not express to the same level. Where $n$=1, representative of 3 coverslips. Calcium studies were also performed in these cells.

### 4.2.3 External LED Light Stimulus Required for Melanopsin Activation in Rat Primary Cortical Astrocytes

Melanopsin light activation was measured using intracellular calcium concentration as a functional output. First, a continual laser stimulus (10% power, 488nm) was used on the confocal using a x40 water objective, as described in section 3.2.3. Fluo-5F AM (1μM) was used as the calcium indicator as this was excited in the 488nm laser stimulus range, allowing for simultaneous receptor stimulation and fluorescence recording. There was no change in the fluorescence of Fluo-5F AM in Opn4 transfected primary rat astrocytes upon green laser light stimulation over 20min (see *Figure 4.9*). It is unclear why this method does not work in optogenetic primary cells when the method has been shown to work in HEK cells, although there are differences in both receptor expression, cell size (astrocytes around 2-4 fold larger than HEK cells), morphology (astrocytes are very flat on a coverslip compared to HEK cells) and transfection efficiency which may affect receptor stimulation.

Receptor activation required different means in the primary cells. In the literature, optogenetic experiments in cell cultures often use an external stimulus, such as an LED or laser (Edward R Siuda *et al.*, 2015; Renault *et al.*, 2015). Using an external LED stimulus of a single wavelength in activation range for melanopsin (470nm), cells were stimulated for 60s during a 5min time course after a 2min baseline, while simultaneously imaged on a confocal microscope to measure X-Rhod-1 fluorescence. A red-shifted excitation and emission wavelength with a precise wavelength filter were important to stop any bleed-through from the LED stimulus photons onto the camera. Primary rat cortical astrocytes transfected with the SNAP-Opn4 produced a calcium response to the external LED stimulus (see *Figure 4.10*). This response was not seen in control astrocytes electroporated with a GFP tagged membrane anchor from the membrane-bound Kras targeting sequence. Kras-transfected cells did not produce calcium transients to LED stimulus, but upon addition of 10μM ATP showed cell viability with a calcium response similar to the photoactivation of Opn4, with $F_{max}/F_0$ ratio (1.75) (see *Figure 4.11*, $n$=3 coverslips, minimum 20 cells per coverslip).

Of interest to note, calcium transients were detected not just in Opn4 transfected astrocytes, but also in other cells on the same coverslip. This observation has been seen in other primary astrocyte optogenetic experiments in cultured astrocytes (see *Figure 4.12*; Li *et al.*, 2012; Berlinguer-Palmini *et al.*, 2014).

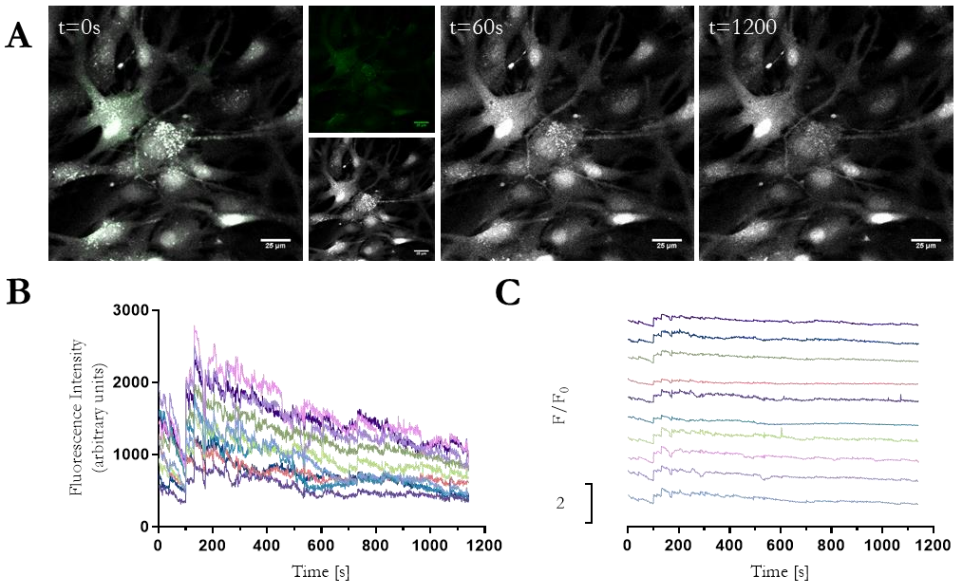


***Figure 4.9* – Calcium recording of continuously laser stimulated Opn4 astrocytes**. A) Primary rat cortical astrocytes (neonatal P3, DIV 14-21) transfected with Opn4 (labelled with SNAP-Surface AF647, 0.2μM) were stimulated with the 488nm laser on a line scanning confocal. Calcium concentration was recorded using Fluo-5F AM (1μM, 30min preincubation, filter BP 495-585nm). B) Raw fluorescence values. There were no detected calcium transients from Fluo-5F fluorescence increase, with the small decrease coming from an imaging artifact. C) Fold fluorescent change is exactly the same for each cell. Representative of *n*=3 experiments where 3 coverslips were used per experiment.

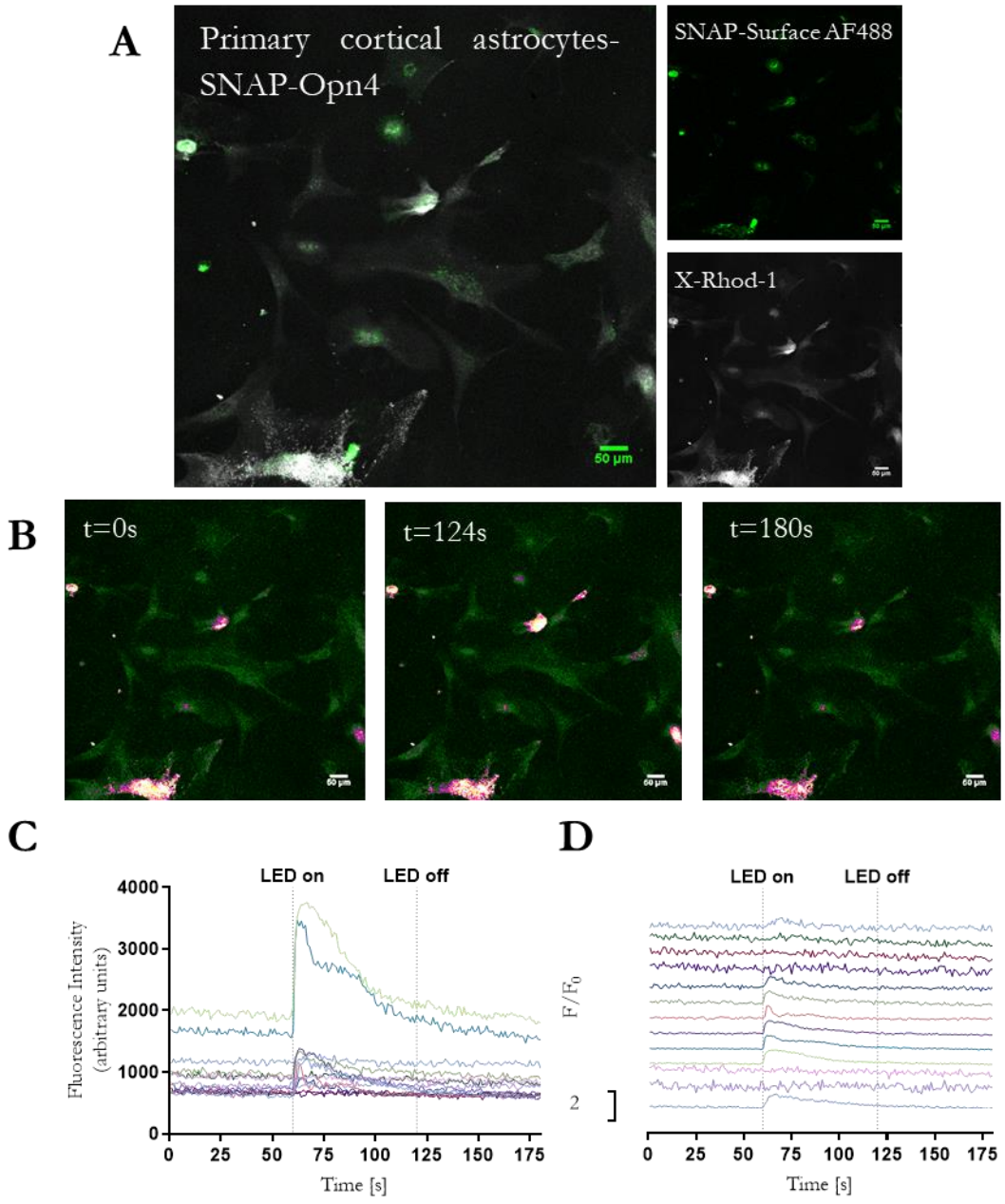


***Figure 4.10*** **– Melanopsin expressing primary cortical astrocytes respond to external LED light sitmulus.** A) Opn4 receptors were labelled with SNAP-Surface AF488 (0.2µM, 30min preincubation) and imaged post calcium timeseries. B) Calcium concentration, measured using X-Rhod-1 AM (1µM, 30min preincubation) fluorescence, increases upon LED (470nm, 25% power) stimulus at 60s, before returning to baseline at the last timepoint, 180s. Images taken at 0s, 60s (stimulation) and 900s (post-stimulation) with false colour Blue Orange to indicate fluorescence intensity changes. C) Raw X-Rhod-1 fluorescence is plotted for all cells, where D) shows fluorescence fold change. Representative of $n$=5 coverslips.

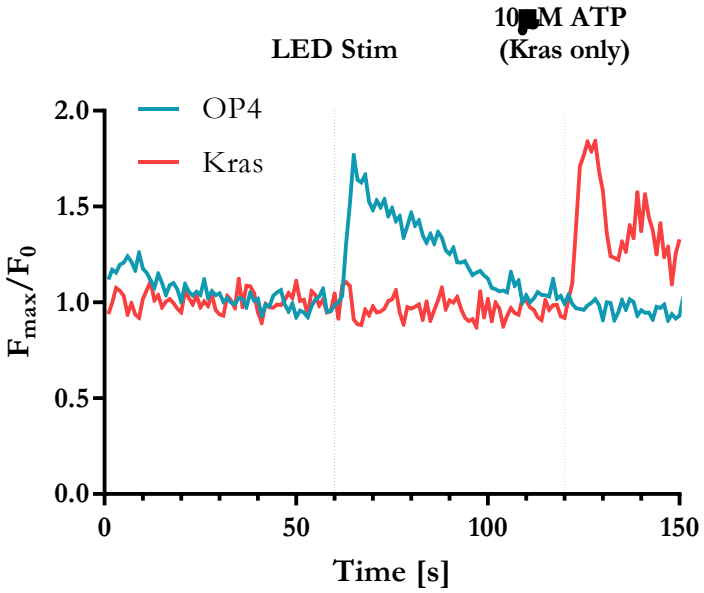


***Figure 4.11* – Timecourse of calcium response in optogenetic and control cells.** Calcium transients were measured using X-Rhod-1 fluorescence change over a period of 3min where an external LED stimulus (25% power) was used after a 60s baseline. In cells transfected with melanopsin, a calcium transient can be seen directly after LED stimulation. Control cells transfected with a GFP tagged Kras membrane protein do not produce a transient in response to the LED, however the calcium response to ATP in these cells show similar fluorescence change as stimulation of melanopsin in optogenetic cells (*n*=1 cell, representative of 3 coverslips with at least 20 cells per coverslip)

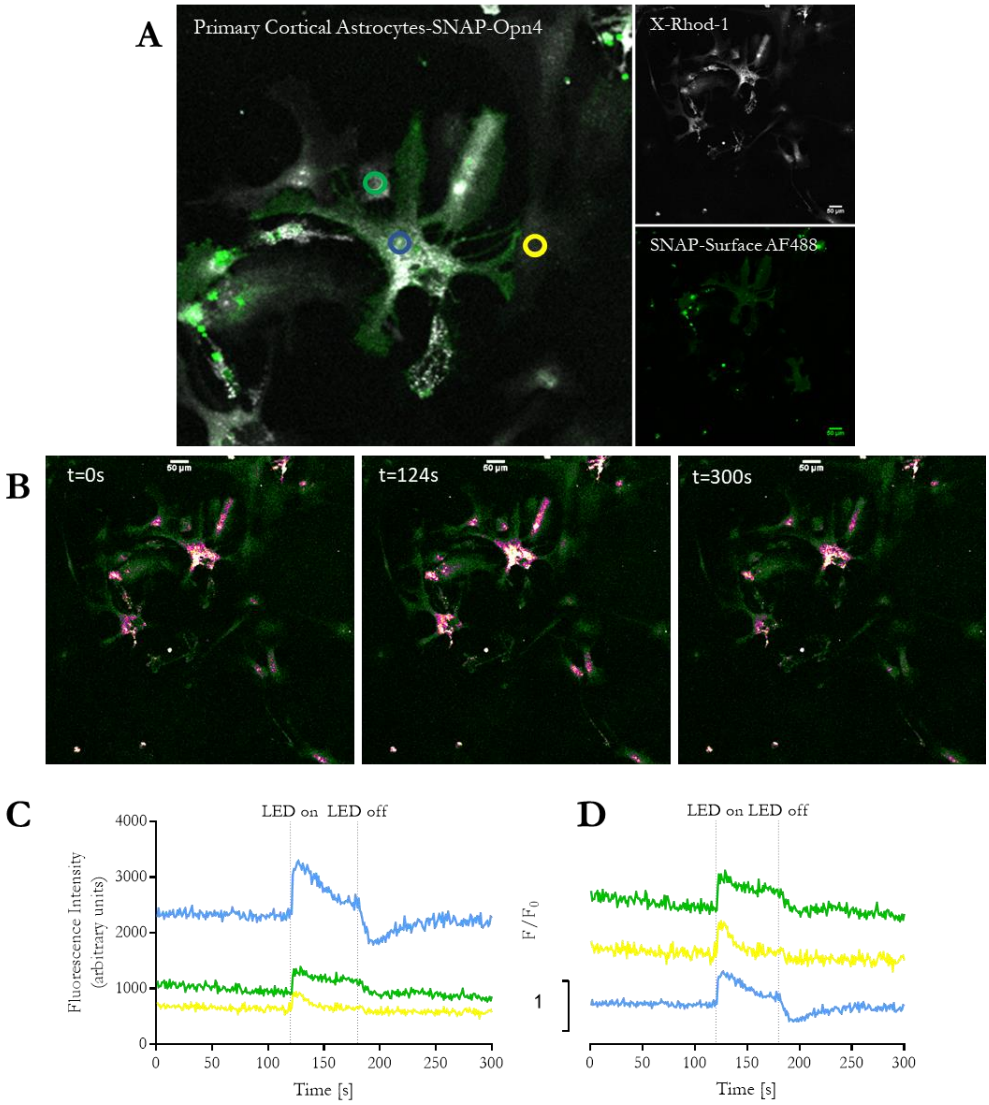


***Figure 4.12*** – **Untransfected astrocytes produce calcium transients in response to photoactivated melanopsin expressing primary astrocytes.** A) Transfected astrocytes in green, labelled with SNAP-Surface AF488 (0.2µM, 30min preincubation) and X-Rhod-1 AM (1µM, 30min preincubation) as the calcium dye. Two untransfected cells have been selected with coloured ROIs (*green* and *yellow*) next to a transfected astrocyte (*blue*). B) Images of X-Rhod-1 fluorescence at the start and end of the timeseries, and one just after LED light activation at 120s (470nm, 5% power). False colour Blue Orange has been applied to help determine intensity. C) Raw fluorescence and D) fold fluorescence recorded for each ROI across the timeseries, where colour matches ROI. Both untransfected cells produce a calcium transient. Representative of some calcium responses, with others more distal, *n*=1 coverslip.

### 4.2.4 Melanopsin Induces Calcium Transients in HEK 293T Cells Similar to the Chimeric Optogenetic Opto-$\alpha_{1A}$AR Receptor

Once it was established that melanopsin presented as a stably expressed receptor in astrocytes with a functional response to an LED stimulus, the receptor was characterised in recombinant HEK 293T cells. As melanopsin has been reported to produce calcium signals but has also been reported as coupled to $G_i$ protein, the calcium response profile of melanopsin was compared to the opto-$\alpha_{1A}$AR used in Chapter 3. Both receptors were expressed in stably transfected cell lines, HEK-SNAP-Opn4 and HEK-SNAP-opto-$\alpha_{1A}$AR, and stimulated with an external single, 60s 470nm LED to replicate the methodology used with astrocyte cultures. The HEK cells expressed the SNAP-Opn4 receptor on the plasma membrane in a similar manner to the SNAP-opto-$\alpha_{1A}$AR receptor (see *Figure 4.13*).

When the HEK-SNAP-opto-$\alpha_{1A}$AR cell line is not supplemented with 9-*cis*-retinal, the cells do not respond to light as readily. This is not the case with the HEK-SNAP-Opn4 cell line which produces a response to LED stimulus independent to 9-*cis*-retinal (1μM) supplementation (see *Figure 4.14*). When the parameters of the fluorescent reads were compared, there was no difference in the percentage of cells, area under the fluorescence curve, latency to the first fluorescence peak, or the fold fluorescence change between supplemented and unsupplemented cells ($n$=3 coverslips, unpaired t-test, $t_{(4)}$=0.3227, p>0.05). For all other Opn4 experiments, 9-*cis*-retinal was supplemented.

Opn4 and opto-$\alpha_{1A}$AR receptors produced a calcium response to a single LED stimulus in HEK 293T cells, measured by Cal-630 red-shifted calcium indicator. For the four different parameters measured (percentage of cells responding to stimulus, fluorescent change in responding cells, time taken to reach $F_{maz}$ and area under the curve of transient) neither receptor was significantly affected by changes in LED brightness (see *Figure 4.15*). Comparing the receptor responses directly for each parameter and stimulus strength, Opn4 activation is more probable at the lower light levels than the opto-$\alpha_{1A}$AR with a 0.5 fold increase in percentage of cells responding (10% and 25% laser power, $n$>4 coverslips, $p$=0.0161 and 0.0062, respectfully) and can produce a larger change in calcium transient fluorescence up to 2 fold larger (75% laser power, $n$>3 coverslips, $p$=0.0294; see *Table 4.1*).

Overall, these results indicate that Opn4 is as good as, and perhaps better than, the opto-$\alpha_{1A}$AR for producing calcium transients in response to light stimulation.

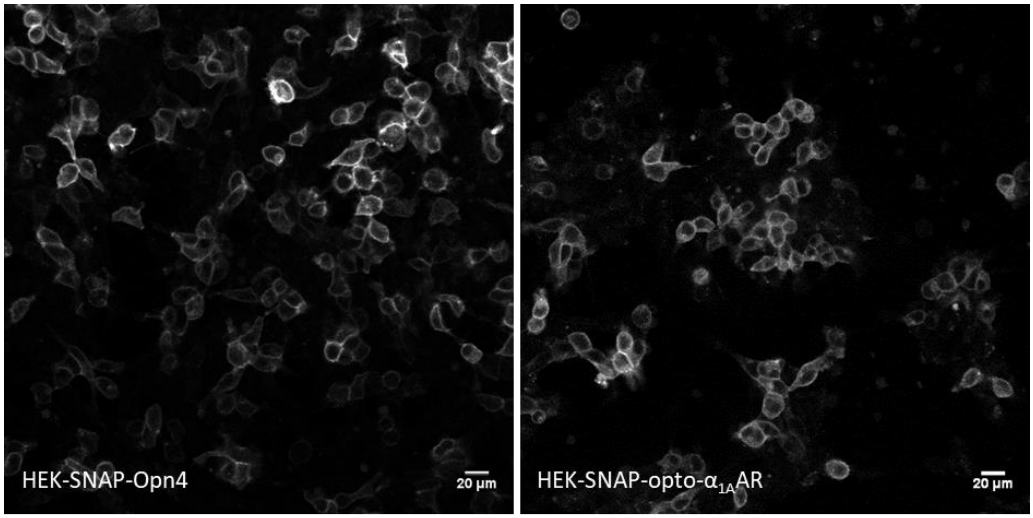


***Figure 4.13*** **– Comparison between Opn4 and opto-$\alpha_{1A}$AR expression in HEK 293T cell**s. Receptors were labelled with SNAP-Surface AF488 (0.2µM) and imaged on a confocal microscope. These images were taken in tandem with the Cal-630 calcium measurements after LED stimulation. Representative of all HEK cell experiments, $n$=1.

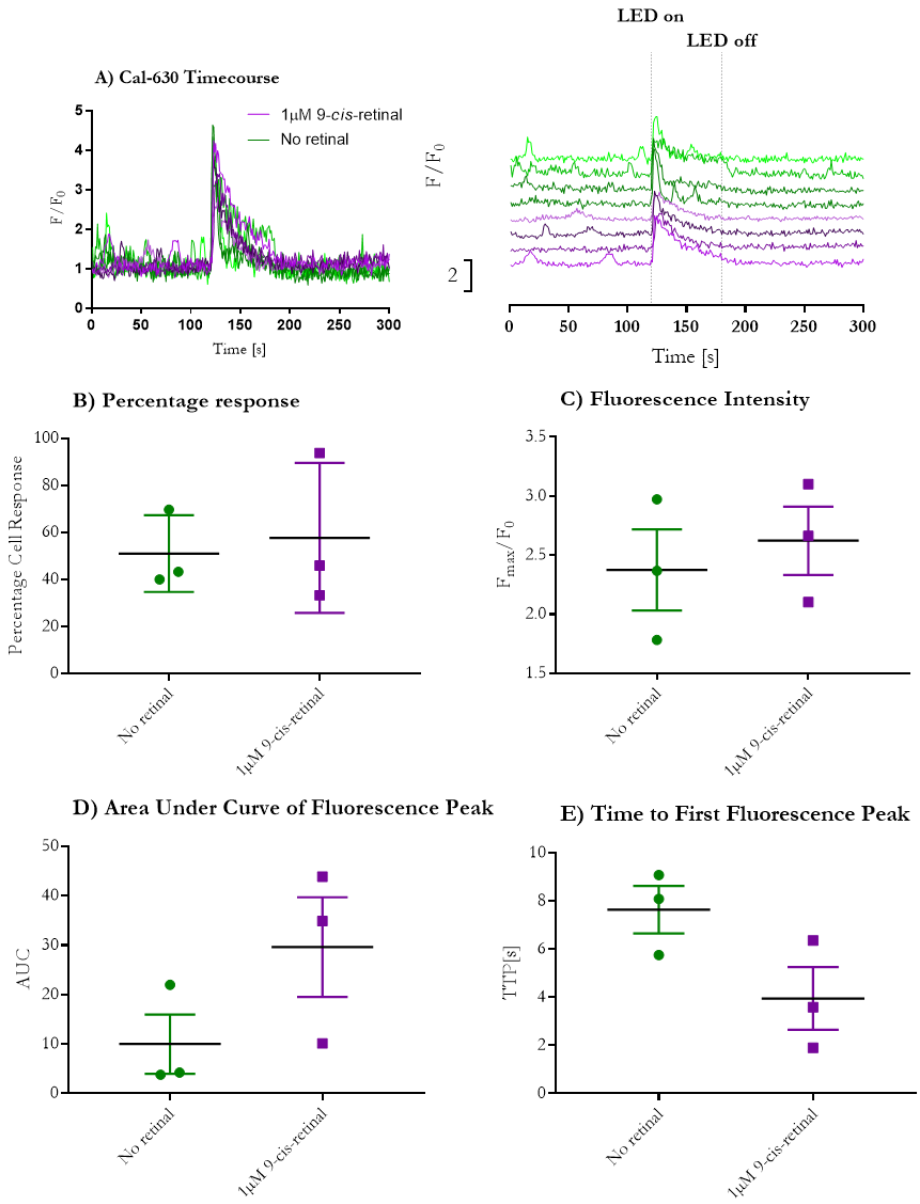


***Figure 4.14* – HEK-SNAP-Opn4 cell line responds to LED light stimulus independent of 9-*cis*-retinal supplementation.** Above, raw fluorescence reads of Cal-630 (1µM) from HEK-SNAP-Opn4 cells, 4 with 9-*cis*-retinal supplementation (1µM; *purple*) and 4 without (*green*), both stimulated at 120s for 60s with 470nm LED (25% power). Cells are randomly chosen from responding cells on 3 coverslips for each condition and show little difference in response profile (>20 cells measured per coverslip). Below, measured calcium response profiles for percentage of cells responding to LED, fold change in Cal-630 fluorescence, area under the curve of fluorescence change and time to reach fluorescence maximum ($n$=3 coverslips where >20 cells were measured per coverslip).

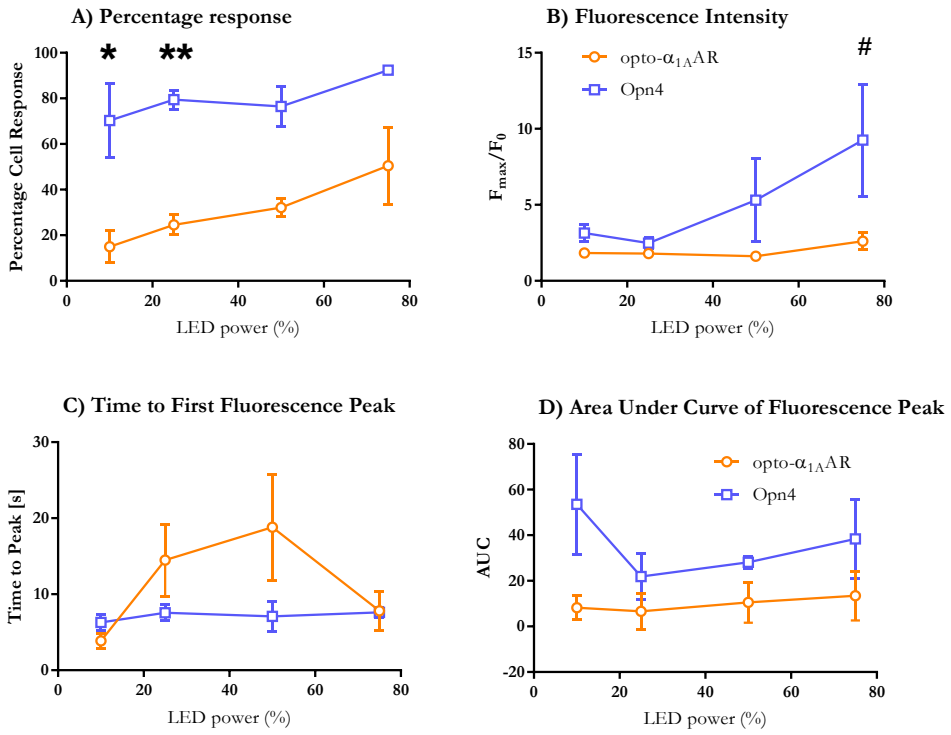


***Figure 4.15* – Different parameters of the calcium response profiles in the HEK-SNAP-opto-$\alpha_{1A}$AR and HEK-SNAP-Opn4 cell lines measured by Cal-630 imaging.** Cells were recorded for 5min and stimulated using a single 60s 470nm LED pulse after 2min ($n \leq 4$ coverslips for each LED power used, at least 20 cells were measured per coverslip). From each cell with a response to LED stimulation in A), the B) fold change of Cal-630 intensity, C) time to reach peak intensity and D) area under the curve of transient response were taken. There was a significant increase in percentage of cells responding with Opn4 expression at the lower light levels and an increase in Cal-630 peak fluorescence at the highest light exposure (one-way ANOVA, Tukey's post hoc; *$p$=0.006, **$p$=0.016, #$p$=0.029).

| $Ca^{2+}$ Imaging Parameter | Sig. Difference? | Stimulus Intensity (% LED power) | Difference Opn4:opto-$\alpha_{1A}$AR | *p* value |
|---|---|---|---|---|
| **Percentage of cells responding** | Yes | 25 | Opn4 55% ↑ | 0.0062 |
| | | 10 | Opn4 55% ↑ | 0.0161 |
| **$F_{max}/F_0$ Cal-630** | Yes | 75 | Opn4 x2 ↑ | 0.0294 |
| **Time to $F_{max}$** | No | | | |
| **AUC of transient** | No | | | |

***Table 4.1* – Comparison of Opn4 and opto-$\alpha_{1A}$AR calcium response profiles to a single 60s 470nm LED stimulus in HEK 293T cells**. Opn4 stimulation produces a 55% increase in the number of cells stimulated on a coverslip compared to the opto-$\alpha_{1A}$AR receptor at the lower LED powers (10% and 25%, one-way ANOVA, Tukey's post hoc). At the highest LED power, Opn4 also produces a fluorescence increase twice the size of opto-$\alpha_{1A}$AR after light stimulation (at 75% power). All data $n \geq 4$ coverslips per receptor, with >20 cells measured per coverslip.

### 4.2.5 Brightness of Stimulus Insufficient to Alter Melanopsin or Truncated Melanopsin Induced Calcium Transients

Developing on the findings in HEK cells, primary astrocytes transfected with Opn4 were stimulated at different LED powers to see if this would affect the calcium response profile of a single cell. Increasing the brightness of a light stimulus has been shown to similarly increase the calcium response in cell populations expressing a $G_q$ coupled optogenetic receptor (Airan *et al.*, 2009). This has often been reported as a population calcium response. Under the conditions outlined with an external LED stimulus of 470nm and using X-Rhod-1 AM as a calcium indicator, no changes in single cell calcium measurements were detected in Opn4 transfected primary rat astrocytes for any of the parameters measured (percentage of cells responding, change in fluorescence, time to reach fluorescent peak and area under the fluorescence transient) between the power range of 1-100% of the LED stimulus (see *Figure 4.16*, $n \geq 3$ coverslips, one-way ANOVA, $p > 0.05$). This indicates that melanopsin is sensitive to low light stimuli and does not require high luminosity for activation. The Opn4-$Ser^{411}$ truncated receptor was also measured using the same methodology to compare response profiles. There was no significant difference between the two receptors for any of the parameters measured, and also no change in the calcium parameters between LED stimulus brightness

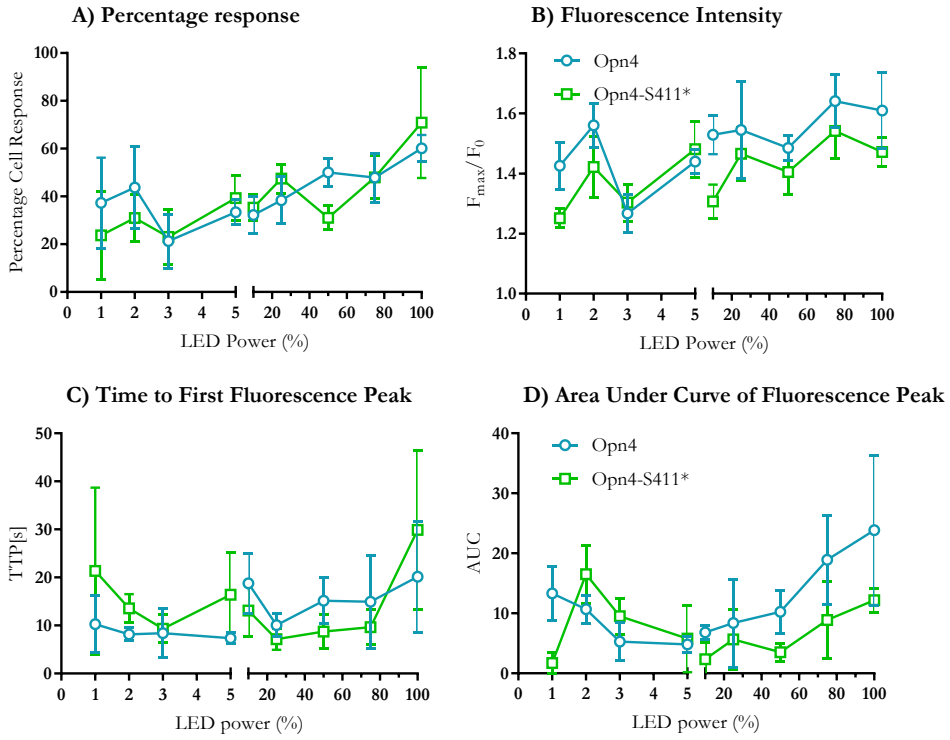


***Figure 4.16* – Calcium response profiles of primary rat neonatal cortical astrocytes expressing SNAP tagged Opn4 or Opn4-S411* mutant.** Astrocytes were transfected 24hr prior to experiment using electroporation and loaded with 1μM X-Rhod-1 calcium indicator and 0.5μM SNAP-Surface AF488 to determine receptor expression. Cells were imaged for 5min on a confocal microscope and stimulated with a 470nm LED after 2min baseline recording at specified brightness (1-100% power). A) shows the percentage of cells on a coverslip responding to LED light stimulation, B) the change in fluorescence upon stimulation of responding cells, C) the time taken to reach peak fluorescence and D) the area under the curve of the peak response.

### 4.2.6 Melanopsin can Induce Calcium Transients to Multiple, Temporally Distinct Light Stimuli

Often a single stimulus is used in optogenetic experiments, whether sustained for a long or short amount of time. Ligand action often does not follow this pattern, with diffusion and unbinding and rebinding of the ligand-receptor complex. In the CNS, there are often multiple stimuli also acting upon an individual cell or group of cells. Replicating this using light can be done by using multiple light on and off signals for a single experiment, potentially offering a more physiologically relevant stimulus pattern than a single, sustained stimulus.

Three different temporal stimulation patterns were selected to test the response of melanopsin in astrocytes under multiple light stimulation in a short period of time; 5s stimulation followed by 5s of darkness 6 times, 10s stimulation with 10s of darkness 3 times, and 20s of stimulation and 20s of darkness 3 times. The patterns were chosen to fit within the 5min time window used in previous experiments with a similar time frame to the 60s stimulus used before. To measure the cell calcium, calcium imaging with X-Rhod-1 AM (1μM) was again used and the cells were stimulated on a confocal with an external LED stimulus at 470nm (25% power, used as the highest power with the least background interference). Both melanopsin and the Opn4-S411 truncated mutant could respond to all three stimuli in the 10s on/off temporal pattern of light (see *Figure 4.17* for examples) and the 20s on/off pattern, although neither receptor could respond to all 6 stimuli under the 5s on/off pattern. The percentage of cells responding to the stimuli did not change between receptor types or under different stimulation patterns, however the average number of transients produced by the light stimulus significantly increased using the Opn4-S411* mutant and longest 20s stimuli by 50-100% (one-way ANOVA, Tukey's post hoc, $p$=0.0299, $n\geq5$, $F_{(5, 26)}$=2.584; see *Figure 4.18*). This indicates that a 5s stimulus is sufficient to stimulate the cell population, and that the Opn4-S411* mutant is more likely to produce a calcium transient in response to a repeated stimulus. The pattern of calcium transients in response to light stimuli are shown in *Figure 4.19* where each responding cell has been represented. Most transients are produced shortly after a light stimulus, and more Opn4-S411* cells respond to the third stimuli of the 20s stimulus than with the Opn4 wild type.

To see if there was a change in calcium influx between the receptors and stimuli patterns, the area under the fluorescent transient and the fold fluorescence change were measured (see *Figure 4.20*). When measuring a generalised AUC and fold change for all calcium transients, there was no detectable significant difference between the mutant and wild type melanopsin receptors, nor the different light stimulus patterns. Investigation of individual responses to each transient revealed that the wild type receptor can produce a 0.25x larger fluorescence transient, and therefore a greater calcium influx, in response to the longest 20s stimulus compared to the Opn4-S411* mutant (two-way ANOVA, Tukey's post hoc, $p<0.0001$, $n\geq3$, $F_{(5, 258)}=6.66$). The 20s stimulus also produced almost 2x greater fluorescence area than the 10s stimulus with the wild type receptor which was not seen in the mutant (two-way ANOVA, Tukey's post hoc, $p=0.0269$, $F_{(5, 258)}=6.66$, $n\geq3$). This suggests that the wild type Opn4 requires a longer light stimulus for activation. Fluorescence fold change was significantly reduced in both the Opn4 and Opn4-S411* by around 0.2x between the first and last 20s stimulus (two-way ANOVA, Tukey's post hoc, $p=0.031$ and $p=0.0131$ respectfully, $F_{(2, 257)}=2.69$, $n\geq3$), indicating that receptor response diminishes under multiple light stimuli.

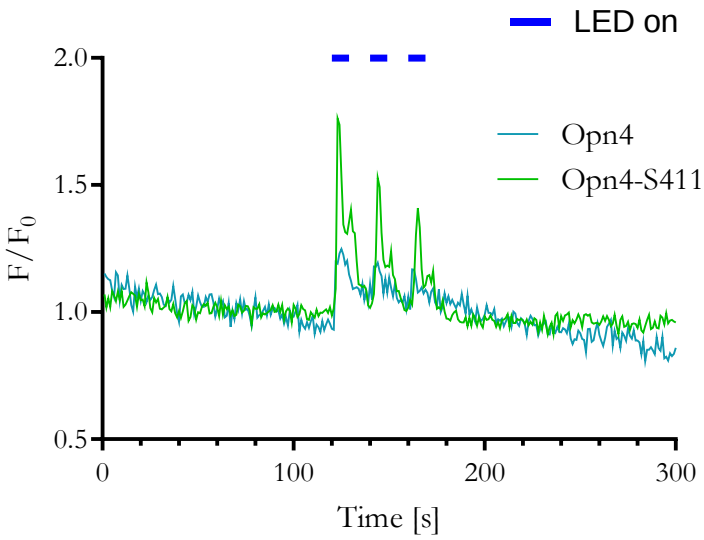


***Figure 4.17* – Astrocytes transfected with melanopsin and its truncated mutant can respond to several distinct stimuli in a single timeframe.** Raw fluorescent values of X-Rhod-1 AM dye are displayed for a single cell under LED 470nm stimulation for Opn4 and Opn4-S411*. Light was turned on after 120s, turned off after 10s and turned back on after 10s, with this repeated three times. The fluorescence trace shows that both receptors can produce a calcium transient in response to all three stimuli in astrocytes, although the peak fluorescence decreases with each stimulation (chosen from $n$=5 coverslips with >20 measured cells).

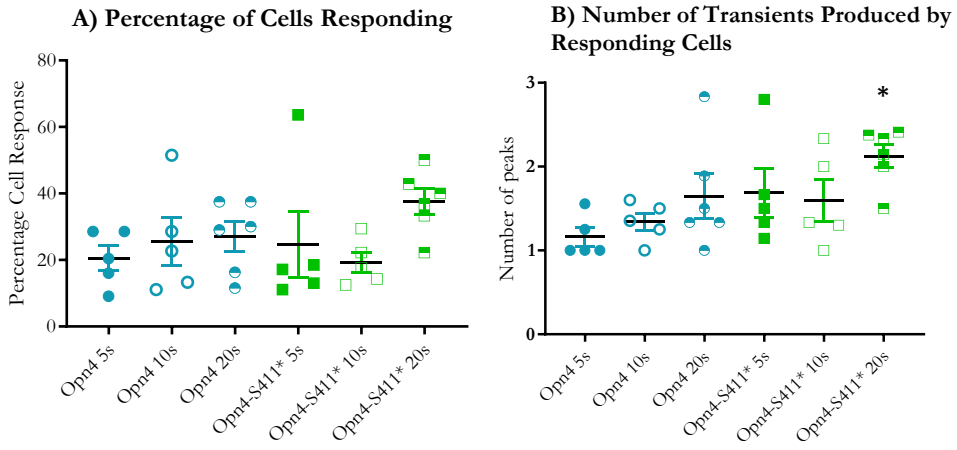


***Figure 4.18*** **– The percentage of astrocytes responding to the light stimuli of different temporal patterns and the number of transients produced by these responding cells.** The patterns used were 5s on 5s off (x6), 10s on 10s off and 20s on 20s off (both x3) after a 2min baseline using an external 25% power 470nm LED, with calcium measured using 1μM X-Rhod-1. Each point represents a coverslip with >20 cells where $n \geq 5$ coverslips for each variable. A) Percentage of cells on a coverslip which produced a transient. B) Average number of transients produced by responding cells. Using a 20s on 20s off stimulation pattern, Opn4-S411* produced a significantly increased number of transients in response to the light pattern (one-way ANOVA, Tukey's post hoc, $*p=0.0299$).

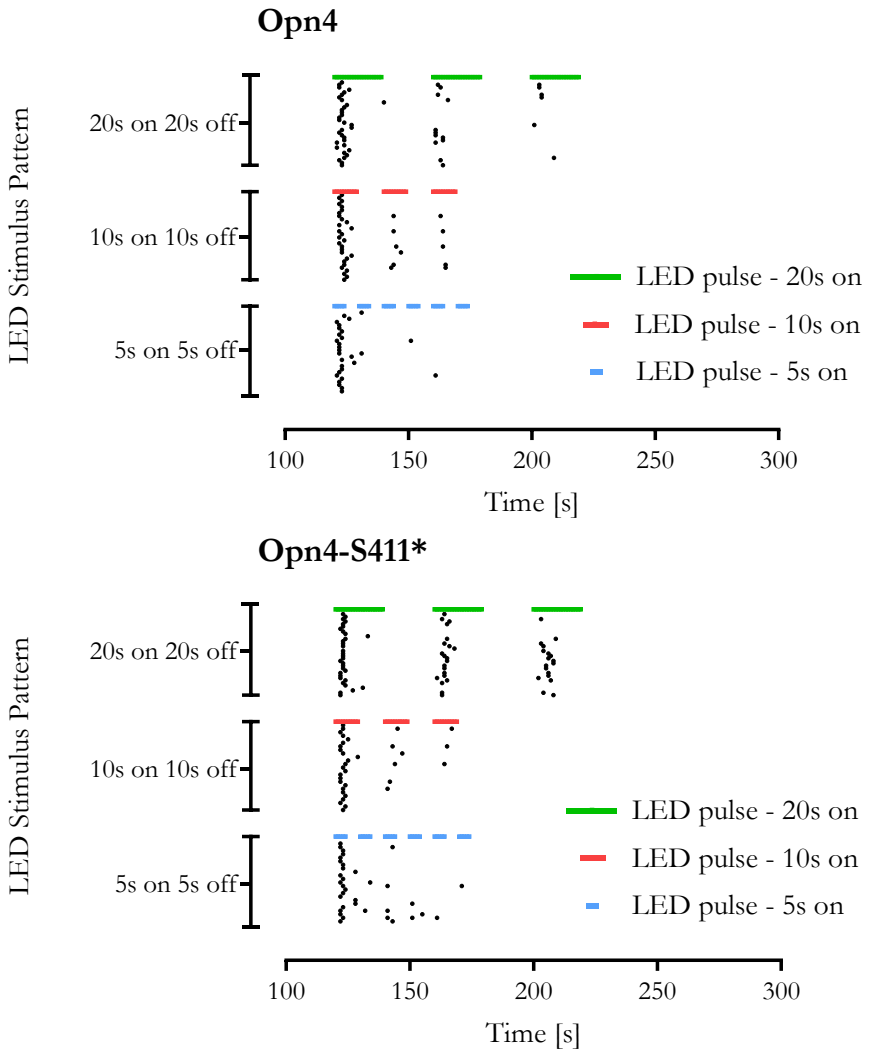


***Figure 4.19* – Raster plot of transients produced by astrocytes transfected with Opn4 and Opn4-S411* and stimulated with different light patterns.** Each row represents a cell, and every black dot represents a peak in the fluorescent trace of a single cell. Only responding cells are shown. Qualitatively, there is a greater cluster of cells responding to the third LED pulse in the 20s stimulus pattern for the mutated Opn4-S411* receptor than the Opn4 wild type. There is an increase in cells responding to the different 5s stimuli for the mutant compared to the wild type. $n \geq 20$ cells per stimulus pattern for each receptor.

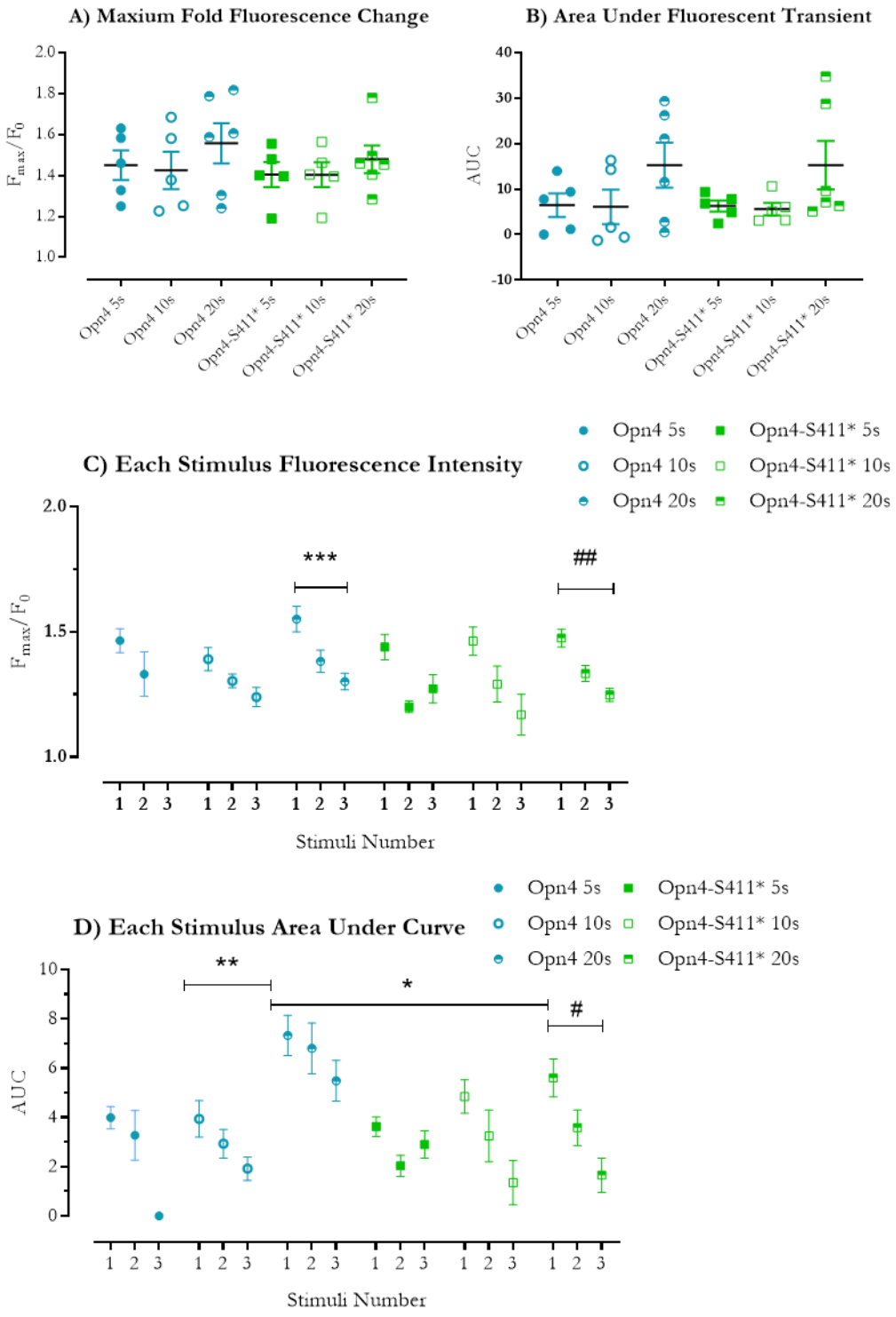
A) Maxium Fold Fluorescence Change
B) Area Under Fluorescent Transient
$F_{max}/F_0$
AUC
Opn4 5s
Opn4 10s
Opn4 20s
Opn4-S411* 5s
Opn4-S411* 10s
Opn4-S411* 20s
C) Each Stimulus Fluorescence Intensity
***
##
Stimuli Number
D) Each Stimulus Area Under Curve
**
*
#
Stimuli Number

***Figure 4.20* – Quantification of fluorescent calcium transients in Opn4 and Opn4-S411* transfected primary astrocytes in response to different temporal patterns of LED stimulation.** Grouped data of A) maximum fluorescence change and B) area under fluorescence curve for the whole experimental timecourse for the Opn4 and Opn4-S411* receptors. C) Fluorescence intensity changes of only responding cells for the first 3 light stimuli, separated into their respective groups. The change in fluorescence intensity is greater for the first stimuli under a 20s stimulus than the third stimuli for both receptors (two-way ANOVA, Tukey's post hoc, $F_{(2, 257)}$=2.69; ***$p$=0.031, ##$p$=0.0131). D) Area under the curve of each transient, separated for each stimulus. The first transient produced by the Opn4 receptor under a 20s LED stimulus has a significantly larger AUC than the first peak produced by the Opn4-S411* receptor under the same stimulus, or by a shorter 10s stimulus with the Opn4 receptor (two-way ANOVA, Tukey's post hoc, $F_{(5, 258)}$=6.66; *$p$<0.0001, **$p$=0.0269). Opn4-S411* produces the greatest AUC on the first LED stimulation, which is significantly lower by the third LED pulse (#$p$=0.031). For each stimuli pattern and receptor, $n$≥3 cells.

### 4.2.7 Inhibition of $G_{i/o}$ Protein in Melanopsin Astrocytes Affects Calcium Response to Multiple Light Stimuli

Melanopsin has been reported to activate both $G_q$ and $G_i$ proteins (Cao *et al.*, 2012; Spoida *et al.*, 2016). To investigate the extent of $G_i$ signalling activation on the calcium responses seen in light-activated Opn4 astrocytes, pertussis toxin (PTX) was used as a selective $G_{i/o}$ protein inhibitor (100ng/mL). The same conditions were used as the previous experiments, with an external 470nm LED for stimulation on a confocal and X-Rhod-1 (1μM) as the calcium indicator. Primary rat cortical astrocytes were transfected, plated, and left to recover for 24hr before treatment with PTX for 24hr. The 24hr delay was required as PTX restricts growth. This did not affect confluency or Opn4 receptor expression in the astrocytes (see *Figure 4.21*).

Treating Opn4 astrocytes with PTX did not affect any of the tested variables for the calcium transients produced under a single 60s 470nm LED stimulation. There was no change between treated and untreated cells for percentage of activation, fold fluorescence change, area under the fluorescence transient or time to the fluorescence peak (see *Figure 4.22*; unpaired *t*-test, $t_{(5)}=0.105$, $n\geq3$ coverslips, >20 cells measured per coverslip). Inhibition of $G_{i/o}$ activation by melanopsin therefore does not alter calcium signals produced by the receptor, indicating that these calcium transients are produced by $G_q$ activation.

The relevance of $G_{i/o}$ activation in melanopsin response to multiple transients was investigated using the 20s on/off protocol used in section 4.2.7, selected due to the increased temporal resolution compared to other patterns of light. Under 20s stimulation, PTX treated cells had an increased percentage of response compared to untreated Opn4 astrocytes from an average of 30% increasing to 50% response (including non-transfected cells; see *Figure 4.23*). There was no difference between the average number of calcium transients detected with X-Rhod-1 AM between untreated and PTX treated astrocytes. No changes in the average area under the curve or fluorescence intensity were detected. When the stimulation time frames were separated, however, there was an increase in area under the curve for the first transient in the stimulation protocol in PTX treated cells (2-way ANOVA, Tukey's post hoc; $p=0.0083$, $F_{(2, 129)}=0.629$, see *Figure 4.24*) and the same drop off in transient

size as seen in untreated cells, both AUC and $F_0/F_{max}$ (2-way ANOVA, Tukey's post hoc, $p$=0.0045, $F_{(2, 129)}$=0.629 and $p$=0.0002, $F_{(2, 127)}$=0.45 respectively, $n$=12-39 responding cells per group).

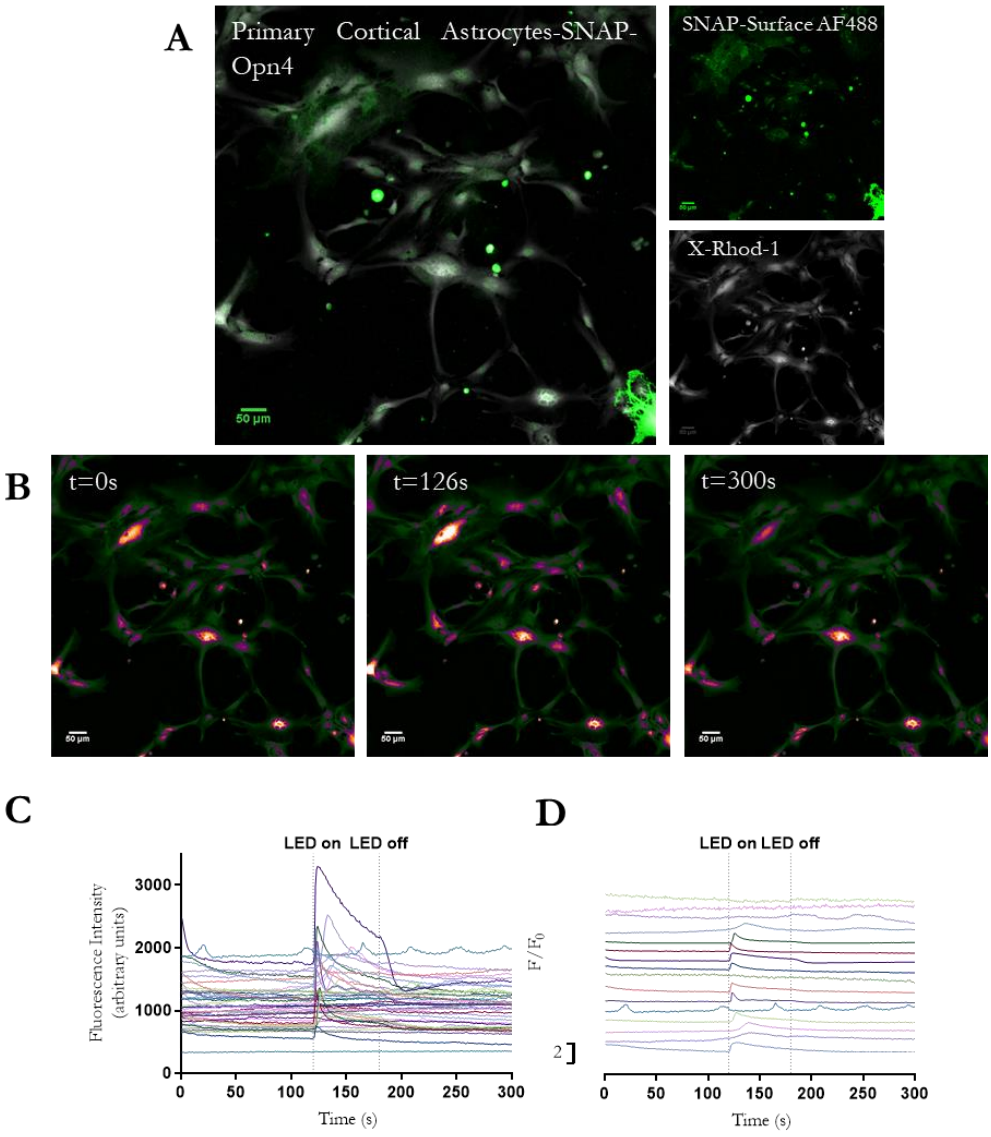


***Figure 4.21*** – **Pertussis toxin incubation does not affect astrocyte morphology, calcium production, nor transfection efficiency.** Primary cortical astrocytes (neonatal P3, DIV 21) were transfected with SNAP-Opn4 and seeded for 24hr, before incubation for 24hr in PTX (100ng/mL). This did not change the astrocyte confluency and morphology in A) and the astrocytes can still respond to LED stimulation, as shown in the B) calcium dye intensity visualised, C) plotted raw fluorescence intensity of every cell and D) normalised fluorescence responses. Representative of 3 coverslips, *n*=1 shown here.

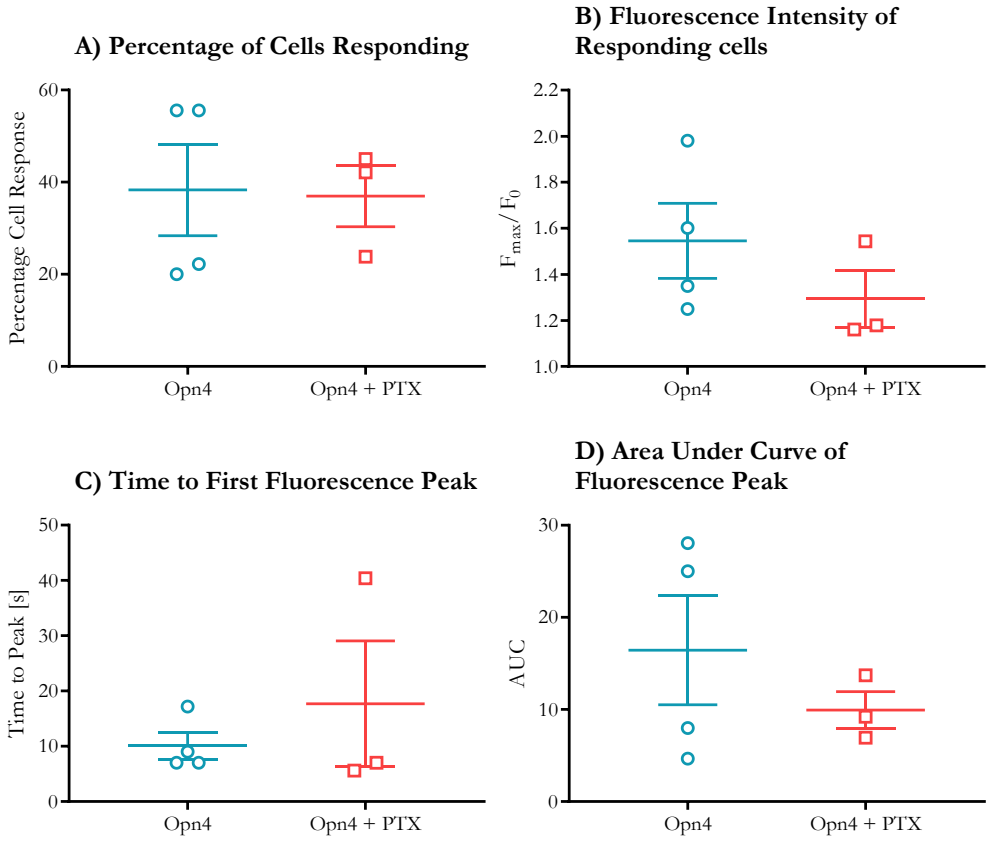


***Figure 4.22*** **– Inhibition of $G_i$ response using pertussis toxin does not affect Opn4 transfected astrocyte's calcium signalling following a single 60s light stimulus.** Astrocytes were incubated with PTX (100ng/mL) for 24hr before stimulation with a 470nm LED after 120s in a 300s timecourse with X-Rhod-1 (1μM) as the calcium indicator. The calcium signalling variables are separated as A) percentage of cells responding, B) fluoresence intensity of the responding cells, C) time to the first fluorescence peak and D) area under the curve of responding fluorescence peaks. $n \geq 3$ coverslips with a minimum 20 cells measured per coverslip, experiments performed on separate days.

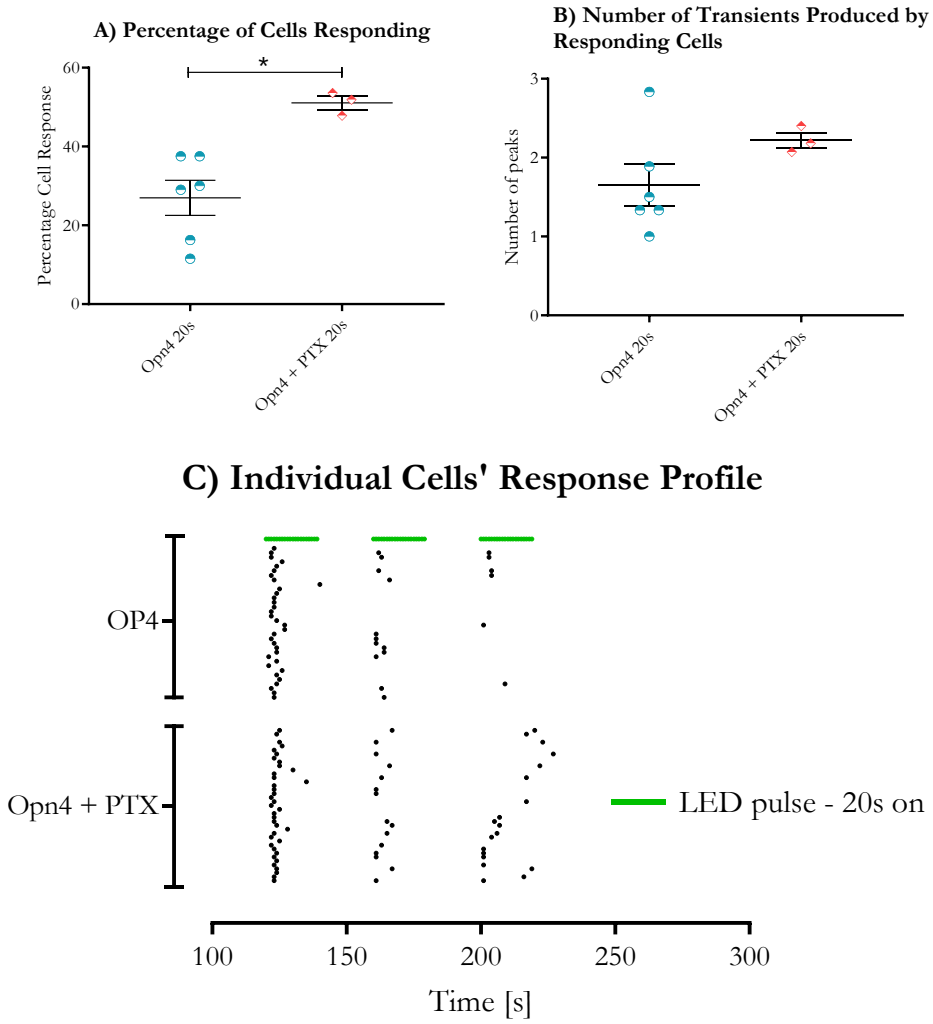


***Figure 4.23*** – **Percentage of Opn4 astrocytes responding and number of calcium transients produced by 3 pulses of light when treated with PTX.** Astrocytes were incubated with PTX (100ng/mL) for 24hr before measuring calcium response with X-Rhod-1 (1μM) to 470nm LED on for 20s, and then off for 20s x3. A) There is an increase in the percentage of astrocytes responding to the multiple stimuli when $G_i$ is inhibited by PTX (unpaired *t*-test, $*p=0.008$, $n \geq 3$ coverslips with >20 cells measured per coverslip). B) There are a similar number of transients produced in responding cells with or without PTX. C) Raster plot comparing Opn4 transfected astrocytes transient peaks with or without PTX. Each row is a single cell and each black dot is a fluorescence transient. PTX increased the number of cells responding to the third LED stimulus, but this was usually with a large delay to the peak of the response.

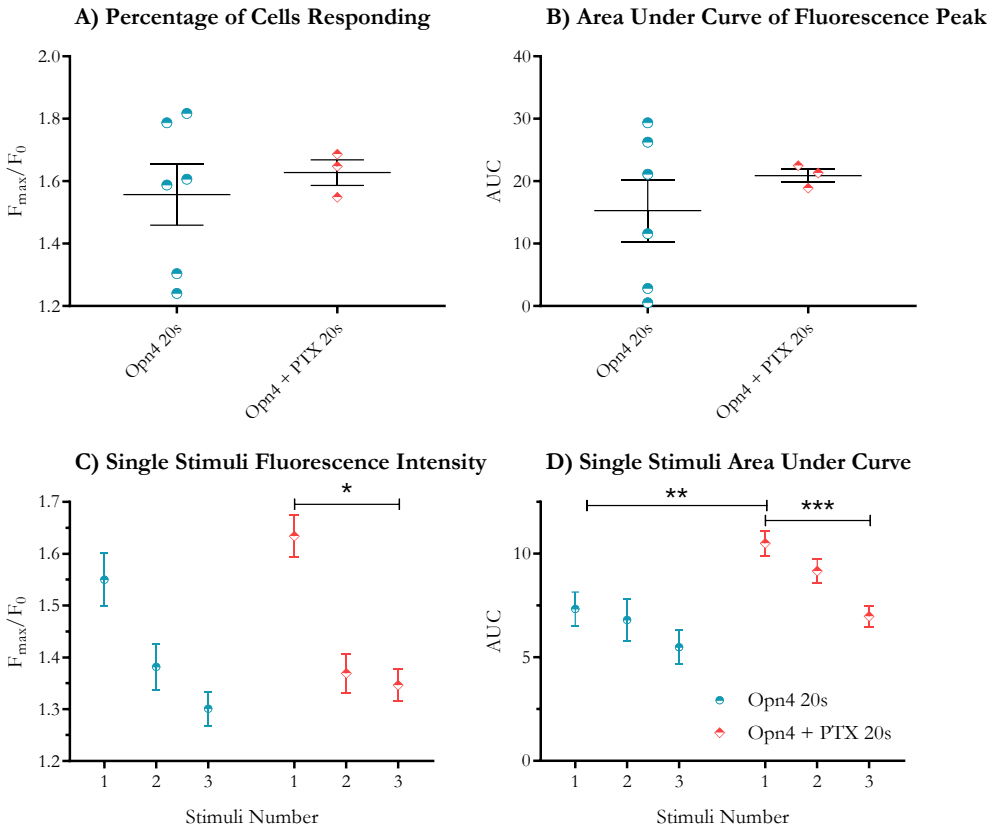


***Figure 4.24* – Size of calcium transients in Opn4 astrocytes produced by 3 pulses of light when treated with PTX.** Astrocytes were incubated with PTX (100ng/mL) for 24hr before measuring calcium response with X-Rhod-1 to 470nm LED on for 20s, and then off for 20s x3. The A) response percentage and B) AUC of fluorescent peaks for all stimuli. C) When single light stimuli responses are separated, an increase in the fluorescence intensity for the first stimuli compared to the final stimuli with PTX SNAP-Opn4-astrocytes can be detected (**p*=0.0002, two-way ANOVA, Tukey's post hoc, $F_{(2, 129)}$=0.629, *n*=12-39 responding cells per group). D) Area under fluorescence curve for each light stimuli. SNAP-Opn4-astrocytes treated with PTX produce a greater area under the curve than cells without PTX (***p*=0.0045), and the first stimuli produces the largest AUC (****p*=0.0083).

## 4.3 Discussion

### 4.3.1 Primary Astrocytes Increase Complexity of Optogenetic Assays

Compared to HEK 293T cells, primary astrocytes proved more difficult to both transfect and stimulate with the optogenetic GPCRs used. Although the opto-$\alpha_{1A}$AR has previously been reported to successfully transfect into primary astrocyte cultures, in this study the cells did not readily take up the receptor (Figueiredo *et al.*, 2014). The main difference is that Figueiredo and colleagues (2014) used adenovirus as their method of gene delivery, compared to the chemo-transfection and electroporation techniques used here. Adenovirus delivery was avoided due to the immune response that the method can produce which would interfere with any physiological studies using the transfected primary astrocytes. Increased transfection rates of the Opn4 receptor compared to the opto-$\alpha_{1A}$AR in primary astrocytes using the same transfection methods may be an indication that Opn4 is a more stable, more easily expressed GPCR optogenetic actuator than the opto-$\alpha_{1A}$AR. This suggests that Opn4 is easier to use for studying general GPCR induced calcium signalling in astrocytes.

Once the Opn4 receptor was successfully expressed, receptor stimulation also proved different to HEK cells. The continuous laser stimulus used in HEK studies did not produce any calcium transients in Opn4 transfected astrocytes. Transfection efficiency differences could be the cause, as HEK cells overexpress the transfected receptors at the plasma membrane more readily and in greater amounts. There could also be an effect due to the difference in morphology between primary astrocytes and HEK cells. Primary astrocytes are larger cells, usually around 100μM in diameter compared to around 20μM for HEK cells, and astrocytes are also a lot flatter and more spread out *in vitro*. One hypothesis is that less receptors are activated by each laser point scan in astrocytes compared to HEK cells due to the spread of receptors and decrease in transfection rate. As astrocytes are also larger, it would suggest that more activated receptors could be required for calcium innovation big enough to produce a whole cell calcium transient. Entire coverslip saturation with LED light proves to be the required method to activate

the Opn4 receptors in astrocytes due to the lack of effectiveness of laser stimulation.

### 4.3.2 Melanopsin vs Opto-$\alpha_{1A}$AR Activation

Although opto-$\alpha_{1A}$AR provides a link to the endogenously expressed $\alpha_{1A}$ adrenoceptor, Opn4 is also coupled to $G_q$ and has the potential to represent a whole subset of $G_q$ protein linked receptors by replicating functional output downstream. Due to the lack of expression of the opto-$\alpha_{1A}$AR receptor in astrocytes, Opn4 activation via LED stimulation was compared to the chimera using stably transfected HEK 293T cell lines. Direct comparison of the two receptors showed little difference in the stimulation profile, although Opn4 did lead to an increase in the number of cells activated by light at lower LED brightness and an increase in the change of Cal-630 fluorescence, and therefore intracellular calcium, for the highest LED power used. This suggests that Opn4 may activate at a lower light level and have a larger window of activity compared to the opto-$\alpha_{1A}$AR. There is also a lower dependence on Opn4 for 9-*cis*-retinal than the opto-$\alpha_{1A}$AR, with HEK-Opn4 cells producing calcium signals to light stimulation without any supplementation in HEK cells. Calcium responses to HEK-Opn4 cells without retinal supplementation were also detected by Spoida *et al.* (2016) and the transients were described to be the same as cells without supplementation, although Bailes and Lucas (2013) reported a decrease in calcium signalling when their HEK-Opn4 cells were not supplemented with retinal. HEK cells do have some retinoid processing machinery, although this is less than most primary cells (Brueggemann and Sullivan, 2002). The HEK retinoid processing was insufficient to allow normal function of the opto-$\alpha_{1A}$AR receptors in Chapter 3, however it appears that the processing is sufficient for melanopsin. As to why this could be the case, melanopsin is very resistant to light bleaching and has been reported to bind *cis*-retinal in a bi- or tristable reversible conformation, unlike rhodopsin which requires liberation of the *trans*-retinal before the receptor can return to its inactive form (Sexton *et al.*, 2012; Emanuel and Do, 2015). This allows faster recycling of the retinal in melanopsin, meaning that less external retinal is required for receptor re-activation. Overall, the studies in HEK cells and the lack of opto-$\alpha_{1A}$AR

transfection in astrocytes promotes melanopsin as a more robust optogenetic tool for studying calcium signalling.

### 4.3.3 Potential Gliotransmission to Non-light sensitive Cultured Astrocytes

An interesting observation from the optogenetic experiments performed on optogenetic cultured astrocytes were calcium transients produced in cells where no fluorescent tag of receptor expression was present, a response not seen in control cultures. One explanation could simply be that the cells in question are expressing the optogenetic receptors but not on the plasma membrane. As the SNAP protein was tagged with SNAP-Surface fluorescence, only receptors on the cell membrane were detected as this represents good translation of the receptor DNA. GPCRs are usually targeted to the membrane, however there is also evidence for endosomal activation of GPCRs inside cells (Tsvetanova *et al.* 2015, see Chapter 1.1.4 for more detail). Primary astrocyte cultures are naturally heterogeneous and transfection differences could occur between cells, nevertheless this would mean that the receptors in question were not expressing to the same extent as the recognisably transfected astrocytes, so any response would probably be reduced. More likely, these results add to the growing evidence in support of transmitters released from calcium-stimulated astrocytes. Optogenetics presents as a useful tool for investigating gliotransmission as only cells with the receptor present can be photostimulated. Studying the potential of gliotransmission with optogenetics, Li *et al.* (2012) used the light-gated $Ca^{2+}$-permeable ionotropic GluR6 receptor to invoke light stimulated calcium elevation in cultured cortical astrocytes, both transfected (LiGluR+) and un-transfected (LiGluR-) with a temporal delay in LiGluR- responses. LiGluR- $Ca^{2+}$ transients were blocked by mGluR and anion channel antagonists but not exocytosis, glutamate-transporter nor hemichannel inhibitors, indicating that glutamate was being released from stimulated LiGluR+ cells via glutamate-sensitive anion channels. Similarly, Berlinguer-Palmini *et al.* (2014) used channelrhodopsin 2 (ChR2) optogenetics in cultured astrocytes to excite surrounding transfected astrocytes and increase synaptic activity of co-cultured neurons. Both studies have a slight caveat that the two photoreceptors used are permeable to different cations as well as calcium, increasing the variables in how the response was triggered (Izquierdo-Serra *et al.*, 2013; Schneider *et al.*, 2013).

Melanopsin provides a more specific response through G protein activation and produces evidence in favour with the previous studies. Further investigation into the mechanisms involved in signal transfer between Opn4+ and Opn4- astrocytes would be of interest.

### 4.3.4 On-Off Light Stimulation of Melanopsin Produces Multiple Calcium Transients in Astrocytes

Primary astrocytes provide an *in vitro* option for increasing translational capacity as their cellular signalling and scaffolding is more complex than recombinant cells with increased heterogeneity. When treated with an $\alpha_1$ adrenoceptor agonist (phenylephrine), the cultured astrocytes produce a variety of different calcium transients to sustained agonist presence such as a sustained increase in intracellular calcium, a single peak response, or multiple transients in an oscillatory style. Using a single, sustained LED pulse with the Opn4 transfected optogenetic astrocytes induced a temporal calcium response with a single peak in calcium concentration. Multiple LED pulses with an on/off pattern could produce a single transient or multiple transients in melanopsin astrocytes, akin to the mix in temporal calcium responses induced with phenylephrine. Rather than using a single, sustained stimulus in GPCR optogenetic experiments, these data suggest multiple pulses produce a more physiologically recognisable response. The opto-$\alpha_{1A}$AR has not yet been utilised in astrocytes this way, with only single light pulses used in a comparative study (Figueiredo *et al.*, 2014). However, low frequency light stimulation of melanopsin expressing astrocytes has been used *in vivo* to induce long-term synaptic plasticity in mice over a short stimulation time of 3min with pulses as short as 5s (Mederos *et al.*, 2018). The most robust responses in the multiple stimuli study were produced using a 20s on/off pattern which can be attributed to the natural length of a calcium transient typically lasting over 40s, as seen with the phenylephrine and melanopsin calcium response timecourses. Shorter patterns would not allow oscillations due to reduced time for recovery from the calcium release, although these are still feasible but decidedly less often. The next stage of optogenetic activation would be to target smaller areas of the cell in order to see the effect of spatial activation and smaller, more controlled calcium puffs.

### 4.3.5 Truncation of the Melanopsin C terminus and the Effect on Receptor Expression and Function in Primary Astrocytes

Removing the phosphorylation sites in the C terminus of the receptor can be used as a method of altering signal output by affecting β-arrestin binding, should the receptor be functional (Gainetdinov *et al.*, 2004, see Chapter 3.1.3 for detailed review). Using the opto-$\alpha_{1A}$AR in chapter 3, different truncations aimed at threonine/serine sites produced different responses to functional outputs of calcium signalling and receptor internalisation. Here, the aim was to use a truncated mutant to alter firing rate of the optogenetic melanopsin tool to allow for different stimulation patterns of the cells.

Only one truncated mutant was used in this investigation; Opn4-S411* was readily expressed in astrocytes following electroporation, whereas Opn4-S375* was not usable. Transfection efficiency was similar for wild type and Opn4-S411* receptors, with neither receptor affecting astrocyte morphology. Truncation of melanopsin at $Ser^{375}$, removing several more phosphorylation sites, caused a reduction in the receptor expression at the astrocyte surface. Lack of surface expression indicates that the protein is not functional or folded correctly after translation. Residues between $Ser^{375}$ and $Ser^{411}$ may therefore have an important role in receptor function and expression. In one study, the phosphorylation of $Ser^{381}$ and $Ser^{398}$ in rat melanopsin were indicated to be important in the production of calcium signalling by light at the receptor, providing evidence that loss of these residues could reduce functional expression (Fahrenkrug *et al.*, 2014). These results were in contrast to experiments in mouse melanopsin which linked C terminal phosphorylation to reduced G protein activation (Blasic, Lane Brown, *et al.*, 2012; Blasic *et al.*, 2014). Whereas rat melanopsin has a similar structure to human, used in this study, mouse melanopsin has a much larger C terminus (Pires *et al.*, 2009). It would therefore be of interest to directly compare these three isoforms to understand the significance in the C terminus differences.

Under multiple stimulations with the LED, the Opn4-S411* mutant responded more often to the final light pulse, producing more transients on average than the wild type melanopsin receptor. Although the receptor could respond more readily to the light pulses, this was at a detriment to the size of the transients and the

calcium produced compared to wild type. Opn4-S411* may therefore be a useful tool in astrocytes to help stimulate the cells in a more translational pattern, as seen using a ligand stimulation for $G_q$, such a phenylephrine, where differing calcium transients are created. Such modifications are already being developed for channelrhodopsin-2 and melanopsin, though not yet tested in astrocytes and using different mechanisms (Tennigkeit *et al.*, 2019). As to how the Opn4-S411* mutant produces a more temporally precise response, these results could indicate an effect on deactivation of the receptor by removing the C terminus region, producing a smaller signal response but allowing for increased response rate. Supporting this theory, Mure *et al.* (2016) found a decrease in response and accelerated deactivation in a mutant similar to the Opn4-S411*, where the mouse melanopsin receptor was truncated at $Ser^{397}$. When serine and threonine residues before this point were mutated to alanine, the opposite occurred with an increase in light sensitivity and reduced deactivation. The mechanism of C terminus phosphorylation and the apparent effect on deactivation is therefore not yet clear. Studies into the components of the phototransduction cascade separate to G protein activation, such as β-arrestin binding and GRK phosphorylation, have yet to investigate the impact on receptor deactivation (Cameron and Robinson, 2014; Sexton and Van Gelder, 2015).

### 4.3.6 Melanopsin $G_i$ Activation and the Effect on Calcium Signalling

Melanopsin may couple to $G_{i/o}$ as well as $G_q$ proteins (Cao *et al.*, 2012; Spoida *et al.*, 2016). $G_{i/o}$ protein is suggested to also produce calcium signalling of its own, although the mechanisms appear to differ slightly to $G_q$ activation; the released $G_{\beta\gamma}$ subunits in the $G_i$ trimer are suggested to directly cause release of calcium from the endoplasmic reticulum through $IP_3$ receptor activation (Zeng *et al.*, 2003; Prole and Taylor, 2016). Nevertheless, treating the astrocytes with $G_{i/o}$ inhibitor PTX did not change photostimulation induced calcium transients to a single light stimulus. Under multiple stimulations, there was an increase in calcium liberation within the PTX treated cells, with increases in the percentage of cells producing a transient and the area under the curve of the first transient when compared to untreated cells. It is unlikely that the $G_{i/o}$ independent effects of PTX are the cause of increase in percentage response as these are usually linked to inhibition of cell growth and

maturation (Mangmool and Kurose, 2011). The increase in calcium could be produced by a decrease in cAMP inhibition, normally caused by $G_i$ activation, allowing an increase in transmission between cells. Thus, the increase in percentage of cells responding would be from untransfected cells through gliotransmission from Opn4 activated astrocytes where $G_i$ protein may be playing a role. To support this hypothesis, there is evidence *in vivo* that glial cells produce an ATP/adenosine dependent transient boost of synaptic transmission in response to optogenetic melanopsin activation (Mederos *et al.*, 2018). The $G_q$ coupled opto-$\alpha_{1A}$AR optogenetic calcium response in astrocytes is also sensitive to ATP degradation and adenosine receptor inhibition (Figueiredo *et al.*, 2014). As well as the impact of adenosine extracellularly, there could be a difference within the astrocytes. In this experiment, X-Rhod-1 was used as a calcium indicator, which typically loads with bias to the mitochondria. The calcium increases measured could be a result of increased cAMP availability to the mitochondria following PTX treatment, although this would need more thorough investigation to prove.

These results using PTX to block one of the signals produced by the cells aid in comprehension of the action of G proteins in astrocytes, which may be more complex than previously thought. Further research into the mechanisms involved in these cell signalling cascades would be of interest.

## 4.4 Conclusions

In this chapter, primary rat cortical astrocytes have been successfully transfected with light-activated melanopsin receptors. The calcium response to light activation in the primary astrocytes and HEK recombinant cells expressing melanopsin was characterised first with a single stimulus, then with multiple stimuli and proved favourable when compared to the chimeric opto-$\alpha_{1A}$AR optogenetic tool. Truncation of melanopsin at $Ser^{411}$ allows for a more temporally responsive receptor, although at the detriment of the maximal calcium response. Calcium signalling by melanopsin occurs independent of $G_i$ activation, but against hypothesis inhibition of $G_{i/o}$ increased the response rate of astrocytes stimulated by light. Taken together, these results provide an insight into the mechanism of melanopsin activation and desensitisation, as well as providing a valid optogenetic GPCR option for astrocytic research.

# Chapter Five
## Optogenetic Receptor Activation by Spatially Targeted Bioluminescence

## 5.1 Introduction

### 5.1.1 Spatially Localised Activation of Optogenetic Receptors in the Cell

Compared to extracellular ligand addition, one of the potential advantages of light activation of receptors is the generate increased control over spatial resolution. Rather than using a chemical to diffuse across the cell environment to activate a large area and many cells, light can be targeted at a single cell, or even a spatially defined area within a cell. This is an increasingly relevant question for GPCR research as compartmentalised signalling is starting to be better understood (see section 1.1.6 for an overview of compartmentalised signalling) (Tsvetanova *et al.*, 2015; Jong *et al.*, 2018). Localisation of the light stimulus is therefore a potential method for single cell and subcellular investigations of cellular signalling using optogenetic receptors.

Two photon excitation microscopy (or 'two photon imaging', a branch of multiphoton imaging) has been used in optogenetic studies to increase the spatial control of light activation of receptors. Originally designed to decrease phototoxicity and photobleaching in fluorescence imaging, two photon imaging aims to increase the detection of a single excitation event (Svoboda and Yasuda, 2006). Rather than a single photon exciting the fluorescent protein, two low energy photons are used to increase the energy state of the fluorescent molecule, emitting a single photon as if excited by a single higher energy photon (Denk *et al.*, 1990; Zipfel *et al.*, 2003). As this event occurs only when the two photons interact simultaneously, there is a non-linear, quadratic drop off of light intensity from the focused laser in the z plane, rather than the standard linear dependence of fluorescence. For example, doubling the intensity produces four times the fluorescence. As the intensity depends on the area, it is greater at the focal point (Zipfel *et al.*, 2003). Two photon imaging is therefore a useful method for localising light and increasing selectivity of activating of optogenetic receptors (Packer *et al.*, 2012; Emiliani *et al.*, 2015; Yang *et al.*, 2018).

Currently, multi photon actuators of optogenetic activation have been used *in vivo* for neuroscience studies into neural networks for specific cell stimulation, often in

combination with other monitoring assays, such as calcium flux or voltage sensing (Scott *et al.*, 2017; Chen *et al.*, 2019). Temporal resolution has been improved to submillisecond levels using faster opsin variants, such as ChETA and Chronos, in conjunction with two photon stimulation without the time delay of scanning laser using holographic parallel illumination (Klapoetke *et al.*, 2014; Ronzitti *et al.*, 2017). However, spatial restriction of optogenetic receptor stimulation with multi photon microscopy is not yet subcellular, and therefore these methods are not yet as useful for *in vitro* studies which usually investigate compartmental cellular signalling rather than network processing. Until further improvements with multi photon imaging, selective subcellular optogenetic stimulation via microscopy is still a challenge.

Although there are limits to defining spatial stimulation using an external light source, optogenetic actuators can be targeted to single areas of a cell, limiting the light activation to subcellular compartments. As outlined in Chapter 1.3.4, optogenetic probes tethered to specific membranes, organelles and areas of the cell can offer subcellular restriction. There are caveats involved which such subcellular targeting, including both the targeting efficiency to the structures concerned, and effects on cell health and potential paradoxical effects when these manufactured proteins are expressed in certain areas of the cell (Rost *et al.*, 2017). Nonetheless, these problems do not outweigh the benefit of using specific subcellular targeting of effectors, a major advantage of light sensitive tools. It would be useful to develop a method of restricting both expression of the optogenetic tool and the illuminated area, which makes the main objective of this thesis chapter clear.

### 5.1.2 Luminopsins

One problem of using light activated receptors in animal systems is the invasiveness of illuminating the desired area, usually requiring surgery to attach a light-delivery system to the animal. Bioluminescence can be produced inside the body using specially designed systems through oxidisation of luciferin by luciferase enzymes, as outlined in Chapter 1.2.4. Using bioluminescent light to activate light-sensitive receptors from the direct area, rather than an external delivery, would therefore be advantageous for decreasing the need for invasive surgical procedures and, of interest to *in vitro* systems, increasing spatial restriction of light activation. Berglund *et al.* (2013) provided the first proof of principle of bioluminescence activation of

optogenetic receptors using a chimera containing *Gaussia* luciferase (GLuc) fused to the N terminus of channelrhodopsin-1, or channelrhodopsin-2, and named them luminopsins. The channelrhodopsins in the luminopsin chimeras were both shown to activate in HEK cells when the small molecule substrate coelenterazine (CTZ) was added, with an inward current observed (Berglund *et al.*, 2013). Luminescence also evoked responses in cultured neurons, increasing the firing rate by 50%. Following *in vitro* success, the preferred GLuc-ChR1 luminopsin chimera was first transfected into mice in the motor cortex of the right hemisphere (Birkner *et al.*, 2014). Mice expressing luminopsins performed repetitive rotations to the left under CTZ administration, indicating that luminopsins were activating neurons in the motor cortex. As well as the excitatory receptors, an inhibitory luminopsin was developed using halorhodopsin and a red shifted *Renilla* luciferase, closer to the activation wavelength of halorhodopsin (Tung *et al.*, 2015). Inhibitory luminopsins have since been used in several animal studies since to study various subjects of neuroscientific interest; demonstrating the need for motorneuron activity post nerve injury, repressing seizure activity in an epileptic mouse model, and investigating the CA3 area of the hippocampus and its effect on spatial and episodic memory (Jaiswal *et al.*, 2017; Song *et al.*, 2018; Tung *et al.*, 2018).

Optimising from the first luminopsins, Berglund *et al.* (2016) investigated different optogenetic receptor-luciferase combinations for increased action potential generation in neurons. Out of the five luciferases tested, the brightest signal was detected in a GLuc variant named 'slow-burn' (sbGLuc). NanoLuc was the second brightest when used with its own substrate furimazine, but not CTZ, perhaps allowing for the use of both luciferase variants in the same system if using luminopsins (Berglund *et al.*, 2016). Brighter luciferase variants increased the amount of action potentials produced by activated neurons using slGLuc-channelrhodopsin-1 luminopsin chimeras treated with CTZ verses normal GLuc, indicating that bioluminescence lumination of the receptors is crucial for luminopsin function. More luciferase-receptor combinations have been produced, such as with GLucM23-channelrhodopsin-1 or sbGLuc-step-function-channelrhodopsin-2, further expanding the toolbox for luminopsin use in optogenetic studies (Berglund *et al.*, 2019; Park *et al.*, 2019).

Luminopsins are not yet fully optimised. As of now, only channelrhodopsins, light activated ion channels, have been used in these studies, however there are many other optogenetic systems that could benefit from bioluminescence activation, broadening the options to deliver a light stimulus in a spatiotemporally regulated manner. A disadvantage of using luminopsins rather than traditional optogenetic techniques is the loss of temporal light control, returning to a process closer to ligand activation of the receptors as bioluminescence production follows the kinetics of photon liberation by the enzymatic conversion of substrate by the luciferase. Perhaps utilising receptor mutants with different temporal activation could be helpful when using these tools.

### 5.1.3 Subcellular Light Targeting and NanoBiT

Luminopsins provide a method of increased spatial targeting of light-activated receptors, however current luminopsin variants illuminate and activate the entirety of receptors expressed throughout the cell. One potential option to localise bioluminescent activation to a subcellular population of receptors is to use protein-fragment complementation of the luciferase component of luminopsins. In protein-fragment complementation, the fluorescent or bioluminescent reporter is divided into complementary fragments and attached to proteins of interest to monitor protein-protein interactions (Ozawa, 2006; Kilpatrick *et al.*, 2015). The beauty of this technique is that the fragments of the reporter only produce a signal when the fused cellular proteins of interest are close enough in proximity. Spatially restricted target proteins could therefore be used to enable luciferase fragment complementation only occurs in selected areas of the cell.

From the previous research on luminopsins, it is clear that bright, sustained bioluminescence is required for optimised optogenetic activation (Berglund *et al.*, 2013, 2016). NanoLuc is one of the brightest of the bioluminescent systems available and produces a sustainable luminescence in the wavelength of blue-green activated optogenetic receptors (Hall *et al.*, 2012; Loh and Proft, 2014). Fortunately, split NanoLuc luciferase systems (NanoLuc Binary Technology, NanoBiT) have been optimised for fragment complementation. These fragments include a 13 amino acid beta-strand of NanoLuc (SmBiT) for complementation with a larger 18kDa polypeptide (LgBiT to form the full luciferase (Dixon *et al.*, 2016).

Importantly Dixon et al (2016) optimised the sequences of both these partners to generate a low affinity pair for complementation that is both rapid and reversible, an issue with previous luminescent and fluorescent complementation reporters (review refs). Most previous GPCR research utilising NanoBiT has focussed on subcellular interactions between two molecules of interest, such as dimerization of receptors, ligand binding, or interactions of receptors with signalling proteins, e.g. G proteins (A. Inoue *et al.*, 2019; Leroy *et al.*, 2019; Wang *et al.*, 2019). This makes NanoBiT a perfect candidate for subcellular targeting in the cell. Using NanoBiT in a luminopsin is therefore feasible, with potential for *in vivo* use in the future.

The next choice to be made is the subcellular target for restricted luminopsin activation. One of the current interests for GPCR investigations is the impact of internalised receptor activation on cellular function, compared to standard plasma membrane stimulation (see section 1.1.4). Much of the evidence supporting endosomal signalling relies on indirect approaches – for example, the sustained timecourse of signalling compared to receptor trafficking, the use of spatially localised second messenger sensors (e.g. cAMP), and the effects of cell permeable versus impermeable receptor ligands and receptor trafficking inhibitors (Jimenez-Vargasa *et al.*, 2018). There is no current method to directly trigger GPCR activation within a specific compartment, and then monitor the consequences. One solution is to use luminopsins activated by NanoBiT complementation with a labelled marker localised to each compartment.

In considering choices for these markers, the Rab proteins, part of the Ras superfamily of small GTPases, offer anchored sites capable of mapping the endosomal pathways open to G protein coupled receptors (Wennerberg *et al.*, 2005). From the available proteins, two were picked for their spatial restriction; the plasma membrane bound Kras, and the early endosome expressing Rab5. For plasma membrane localisation of the luciferase LgBiT fragment, we used the membrane targeting motif of Kras, a plasma membrane localised RAS GTPase involved in cell proliferation (Welman *et al.*, 2000; Dharmaiah *et al.*, 2019). This sequence contains a polybasic sequence followed by the prenylation motif, and has previously been used in several studies to localise biosensors and fluorescent proteins in BRET studies (Tsai *et al.*, 2015; Bery *et al.*, 2018). Rab5 is localised to early endosomes where it is involved in guiding vesicle fusion after clathrin

mediated endocytosis, and through interaction with other effectors the maturation of early endosomes destined for other compartments (Arriagada *et al.*, 2019). Rab5-GFP has often been used as a marker for early endosomes in studies of receptor trafficking, showing its potential usefulness as an assay protein (Holliday *et al.*, 2007). Thus the Kras sequence and Rab5 offer promising starting candidates to generate spatially localised LgBiT fragments, that then confer restricted bioluminescence stimulation of the optogenetic receptors through complementation as they pass through these subcellular domains.

### 5.1.4 Chapter Aims

The aims of this chapter are three fold;

i. To develop a complementation based luminopsin system for controlling subcellular receptor activation, by combining SmBiT tagged optogenetic $G_q$ coupled GPCRs (opto-$\alpha_{1A}$AR and melanopsin) constructs with spatially localised LgBiT marker proteins (see *Figure 5.1*).
ii. To confirm light-activation of the new constructs via calcium signalling assay, and bioluminescence production after furimazine addition on co-expressing the tagged luminopsins and NanoBiT markers.
iii. Using calcium mobilisation and OptoXR internalisation assays to assess GPCR luminopsin activation by complemented luminescence stimulation, from the plasma membrane or endosomal localised LgBiT fragments.

Optogenetic receptors opto-$\alpha_{1A}$AR and melanopsin, already expressing an N terminal SNAPtag, were fused to two different SmBiT fragments (smBiT114, low affinity $K_d$=190μM, and smBiT86, high affinity $K_d$=0.7nM; Dixon *et al.* 2016, supplementary s2) of the NanoBiT luciferase to create four new luminopsin receptor variants (SNAP-opto-$\alpha_{1A}$AR-smBiT114, SNAP-opto-$\alpha_{1A}$AR-smBiT86, SNAP-Opn4-smBiT114 and SNAP-Opn4-smBiT86). The receptor constructs were then stably expressed in HEK 293T cells and co-transfected with either LgBiT-Kras (plasma membrane target) or LgBiT-Rab5 (early endosome target) to restore functioning luciferase close to the receptor via NanoBiT complementation. Through the use of $Ca^{2+}$-sensitive dyes to measure cellular calcium transients and fluorescent SNAP labelling to monitor receptor internalisation, luminopsins generated by spatially restricted complementation were tested for functional response to bioluminescence production from furimazine addition in HEK cells. Bioluminescence imaging using the Olympus LV200 specialised bioluminescence microscope analysed the spatial distribution of the bioluminescence produced by NanoBiT complementation and furimazine in the designed luminopsins.

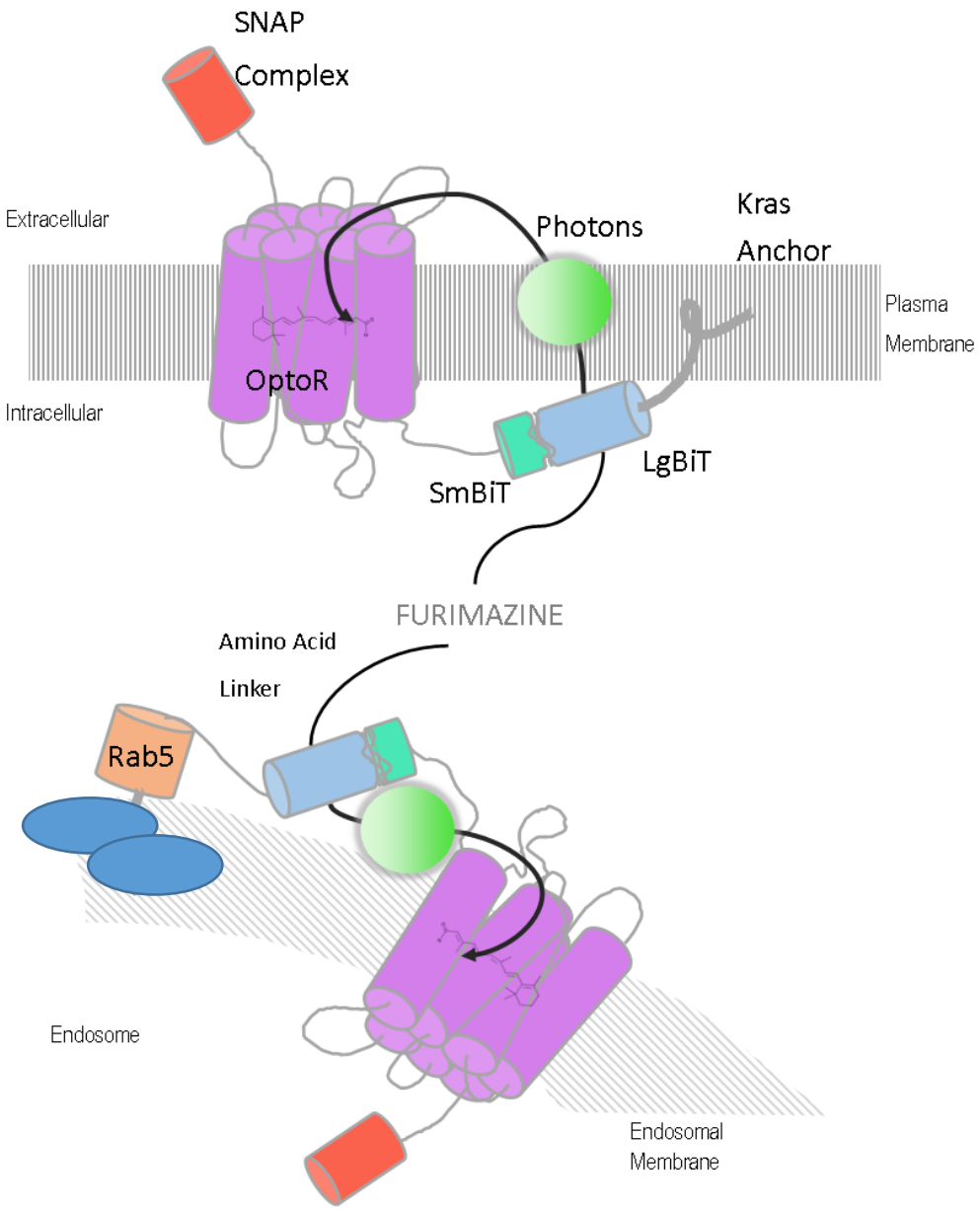


***Figure 5.1* – The proposed subcellular targeting of optogenetic receptor (OptoR) activation by NanoBiT complementation with localised marker proteins.** When the smBiT tagged receptor is close enough to the LgBiT to promote NanoBiT complementation, supplemented furimazine is enzymatically converted to product by NanoBiT, releasing photons from the complex to photoisomerise the retinal analogue present within the optogenetic receptor. Although both the Kras plasma membrane anchor and the Rab5 tagged protein are shown, only one LgBiT-protein complex was investigated per experiment.

## 5.2 Results

### 5.2.1 SNAP Tagged Optogenetic Opto-$\alpha_{1A}$AR-SmBiT Constructs Stably Express in HEK293T Cells and Produce Calcium Signals in Response to LED Stimulation

There are two options for the small protein component of the NanoBiT protein; the high affinity, SmBiT86, which generates stable slowly reversible NanoBiT complexes, and the low affinity, SmBiT114 which is rapidly reversible. For NanoBiT construct production, the smBiT114 or smBiT86 proteins were fused in frame to the C terminus of the optogenetic receptors. To achieve this, a PCR amplified SNAP-opto-$\alpha_{1A}$AR lacking the STOP codon construct was successfully ligated into the p3.1$_{ZEO}$-smBiT114 or p3.1$_{ZEO}$-smBiT86 vectors after subcloning using the flanking restriction sites (XhoI/KpnI) introduced by PCR primers. Successful insertion of the receptor DNA in the new constructs was detected by restriction digestion using the flanking restriction enzymes (XhoI, KpnI) and agarose gel electrophoresis of maxiprep samples, where an additional band was shown when the receptor is present compared to the vector backbone (5.0 kbp alone) – the predicted band for the SNAP- opto-$\alpha_{1A}$AR was at 2.0kbp (see Figure 5.2). The sequence was verified in the maxiprep DNA preparation by sequencing with T7 and BGHrev primers to confirm no PCR errors and that an in frame fusion protein (N terminal signal sequence, followed by SNAP tag, followed by receptor cDNA, followed by smBiT protein and STOP codon) was correctly encoded. Following stable transfection, mixed population cell lines expressing the opto-$\alpha_{1A}$AR-smBiT receptors were visualised by labelling the SNAP receptor protein with the appropriate SNAP fluorophore. HEK293T cells stably expressing SNAP-opto-$\alpha_{1A}$AR-smBiT114 or SNAP-opto-$\alpha_{1A}$AR-smBiT86 showed a plasma membrane localised expression and in a majority of the cell population following membrane impermeant SNAP Surface AF-647 labelling (see *Figure 5.3*).

Functionality of the SNAP-opto-$\alpha_{1A}$AR-smBiT receptor constructs was compared to the SNAP-opto-$\alpha_{1A}$AR in HEK cells to test if the C terminal smBiT tag would interfere with receptor activation. The calcium response to a single 60s LED stimulus of 470nm wavelength was compared using the four parameters described

in Chapter 4.2.5; percentage cell response, maximal fold change, latency to first calcium transient and the area under the curve of the fluorescent peak (see *Figure 5.4*). When supplemented with 9-*cis*-retinal (1μM), both the HEK-SNAP-opto-$\alpha_{1A}$AR-smBiT114 and HEK-SNAP-opto-$\alpha_{1A}$AR-smBiT86 cell lines had the similar responses to the light stimulus as for SNAP-opto-$\alpha_{1A}$AR expressing cells for the tested parameters

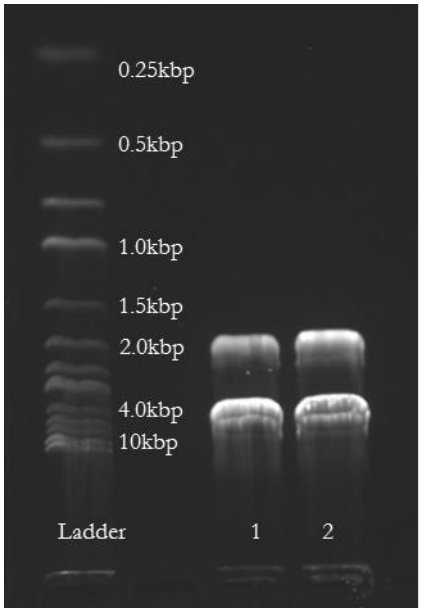


***Figure 5.2* – Agarose gel electrophoresis of the p3.1$_{NEO}$-SNAP-opto-$\alpha_{1A}$AR-smBiT plasmids (numbered lanes 1 and 2) using a double restriction digestion of Kpn I and Xho I.** The left lane contains a diagnostic 1kbp DNA ladder of known molecular weight bands. Lane 1 is the SNAP-opto-$\alpha_{1A}$AR with a band at 2.0kbp and the p3.1$_{ZEO}$-smBiT86 vector at the 5kbp range, with lane 2 displaying the SNAP-opto-$\alpha_{1A}$AR again at 2.0kbp but cut from the p3.1$_{ZEO}$-smBiT114 vector at around 5kbp.

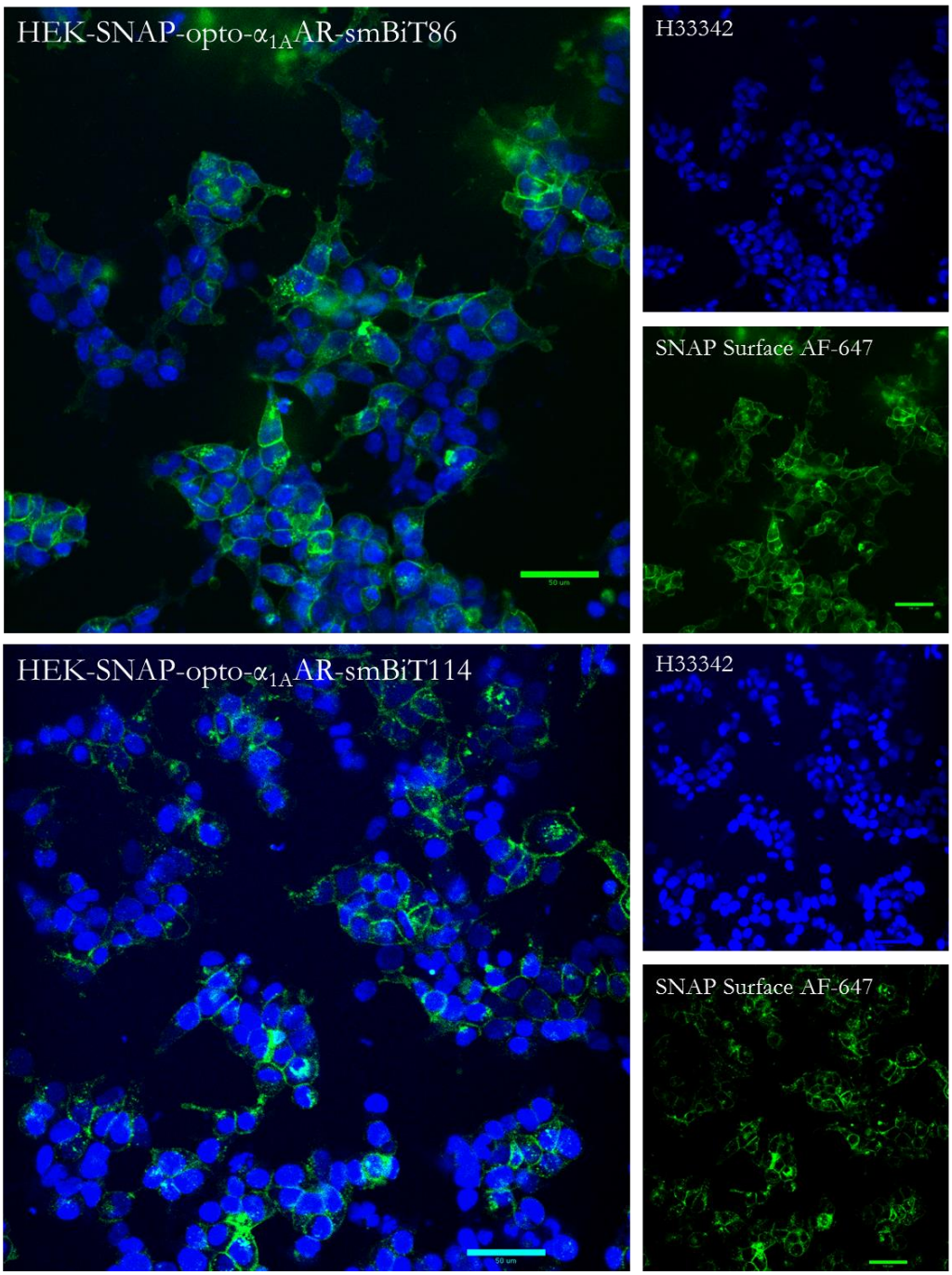


***Figure 5.3* – Stable expression of SNAP-opto-$\alpha_{1A}$AR-smBiT constructs in HEK293 cells.** Receptors were visualised using SNAP-Surface AF-647 (0.2μM, 30 min, 37°C) in combination with H33342 nuclear stain to detect cells ($n$=1 representative of 5 experiments). Images were taken at 40x objective using the IX Ultra confocal plate reader.

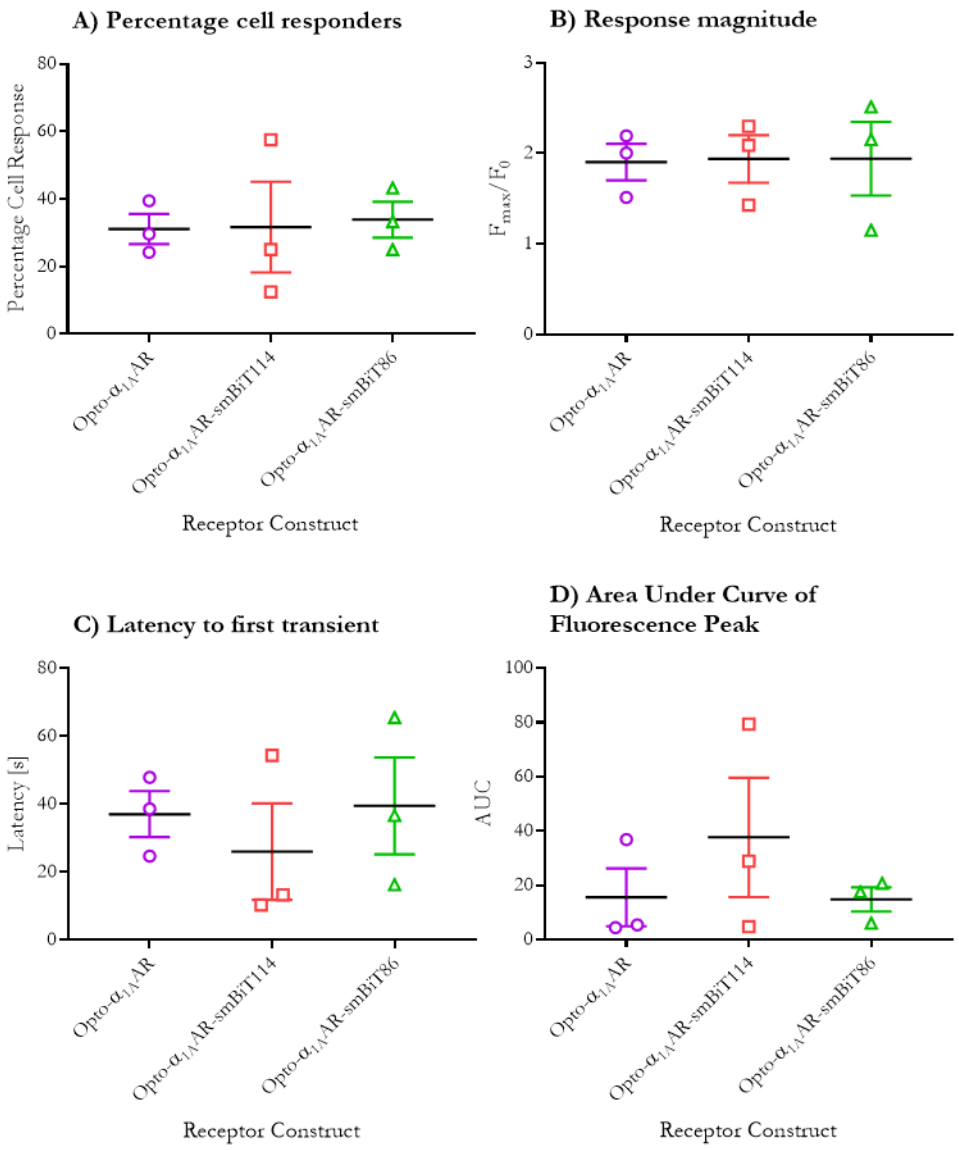


***Figure 5.4* – Comparison of intracellular calcium mobilisation in response to a single LED light pulse between HEK-SNAP-opto-$\alpha_{1A}$AR wild type and HEK-SNAP-opto-$\alpha_{1A}$AR-smBiT cell lines.** Cellular calcium was recorded for 5min using Cal-630 AM (1μM). A single stimulation 60s LED pulse (25% power, 470nm) was performed after 120s. All cells were treated with 9-*cis*-retinal (1μM) 1hr prior to experimentation. The variables measured and averaged over a coverslip were; A) percentage of cells producing at least one calcium transient on a coverslip, B) fluorescence increase of Cal-630 for every cell producing a transient, C) the latency taken until first transient, and D) the area of the curve underneath calcium transients (*n*=3 experiments with a minimum of 25 cells measured per experiment).

### 5.2.2 HEK-SNAP-Opto-$\alpha_{1A}$AR-SmBiT Cell Lines Produce Bioluminescence when Co-Transfected with LgBiT Marker Constructs and Treated with Furimazine

NanoBiT requires a second, larger protein named the LgBiT to complement the SmBiT and form the full luciferase protein. Addition of the substrate, furimazine, then triggers bioluminescence from the luciferase enzyme that is proportional to the level of complementation achieved. The stable HEK-SNAP-opto-$\alpha_{1A}$AR-smBiT cell lines were used to transiently transfect in different LgBiT constructs (LgBiT-Kras, LgBiT-Rab5, LgBiT-LL-Kras, LgBiT-LL-Rab5) predicted to targeted to the plasma membrane (Kras) or early endosomes (Rab5) respectively. Two marker constructs additional contained a 15 Gly-Ser long linker (LL) to increase flexibility between the LgBiT and target sequence for increased ability to interact with the receptor C terminal

Cells were used 48hr post transient transfection of the marker constructs to investigate the production of complemented bioluminescence, measured using the PheraSTAR platereader. All combinations of opto-$\alpha_{1A}$AR-smBiT-LgBiT complementation produced bioluminescence in HEK293T cells in a furimazine concentration-dependent manner (LgBiT-Rab5 was not used in this study). For the LgBiT-Kras and LgBiT-LL-Kras, bioluminescence lasted for the duration of the reading (26min) with a distinguishable peak at 5min in the highest concentrations (10μM and 1μM; see *Figure 5.5*). As expected, the addition of the 18 amino acid linker in the LgBiT-LL-Kras increases bioluminescence output from NanoBiT complexes by 2 fold compared to LgBiT-Kras transfected cells (see *Figure 5.6*). When the raw bioluminescence values are compared, opto-$\alpha_{1A}$AR-smBiT86 transfected cells were characterised by a 10 fold increase in bioluminescence output when co-expressed with the LgBiT-LL-Kras compared to the opto-$\alpha_{1A}$AR-smBiT114 cell line. The bioluminescence time-profiles for LgBiT-LL-Rab5 co-transfected cells were also similar, peaking at 5min following furimazine addition (*Figure 5.7*). In the opto-$\alpha_{1A}$AR -smBiT86 cell line, the bioluminescence intensities observed following transfection with LgBiT-LL-Kras or LgBiT-LL-Rab5 were similar. However a 3 fold greater luminescent signal was observed in the opto-$\alpha_{1A}$AR-smBiT114 cell line following transfection of the Kras marker compared to Rab5, measured on the same day. This would be consistent with the predominantly

plasma membrane localised expression of SNAP-opto-$\alpha_{1A}$AR-smBiT114 observed in *Figure 5.3*, a difference that is obscured in the brighter sm86 system because of the ability of this high affinity fragment to form stable complemented luciferase, which then accumulates. Overall, these results show that NanoBiT complementation with OptoRs can occur within either spatially targeted site (Kras/Rab5), generating bioluminescence with potential to activate for the optogenetic receptors.

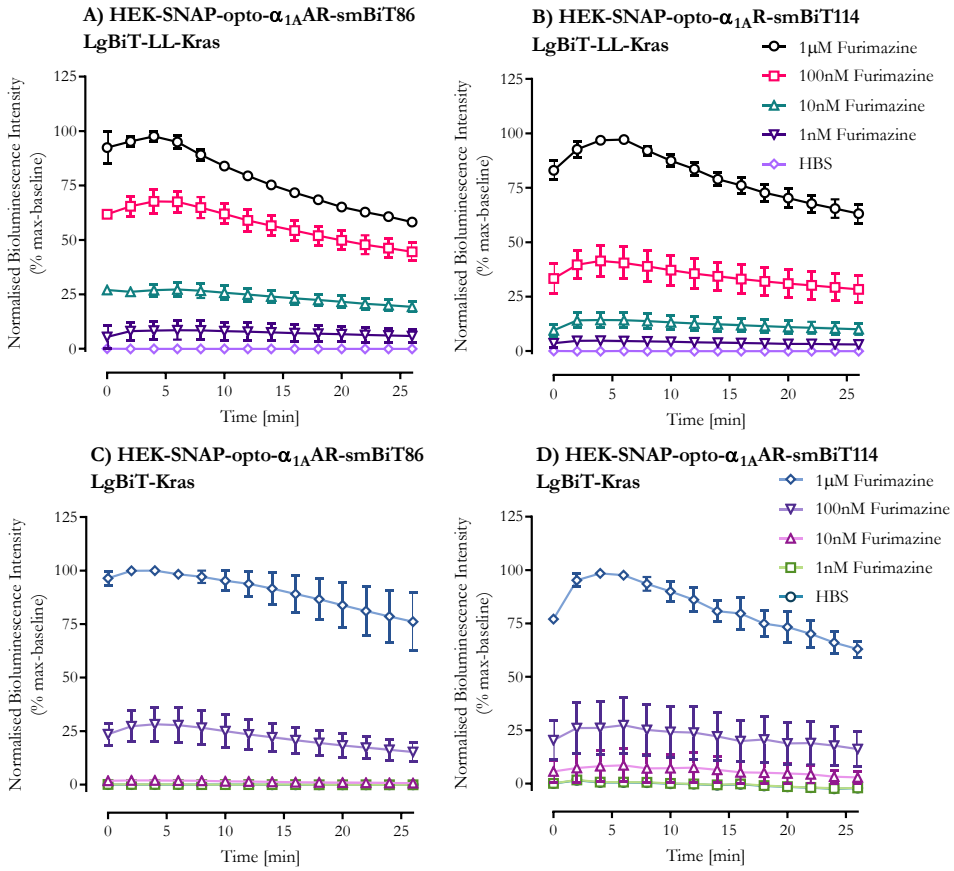


***Figure 5.5* – Bioluminescence produced by HEK-SNAP-opto-$\alpha_{1A}$AR-smBiT86 (A, C) and HEK-SNAP-opto-$\alpha_{1A}$AR-smBiT114 (B, D) stable cell lines transfected with two different LgBiT-Kras constructs and treated with furimazine.** Cells were transiently transfected with LgBiT constructs 48hr before experiment and plated 24hr before bioluminescence readings were taken on the PheraSTAR plate reader every 2min for 26min. In A) and B) the marker construct contained the 18 amino acid linker (LL) between LgBiT and the Kras sequence, whereas C) and D) were co-transfected with the LgBiT-Kras structure with the minimal 2 amino acid linker. $n \geq 3$ experiments with each condition in duplicate for each experiment. Data normalised to 100%=max response, 0%=lowest response across the data set for each experiment and condition.

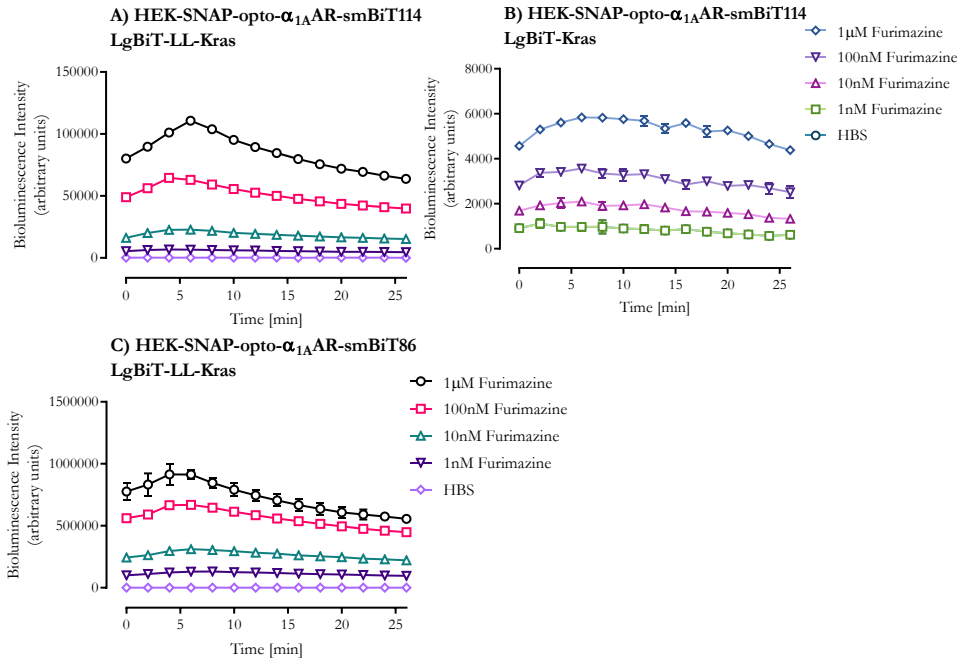


***Figure 5.6* – Raw bioluminescence reads for HEK-SNAP-opto-$\alpha_{1A}$AR-smBiT cell lines co-expressing LgBiT-Kras constructs.** Cells were transiently transfected with LgBiT constructs 48hr before experiment and plated 24hr before bioluminescence readings were taken on the PheraSTAR plate reader every 2min for 26min. A) without a linker in the LgBiT-Kras construct compared to B) adding an 18 amino acid linker between the Kras and the LgBiT proteins. C) Cells expressing opto-$\alpha_{1A}$AR-smBiT86, generating high affinity complementation with the LgBiT-LL-kRas marker produced the highest bioluminescence output, 10 fold greater than the low affinity smBiT114 at the highest concentration of furimazine (1μM). *n*=1 experiment performed in duplicate, representative of a minimum 3 experiments for the 3 variables.

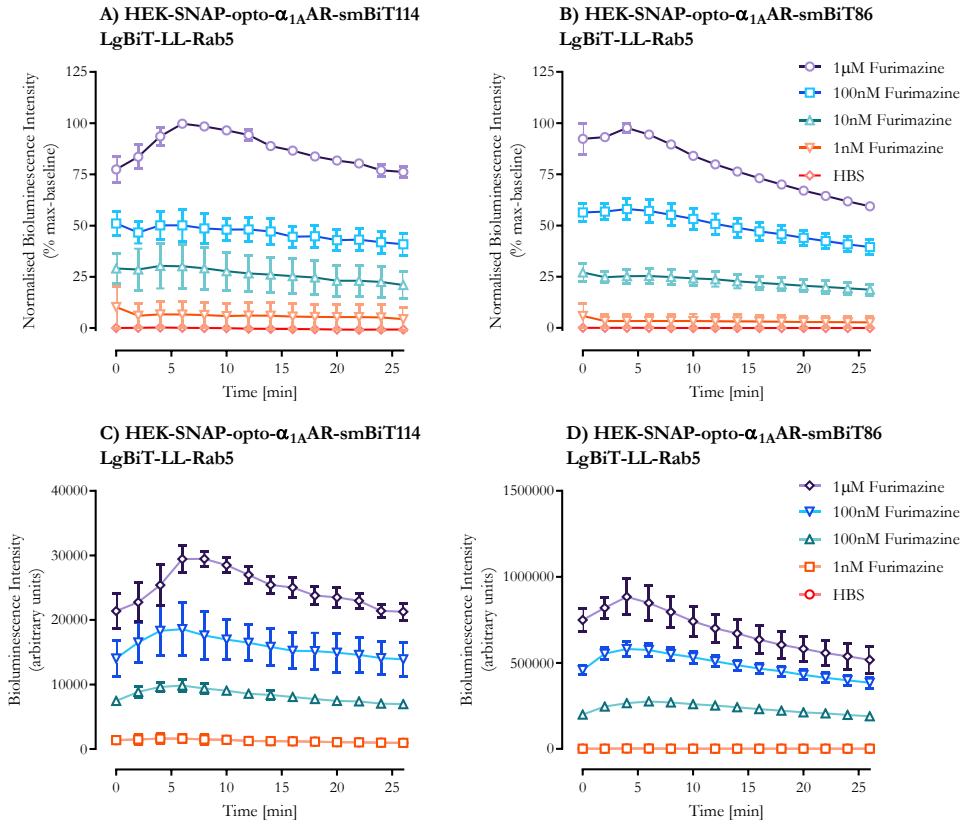


***Figure 5.7* – Bioluminescence produced by HEK-SNAP-opto-$\alpha_{1A}$AR-smBiT cell lines transfected with LgBiT-LL-Rab5 constructs and treated with furimazine.** Cells were transiently transfected with LgBiT-LL-Rab5 48hr before experiment and plated 24hr before bioluminescence readings were taken on the PheraSTAR plate reader every 2min for 26min.A) OptoR-smBiT114 and B) OptoR-smBiT86 normalised responses from $n \geq 3$ experiments with each condition in duplicate wells for each experiment. Both the smBiT114 and smBiT86 produce bioluminescence with LgBiT-LL-Rab5 for the full period of the reading, with a peak at around 5min.. Cells expressing OptoR- smBiT86 produced a 20 fold increase in raw bioluminescence output (C) compared to the OptoR-smBiT114 cell line (D) co-transfected with LgBiT-LL-Rab5 (n=1, in duplicate). All raw values shown were taken in the same experiment as *Figure 5.5* for direct comparison.

### 5.2.3 Luciferase complemented SNAP-Opto-$\alpha_{1A}$AR-SmBiT86 receptors do not Produce Calcium Transients in Response to Furimazine Addition

To investigate the ability of the bioluminescence produced by the NanoBiT complementation to activate the opto-$\alpha_{1A}$AR, intracellular calcium was recorded at a single cell level using a red-shifted calcium sensitive dye (Cal-630) during furimazine stimulation. HEK-SNAP-opto-$\alpha_{1A}$AR-smBiT86 cells were co-transfected with either LgBiT-LL-Kras or LgBiT-LL-Rab5 48hr prior to experimentation. The long linker LgBiT combination, together with the receptor labelled with Sm86 was the test combination initially chosen due to the brightest bioluminescent signal, with the greatest probability of activating the light sensitive receptor. Cells were treated with 1μM 9-*cis*-retinal and loaded with 1μM Cal-630 AM 1hr before experimentation, and also labelled SNAP Surface AF-488 30min prior. During experimentation, cells were mounted on a confocal microscope in the dark and imaged for 5min at 1 frame per second using the 647nm laser. To induce bioluminescence production, 1μM furimazine was added after a 2min baseline. No furimazine induced calcium transients were detected in the HEK cells for either LgBiT construct for all 6 experiments performed (3 for each LgBiT construct; see *Figure 5.8*). Towards the end of each experiment, there was a general increase in baseline fluorescence seen in all cells. However, this may not reflect in an increase in cellular calcium, but bleed through the emission filter from the luminescent signal. Thus although the opto-$\alpha_{1A}$AR-smBiT construct is activated to produce calcium signalling by LED light sources, the bioluminescence produced by the complemented luminopsin constructs was not sufficient in the HEK cell line to activate these transients.

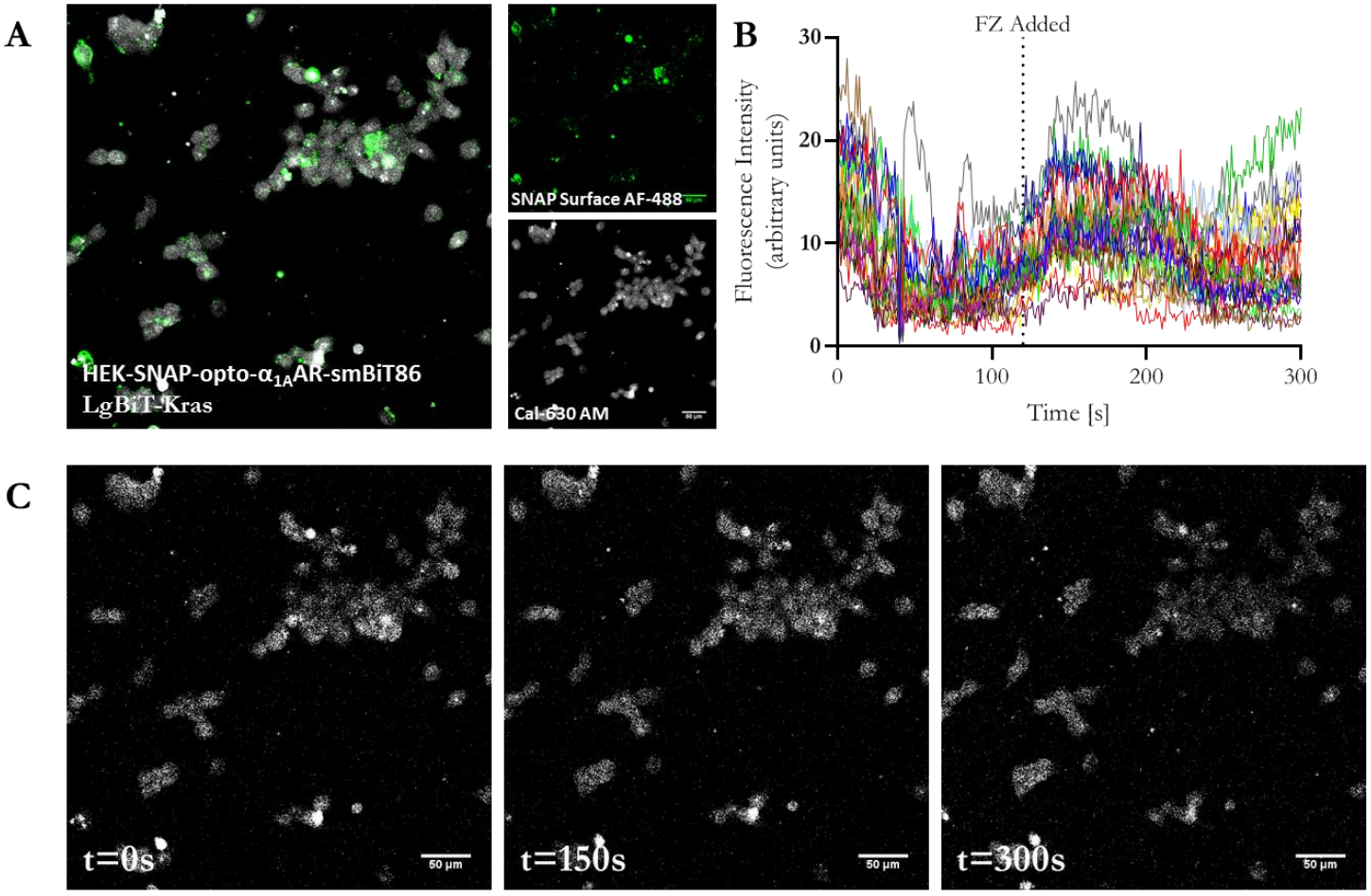
A
HEK-SNAP-opto-α1AAR-smBiT86
LgBiT-Kras
SNAP Surface AF-488
Cal-630 AM
B
FZ Added
Fluorescence Intensity
(arbitrary units)
30
20
10
0
0
100
200
300
Time [s]
C
t=0s
50 µm
t=150s
50 µm
t=300s
50 µm

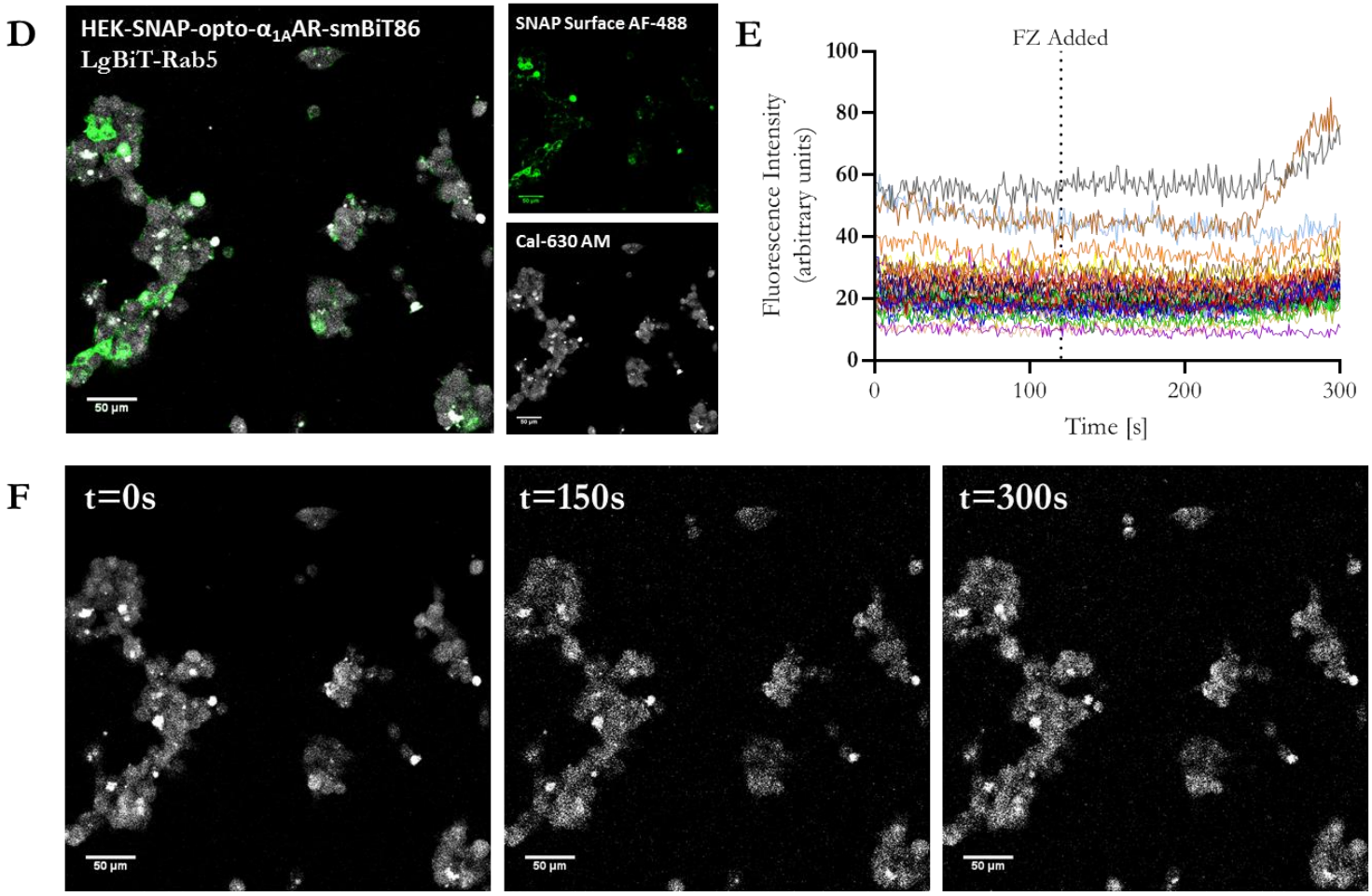
D
HEK-SNAP-opto-α1AAR-smBiT86
LgBiT-Rab5
50 µm
SNAP Surface AF-488
Cal-630 AM
E
FZ Added
Fluorescence Intensity
(arbitrary units)
100
80
60
40
20
0
0
100
200
300
Time [s]
F
t=0s
t=150s
t=300s
50 µm
50 µm
50 µm

***Figure 5.8* – Intracellular calcium measurements in the stable HEK-SNAP-opto-$\alpha_{1A}$AR-smBiT86 cell line co-transfected with LgBiT-LL-Rab5 or LgBiT-LL-Kras, after furimazine addition.** Cells were transiently transfected with LgBiT-Rab5 48hr prior to experiment and treated with 9-*cis*-retinal (1μM) 1hr before readings and SNAP Surface AF-488 (0.2μM) 30min prior. Cal-630 AM (1μM) was used as the calcium indicator with readings taken every 1s for 5min on a confocal microscope. Furimazine (FZ, 1μM) was added after a 120s baseline recording. A) and D) SNAP labelled SNAP-opto-$\alpha_{1A}$AR-smBiT86 cells taken after either experiment at 470nm. B) Cal-630 fluorescence intensity (ex/em 607/625nm) of all cells on the coverslip over the 5min time period transfected with LgBiT-LL-Kras, with E) showing LgBiT-LL-Rab5. C) Images taken at 0s, 150s and 300s for cells co-transfected with LgBiT-LL-Kras. LgBiT-LL-Rab5 is similarly shown in F). Single experiment representative of n=3, for each LgBiT construct.

### 5.2.4 Investigation of SNAP-Opn4-SmBiT receptors as alternative OptoRs for luciferase complementation

In Chapter 4, the melanopsin receptor Opn4 was used as a native optogenetic GPCR with increased signalling at lower light intensities and a lower dependence on 9-*cis*-retinal supplementation compared to the opto-$\alpha_{1A}$AR (see Chapter 4.2.5). It was therefore hypothesised that the melanopsin receptor could be a better target for bioluminescence activation. SmBiT constructs with the Opn4 receptor were made in the same manner as the SNAP-opto-$\alpha_{1A}$AR-smBiT constructs (see 5.2.1) with the smBiT protein attached to the C terminus of the receptor. Briefly, the p3.1$_{NEO}$-SNAP-Opn4$^{-}$* vector was used to digest out SNAP-Opn4$^{-}$* (using KpnI and XhoI) and ligate the receptor into the p3.1$_{ZEO}$-smBiT114 and p3.1$_{ZEO}$-smBiT86 vectors to create p3.1$_{ZEO}$-SNAP-Opn4-smBiT114 and p3.1$_{ZEO}$-SNAP-Opn4-smBiT86 cDNA for transfection (see *Figure 5.9*). The sequence was verified in the maxiprep DNA preparation by sequencing with T7 and BGHrev to confirm no PCR errors and that an in frame fusion protein (N terminal signal sequence, followed by SNAP tag, followed by receptor cDNA, followed by smBiT protein and STOP codon) was correctly encoded. Stable cell lines were then established in HEK293T cells with receptor expression detected by SNAP Surface AF-488 fluorescence on the plasma membrane (see *Figure 5.10*).

As with the opto-$\alpha_{1A}$AR, stable HEK-SNAP-Opn4-smBiT cell lines were used to transiently transfect in LgBiT constructs. With furimazine concentrations between 300nM and 10μM, bioluminescence was produced in both the HEK-SNAP-Opn4-smBiT114 and HEK-SNAP-Opn4-smBiT86 cell lines co-transfected with all LgBiT marker constructs (LgBiT-Kras, LgBiT-LL-Kras, LgBiT-Rab5, LgBiT-LL-Rab5; see *Figure 5.11* and *Figure 5.12*). Bioluminescence was produced for the entire reading with maximal peak at 5min. Furimazine appeared somewhat more potent comparing signals resulting fromsmBiT86-LgBiT complementation compared to the smBiT114-LgBiT, although $R_{max}$ values were not reached with the concentrations of furimazine used and full concentration response curves were not generated (see *Figure 5.14*).

When raw bioluminescence intensities were compared the smBiT86 constructs produced a 10 fold increase in maximal intensity compared to the smBiT114 with all LgBiT markers (see *Figure 5.13*). Replicating the results from the opto-$\alpha_{1A}$AR-smBiT receptors, LgBiT-LL-Rab5 produces a comparable bioluminescence compared to LgBiT-LL-Kras with both smBiTs when expressed with the Opn4-smBiT receptors, although LgBiT-Kras produces a 2 fold increase in bioluminescence than LgBiT-Rab5 in Opn4-smBiT114 receptors. The difference without the linker could be down to the reduced efficiency of complementation without the linker.

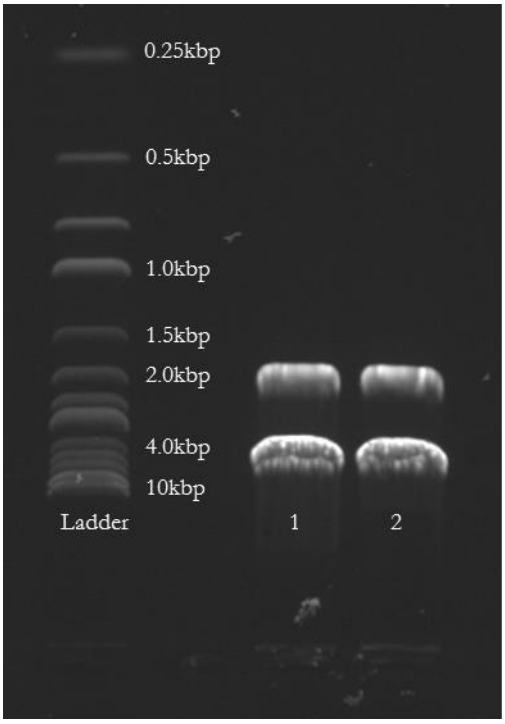


***Figure 5.9*** **– Agarose gel electrophoresis of the p3.1$_{NEO}$-SNAP-Opn4-smBiT plasmids (numbered lanes 1 and 2) using a double restriction digestion of Kpn I and Xho I.** The left lane contains a diagnostic DNA ladder of known molecular weight bands. Lane 1 is SNAP-Opn4 with a band at 1.9kbp and the p3.1$_{ZEO}$-smBiT86 vector at the 5kbp range, with lane 2 displaying SNAP-Opn4 again at 1.9kbp, but cut from the p3.1$_{ZEO}$-smBiT114 vector at around 5kbp.

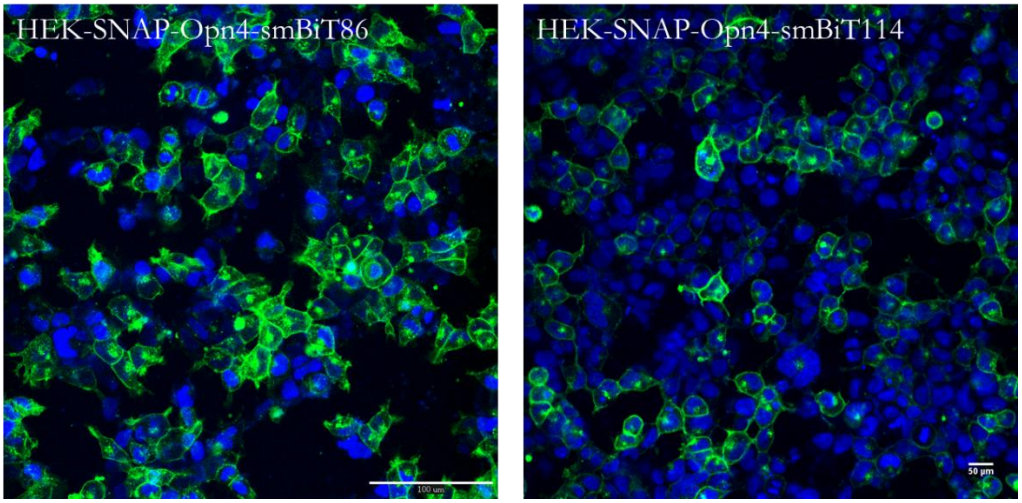


***Figure 5.10* – SNAP-Opn4-smBiT114 and SNAP-Opn4-smBiT86 receptor expression in stably transfected HEK293 cells.** Receptors were visualised using SNAP-Surface AF647 (0.2μM, 30min, 37º) in combination with H33342 nuclear stain to detect cells (*n*=1 representative of 5 experiments). Images were taken at 40x objective using the IX Ultra confocal plate reader.

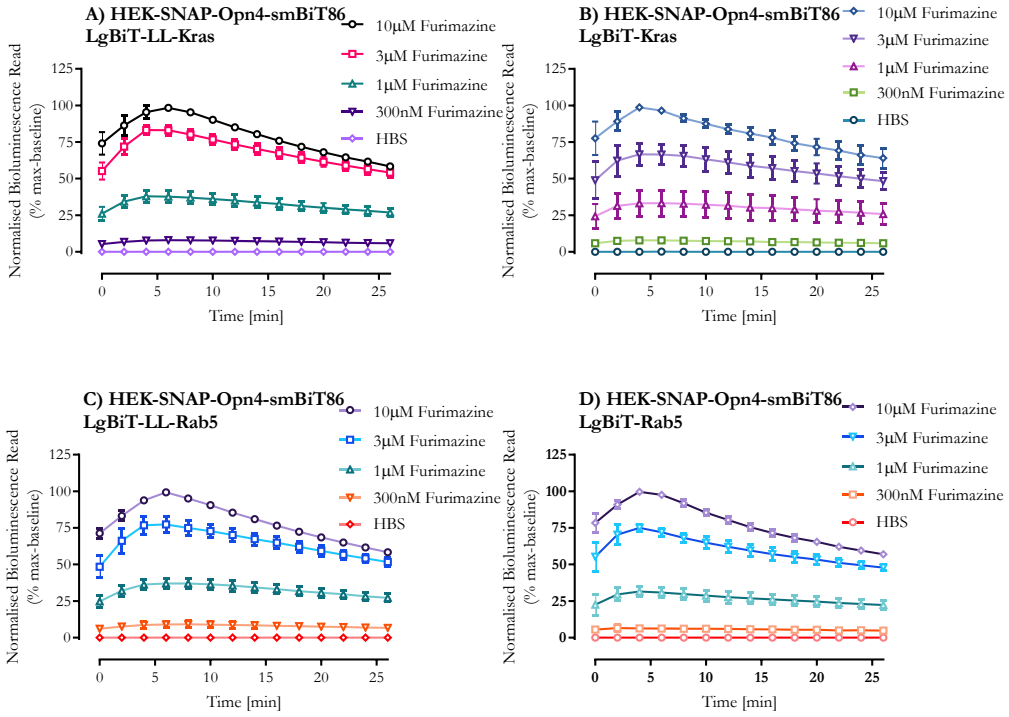


***Figure 5.11* – Bioluminescence intensity produced by the HEK-SNAP-Opn4-smBiT86 stable cell line co-transfected with different LgBiT constructs.** Cells were transiently transfected with LgBiT constructs 48hr before experiment and plated 24hr before bioluminescence readings were taken on the PheraSTAR plate reader every 2min for 26min after furimazine addition. All LgBiT constructs, A) LgBiT-LL-Kras, B) LgBiT-Kras, C) LgBiT-LL-Rab5 and D) LgBiT-Rab5, produce bioluminescence dependent on furimazine concentration. $n \geq 3$ experiments with each condition in duplicate for each experiment.

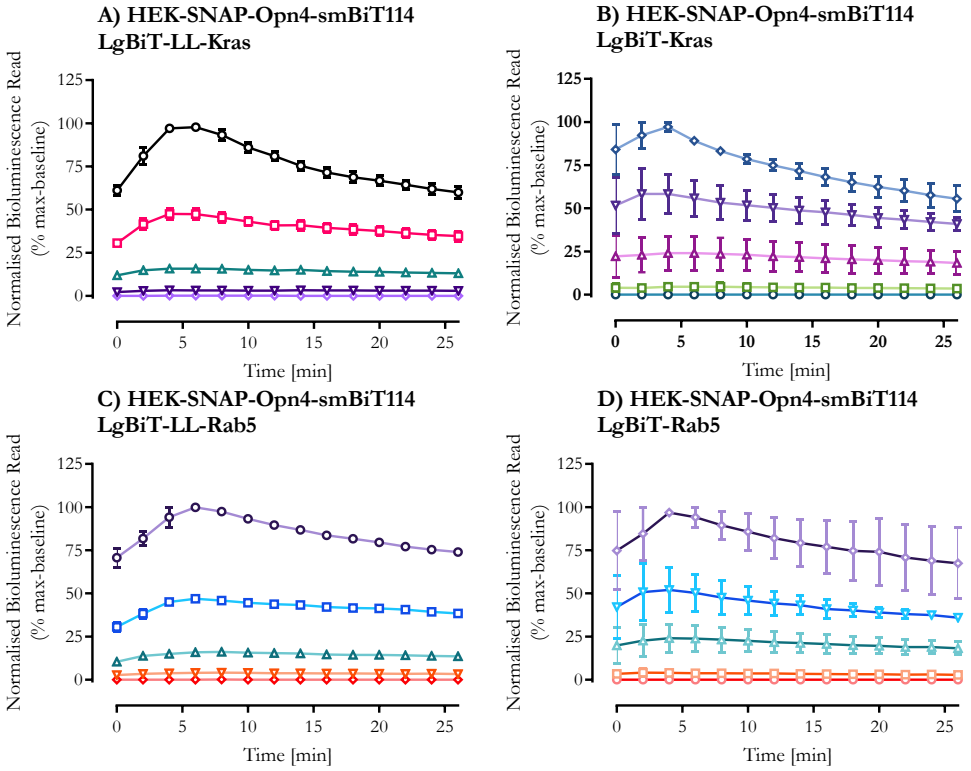


***Figure 5.12* – Bioluminescence intensity produced by the HEK-SNAP-Opn4-smBiT114 stable cell line transfected with different LgBiT constructs.** Cells were transiently transfected with LgBiT constructs 48hr before experiment and plated 24hr before bioluminescence readings were taken on the PheraSTAR plate reader every 2min for 26min. All LgBiT constructs, A) LgBiT-LL-Kras, B) LgBiT-Kras, C) LgBiT-LL-Rab5 and D) LgBiT-Rab5, produce bioluminescence dependent on furimazine concentration. $n \geq 3$ experiments with each condition in duplicate for each experiment.

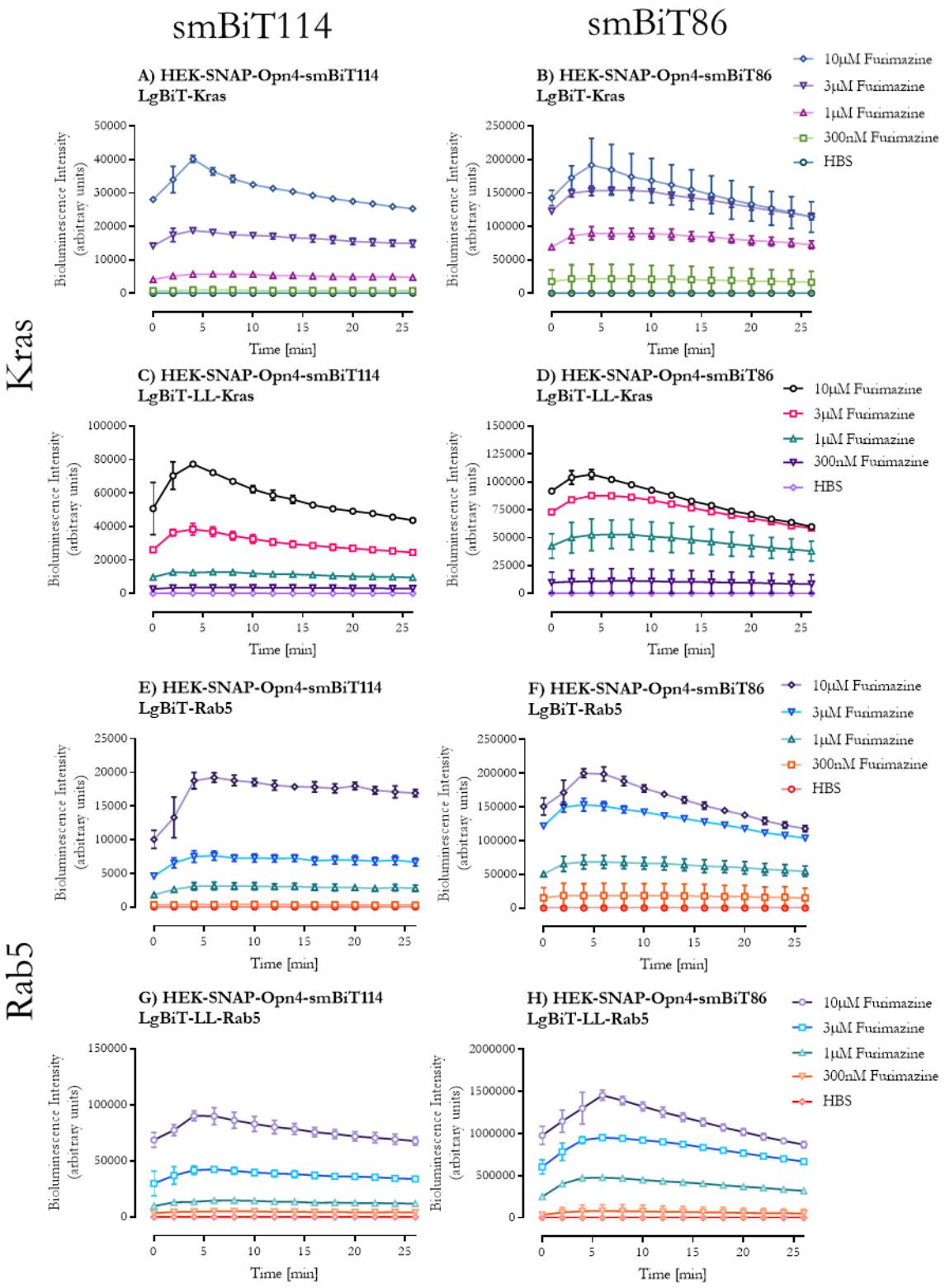
smBiT114
smBiT86
Kras
Rab5
A) HEK-SNAP-Opn4-smBiT114
LgBiT-Kras
B) HEK-SNAP-Opn4-smBiT86
LgBiT-Kras
C) HEK-SNAP-Opn4-smBiT114
LgBiT-LL-Kras
D) HEK-SNAP-Opn4-smBiT86
LgBiT-LL-Kras
E) HEK-SNAP-Opn4-smBiT114
LgBiT-Rab5
F) HEK-SNAP-Opn4-smBiT86
LgBiT-Rab5
G) HEK-SNAP-Opn4-smBiT114
LgBiT-LL-Rab5
H) HEK-SNAP-Opn4-smBiT86
LgBiT-LL-Rab5
10µM Furimazine
3µM Furimazine
1µM Furimazine
300nM Furimazine
HBS
Bioluminescence Intensity (arbitrary units)
Time [min]

***Figure 5.13* – Comparison of raw bioluminescence values between HEK-SNAP-Opn4-smBiT86 and HEK-SNAP-Opn4-smBiT114 cell lines when co-transfected with LgBiT-Rab5 or LgBiT-Kras and treated with furimazine.** Single experiments performed in duplicate on the same day, $n$=1, representative of $n \geq 3$ experiments, used in normalised results as shown in *Figure 5.11* and *Figure 5.12*. The Opn4-smBiT86 cell line produced an almost 10 fold increase in bioluminescence with both the LgBiT-Kras (A, B) and LgBiT-LL-Kras (C, D) compared to Opn4-smBiT114 expressing cells. In the HEK-SNAP-Opn4-smBiT114 cell line, the LgBiT kRas construct designs including long linker provided a 2 fold increase in bioluminescence compared to the minimal linker versions, whereas this is further increased in the HEK-SNAP-Opn4-smBiT86 cell line to a 5 fold increase. Similar increases in luminescence intensity were observed in Opn4-smBiT86 cells co-transfected withLgBiT-Rab5 (E, F) or LgBiT-LL-Rab5 (G, H) compared to the Opn4-smBiT114, with an improved response using the long linker versions of the marker constructs

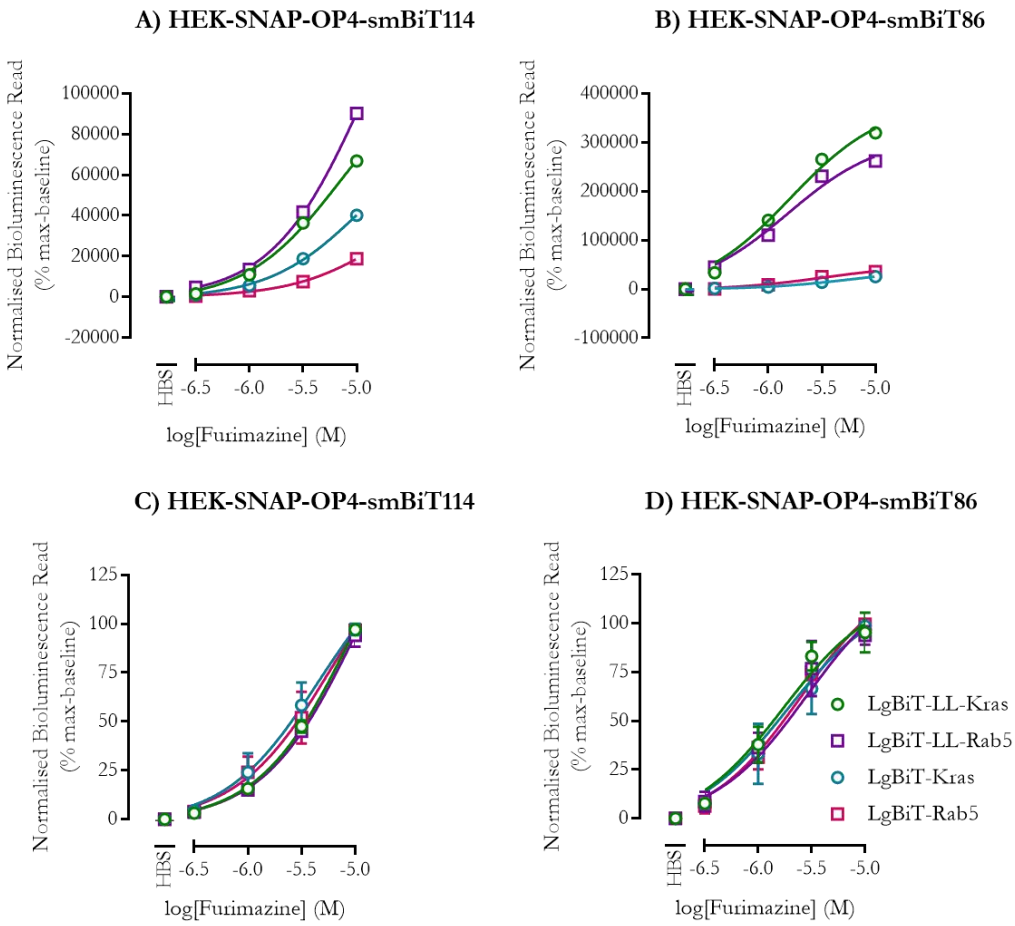


***Figure 5.14* – Furimazine concentration bioluminescence curve in HEK-SNAP-Opn4-smBiT86 and HEK-SNAP-Opn4-smBiT114 cells in combination with various transfected LgBiT constructs.** Luminescence measurements were taken at 4 min (bioluminescence peak) following furimazine addition. A) and B) are representative raw values from the PheraSTAR platereader ($n$=1 experiment in duplicate). C) and D) are normalised to vehicle and expressed as a percentage of the 10μM effect. Using the data from section 5.2.5, $n \geq 3$ where experiments were performed in duplicate.

### 5.2.5 The HEK-SNAP-Opn4-SmBiT86 Cell Line Co-Transfected with LgBiT Constructs can Produce Furimazine Induced Calcium Signalling

Once bioluminescence production was shown using the NanoBiT Opn4 constructs after complementation, functional activation of the Opn4 receptors stimulated by luminescence was investigated. As with the opto-$\alpha_{1A}$AR receptors, the main functional output of melanopsin upon light stimulation is an increase in calcium via $G_q$ activation. The HEK-SNAP-Opn4-smBiT86 and HEK-SNAP-Opn4-smBiT114 cell lines were therefore used in a calcium mobilisation assay using Cal-630 AM (1μM) calcium indicator due to the red shifted wavelength of the dye.

Well based high-throughput fluorescence measurement of the cells using a Flexstation 96 well platereader with automated furimazine addition did not produce any population calcium transients over a 2min period (data not shown).

In contrast, single cell confocal imaging detected individual responding cells post furimazine addition in the HEK-SNAP-Opn4-smBiT86 stable cell line co-transfected with LgBiT constructs (see *Figure 5.15* and *Figure 5.16*). Cells were transiently transfected with LgBiT constructs 48hr prior to imaging where the red-shifted Cal-630 AM was used to measure intracellular calcium for 10min. Calcium transients were not observed in the HEK-SNAP-opto-$\alpha_{1A}$AR-smBiT86 cell line or the HEK-SNAP-Opn4-smBiT114 cell line without furimazine, demonstrating that the response is due to receptor activation rather than a furimazine addition off target effect. Once furimazine was added, there was a general increase in background fluorescence due to bioluminescence bleed through, but intracellular calcium transients could still be seen within the fluorescent readout. Not all experiments produced a response, potentially due to low receptor-LgBiT co-expression following transfection in cells, but compared to vehicle control cells without furimazine addition there was a general increase in the percentage of cell activation, fluorescence intensity and the number of calcium transients, although this was not statistically significant, potentially due to low *n* numbers of response (see *Figure 5.17*).

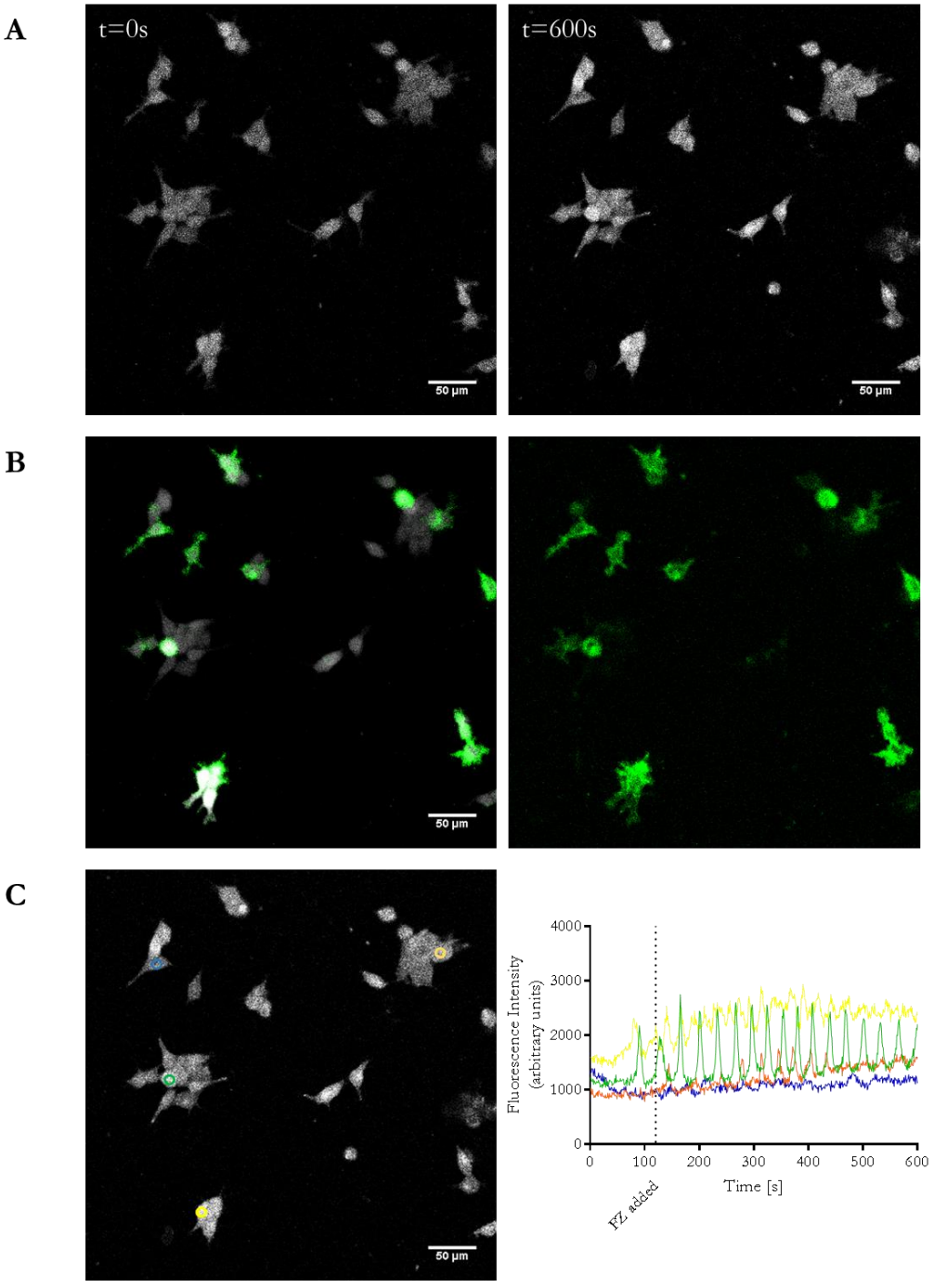
A
t=0s
t=600s
50 µm
50 µm
B
50 µm
C
50 µm
Fluorescence Intensity (arbitrary units)
4000
3000
2000
1000
0
0
100
200
300
400
500
600
Time [s]
PZ added

***Figure 5.15* – Cal-630 calcium measurements in the HEK-SNAP-Opn4-smBiT86 stable cell line co-transfected with LgBiT-LL-Rab5.** Cells were loaded with 1μM Cal-630 AM and treated with 1μM 9-*cis*-retinal 1hr before experiment. Confocal images were taken at 1 frame per second for 10min using the 647nm laser and 1μM furimazine (FZ) was added after 120s. A) Images of Cal-630 fluorescence before (t=0s) and after (t=600s) FZ addition. B) SNAP-Opn4-smBiT86 expression in HEK cells detected with SNAP-Surface AF488 labelling (0.2μM), taken post Cal-630 imaging. LgBiT-Rab5 expression could not be visualised. C) Representative ROIs from SNAP-Opn4-smBiT86 expressing cells and the matching colours are traced for fluorescence intensity across the 10min. *Green* and *yellow* cells were active before FZ addition but increase in calcium mobilisation transients post FZ. *Orange* produced transients post FZ addition, and *blue* produces no calcium transients.

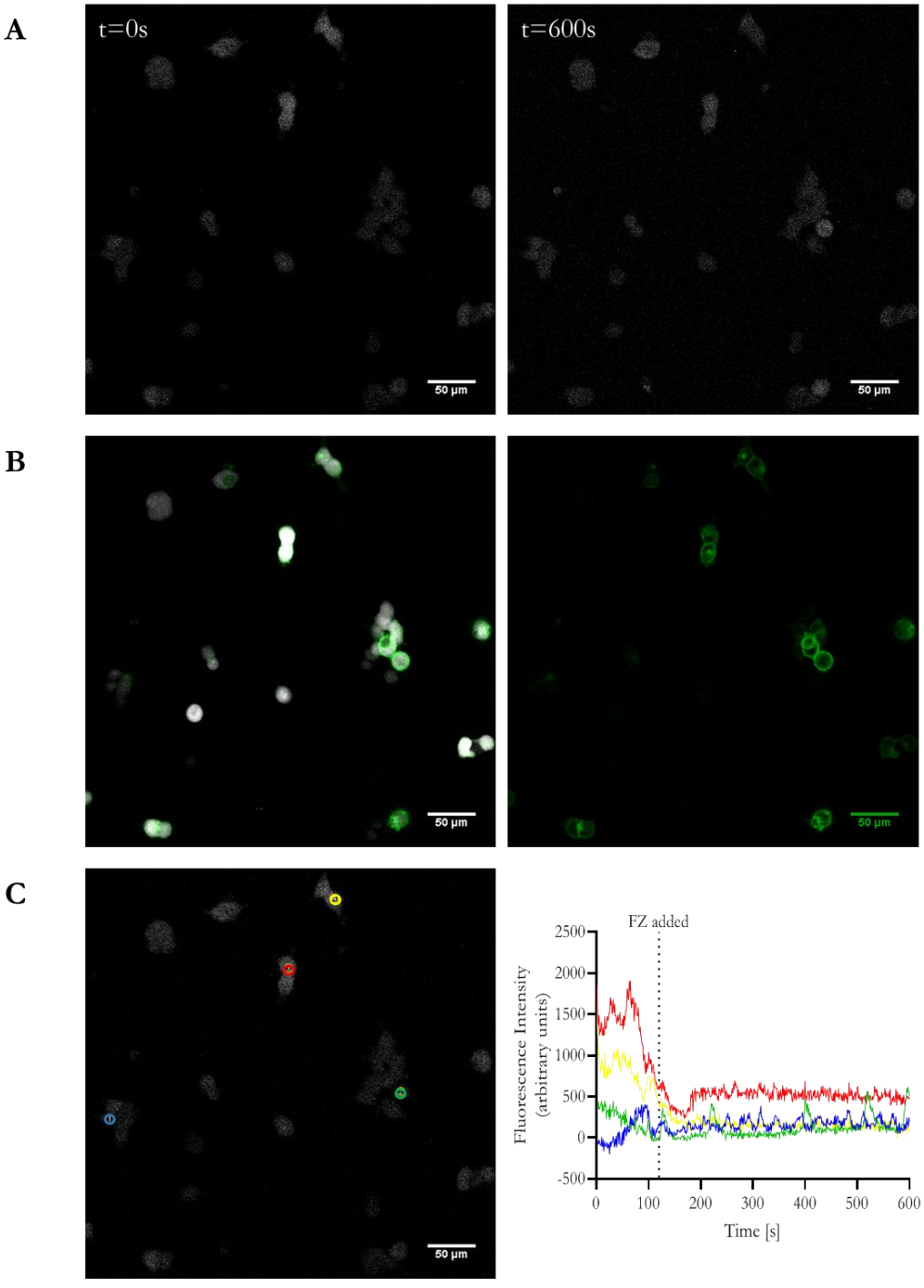
A
t=0s
t=600s
50 µm
50 µm
B
50 µm
50 µm
C
50 µm
FZ added
Fluorescence Intensity (arbitrary units)
2500
2000
1500
1000
500
0
-500
0
100
200
300
400
500
600
Time [s]

***Figure 5.16* – Cal-630 fluorescence in the HEK-SNAP-Opn4-smBiT86 stable cell line co-transfected with LgBiT-LL-Kras.** Cells were loaded with 1μM Cal-630 AM and treated with 1μM 9-*cis*-retinal 1hr before experiment. Confocal images were taken at 1 frame per second for 10min using the 647nm laser and 1μM furimazine (FZ) was added after 120s. A) Images of Cal-630 fluorescence before (t=0s) and detected with SNAP-Surface AF488 labelling (0.2μM), taken post Cal-630 imaging. LgBiT-Kras expression could not be visualised. C) Representative ROIs from SNAP-Opn4-smBiT86 expressing cells and the matching colours are traced for fluorescence intensity across the 10min.

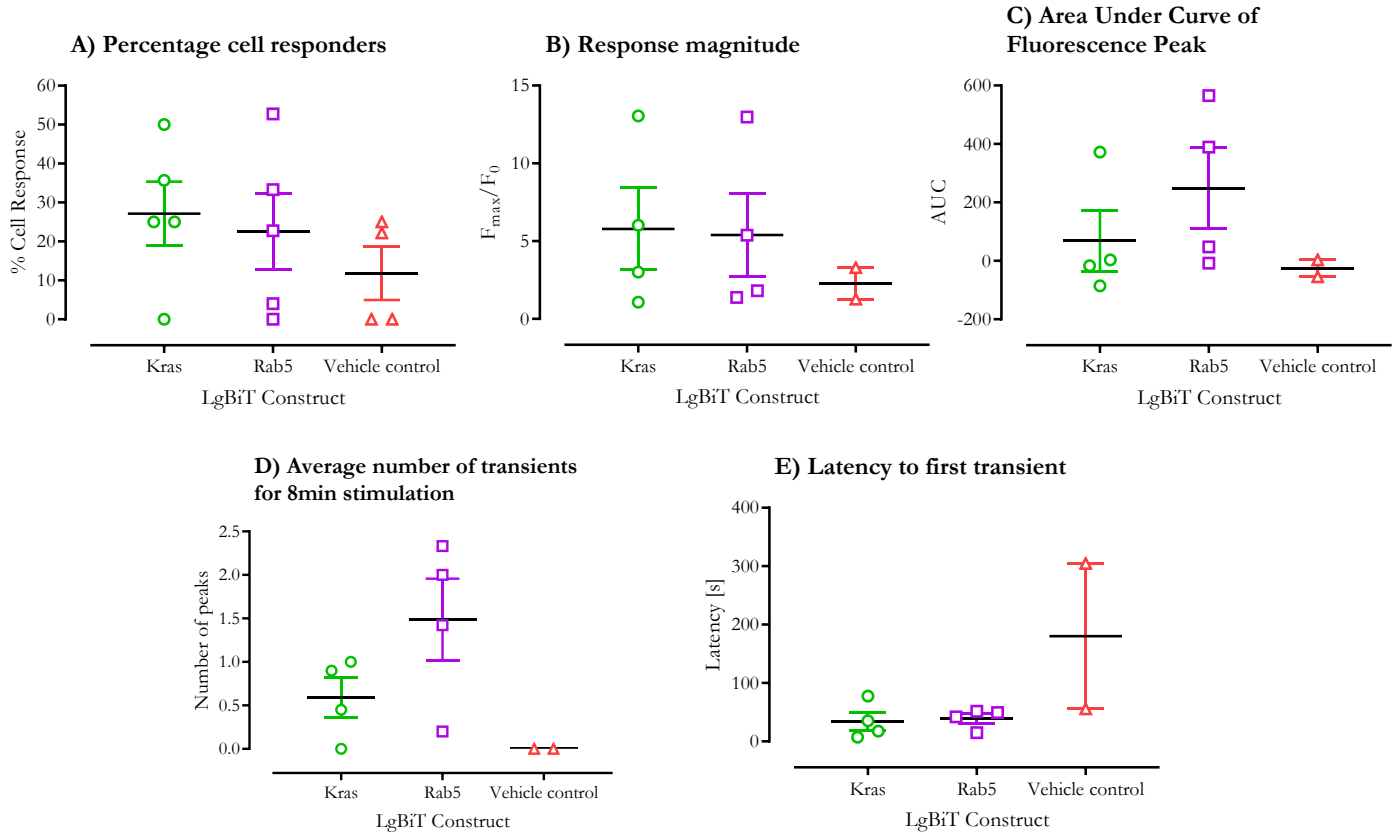
A) Percentage cell responders
% Cell Response
60
50
40
30
20
10
0
Kras
Rab5
Vehicle control
LgBiT Construct
B) Response magnitude
$F_{max}/F_0$
15
10
5
0
Kras
Rab5
Vehicle control
LgBiT Construct
C) Area Under Curve of Fluorescence Peak
AUC
600
400
200
0
-200
Kras
Rab5
Vehicle control
LgBiT Construct
D) Average number of transients for 8min stimulation
Number of peaks
2.5
2.0
1.5
1.0
0.5
0.0
Kras
Rab5
Vehicle control
LgBiT Construct
E) Latency to first transient
Latency [s]
400
300
200
100
0
Kras
Rab5
Vehicle control
LgBiT Construct

***Figure 5.17* – Summary of the calcium response profiles in the HEK-SNAP-Opn4-smBiT86 stable cell line stimulated with furimazine and measured by Cal-630, in the presence and absence of LgBiT subcellular markers** Cells were stimulated with 1μM furimazine after 2min and Cal-630 (1μM) fluorescence was recorded at 1 frame per second for 10min ($n \geq 4$ coverslips from separate experiments with a minimum of 25 cells per coverslip). A) The percentage of cells on a coverslip responding to furimazine addition. Out of the 5 experiments performed with each LgBiT construct (LgBiT-LL-Rab5 and LgBiT-LL-Kras), only 4 experiments produced calcium transients. Without furimazine, 2 experiments produced transients. B) Peak magnitude of calcium transients in responding cells, measured using fluorescence intensity increase over baseline. C) Area under the curve of the fluorescence peak for the entire read. The baseline decline in Cal-630 fluorescence resulted in some negative values calculated for AUC, when there was no response. D) The average number of calcium transients produced by HEK cells after furimazine addition, reduced when no furimazine was added. E) The latency to the peak of the first transient after furimazine addition. Both LgBiT constructs have low latencies, however in one control experiment, cells did not respond until 5min post vehicle addition, indicating that this response was not produced by addition of liquid.

### 5.2.6 Furimazine Stimulated Opn4-sm86 Receptor Internalisation Following LgBiT Marker Complementation

Once it was established that the luminopsin OP4 receptors could potentially activate $G_q$ protein pathways by bioluminescence stimulation, an internalisation assay was established as another readout of light stimulated receptor activation. Receptors were tagged with SNAP Surface AF647 (0.2μM) in the HEK-SNAP-Opn4-smBiT86/114 cell lines with or without incubation with endocytosis inhibitors (Pitstop 2 and Dyngo 4a, 30μM; see Chapter 3.2.5 for overview). Cells then underwent 30min stimulation with furimazine and the bioluminescence produced was measured on the PheraSTAR platereader. Transferrin AF-546 (1:1000 dilution) was also present during this step to label early and recycling endosomes. Post stimulation, cells were fixed and imaged on the IX Ultra platereader. Images were analysed by an algorithm that measured the co-localisation of the endosomal label with the SNAPtagged receptors. Treatment with Dyngo 4a did not cause any change in bioluminescence production, however Pitstop 2a caused a 3 fold reduction in the bioluminescence produced by furimazine in the cells (see *Figure 5.22*).

The stable HEK-SNAP-OP4-smBiT86 cell line, cotransfected with LgBiT-LL-kRas, with high furimazine concentrations increased the amount of endocytosed SNAP Surface AF-647 fluorescence, although the percentage of cells showing significant stimulated internalisation was relatively small (see *Figure 5.18*). As with the calcium assay, low receptor/NanoBiT co-expression after transient co-transfection is a potential reason for the small response window. The stable HEK-SNAP-OP4-smBiT114 cell line did not show internalisation linked to furimazine addition when co-transfected (see *Figure 5.19*). Lack of both internalisation and calcium mobilisation using the smBiT114 indicates that the bioluminescence produced by complementation with this luciferase construct is not bright enough for receptor activation.

When the images were quantified via the translocation algorithm, furimazine produced a concentration response in HEK-SNAP-OP4-smBiT86 receptor translocation to endosomes with both the LgBiT-LL-Kras and LgBiT-LL-Rab5 (see *Figure 5.20*). Addition of Dyngo 4a, a clathrin-dependent inhibitor, did not

cause a reduction in internalisation of the OP4 receptors with both LgBiT constructs. Pitstop 2 only produced a reduction in cells co-transfected with LgBiT-LL-Kras. The internalisation response was less marked in cells co-transfected with the minimal linker LgBiT constructs, and the internalisation effect seen with these constructs was also not sensitive to endocytosis inhibitors Pitstop 2 or Dyngo 4a. The HEK-SNAP-OP4-smBiT114 cell line did not produce a concentration dependent internalisation response to furimazine when co-transfected with any of the LgBit constructs (see *Figure 5.21*).

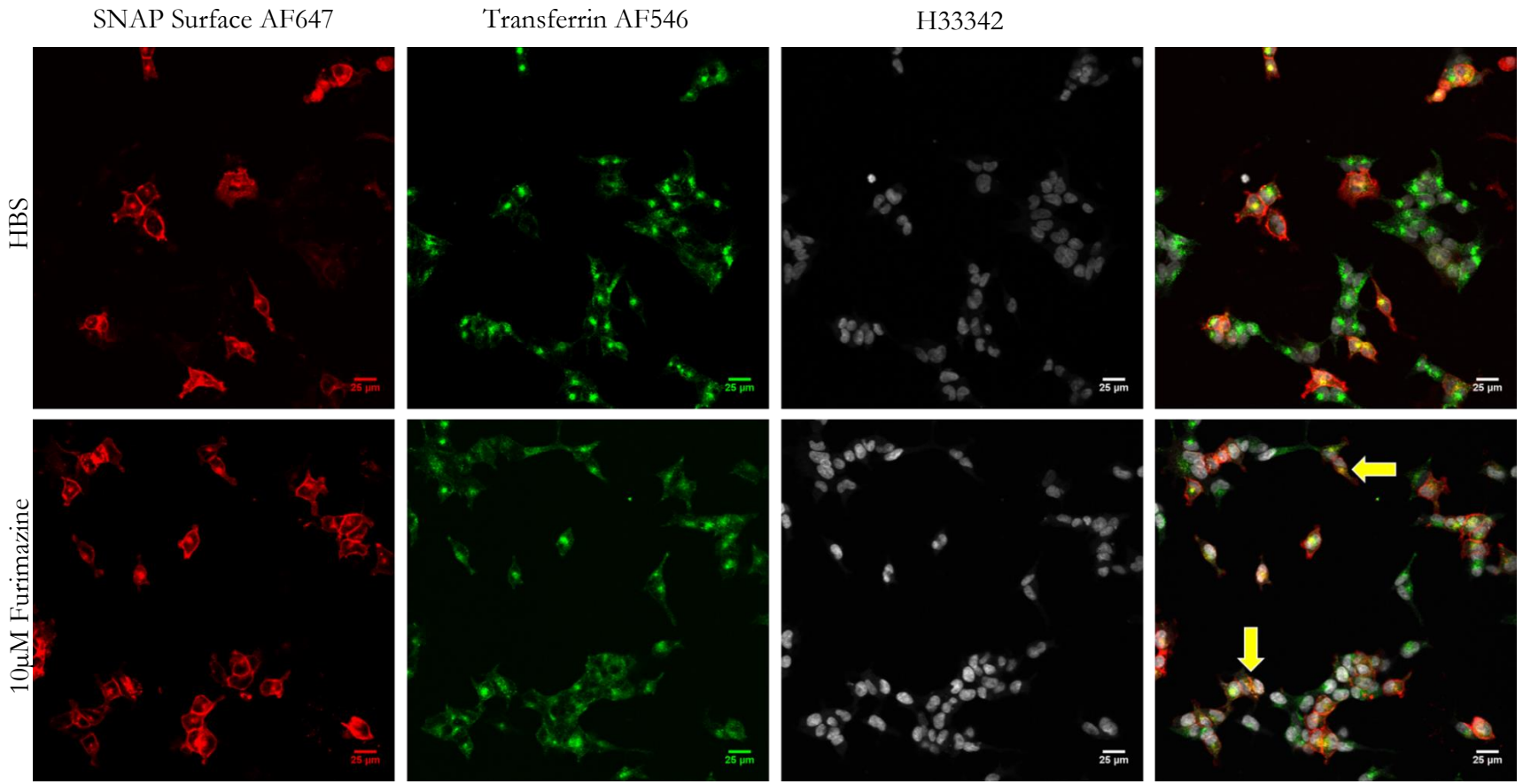
SNAP Surface AF647
Transferrin AF546
H33342
HBS
10μM Furimazine
25 μm

***Figure 5.*18 – Co-localisation of SNAP tagged Opn4-smBiT86 receptors with transferrin-AF546 in HEK 293T cells transfected with LgBiT-LL-Kras.** Cells were transfected with LgBiT-LL-Kras 48hr before experiment. Receptors were labelled using SNAP-Surface AF647 (0.2μM, 30min, 37º) and transferrin-AF546 (10μg.mL$^{-1}$). Cells were treated with furimazine or HBS for 30min prior to fixing and imaging on a confocal plate reader. Yellow arrows in the combined image show cells with high co-localisation. Representative $n$=1 site of 4 sites from 1 well of a duplicate experiment repeated 4 times.

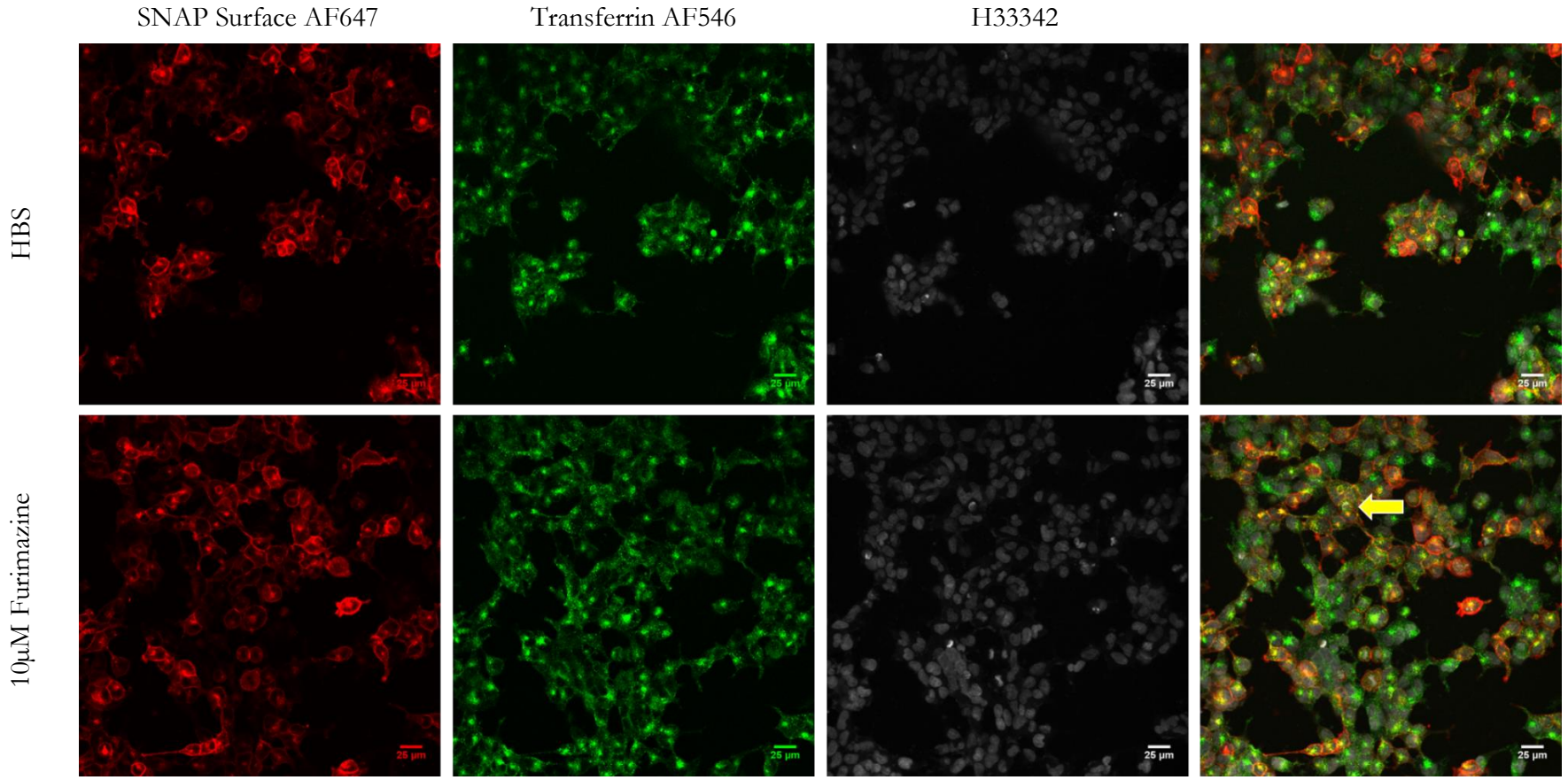
SNAP Surface AF647
Transferrin AF546
H33342
HBS
10μM Furimazine
25 μm

***Figure 5.19*** **– Co-localisation of SNAP tagged Opn4-smBiT114 receptors with transferrin in HEK 293T cells transfected with LgBiT-LL-Kras.** Cells were transfected with LgBiT-LL-Kras 48hr before experiment. Receptors were labelled using SNAP-Surface AF-647 (0.2μM, 30min, 37º) and transferrin using transferrin AF-546. Cells were treated with furimazine or HBS for 30min prior to fixing and imaging on a confocal plate reader. Yellow arrow in the combined image show cells with high co-localisation. Representative $n$=1 site of 4 sites from 1 well of a duplicate experiment repeated 4 times.

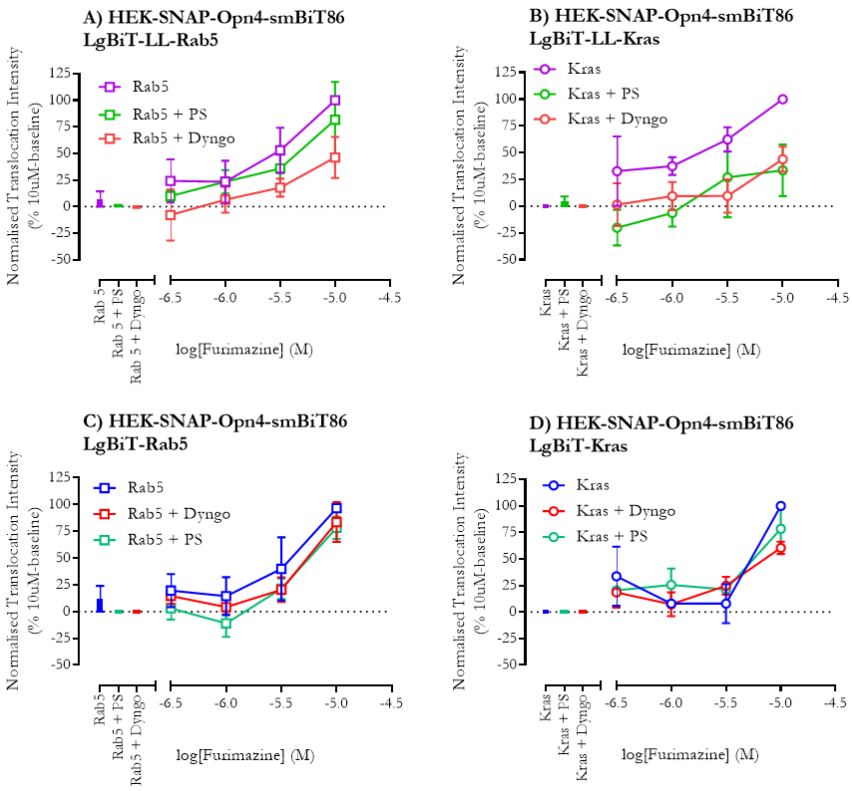


***Figure 5.20* – Analysis of SNAP tagged receptor translocation to transferrin labelled endosomes in the HEK-SNAP-Opn4-smBiT86 stable cell line with co-transfected LgBiT constructs.** Cells were transfected with LgBiT constructs 48hr prior to experimentation where they were labelled with SNAP-Surface AF-647 (0.2μM), treated with 9-*cis*-retinal (1μM) and in the presence and absence of Pitstop 2 (PS) or Dyngo 4a (Dyngo) endocytosis inhibitors (both 30μM). After 30min stimulation with furimazine and labelling with transferrin AF-548 (1:1000 dilution), cells were imaged on the IX Ultra platereader and a translocation algorithm was used to measure SNAPtag fluorescence against transferrin for co-localisation of receptors with endosomes. A) and B) show the LgBiT constructs with an added amino acid linker to Rab5 and Kras, respectively. There was a concentration-dependent response to furimazine which is reduced using Dyngo 4a, but only significantly by Pitstop 2 in the Kras anchored bioluminescence (one way ANOVA, Tukey's post hoc, $p=0.05$). C) and D) are the LgBiT constructs without a linker, where no internalisation inhibition was seen by the endocytosis inhibitors. $n \geq 3$ experiments, where the long linker constructs data were taken on different days to the LgBiT without a linker. Bars on the left represent averaged vehicle responses.

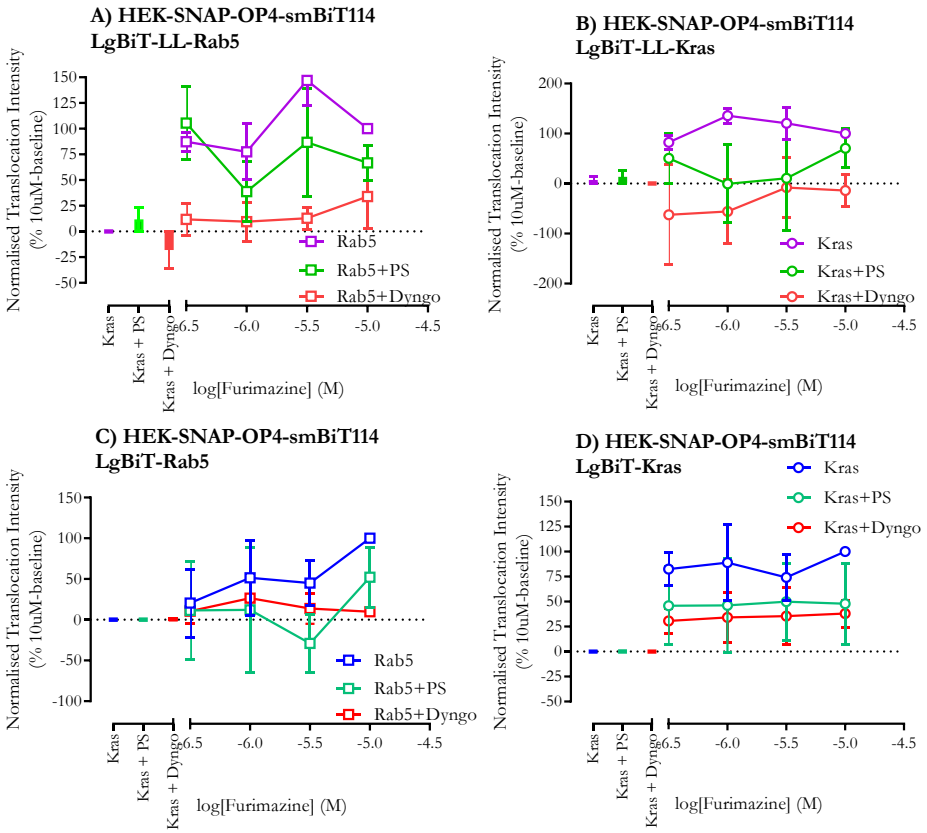


***Figure 5.21* – Analysis of SNAP tagged receptor translocation to endosomes in the HEK-SNAP-Opn4-smBiT114 stable cell line with transient LgBiT constructs.** Cells were transfected with LgBiT constructs 48hr prior to experimentation where they were labelled with SNAP-Surface AF647 (0.2μM), treated with 9-*cis*-retinal (1μM) and in the presence and absence of Pitstop 2 (PS) or Dyngo 4a (Dyngo) endocytosis inhibitors (both 30μM). After 30min stimulation with furimazine and labelling with transferrin AF548 (1:1000 dilution), cells were imaged on the IX Ultra platereader and a translocation algorithm was used to measure SNAPtag fluorescence against transferrin for co-localisation of receptors with endosomes. A) and B) show the LgBiT constructs with an added amino acid linker to Rab5 and Kras, respectively. C) and D) represent the LgBiT constructs without a linker. For all conditions, there was a lack of concentration-dependent response to furimazine. Dyngo 4a also had the least internalisation for all conditions. $n \geq 3$ experiments, where the long linker constructs data were taken on different days to the LgBiT without a linker. Bars on the left represent averaged vehicle responses.

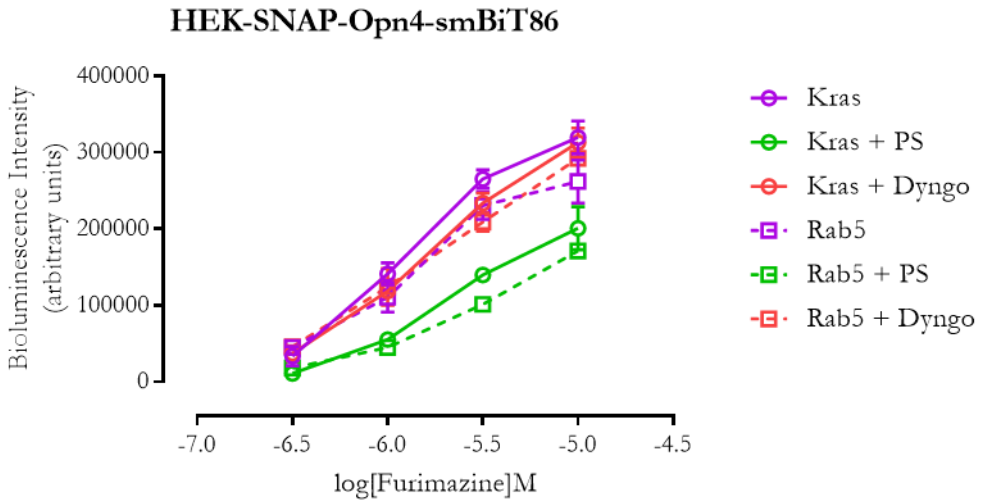


***Figure 5.22* – Effect of Pitstop 2 and Dyngo 4a on bioluminescence production in the HEK-SNAP-Opn4-smBiT86 stable cell line when co-transfected with LgBiT-LL-Kras or LgBiT-LL-Rab5.** Cells were incubated with Pitstop 2 or Dyngo 4a (both 30μM) for 30min prior to stimulation with furimazine for 30min while bioluminescence was measured on the PheraSTAR platereader. There was no difference in bioluminescence production when cells were treated with Dyngo 4a, however Pitstop 2 reduced the bioluminescence brightness released by furimazine by 3.2 fold at the highest concentration. Representative of $n$=4 experiments, from 1 experiment performed in duplicate.

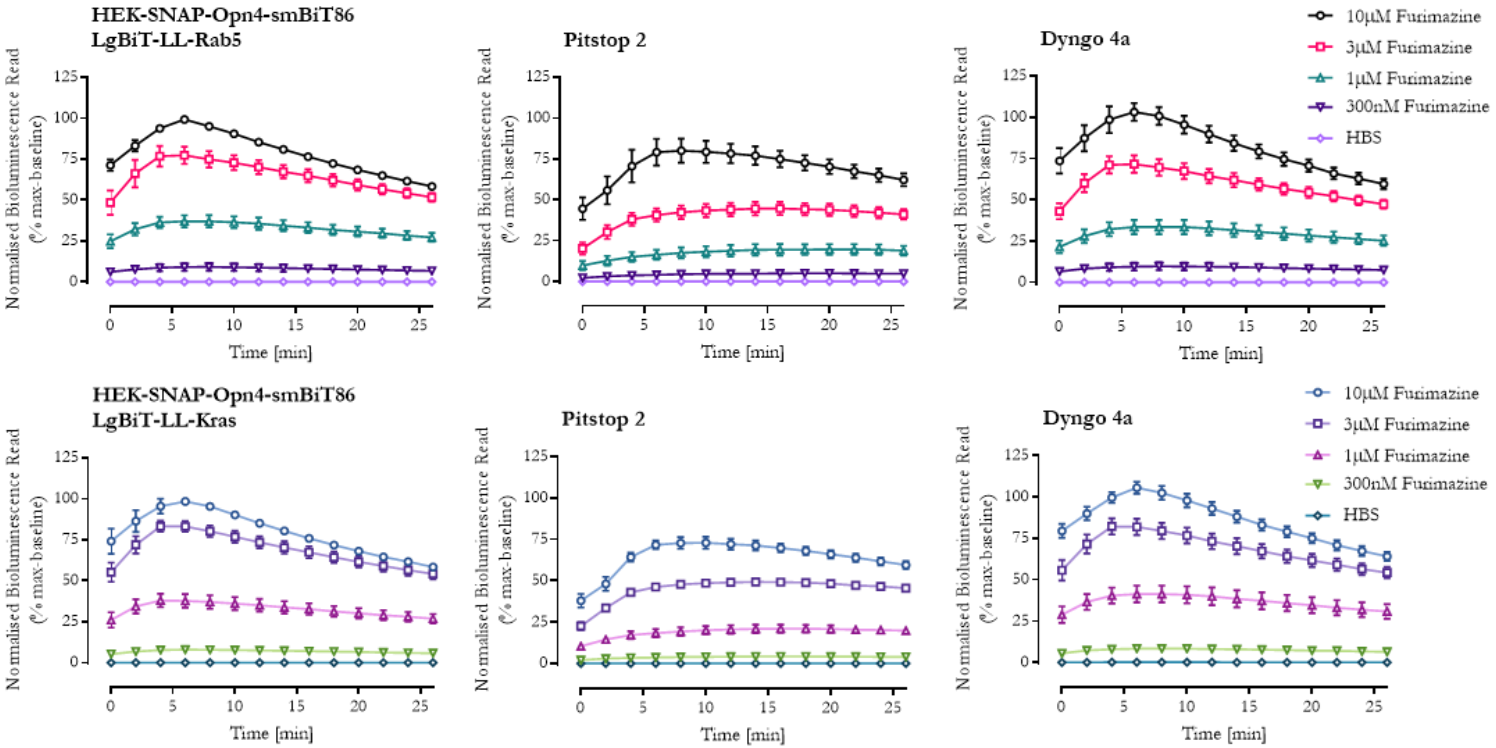


***Figure 5.23*** **– Effect of endocytosis inhibitors Pitstop 2 and Dyngo 4a on bioluminescence produced by HEK-SNAP-Opn4-smBiT89 stable cell line transfected with LgBiT-LL-Rab5 or Kras constructs.**

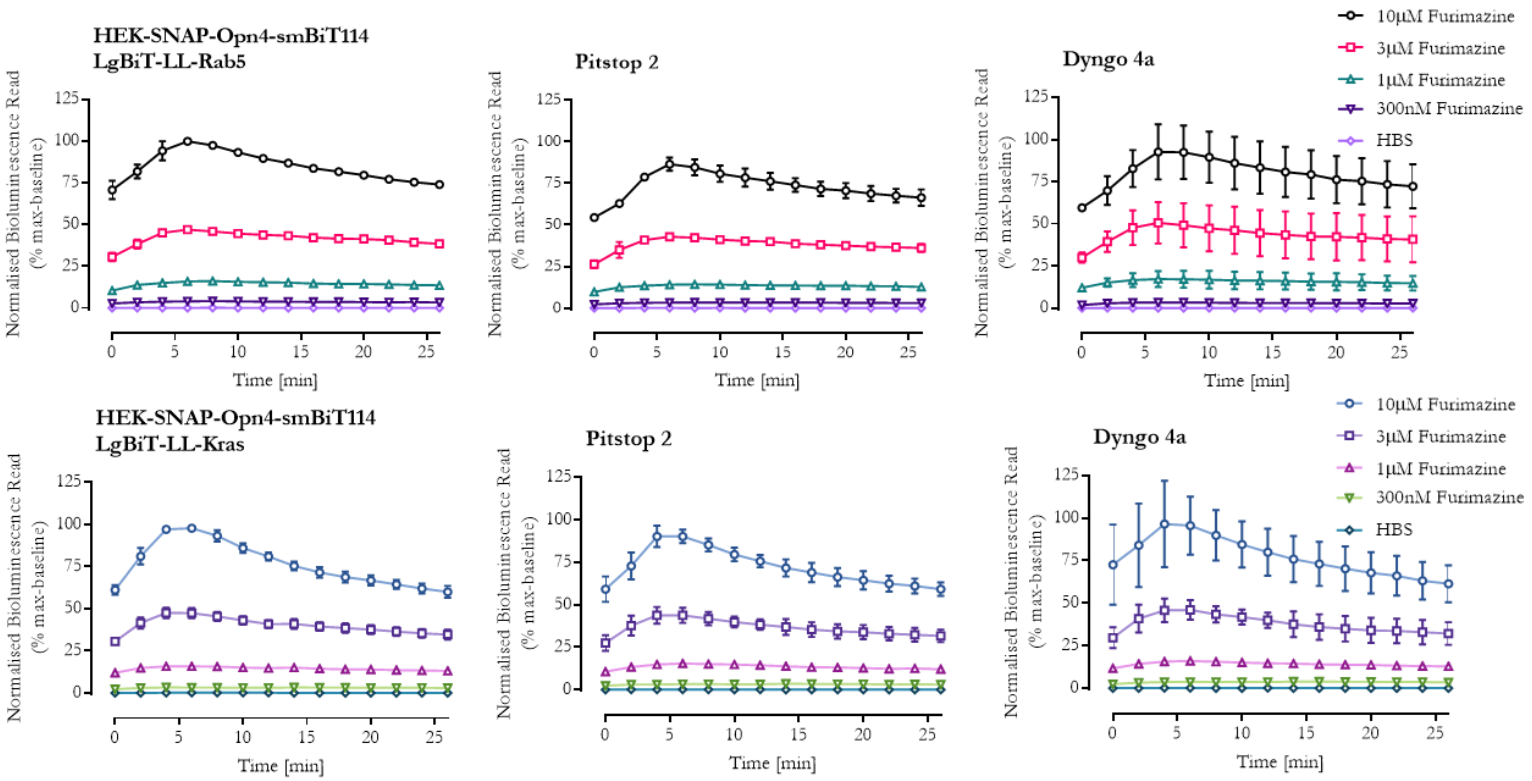


***Figure 5.24*** **– Effect of endocytosis inhibitors Pitstop 2 and Dyngo 4a on bioluminescence produced by HEK-SNAP-Opn4-smBiT114 stable cell line transfected with LgBiT-LL-Rab5 and Kras constructs.**

### 5.2.7 Subcellular Localisation of Opn4-NanoBiT Bioluminescence Following Complementation with Different LgBiT Anchor Proteins

Although the smBiT86 could produce cellular signalling in response to furimazine addition, the smBiT114 did not. The most likely explanation would be that the increase in brightness and stable complementation of the smBiT86 with the LgBiT protein allows for better receptor activation. However, one issue that may arise is that the increased brightness and stable complementation produced by the smBiT86 may be less localised to the LgBiT area of expression, therefore decreasing the spatial advantage of the assay.

The spatial properties of the bioluminescence produced in the luminopsins were investigated with bioluminescence imaging, also presenting an opportunity to investigate the co-expression levels of the SNAP-Opn4-smBiT receptors with the LgBiT contracts in transfected HEK cells. Using the Olympus LV200 microscope, with specialist capacity for low light capture, bioluminescence was imaged on a single cell level in the stable HEK-SNAP-Opn4-smBiT cell lines using the brighter LgBiT-LL-Kras and LgBiT-LL-Rab5 constructs as co-transfected proteins. Qualitatively, the LgBiT-LL-Kras produced brighter membrane-bound bioluminescence than the LgBiT-LL-Rab5 when complementing both the Opn-smBiT86 and Opn-smBiT114 (see *Figure 5.23* and *Figure 5.24*). It was expected that the smBiT86 would not have bioluminescence localisation due to its ability to produce stable high affinity complexes with LgBiT, allowing the bioluminescent construct to be trafficked to other areas of the cell. In the Opn4-smBiT86, the brightest bioluminescence was observed at the plasma membrane with the LgBiT-Kras construct and appeared more endosomal (though not exclusively so) when complexed the LgBiT-Rab5. Bioluminescent images from the OP4- smBiT114 cell line were less bright but showed a qualitatively similar pattern of predominant plasma membrane (LgBiT-kras) or endosomal distribution (LgBiT-Rab5). In each case, a limited percentage of cells generated a bioluminescent signal, compared to previous observations in identifying the SNAP-Opn4-SmBiT receptors by SNAP labelling (*Figure 5.10*), reflecting the transient co-transfection efficiency of the LgBiT constructs. These images provided qualitative reassurance that the LgBiT marker proteins were indeed targeted to plasma membrane or endosomal compartments as designed.

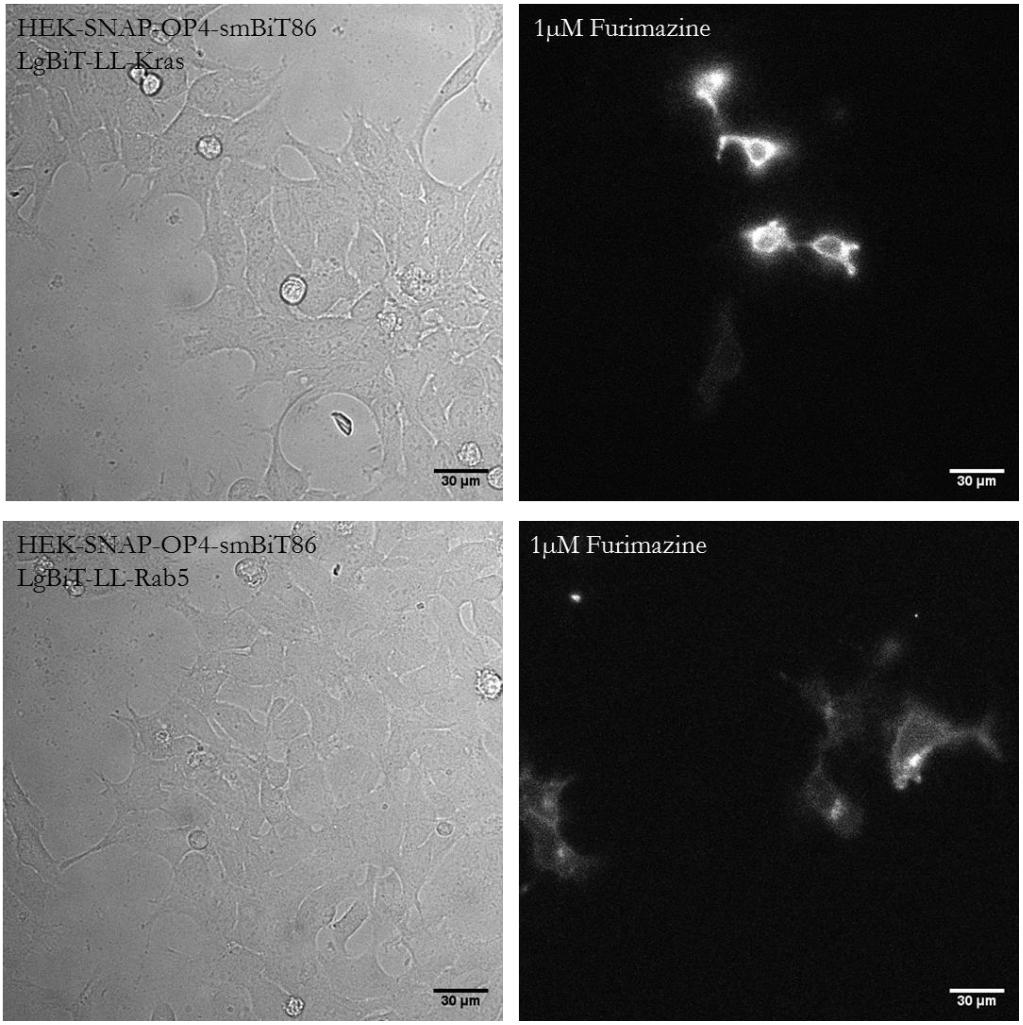


***Figure 5.25* – Images of bioluminescence produced by HEK-SNAP-Opn4-smBiT86 stable cell line transfected with LgBiT-LL-Kras and LgBiT-LL-Rab5.** Cells were transfected 48hr prior to experiments and plated 24hr before onto glass bottomed Petri dishes. Furimazine (1μM) was added to the cells and the Petri dish was scanned for bioluminescence and once expression was found, cells were imaged for 2hr where bioluminescence was continuously emitted. The co-transfected LgBiT-LL-Kras appears to produce a more predominantly membrane located bioluminescence than the LgBiT-LL-Rab5. Representative of $n$=2 for both LgBiT constructs, images shown taken on the same day.

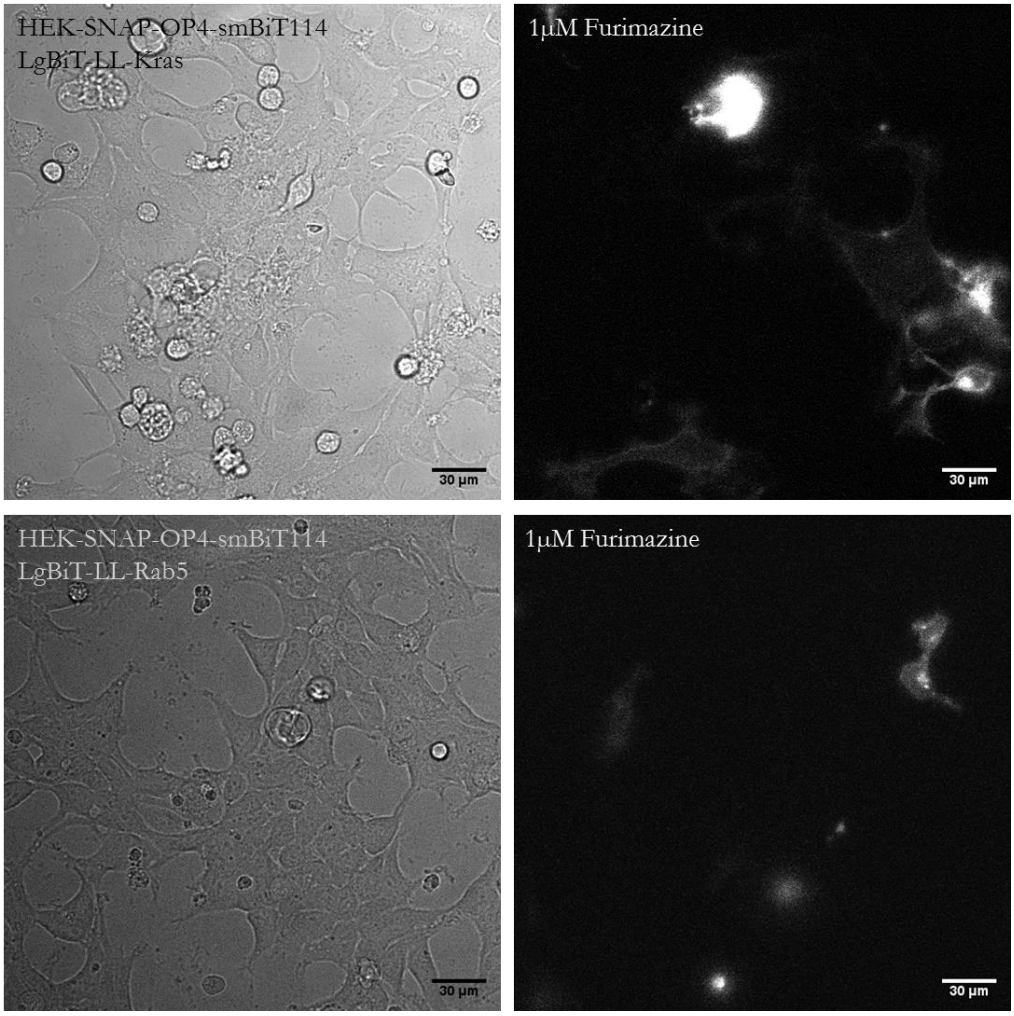


***Figure 5.26* – Images of bioluminescence produced by HEK-SNAP-Opn4-smBiT114 stable cell line transfected with LgBiT-LL-Kras and LgBiT-LL-Rab5.** Cells were transfected 48hr prior to experiments and plated 24hr before onto glass bottomed Petri dishes. Furimazine (1μM) was added to the cells and the Petri dish was scanned for bioluminescence and once expression was found, cells were imaged for 2hr over which time bioluminescence was continuously emitted. Representative of $n$=2 for both LgBiT constructs.

## 5.3 Discussion

### 5.3.1 NanoBiT Complementation using Compartmental Markers is Sufficient to Generate Robust Bioluminescence with SmBiT Tagged Optogenetic Receptors Opto-$\alpha_{1A}$AR and OP4

The two parts of the NanoBiT luciferase are required to be in close proximity in order to form the whole complex and allow enzymatic digestion of furimazine to generate the bioluminescence stimulus. Using both Rab5 and Kras as protein 'anchors' for the LgBiT managed to produce bioluminescence when using either opto-$\alpha_{1A}$AR or OP4, showing that the two proteins are close enough to create the required complementation. For both optogenetic receptors, bioluminescence was greater when using LgBiT fused to the Kras anchor, rather than the Rab5 protein. This is consistent with the distribution of the receptors, with both opto-$\alpha_{1A}$AR and Opn4 expressing predominantly on the plasma membrane, as shown by SNAP labelling, rather than endosomes.

It would be of interest to measure the difference in bioluminescence production post receptor stimulation with light when receptors will be actively endocytosed to determine if this is indeed the case. Another potential explanation could be due to a difference in expression efficiency between the two LgBiT constructs. This could be measured by adding a tag to the LgBiT constructs to be able to measure its independent expression in cells, a process not performed in the current study due to potential interference from the tag interacting with the assay.

When an amino acid linker was added between the LgBiT and anchor protein, bioluminescence production increased for both smBiT constructs. This linker increases flexibility and distance between the complementation fragment and the tether (e.g. the membrane lipid tag provided by the Kras sequence), allowing for complementation between the LgBiT and SmBiT when the two target proteins are in different orientations or slightly further apart. Storme *et al.* (2018) also varied the protein linker between LgBiT and their target of interest, the $A_3$ adenosine receptor. Due to potential interactions between the receptor and the serine residues in the LgBiT linker, the linker was shortened from 21 amino acids to 9. In this case, the change in linker did not affect the bioluminescence readout (Storme *et al.*, 2018). One explanation could be that the investigators were using β-arrestin-2 as their

target effector, a cytosolic molecule that would not have the same spatial restrictions as the Kras or Rab5 protein anchors used in this study. For example, the LgBiT-Kras sequence without a linker is likely to place the marker very close to the inner leaflet of the plasma membrane when it is lipid modified. Opn4 and opto-$\alpha_{1A}$AR both have a reasonably large C terminus following the potential palmitoylation site located at the membrane, therefore the SmBiT tag may be located some way away from the juxtamembrane localised LgBiT, making the LgBiT less likely to complement. Adding the linker extends the LgBiT away from the membrane and therefore produces a greater chance of interaction between the fragments.

### 5.3.2 Bioluminescence from NanoBiT Complementation does not Induce Calcium Signalling in Opto-$\alpha_{1A}$AR

Unfortunately, the combination of using opto-$\alpha_{1A}$AR and NanoBiT as the opsin and luciferase components of the luminopsin construct was unsuccessful in producing calcium signalling. The main possibility would be that the NanoBiT construct does not produce enough bioluminescence from the furimazine substrate for the chimeric receptor, which requires a bright light for activation, unlike the melanopsin which can be activated at very low light levels (Airan *et al.*, 2009; van Wyk *et al.*, 2015). When developing luminopsins, several different luciferases have been investigated for their bioluminescence production and ability to activate channelrhodopsin-1/2 (Berglund *et al.*, 2016; Park *et al.*, 2019).

### 5.3.3 High Affinity SmBiT86 can Activate OP4 Calcium Mobilisation and Receptor Trafficking, but not Low Affinity SmBiT114

Intracellular calcium signalling was measured in the HEK-SNAP-OP4-smBiT86 stable cell line when co-transfected with LgBiT-LL-Kras or LgBiT-LL-Rab5 and treated with 1μM furimazine. Melanopsin has been shown to activate at lower light levels than the opto-$\alpha_{1A}$AR in this body of work (see Chapter 4.2.5). It is therefore not a surprise that the OP4 construct had a greater success with the bioluminescence activator, although the lower bioluminescence produced using the smBiT114 was not sufficient for receptor activation in single cell calcium measurements. It would have been useful to increase the robust measurement of the single cell calcium responses, in part limited by the relatively low transfection

efficiency of the LgBiT constructs. This could in future by achieved by including a fluorescent marker for the LgBiT co-transfection (e.g. inclusion of GFP DNA, or a LgBiT also tagged with fluorescent protein) – so that only co-transfected cells were monitored for calcium responses, rather than the whole field. Alternatively, dual stable co-transfected cell lines could be generated to increase the expression of the LgBiT.

One concern with the luminopsin methodology is that substrate binding kinetics have to be considered in the light-activated system, alongside the kinetics of opsin activation. Under the general experimental conditions of the assays used, the luminescence generation by the complemented luciferase occurred rapidly (within seconds) but did not peak until approximately 5 min following furimazine addition. This peak response in fact occurred after the endpoint of single cell calcium measurements. As would be expected for an all-or-nothing response, variations in the latency to trigger a calcium transient were observed following furimazine addition. Together with the relatively low transient transfection efficiency of the LgBiT markers in the test assays, this made population calcium measurements impossible. In order to improve the temporal aspect and potentially enable population response measures, a substrate with improved, faster cell permeability could help quicken bioluminescence production, or perhaps the development of luciferases with improved catalytic turnover of the substrate for a brighter, more rapid signal. Currently, NanoBiT offers the best kinetics of the split luciferases. As a relatively new and developing methodology, where the first split luciferase was described by Ozawa *et al.* (2001), there is still the possibility of better substrates or improved catalysis in the future.

This assay did provide evidence of Opn4 activation and endocytosis in response to luminescence in the HEK-SNAP-Opn4-smBiT86 cell line when co-transfected with either LgBiT-LL-Kras or LgBiT-LL-Rab5. Although the quantified internalisation effect was relatively modest, a selective effect on internalisation was supported by the inhibitory effect of Dyngo 4a. Interestingly, Pitstop 2 inhibited furimazine induced internalised receptors only in the HEK-SNAP-OP4-smBiT86 cell line when co-transfected with LgBiT-LL-Kras, and not with LgBiT-LL-Rab5. This could be due to a mechanistic difference between the way Pitstop 2 and Dyngo 4a act. Unlike Dyngo 4a, which is clathrin-dependent, Pitstop 2 has been suggested to also inhibit clathrin-independent endocytosis, potentially through altering the

mobility of integral membrane proteins (Dutta *et al.*, 2012; Willox *et al.*, 2014). If these proteins are important for plasma membrane endocytosis, but not endosome function, this could perhaps answer why Pitstop 2 caused a decrease in internalisation for receptors at the membrane in close proximity to Kras, rather than promote the internalisation of activated receptors in endosomes near Rab5. Unfortunately, Pitstop 2 treatment also showed a reduction in bioluminescence production, which could confound the results.

### 5.3.4 Evaluating the Potential for Split Complementation Luminopsins to Investigate Spatially Localised Signalling from Membrane and Endosomes.

Calcium signalling responses were detected in Opn4-Nanobit constructs using both a plasma membrane marker and, interestingly, an early endosome marker. Previous investigations into endosomal signalling largely consider $G_s$ coupled receptor responses. Once established, a Gq stimulus pathway in endosomes could be interesting. For example, the PLC pathway activation from Golgi localised $\beta_1$ adrenoceptors in the heart has recently been shown as separate to plasma membrane stimulation, indicating compartmentalised $G_q$ signalling may be important for treatment targets (Nash *et al.*, 2019).

A crucial component of using a split luciferase rather than a full luciferase for receptor activation is the spatial advantage gained by allowing specific tethering of the luciferase fragments. Bioluminescence imaging provided evidence that the spatial difference between the Kras and Rab5 tethered LgBiT component does exist, and that the bioluminescence was targeted to the correct place, although the extent of this difference was not quantified. It could be possible to measure bioluminescence intensity at different areas of the cell, should these areas be defined by perhaps other dyes or indicators.

There were some limitations to developing the new luminopsin technology. As the smBiT86 produced a response and not the low affinity smBiT114, this could show a lack of location specificity as smBiT86 produces a stable complex with the LgBiT and may be trafficked to other compartments, such as the endosomes.

The efficiency of the activation by luciferase was also not very robust, with a lack of statistical significance from the calcium responses and low internalisation levels.

There is also the potential that luminescent light could activate non-complemented receptors in other areas, e.g. early endosomes are close to the plasma membrane and may stimulate receptors at these areas too. Therefore the evidence is not yet sufficient to interpret data as a response originating from endosomal localised receptors.

### 5.3.5 Next Steps

In future, alternative assays investigating the cumulative consequences of $G_q$ activation could be considered, rather than the rapid generation of a calcium transient shortly after furimazine addition. An example would be the measurement of inositol phosphate (IP) generation (e.g. using the CisBio $IP_1$ assay), which could measure the effect of sustained light generation by the luciferase over an extended period (mins – hrs) (Zhang *et al.*, 2010). This was one purpose of investigating receptor internalisation as an alternative readout of luciferase based OptoR stimulation and reflects a longer term stimulatory effect of luminescence signal generated, potentially offering greater sensitivity compared to rapid calcium mobilisation. As discussed in chapter 4.3.5, for Opn4 internalisation is likely to reflect an arrestin driven process though this was not directly determined (Blasic, Brown, *et al.*, 2012). The luminopsin coupling could also be improved, for example by shortening the C terminus to make the luciferase close to the optogenetic receptor, or by using alternative optogenetic GPCRs.

Another factor to consider with the spatial localisation of the bioluminescence produced is the drop off in intensity from the vicinity of activation. Unlike the spatially restricted two-photon microscopy described in 5.1.1 which has quadratic decrease of light intensity from the area of illumination, normal fluorescence and bioluminescence has a linear decrease in intensity, causing the photon excitation to 'bleed' further from the source (Svoboda and Yasuda, 2006). A potential solution for decreasing the spread of the bioluminescence to other areas could be to use a cell impermeable or permeable (depending on target site) luciferase inhibitor for the NanoBiT. Such inhibitors have recently been developed for NanoLuc, although these have yet to be tried with the NanoBiT constructs (Walker *et al.*, 2017). The opsin would be tagged on the extracellular N terminus with the smBiT. Plasma membrane or endosomal markers that localise the LgBiT to the extracellular (or internal endosome) surface could then be generated so that addition of a cell

impermeable inhibitor would prevent luciferase stimulation of receptors at the membrane.

Although the full NanoLuc and its substrate furimazine was shown to be the second brightest out of the luciferases tested, the NanoBiT was not investigated (Berglund *et al.*, 2016). A risk with using split reporter proteins is that there is the potential for loss of response and potency compared to the in-tact protein, for example with the split RLuc, bioluminescence was reduced (Paulmurugant and Gambhir, 2003). NanoBiT and NanoLuc have not been directly compared in current literature for the brightness of bioluminescence signal, only reported to have the same linear increase in signal with DNA expression (Dixon *et al.*, 2016). However, the possibility remains that the loss in brightness between the NanoLuc and NanoBiT could be the cause in discrepancy, a point that would be worth further investigation. The only brighter luciferase used in luminopsin development is the so-called 'slow-burn' *Gaussia* Luciferase (Berglund *et al.*, 2016). If a fragment based reporter of sbGLuc is made accessible, this could also be of interest to activating receptors that require bright light as a stimulus.

## 5.4 Conclusions

Although ion channels have successfully been activated using receptor-tethered luciferase constructs, these data provide the first attempt at using bioluminescence to activate light-sensitive GPCRs. Spatial restriction of the receptor activation to individual cellular compartments was also achieved using a split version of the NanoLuc luciferase (NanoBiT) with one fragment fused to spatially restricted proteins at either the plasma membrane (Kras) or early endosomes (Rab5) to allow for area specific complementation with the receptor-based NanoBiT fragment.

Opn4 was demonstrated as a good candidate for bioluminescence stimulation. The chimeric opto-$\alpha_{1A}$AR was not a good candidate for bioluminescence activation, presumably due to a low light sensitivity that was not met by the brightness of the NanoBiT luciferase. When using melanopsin as the opsin for activation, an internal calcium signalling response was measured from furimazine digestion by the attached NanoBiT luciferase and photon release for both Kras and Rab5 tethered bioluminescence. This provides some preliminary evidence that endosomal compartmentalised receptors are capable of $G_q$ signalling to calcium. The SNAPtagged melanopsin receptors also showed increased internalisation to endosomes in response to bioluminescence activation, which response was different between the two spatially restricted areas, only being sensitive to Pitstop 2 endocytosis inhibitor when activated at the plasma membrane by the Kras tethered luciferase. The new methodology described does require optimisation before use, as currently a low expression rate of the target proteins and slow catalysis response of the NanoBiT-furimazine interaction could be causing the lack of robust responses measured. However, based on this initial study, the complementation can be refined to improve the design (e.g. fusing the bioluminescence source closer to the retinal binding pocket, or using a tagged LgBiT for specific cell analysis) and potentially allow analysis of spatially restricted luminopsins in the future.

# Chapter Six
General Discussion

## 6.1 Summary of Thesis Findings

Optogenetic $G_q$ coupled receptor constructs of opto-$\alpha_{1A}$AR (the bovine rhodopsin-human $\alpha_{1A}$ adrenoceptor chimera) and human melanopsin have been utilised for light activated calcium signalling in the HEK293 model cell line and primary astrocyte cultures. Fluorescent assays to monitor calcium signalling and receptor trafficking of opto-$\alpha_{1A}$AR post light activation were developed in HEK293 cells, where addition of 9-*cis*-retinal, but not all-*trans*-retinal, proved crucial for receptor activation. Melanopsin was successful in producing astrocytic calcium transients following several different patterns of light stimulation, further strengthening the evidence for its use as an optogenetic GPCR tool (Beiert *et al.*, 2014; Spoida *et al.*, 2016; Mederos *et al.*, 2018). Despite the links to melanopsin and $G_{i/o}$ induced calcium signalling, inhibition of the $G_{i/o}$ proteins in melanopsin(+) astrocytes instead led to an increase in calcium response (Cao *et al.*, 2012; Spoida *et al.*, 2016).

Temporal characteristics of receptor signalling were also tuned using C terminal truncation mutants. The opto-$\alpha_{1A}$AR mutant truncated at $Ser^{371}$ to remove all potential PKC phosphorylation sites produced an increase in calcium transients in response to constant laser stimulation, indicating the mutant receptor has a better chance of producing receptor activation by a light stimulus. There was also a reduction in opto-$\alpha_{1A}$AR trafficking under constant laser light stimulation, supporting evidence that the C terminal of the $\alpha_{1A}$ adrenoceptor is important in receptor endocytosis (Lattion *et al.*, 1994; Cabrera-Wrooman *et al.*, 2010). This increase in calcium transients was not seen in truncations at $Ser^{421}$ or $Thr^{471}$, both of which leave several phosphorylation sites at the C terminal end of the receptor. When melanopsin was truncated at $Ser^{411}$, there was an increased calcium response to multiple light stimuli in astrocytes compared to the wild type receptor, suggesting that the mutant is more readily stimulated by a single stimulus. This Opn4-S411* mutant could be useful for studies requiring multiple stimulations of the receptor.

Following success in receptor stimulation and temporal tuning, the potential for compartmental, subcellular activation of GPCRs was developed using opto-$\alpha_{1A}$AR and melanopsin in a 'luminopsin' construct with NanoBiT fragment-based bioluminescence light. With the high affinity smBiT86 of the NanoBiT luciferase

on C terminus of melanopsin and the LgBiT fused via an 18 amino acid Gly/Ser linker to Kras (plasma membrane targeting sequence) or Rab5 (early endosome protein), furimazine addition could induce calcium transients in HEK293 cells. Increased bioluminescence intensity with increased furimazine concentration was also shown to link to relocation of receptors to transferrin-tagged endosomes, demonstrating bioluminescence induced endocytosis. This response was also found to be sensitive to endocytosis inhibitors Pitstop 2 and Dyngo 4a. Bioluminescence imaging revealed the restriction of the bioluminescence signal to the areas of interest, at the plasma membrane or in endosomes.

## 6.2 Contribution of Work to the Research Field

The success of our truncation mutants of the opto-$\alpha_{1A}$AR and melanopsin have allowed us to develop GPCR optogenetic tools that have improved signalling profiles for repeated light stimuli. Although the microbial optogenetic ion channels have fast on and off kinetics, GPCRs have a second messenger system. By allowing for increased temporal control of the activation, there is an increased ability for the downstream effectors to also be controlled. This will be particularly useful in neuroscience research where the temporal aspects of cell signalling are fast and complex.

The ability to use melanopsin as an optogenetic tool was only established during this body of work. Natural coupling to $G_q$ proteins is desirable in research involving astrocytes as their signalling is heavily linked to release of $Ca^{2+}$ from intracellular stores (Hirase *et al.*, 2014). Although ChR2 and other permeable ion channels can allow the entry of $Ca^{2+}$, their use as calcium channels are debated as to the efficiency of such methods (Xie *et al.*, 2015). It was only recently that melanopsin was used *in vivo* to stimulate astrocytic calcium responses (Mederos *et al.*, 2018). Further development of melanopsin stimulation to allow for increased spatiotemporal resolution will be useful for unravelling the complexity of astrocytic calcium responses (Bazargani and Attwell, 2016). There are distinct nanoscopic profiles in astrocytes and spatial constraints for the calcium signalling which are not yet fully understood (Rusakov, 2015).

An exciting prospect of this thesis is the ability to spatially activate optogenetic receptors with bioluminescence. To our knowledge, there is currently no method that allows for stimulation of GPCRs only in one cellular compartment in multiple

cells simultaneously. These initial data provide a foundation for the development of compartmentalised light activation and provide future insight into whether $G_q$ protein endosomal signalling can occur, a response that is not yet well characterised (Tsvetanova *et al.*, 2015).

## 6.3 Methodological Considerations

A key area for improvement using luminopsin based melanopsin-NanoBiT constructs involved co-expression of the receptor and marker constructs. This could potentially be overcome by using different methods of transfection, such as the higher transfection efficiency method of electrophoresis, or generation of dual stably transfected lines, potentially using a single clone. Second, we were less able to demonstrate clear activation of melanopsin when the low affinity NanoBiT partner (smBiT114) was used. This is a disadvantage when wishing to localize the subcellular stimulus, since complementation using the smBiT86 HiBiT peptide is long lasting and may not be as restricted to the domain identified by the marker. In the future, bioluminescence-based activation could be applied to other types of optogenetic tool that may be more sensitive to the levels of light produced (Bailes *et al.*, 2012). For example, photoactivated adenylyl cyclase found in bacteria (*Beggiatoa*) and algae (*Euglena gracilis*) can be used for direct blue light stimulation of cAMP (Stierl *et al.*, 2011; Z. Zhou *et al.*, 2016). There are also light oxygen voltage sensing proteins (LOV) domain-based tools – the photosensory modules found in plants, bacteria and algae – which can be coupled to non-endogenous effector proteins to cause blue light activation (Salomon *et al.*, 2000). These were first developed as an allosteric activator for GTPase Rac1, in which the LOV2 domain was sterically bound to inhibit Rac1 and, upon light exposure, the GTPase activity is restored (Wu *et al.*, 2009). Rost *et al.* (2017) offers a thorough summary of current available tools and targeting motifs, which include light inducible soluble cyclases, phosphodiesterases, LOV domain allosteric activation, phytochromes and cryptochromes.

Developed assays for measuring the responses of the opto-$\alpha_{1A}$AR and melanopsin light activated receptors focused on only two major responses; increase in intracellular $Ca^{2+}$ and receptor trafficking. The results could be strengthened through the use of more assays focusing on other downstream signals of receptor

activation. Calcium signalling assays using fluorescent calcium dyes were used to measure receptor activation. Calcium indicators are a robust method of measuring intracellular [$Ca^{2+}$], however it should be noted that these indicators only measure changes in the cytosolic free [$Ca^{2+}$], of which are in equilibrium with $Ca^{2+}$ that are bound to endogenous calcium buffers, such as parvalbumin (Grienberger and Konnerth, 2012). The dyes also act as a calcium buffer, contributing to the intracellular calcium dynamics (Helmchen *et al.*, 1996). Calcium is also not the only signalling molecule produced in $G_{q/11}$ activation that can be measured through cellular assays. Inositol monophosphate ($IP_1$) is an indirect measure of $IP_3$, which is produced in hydrolysis of phosphoinositide by PLC. As $IP_3$ has an extremely short half-life, it is rapidly hydrolysed to $IP_1$, which then accumulates in cells. $IP_1$ is therefore a less downstream indication of $G_q$ protein activation which can be measured using a variety of methods, including the use of radioactive [$^3$H] inositol, or homogeneous time-resolved fluorescence with cryptate-labeled anti-$IP_1$ monoclonal antibody (Zhang *et al.*, 2010).

Receptor trafficking was measured in cells as an indication of endocytosis, although the molecules and mechanisms involved in the trafficking were not directly elucidated. Recruitment of β-arrestin can be directly measured using the co-expression of β-arrestin as a fusion protein in several different technologies that are commercially available (Song *et al.*, 2009). NanoBiT technology, the system used in the bioluminescence experiments, can also be used to monitor β-arrestin or G protein recruitment of a receptor under stimulation by co-expressing the two fragments on the receptor and effector and measuring the bioluminescence (Reyes-Alcaraz *et al.*, 2018; Fumagalli *et al.*, 2019). This could result in unwanted stimulation of the optogenetic receptor, although this has been performed in an optogenetic system with the full NanoLuc in a bioluminescence resonance energy transfer assay (Yang *et al.*, 2016).

Further to the limitations in the assays used, the cell cultures that the experiments have been performed in also have their downsides. HEK293 cells are useful model systems, but they do not express all cell processing machinery and scaffolding that can be found in native cells and have a high division rate, causing a lot of movement, as seen in this thesis (Chapter 3) with the receptor trafficking assay

(Thomas and Smart, 2005). Constitutive expression of receptors is also usually a downside of HEK293 cells in pharmacological studies but should not impact optogenetic work. Cultured astrocytes, although translational, do not represent true, *in vivo* morphology or microenvironment. In animals, astrocytes have hundreds to thousands of processes with other cells in a complex, 3D structure (Lang *et al.*, 2016). If cultured, these astrocytes lose this morphology, instead becoming flat, almost 2D structures, usually with a comparatively low number of processes. Culturing of primary astrocytes can also differ greatly between labs as there is a lack of a standardized process, perhaps making results obtained with these cells less reproducible (Lang *et al.*, 2016). Also, as mature astrocytes don't divide, cultured astrocytes are usually derived from developing astrocytes (Norton and Farooq, 1989). Using the new-born rats as cell donors is also problematic as the astrocytes are still immature and yet to form a working syncytium that are key for regular astrocyte function (Hertz *et al.*, 1998).

Overall, although optogenetics offers many advantages over traditional pharmacological or electrophysiological methods, there are still several caveats to using this method. For one, the optogenetic receptor itself does not directly compare to activation of an endogenous receptor, and as the optogenetic receptors have to be introduced into the system, the cell signalling response is from an overexpression of these receptors. When using the optogenetic tools for *in vitro* imaging, it is often required to use light to find the cells on the coverslip/culture surface, and passaging and handling of these cells requires some background light. This could lead to unwanted stimulation of the receptors if the environment surrounding the lab is not set up for such techniques. It is also unfortunate that many cell signalling assays use a form of fluorescence as an output read, again perhaps leading to some confounding light activation factors. For example, the melanopsin receptor may be tristable with two dark states, one activated by blue light and the other in the red (Emanuel and Do, 2015). Using the red-shifted fluorescent markers may therefore be affecting receptor response. In this thesis, stimulations using a sustained, non-scanning light source did not produce multiple signalling events, even in astrocytes which have inherent calcium wave propagation dynamics. This also impacts on the translation of the light stimulus to a ligand activation, where the ligand is free to bind, dissociate and diffuse in and out of the

binding pocket. There was also no observed change in the calcium response to different light intensities for either melanopsin or opto-$\alpha_{1A}$AR when stimulated with varied 470nm LED brightness (see sections 4.2.5 and 6). As ligand concentration response studies are usually carried out using log[ligand], it would make sense that the low levels of difference in LED brightness intensity (eg. 100 fold difference with the LED source vs 100,000 fold using a ligand dilution method) do not produce an intensity level dependent response. Although this digital on-off system using light could be useful to some studies, it can be difficult to identify the size of the stimulus needed to produce a response.

## 6.4 Future Steps

One of the developments that was not completed in time for this body of work was a high throughput system for the optogenetic calcium response experiments. As the assay requires measurements from live cells over time with an external light source, the IX Ultra confocal platereader could not be used. A new 96 well plate set-up was conceived with an algorithm to program the confocal microscope's stage to select a well, stimulate with the affixed LED light source and record the images over time. Such a technological development will vastly improve the amount of data that can be gathered in a given time period, allowing for more variables to be tested at once. The drawback of such a method is that the first well of the plate will have a different incubation time in the imaging buffer compared to the last well. Good experimental design with changing positions of the variables across repeats could combat this.

Another study that was not fully optimised aimed to link optogenetic stimulation in cultured astrocytes to functional responses. Experiments investigating changes in astrocyte morphology in response to $G_q$ protein light-activation were undertaken with an endpoint of the number of stellate processes, calculated from images of immunofluorescence GFAP and calcein stains. Astrocytic stellation has been linked with gliosis, a form of immune response (Adzic *et al.*, 2017). There are links between these morphological changes and several membrane receptors, such as dopamine receptors, adrenoceptors and purinergic ATP receptors (Adzic *et al.*, 2017; Koppel *et al.*, 2018). The mechanism of stellation is thought to involve Rho-GTPase signalling, which can re-arrange the actin skeleton (Zhang *et al.*, 2019). It would therefore be interesting to see the direct effect of $G_q$ calcium release on this

physiological process. Future experiments can address this, giving further insight into the mechanism of stellation.

The optogenetic GPCRs themselves could be further improved through several variables. Wavelength tuning of the receptors will be useful for using alongside fluorescent assays or for access *in vivo*. When stimulating receptors in tissue, longer wavelengths are desired to allow deeper penetration. There has been suggestions of using receptors that are sensitive to radio-waves through the use of iron oxide nanoparticles, demonstrated in the TRPV1 receptor (Stanley *et al.*, 2012). Although the TRPV1 receptor is already temperature sensitive, there is the possibility that other receptors could be targeted to these long, infra-red wavelengths as we start to understand the molecular mechanisms behind wavelength selection of light activated receptors (Zaccardi *et al.*, 2006; Matsuyama *et al.*, 2012; Proft and Weiss, 2012). Moves are already being made in such a direction, such as the development of a 40nm red-shifted sodium-pump rhodopsin, KR2 (K. Inoue *et al.*, 2019). Another variable that would be desirable to control is the on/off switching of the receptor. This has been addressed using the tristable melanopsin in this thesis, however there is the opportunity for further development of retinal activation and deactivation. Although the receptors in this study were mutated to potentially change the desensitisation profile, and perhaps β-arrestin binding, of the receptors, other mutations could potentially alter the G protein coupling efficacy. This has been demonstrated in the muscarinic DREADDs, and would be a useful tool to compare the G protein and β-arrestin response with a spatiotemporal probe such as these optogenetic GPCRS (Nakajima and Wess, 2012).

Another methodology that is currently being developed is the used of optogenetic stem cell lines. Through the culturing of human embryonic stem cells to specific phenotypes, cells can be grafted to sites of damage or behavioural deficit to help correct disease phenotypes; for example, growth of dopamine phenotype neurons to correct motor asymmetry and functional deficits in Parkinsonian rats (Yang *et al.*, 2008; Hargus *et al.*, 2010). Through genetic manipulation of these stem cells, they can become optogenetic to allow for direct, selective control of these cells. Such stem cells have the ability to fully integrate and functionally regulate an existing neural network (Weick *et al.*, 2010). Perhaps the use of human stem cell astrocyte lineages with melanopsin expression could be useful for astrocytic investigations.

Alongside the use of optogenetic GPCRs, there is the potential for using light-activated ligands to control receptor activation, either photoswitchable or caged compounds. This would lose the beneficial fast on kinetics of the retinal-bound GPCRs, but would allow for translation to ligand kinetics, a crucial part of drug design. Such compounds exist for many receptors, and it will be expected that many more will be developed in the future ( for through reviews, see Kim, 2016; Ricart-Ortega *et al.*, 2019). It could even be possible to use bioluminescence, as demonstrated in this work with GPCR stimulation, to instead activate photoswitchable ligands only in certain cells expressing the genetic luciferase probes. This would be invaluable to work investigating the use of tissue-specific drug targets.

# Chapter Seven
## References


Abrams, P., Andersson, K. E., Buccafusco, J. J., Chapple, C., De Groat, W. C., Fryer, A. D., Kay, G., Laties, A., Nathanson, N. M., Pasricha, P. J. and Wein, A. J. (2006) 'Muscarinic receptors: Their distribution and function in body systems, and the implications for treating overactive bladder', *British Journal of Pharmacology*, 148(5), pp. 565–578.

Adzic, M., Stevanovic, I., Josipovic, N., Laketa, D., Lavrnja, I., Bjelobaba, I. M., Bozic, I., Jovanovic, M., Milosevic, M. and Nedeljkovic, N. (2017) 'Extracellular ATP induces graded reactive response of astrocytes and strengthens their antioxidative defense in vitro', *Journal of Neuroscience Research*, 95(4), pp. 1053–1066.

Agulhon, C., Boyt, K. M., Xie, A. X., Friocourt, F., Roth, B. L., Mccarthy, Ken D and Mccarthy, K D (2013) 'Modulation of the autonomic nervous system and behaviour by acute glial cell $G_q$ protein-coupled receptor activation in vivo', *The Journal of Physiology*, 591(22), pp. 5599–5609.

Airan, R. D., Thompson, K. R., Fenno, L. E., Bernstein, H. and Deisseroth, K. (2009) 'Temporally precise *in vivo* control of intracellular signalling', *Nature*, 458(7241), pp. 1025–1029.

Alberts, B., Johnson, A., Lewis, J., Raff, M., Roberts, K. and Walter, P. (2008) *Molecular Biology of the Cell*. 5th edn. New York Garland Science

Alcántara-hernández, R., Hernández-méndez, A. and Romero-ávila, M. T. (2017) 'Noradrenaline, oxymetazoline and phorbol myristate acetate induce distinct functional actions and phosphorylation patterns of $\alpha_{1A}$-adrenergic receptors', *BBA - Molecular Cell Research*, 1864(12), pp. 2378–2388.

Alexander, G. M., Rogan, S. C., Abbas, A. I., Armbruster, B. N., Pei, Y., Allen, J. a, Nonneman, R. J., Hartmann, J., Moy, S. S., Nicolelis, M. a, Mcnamara, J. O. and Roth, B. L. (2009) 'Remote control of neuronal activity in transgenic mice expressing evolved G protein-coupled receptors', *Neuron*, 63(1), pp. 27–39.

Alloway, P. G., Howard, L. and Dolph, P. J. (2000) 'The Formation of Stable Rhodopsin-Arrestin Complexes Induces Apoptosis and Photoreceptor Cell Degeneration', *Neuron*, 28, pp. 129–138.

Alvarez-Curto, E., Inoue, A., Jenkins, L., Raihan, S. Z., Prihandoko, R., Tobin, A. B. and Milligan, G. (2016) 'Targeted elimination of G proteins and arrestins defines their specific contributions to both intensity and duration of G protein-coupled receptor signaling', *Journal of Biological Chemistry*, 291(53), pp. 27147–27159.

Araque, A., Parpura, V., Sanzgiri, R. and Haydon, P. (1999) 'Tripartite synapses: glia, the unacknowledged partner', *Trends in neurosciences*, 22(5), pp. 208–215.

Araque, A., Sanzgiri, R., Parpura, V. and Haydon, P. (1998) 'Calcium elevation in astrocytes causes an NMDA receptor-dependent increase in the frequency of miniature synaptic currents in cultured hippocampal neurons', *The Journal of Neuroscience*, 18(17), pp. 6822–6829.

Armbruster, B. N., Li, X., Pausch, M. H., Herlitze, S. and Roth, B. L. (2007) 'Evolving the lock to fit the key to create a family of G protein-coupled receptors potently activated by an inert ligand.', *PNAS*, 104(12), pp. 5163–8.

Armbruster, B. N. and Roth, B. L. (2005) 'Mining the receptorome', *Journal of Biological Chemistry*, 280(7), pp. 5129–5132.

Arriagada, C., Silva, P., Millet, M., Solano, L., Moraga, C. and Torres, V. A. (2019) 'Focal adhesion kinase-dependent activation of the early endocytic protein Rab5 is associated with cell migration', *Journal of Biological Chemistry*, 294, pp. 12836–12845.

Aslanoglou, D., Alvarez-Curto, E., Marsango, S. and Milligan, G. (2015) 'Distinct Agonist Regulation of Muscarinic Acetylcholine $M_2$-$M_3$ Heteromers and Their Corresponding Homomers', *Journal of Biological Chemistry*, 290(23), pp 14785-96.

Bahouth, S. W. and Nooh, M. M. (2017) 'Barcoding of GPCR trafficking and signaling through the various trafficking roadmaps by compartmentalized signaling networks', *Cellular Signalling*, 36, pp. 42–55.

Bailes, H. J. and Lucas, R. J. (2013) 'Human melanopsin forms a pigment maximally sensitive to blue light ($\lambda_{max} \approx 479$ nm) supporting activation of $G_{q/11}$ and $G_{i/o}$ signalling cascades', *Proceedings of the Royal Society B*, 280(20122987).

Bailes, H. J., Milosavljevic, N., Zhuang, L.-Y., Gerrard, E. J., Nishiguchi, T., Ozawa, T. and Lucas, R. J. (2017) 'Optogenetic interrogation reveals separable G-protein-dependent and -independent signalling linking G-protein-coupled receptors to the circadian oscillator', *BMC Biology*, 15(1), p. 40.

Bailes, H. J., Zhuang, L. Y. and Lucas, R. J. (2012) 'Reproducible and sustained regulation of $G_{\alpha s}$ signalling using a metazoan opsin as an optogenetic tool', *PLoS ONE*, 7(1), p. e30774.

Banghart, M., Borges, K., Isacoff, E., Trauner, D. and Kramer, R. H. (2004) 'Light-activated ion channels for remote control of neuronal firing', *Nature Neuroscience*, 7(12), pp. 1381–1386.

Bauman, A. L., Soughayer, J., Nguyen, B. T., Willoughby, D., Carnegie, G. K., Wong, W., Hoshi, N., Langeberg, L. K., Cooper, D. M. F., Dessauer, C. W. and Scott, J. D. (2006) 'Dynamic Regulation of cAMP Synthesis through Anchored PKA-Adenylyl Cyclase V/VI Complexes', *Molecular Cell*, 23(6), pp. 925–931.

Bazargani, N. and Attwell, D. (2016) 'Astrocyte calcium signaling: the third wave', *Nature Neuroscience*, 19(2), pp. 182–189.

Beautrait, A., Paradis, J. S., Zimmerman, B., Giubilaro, J., Nikolajev, L., Armando, S., Kobayashi, H., Yamani, L., Namkung, Y., Heydenreich, F. M., Khoury, E., Audet, M., Roux, P. P., Veprintsev, D. B., Laporte, S. A. and Bouvier, M. (2017) 'A new inhibitor of the β-arrestin/AP2 endocytic complex reveals interplay between GPCR internalization and signalling', *Nature Communications*, 8(15054).

Beiert, T., Bruegmann, T. and Sasse, P. (2014) 'Optogenetic activation of $G_q$ signalling modulates pacemaker activity of cardiomyocytes', *Cardiovascular Research*, 102(3), pp. 507–516.

Bekar, L. K., He, W. and Nedergaard, M. (2008) 'Locus coeruleus a-adrenergic-mediated activation of cortical astrocytes in vivo', *Cerebral Cortex*, 18(12), pp. 2789–2795.

Berg, K. A., Maayani, S., Goldfarb, J., Scaramellini, C., Leff, P. and Clarke, W. P. (1998) 'Effector Pathway-Dependent Relative Efficacy at Serotonin Type 2A and

2C Receptors: Evidence for Agonist-Directed Trafficking of Receptor Stimulus', *Molecular Pharmacology*, 54, pp. 94–104.

Berglund, K., Birkner, E., Augustine, G. J. and Hochgeschwender, U. (2013) 'Light-Emitting Channelrhodopsins for Combined Optogenetic and Chemical-Genetic Control of Neurons', *PLoS ONE*, 8(3), p. e59759.

Berglund, K., Clissold, K., Li, H. E., Wen, L., Park, S. Y., Gleixner, J., Klein, M. E., Lu, D., Barter, J. W., Rossi, M. a., Augustine, G. J., Yin, H. H. and Hochgeschwender, U. (2016) 'Luminopsins integrate opto- and chemogenetics by using physical and biological light sources for opsin activation', *PNAS*, 113(3), pp. E358–E367.

Berglund, K., Fernandez, A. M., Gutekunst, C. A. N., Hochgeschwender, U. and Gross, R. E. (2019) 'Step-function luminopsins for bimodal prolonged neuromodulation', *Journal of Neuroscience Research*, 98(3), pp. 407–409.

Berlinguer-Palmini, R., Narducci, R., Merhan, K., Dilaghi, A., Moroni, F., Masi, A., Scartabelli, T., Landucci, E., Sili, M., Schettini, A., McGovern, B., Maskaant, P., Degenaar, P. and Mannaioni, G. (2014) 'Arrays of MicroLEDs and astrocytes: Biological amplifiers to optogenetically modulate neuronal networks reducing light requirement', *PLoS ONE*, 9(9), p. e108689.

Berry, J., Frederiksen, R., Yao, Y., Nymark, S., Chen, J. and Cornwall, C. (2016) 'Effect of rhodopsin phosphorylation on dark adaptation in mouse rods', *Journal of Neuroscience*, 36(26), pp. 6973–6987.

Bery, N., Cruz-Migoni, A., Bataille, C. J., Quevedo, C. E., Tulmin, H., Miller, A., Russell, A., Phillips, S. E., Carr, S. B. and Rabbitts, T. H. (2018) 'BRET-based RAS biosensors that show a novel small molecule is an inhibitor of RAS-effector protein-protein interactions', *eLife*, 7(e37122).

Bieluszewska, A., Weglewska, M., Bieluszewski, T., Lesniewicz, K. and Poreba, E. (2018) 'PKA-binding domain of AKAP8 is essential for direct interaction with DPY30 protein', *FEBS Journal*, 285(5), pp. 947–964.

Birkner, E., Berglund, K., Klein, M. E., Augustine, G. J. and Hochgeschwender, U. (2014) 'Non-invasive activation of optogenetic actuators', *Proceedings, SPIE Optical Engineering*, 1(8928).

Bishop, A., Buzko, O., Heyeck-Dumas, S., Jung, I., Kraybill, B., Liu, Y., Shah, K., Ulrich, S., Witucki, L., Yang, F., Zhang, C. and Shokat, K. M. (2000) 'Unnatural Ligands for Engineered Proteins: New Tools for Chemical Genetics', *Annu. Rev. Biophys. Biomol. Struct.*, 29, pp. 577–606.

Black, J. B., Premont, R. T. and Daaka, Y. (2016) 'Feedback regulation of G protein-coupled receptor signaling by GRKs and arrestins', *Seminars in Cell and Developmental Biology*, 50, pp. 95–104.

Blasic, J. R., Brown, R. L. and Robinson, P. R. (2012) 'Phosphorylation of Mouse Melanopsin by Protein Kinase A', *PLoS ONE*, 7(9), p. e45387.

Blasic, J. R., Lane Brown, R. and Robinson, P. R. (2012) 'Light-dependent phosphorylation of the carboxy tail of mouse melanopsin', *Cellular and Molecular Life Sciences*, 69(9), pp. 1551–1562.

Blasic, J. R., Matos-Cruz, V., Ujla, D., Cameron, E. G., Hattar, S., Halpern, M. E. and Robinson, P. R. (2014) 'Identification of critical phosphorylation sites on the carboxy tail of melanopsin', *Biochemistry*, 53(16), pp. 2644–2649.

Bouzier-Sore, A.-K. and Pellerin, L. (2013) 'Unraveling the complex metabolic nature of astrocytes.', *Frontiers in Cellular Neuroscience*, 7(179).

Boyden, E. S., Zhang, F., Bamberg, E., Nagel, G. and Deisseroth, K. (2005) 'Millisecond-timescale, genetically targeted optical control of neural activity.', *Nature Neuroscience*, 8(9), pp. 1263–8.

Brueggemann, L. I. and Sullivan, J. M. (2002) 'HEK293S Cells Have Functional Retinoid Processing Machinery', *The Journal of General Physiology*, 119, pp. 593–612.

Budd, D. C., McDonald, J. E. and Tobin, A. B. (2000) 'Phosphorylation and regulation of a $G_{q/11}$-coupled receptor by casein kinase 1α', *Journal of Biological Chemistry*, 275(26), pp. 19667–19675.

Bünemann, M., Frank, M. and Lohse, M. J. (2003) 'Gi protein activation in intact cells involves subunit rearrangement rather than dissociation', *PNAS*, 100(26), pp. 16077–16082.

Bygrave, F. L. and Benedetti, A. (1996) 'What is the concentration of calcium ions in the endoplasmic reticulum?', *Cell Calcium*, 19(6), pp. 547–551.

Cabrera-Wrooman, A., Romero-Ávila, M. T. and García-Sáinz, J. A. (2010) 'Roles of the $\alpha_{1A}$-adrenergic receptor carboxyl tail in protein kinase C-induced phosphorylation and desensitization', *Naunyn-Schmiedeberg's Archives of Pharmacology*, 382(5–6), pp. 499–510.

Calebiro, D. (2011) 'Thyroid-stimulating hormone receptor activity after internalization', *Annales d'Endocrinologie*, 72(2), pp. 64–67.

Callaway, E. M. and Katz, L. C. (1993) 'Photostimulation using caged glutamate reveals functional circuitry in living brain slices.', *PNAS*, 90(16), pp. 7661–5.

Cameron, E. G. and Robinson, P. R. (2014) 'β-Arrestin-Dependent Deactivation of Mouse Melanopsin', *PLoS ONE*, 9(11), p. e113138.

Cao, P., Sun, W., Kramp, K., Zheng, M., Salom, D., Jastrzebska, B., Jin, H., Palczewski, K. and Feng, Z. (2012) 'Light-sensitive coupling of rhodopsin and melanopsin to $G_{i/o}$ and $G_q$ signal transduction in Caenorhabditis elegans', *The FASEB Journal*, 26(2), pp. 480–491.

Carpenter, B., Nehmé, R., Warne, T., Leslie, A. G. W. and Tate, C. G. (2016) 'Structure of the adenosine $A_{2A}$ receptor bound to an engineered G protein', *Nature*, 536(7614), pp. 104–107.

Chakravorty, D. and Assmann, S. M. (2018) 'G protein subunit phosphorylation as a regulatory mechanism in heterotrimeric G protein signaling in mammals, yeast, and plants', *Biochemical Journal*, 475(21), pp. 3331–3357.

Chalothorn, D., McCune, D. F., Edelmann, S. E., García-Cazarín, M. L., Tsujimoto, G. and Piascik, M. T. (2002) 'Differences in the Cellular Localization and Agonist-Mediated Internalization Properties of the $a_1$-Adrenoceptor Subtypes', *Molecular pharmacology*, 61(5), pp. 1008–16.

Chen, I.-W., Ronzitti, E., Lee, B. R., Daigle, T. L., Dalkara, D., Zeng, H., Emiliani, V. and Papagiakoumou, E. (2019) '*In vivo* sub-millisecond two-photon optogenetics with temporally focused patterned light', *The Journal of Neuroscience*, 39(18), pp. 3484–3497.

Chen, J., Makino, C. L., Peachey, N. S., Baylor, D. A. and Simon, M. I. (1995) 'Mechanisms of Rhodopsin Inactivation *in Vivo* as Revealed by a COOH-Terminal Truncation Mutant', *Science*, 267(5196), pp. 374–377.

Chen, N., Sugihara, H., Sharma, J., Perea, G., Petravicz, J., Le, C. and Sur, M. (2012) 'Nucleus basalis-enabled stimulus-specific plasticity in the visual cortex is mediated by astrocytes', *PNAS*, 109(41), pp. E2832–E2841.

Chen, X., Choo, H., Huang, X. P., Yang, X., Stone, O., Roth, B. L. and Jin, J. (2015) 'The first structure-activity relationship studies for designer receptors exclusively activated by designer drugs', *ACS Chemical Neuroscience*, 6(3), pp. 476–484.

Chew, K. S., Schmidt, T. M., Rupp, A. C., Kofuji, P. and Trimarchi, J. M. (2014) 'Loss of $G_{q/11}$ genes does not abolish melanopsin phototransduction', *PLoS ONE*, 9(5), p. e98356.

Choe, H. W., Kim, Y. J., Park, J. H., Morizumi, T., Pai, E. F., Krau, N., Hofmann, K. P., Scheerer, P. and Ernst, O. P. (2011) 'Crystal structure of metarhodopsin II', *Nature*, 471(7340), pp. 651–655.

Chung, K. Y., Rasmussen, S. G. F., Liu, T., Li, S., Devree, B. T., Chae, P. S., Calinski, D., Kobilka, B. K., Woods Jr., V. L. and Sunahara, R. K. (2012) 'β2 adrenergic receptor-induced conformational changes in the heterotrimeric G protein $G_s$', *Nature*, 477(7366), pp. 611–615.

Cideciyan, A. V, Zhao, X., Nielsen, L., Khani, S. C., Jacobson, S. G. and Palczewski, K. (1998) 'Null mutation in the rhodopsin kinase gene slows recovery kinetics of rod and cone phototransduction in man', *PNAS*, 95, pp. 328–333.

Cieślik, P., Domin, H., Chocyk, A., Gruca, P., Litwa, E., Płoska, A., Radulska, A., Pelikant-Małecka, I., Brański, P., Kalinowski, L. and Wierońska, J. M. (2019) 'Simultaneous activation of mGlu2 and muscarinic receptors reverses MK-801-induced cognitive decline in rodents', *Neuropharmacology*, p. 107866.

Claeysen, S., Joubert, L., Sebben, M., Bockaert, J. and Dumuis, A. (2003) 'A single mutation in the 5-$HT_4$ receptor (5-$HT_4$-R D100(3.32)A) generates a $G_s$-coupled receptor activated exclusively by synthetic ligands (RASSL)', *Journal of Biological Chemistry*, 278(2), pp. 699–702.

Clapham, D. E. (2007) 'Calcium Signaling', *Cell*, 131(6), pp. 1047–1058.

Conklin, B. R., Hsiao, E. C., Claeysen, S., Dumuis, A., Forsayeth, J. R., Guettier, J., Chang, W. C., Pei, Y., Ken, D., Nissenson, R. A., Wess, J., Bockaert, J. and Roth, B. L. (2008) 'Engineering GPCR signaling pathways with RASSLs', *Nature Methods*, 5(8), pp. 673–678.

Cornell-Bell, A. H., Finkbeiner, S. M., Cooper, M. S. and Smith, S. J. (1990) 'Glutamate Induces Calcium Waves in Cultured Astrocytes: Long-Range Glial Signaling', *Science*, 247(4941), pp. 470–73.

Coward, P., Wada, H. G., Falk, M. S., Chan, S. D., Meng, F., Akil, H. and Conklin,

B. R. (1998) 'Controlling signaling with a specifically designed $G_i$-coupled receptor.', *PNAS*, 95(1), pp. 352–7.

Croft, W., Reusch, K., Tilunaite, A., Russell, N. A., Thul, R. and Bellamy, T. C. (2016) 'Probabilistic encoding of stimulus strength in astrocyte global calcium signals', *Glia*, 64(4), pp. 537–552.

Cukkemane, A., Seifert, R. and Kaupp, U. B. (2011) 'Cooperative and uncooperative cyclic-nucleotide-gated ion channels', *Trends in Biochemical Sciences*, 36(1), pp. 55–64.

Damez-Werno, D. M. and Kenny, P. J. (2015) 'Using Opioid Receptors to Expand the Chemogenetic and Optogenetic Toolbox', *Neuron*, 86, pp. 853–855.

Dascal, N. and Kahanovitch, U. (2015) 'Chapter Two - The Roles of $G_{\beta\gamma}$ and $G_{\alpha}$ in Gating and Regulation of GIRK Channels', in Slesinger, P. A. and Wickman, K. (eds) *International Review of Neurobiology*, pp. 27–85.

DeFea, K. A., Zalevsky, J., Thoma, M. S., Dery, O., Mullins, R. D. and Bunnett, N. W. (2000) 'β-Arrestin-dependent endocytosis of proteinase-activated receptor 2 is required for intracellular targeting of activated ERK1/2', *Journal of Cell Biology*, 148(6), pp. 1267–1281.

Deisseroth, K. (2011) 'Optogenetics', *Nature Methods*, 8(1), pp. 26–29.

Deisseroth, K. (2015) 'Optogenetics: 10 years of microbial opsins in neuroscience.', *Nature neuroscience*, 18(9), pp. 1213–1225.

Denk, W., Strickler, J. and Web, W. W. (1990) 'Two-Photon Laser Scanning Fluorescence Microscopy', *Science*, 248(4951), pp. 73–76.

DeWire, S. M., Ahn, S., Lefkowitz, R. J. and Shenoy, S. K. (2007) 'β-Arrestins and Cell Signaling', *Annual Review of Physiology*, 69(1), pp. 483–510.

Dharmaiah, S., Tran, T. H., Messing, S., Agamasu, C., Gillette, W. K., Yan, W., Waybright, T., Alexander, P., Esposito, D., Nissley, D. V., McCormick, F., Stephen, A. G. and Simanshu, D. K. (2019) 'Structures of N-terminally processed KRAS provide insight into the role of N-acetylation', *Scientific Reports*, 9(10512).

Di Bari, M., Di Pinto, G., Reale, M., Mengod G. and Tata A. M. 'Cholinergic System and Neuroinflammation: Implication in Multiple Sclerosis', *Central Nervous System Agents in Medicinal Chemistry* (2017) 17: 109.

Díaz, N. M., Morera, L. P. and Guido, M. E. (2016) 'Melanopsin and the Non-visual Photochemistry in the Inner Retina of Vertebrates', *Photochemistry and Photobiology*, 92, pp. 29–44.

Ding, F., O'Donnell, J., Thrane, A. S., Zeppenfeld, D., Kang, H., Xie, L., Wang, F. and Nedergaard, M. (2013) '$\alpha_1$-adrenergic receptors mediate coordinated $Ca^{2+}$ signaling of cortical astrocytes in awake, behaving mice', *Cell Calcium*, 54(6), pp. 387–394.

Dixon, A. S., Schwinn, M. K., Hall, M. P., Zimmerman, K., Otto, P., Lubben, T. H., Butler, B. L., Binkowski, B. F., MacHleidt, T., Kirkland, T. A., Wood, M. G., Eggers, C. T., Encell, L. P. and Wood, K. V. (2016) 'NanoLuc Complementation Reporter Optimized for Accurate Measurement of Protein Interactions in Cells', *ACS Chemical Biology*, 11(2), pp. 400–408.

Do, M. T. H., Kang, S. H., Xue, T., Zhong, H., Liao, H. W., Bergles, D. E. and Yau, K. W. (2009) 'Photon capture and signalling by melanopsin retinal ganglion cells', *Nature*, 457(7227), pp. 281–287.

Downes, G. B. and Gautam, N. (1999) 'The G protein subunit gene families', *Genomics*, 62(3), pp. 544–552.

Dubouskaya, T. G., Hrynevich, S. V., Waseem, T. V. and Fedorovich, S. V. (2018) 'Calcium release from intracellular stores is involved in mitochondria depolarization after lowering extracellular pH in rat brain synaptosomes', *Acta Neurobiologiae Experimentalis*, 78, pp. 343–351.

DuBridge, R. B., Tang, P., Chao Hsia, H., Leong, P.-M., Miller, J. H. and Calos, M. P. (1987) 'Analysis of Mutation in Human Cells by Using an Epstein-Barr Virus Shuttle System', *Molecular and Cellular Biology*, 7(1), pp. 379–387.

Duc, N. M., Kim, H. R. and Chung, K. Y. (2015) 'Structural mechanism of G protein activation by G protein-coupled receptor', *European Journal of Pharmacology*, 763, pp. 214–222.

Dunn, V. K. and Gleason, E. (2018) 'Inhibition of endocytosis suppresses the nitric oxide-dependent release of $Cl^-$ in retinal amacrine cells', *PLoS ONE*, 13(7), p. e0201184.

Dupont, G., Combettes, L., Bird, G. S. and Putney, J. W. (2011) 'Calcium Oscillations', *Cold Spring Harbor Perspectives in Biology*, 3, pp. 1–18.

Durkee, C. A., Covelo, A., Lines, J., Kofuji, P., Aguilar, J. and Araque, A. (2019) '$G_{i/o}$ protein-coupled receptors inhibit neurons but activate astrocytes and stimulate gliotransmission', *Glia*, 67(6), pp. 1076–1093.

Dutta, D., Williamson, C. D., Cole, N. B. and Donaldson, J. G. (2012) 'Pitstop 2 Is a Potent Inhibitor of Clathrin-Independent Endocytosis', *PLoS ONE*, 7(9), pp. 1–9.

Eason, M. G. and Liggett, S. B. (1996) 'Chimeric mutagenesis of putative G-protein coupling domains of the $\alpha_{2A}$-adrenergic receptor', *The Journal of Biological Chemistry*, 271(22), pp. 12826–12832.

Elhusseiny, A., Cohen, Z., Olivier, A., Stanimirović, D. B. and Hamel, E. (1999) 'Functional acetylcholine muscarinic receptor subtypes in human brain microcirculation: Identification and cellular localization', *Journal of Cerebral Blood Flow and Metabolism*, 19(7), pp. 794–802.

Emanuel, A. J. and Do, M. T. H. (2015) 'Melanopsin tristability for sustained and broadband phototransduction', *Neuron*, 85, pp. 1043–1055.

Emiliani, V., Cohen, A. E., Deisseroth, K. and Häusser, M. (2015) 'All-Optical Interrogation of Neural Circuits', *The Journal of Neuroscience*, 35(41), pp. 13917–13926.

Van Eps, N., Caro, L. N., Morizumi, T., Kusnetzow, A. K., Szczepek, M., Hofmann, K. P., Bayburt, T. H., Sligar, S. G., Ernst, O. P. and Hubbell, W. L. (2017) 'Conformational equilibria of light-activated rhodopsin in nanodiscs', *PNAS*, 114(16), pp. E3268–E3275.

Fahrenkrug, J., Falktoft, B., Georg, B., Hannibal, J., Kristiansen, S. B. and Klausen,

T. K. (2014) 'Phosphorylation of rat melanopsin at Ser-381 and Ser-398 by light/dark and its importance for intrinsically photosensitive ganglion cells (ipRGCs) cellular $Ca^{2+}$ signaling', *Journal of Biological Chemistry*, 289(51), pp. 35482–35493.

Fan, J., Rohrer, B., Moiseyev, G., Ma, J.-X. and Crouch, R. K. (2003) 'Isorhodopsin rather than rhodopsin mediates rod function in RPE65 knock-out mice', *PNAS*, 100(23), pp. 13662–13667.

Favre, N., Fanelli, F., Missotten, M., Nichols, A., Wilson, J., Di Tiani, M., Rommel, C. and Scheer, A. (2005) 'The DRY motif as a molecular switch of the human oxytocin receptor', *Biochemistry*, 44(30), pp. 9990–10008.

Feinstein, T. N., Yui, N., Webber, M. J., Wehbi, V. L., Stevenson, H. P., King, J. D., Hallows, K. R., Brown, D., Bouley, R. and Vilardaga, J. P. (2013) 'Noncanonical control of vasopressin receptor type 2 signaling by retromer and arrestin', *Journal of Biological Chemistry*, 288(39), pp. 27849–27860.

Ferrandon, S., Feinstein, T. N., Castro, M., Wang, B., Bouley, R., Potts, J. T., Gardella, T. J. and Vilardaga, J.-P. (2009) 'Sustained cyclic AMP production by parathyroid hormone receptor endocytosis', *Nature Chemical Biology*, 5(10), pp. 734–742.

Figueiredo, M., Lane, S., Stout, R. F., Liu, B., Parpura, V., Teschemacher, A. G. and Kasparov, S. (2014) 'Comparative analysis of optogenetic actuators in cultured astrocytes.', *Cell calcium*, 56(3), pp. 208–14.

Flock, T., Hauser, A. S., Lund, N., Gloriam, D. E., Balaji, S. and Babu, M. M. (2017) 'Selectivity determinants of GPCR-G protein binding', *Nature*, 545(7654), pp. 1–33.

Frederiksen, R., Nymark, S., Kolesnikov, A. V, Berry, J. D., Iv, L. A., Koutalos, Y., Kefalov, V. J. and Cornwall, M. C. (2016) 'Rhodopsin kinase and arrestin binding control the decay of photoactivated rhodopsin and dark adaptation of mouse rods', 148(1), pp. 1–11.

Freeley, M., Kelleher, D. and Long, A. (2011) 'Regulation of Protein Kinase C function by phosphorylation on conserved and non-conserved sites', *Cellular Signalling*, 23(5), pp. 753–762.

Fritze, O., Filipek, S., Kuksa, V., Palczewski, K., Peter Hofmann, K. and Ernst, O. P. (2003) 'Role of the conserved $NPxxY(x)_{5,6}F$ motif in the rhodopsin ground state and during activation', *PNAS*, 100(5), pp. 2290–2295.

Fujita, T., Umemura, M., Yokoyama, U., Okumura, S. and Ishikawa, Y. (2017) 'The role of Epac in the heart', *Cellular and Molecular Life Sciences*, 74, pp. 591–606.

Fumagalli, A., Zarca, A., Neves, M., Caspar, B., Hill, S. J., Mayor, F., Smit, M. J. and Marin, P. (2019) 'CXCR4/ACKR3 phosphorylation and recruitment of interacting proteins: key mechanisms regulating their functional status', *Molecular Pharmacology*, 96(6), pp. 794–808.

Gainetdinov, R. R., Premont, R. T., Bohn, L. M., Lefkowitz, R. J. and Caron, M. G. (2004) 'Desensitization of G protein–coupled receptors and neuronal functions', *Annual Review of Neuroscience*, 27(1), pp. 107–144.

Galés, C., Van Durm, J. J. J., Schaak, S., Pontier, S., Percherancier, Y., Audet, M., Paris, H. and Bouvier, M. (2006) 'Probing the activation-promoted structural rearrangements in preassembled receptor-G protein complexes', *Nature Structural and Molecular Biology*, 13(9), pp. 778–786.

Galés, C., Rebois, R. V., Hogue, M., Trieu, P., Breit, A., Hébert, T. E. and Bouvier, M. (2005) 'Real-time monitoring of receptor and G-protein interactions in living cells', *Nature Methods*, 2(3), pp. 177–184.

García-Nafría, J., Nehmé, R., Edwards, P. C. and Tate, C. G. (2018) 'Cryo-EM structure of the serotonin 5-$HT_{1B}$ receptor coupled to heterotrimeric $G_o$', *Nature*, 558(7711), pp. 620–623.

García-Nafría, J. and Tate, C. G. (2019) 'Cryo-EM structures of GPCRs coupled to $G_s$, $G_i$ and $G_o$', *Molecular and Cellular Endocrinology*, 488, pp. 1–13.

Gee, K. R., Brown, K. A., Chen, W. N., Bishop-Stewart, J., Gray, D. and Johnson, I. (2000) 'Chemical and physiological characterization of fluo-4 $Ca^{2+}$-indicator dyes', *Cell Calcium*, 27(2), pp. 97–106.

Gerits, A., Vancraeyenest, P., Vreysen, S., Laramée, M.-E., Michiels, A., Gijsbers, R., Van den Haute, C., Moons, L., Debyser, Z., Baekelandt, V., Arckens, L. and Vanduffel, W. (2015) 'Serotype-dependent transduction efficiencies of recombinant adeno-associated viral vectors in monkey neocortex', *Neurophotonics*, 2(3), p. 031209.

Giaume, C., Leybaert, L., Naus, C. C. and Sáez, J. C. (2013) 'Connexin and pannexin hemichannels in brain glial cells: Properties, pharmacology, and roles', *Frontiers in Pharmacology*, 4(88), pp. 1–17.

Gomez, J. L., Bonaventura, J., Lesniak, W., Mathews, W. B., Sysa-Shah, P., Rodriguez, L. A., Ellis, R. J., Richie, C. T., Harvey, B. K., Dannals, R. F., Pomper, M. G., Bonci, A. and Michaelides, M. (2017) 'Chemogenetics revealed: DREADD occupancy and activation via converted clozapine', *Science*, 357(6350), pp. 503–507.

Gonçalves-pimentel, C., Machado, G., Moreno, M., Soares, B., Rosendo, A., Claudio, I., Rodrigues, G. and Savariradjane, M. (2018) 'Cellulose exopolysaccharide from sugarcane molasses as a suitable substrate for 2D and 3D neuron and astrocyte primary cultures', *Journal of Materials Science: Materials in Medicine*.

Gould, R. W., Gunter, B. W., Bubser, M., Matthews, R. T., Teal, L. B., Ragland, M. G., Bridges, T. M., Garrison, A. T., Winder, D. G., Lindsley, C. W. and Jones, C. K. (2019) 'Acute Negative Allosteric Modulation of $M_5$ Muscarinic Acetylcholine Receptors Inhibits Oxycodone Self-Administration and Cue-Induced Reactivity with No Effect on Antinociception', *ACS Chemical Neuroscience*, 10(8), pp. 3740–3750.

Govorunova, E. G., Sineshchekov, O. A., Li, H. and Spudich, J. L. (2017) 'Microbial Rhodopsins: Diversity, Mechanisms, and Optogenetic Applications', *Annu. Rev. Biochem.*, 86, pp. 845–72.

Govorunova, E. G., Sineshchekov and Spudich, J. L. (2019) 'Three Families of Channelrhodopsins and Their Use in Optogenetics (review)', *Neuroscience and Behavioral Physiology*, 49(2), pp. 163–168.

Graham, D. M., Wong, K. Y., Shapiro, P., Frederick, C., Pattabiraman, K. and Berson, D. M. (2008) 'Melanopsin ganglion cells use a membrane-associated rhabdomeric phototransduction cascade', *Journal of Neurophysiology*, 99(5), pp. 2522–2532.

Grienberger, C. and Konnerth, A. (2012) 'Imaging Calcium in Neurons', *Neuron*, 73(5), pp. 862–885.

Guettier, J.-M., Gautam, D., Scarselli, M., Ruiz de Azua, I., Li, J. H., Rosemond, E., Ma, X., Gonzalez, F. J., Armbruster, B. N., Lu, H., Roth, B. L. and Wess, J. (2009) 'A chemical-genetic approach to study G protein regulation of beta cell function in vivo.', *PNAS*, 106(45), pp. 19197–202.

Gundry, J., Glenn, R., Alagesan, P. and Rajagopal, S. (2017) 'A Practical Guide to Approaching Biased Agonism at G Protein Coupled Receptors', *Frontiers in Neuroscience*, 11, pp. 1–6.

Gupta, M. K., Papay, R. S., Jurgens, C. W. D., Gaivin, R. J., Shi, T., Doze, V. A. and Perez, D. M. (2009) '$\alpha_1$-Adrenergic Receptors Regulate Neurogenesis and Gliogenesis', *Molecular Pharmacology*, 76(2), pp. 314–326.

Gurevich, E. V., Tesmer, J. J. G., Mushegian, A. and Gurevich, V. V. (2012) 'G protein-coupled receptor kinases: More than just kinases and not only for GPCRs', *Pharmacology and Therapeutics*, 133, pp. 40–69.

Hall, M. P., Unch, J., Binkowski, B. F., Valley, M. P., Butler, B. L., Wood, M. G., Otto, P., Zimmerman, K., Vidugiris, G., MacHleidt, T., Robers, M. B., Benink, H. A., Eggers, C. T., Slater, M.l R., Meisenheimer, P. L., Klaubert, D. H., Fan, F., Encell, L. P. and Wood, K. V. (2012) 'Engineered luciferase reporter from a deep sea shrimp utilizing a novel imidazopyrazinone substrate', *ACS Chemical Biology*, 7(11), pp. 1848–1857.

Halls, M. L. and Cooper, D. M. F. (2017) 'Adenylyl cyclase signalling complexes – Pharmacological challenges and opportunities', *Pharmacology and Therapeutics*, 172, pp. 171–180.

Hamann, A., Nguyen, A. and Pannier, A. K. (2019) 'Nucleic acid delivery to mesenchymal stem cells: a review of nonviral methods and applications', *Journal of Biological Engineering*, 13(7).

Hankins, M. W., Peirson, S. N. and Foster, R. G. (2008) 'Melanopsin: an exciting photopigment', *Trends in Neurosciences*, 31(1), pp. 27–36.

Hargus, G., Cooper, O., Deleidi, M., Levy, A., Lee, K., Marlow, E., Yow, A., Soldner, F., Hockemeyer, D., Hallett, P. J., Osborn, T., Jaenisch, R. and Isacson, O. (2010) 'Differentiated Parkinson patient-derived induced pluripotent stem cells grow in the adult rodent brain and reduce motor asymmetry in Parkinsonian rats', *PNAS*, 107(36), pp. 15921–15926.

Henneberger, C., Papouin, T., Oliet, S. H. R. and Rusakov, D. A. (2010) 'Long-term potentiation depends on release of D-serine from astrocytes', *Nature*, 463(7278), pp. 232–236.

Harjes, U. (2019) 'A source of calcium', *Nature Reviews Cancer*, 19, p. 3.

Helmchen, F., Imoto, K. and Sakmann, B. (1996) '$Ca^{2+}$ Buffering and Action

Potential-Evoked Ca2+ Signaling in Dendrites of Pyramidal Neurons', *Biophysical Journal*, 70, pp. 1069–1081

Hertz, L., Peng, L. and Lai, J. C. K. (1998) 'Functional Studies in Cultured Astrocytes', *Methods*, 16(3), pp. 293–310.

Hinz, L., Ahles, A., Ruprecht, B., Ku, B. and Engelhardt, S. (2017) 'Two serines in the distal C-terminus of the human ß$_1$-adrenoceptor determine ß-arrestin2 recruitment', *PLoS ONE*, 12(5), p. e0176450.

Hirase, H., Iwai, Y., Takata, N., Shinohara, Y. and Mishima, T. (2014) 'Volume transmission signalling via astrocytes', *Philosophical Transactions of the Royal Society B*, 369(20130604).

Holliday, N. D., Holst, B., Rodionova, E. A., Schwartz, T. W. and Cox, H. M. (2007) 'Importance of constitutive activity and arrestin-independent mechanisms for intracellular trafficking of the ghrelin receptor', *Molecular Endocrinology*, 21(12), pp. 3100–3112.

Holliday, N. D., Lam, C. W., Tough, I. R. and Cox, H. M. (2005) 'Role of the C terminus in neuropeptide Y $Y_1$ receptor desensitization and internalization', *Molecular Pharmacology*, 67(3), pp. 655–664.

Horowitz, L. F., Hirdes, W., Suh, B. C., Hilgemann, D. W., Mackie, K. and Hille, B. (2005) 'Phospholipase C in living cells: Activation, inhibition, $Ca^{2+}$ requirement, and regulation of M current', *Journal of General Physiology*, 126(3), pp. 243–262.

Hu, J., Stern, M., Gimenez, L. E., Wanka, L., Zhu, L., Rossi, M., Meister, J., Inoue, A., Beck-Sickinger, A. G., Gurevich, V. V. and Wess, J. (2016) 'A G Protein-Biased Designer G Protein-Coupled Receptor Useful for Studying the Physiological Relevance of $G_{q/11}$-Dependent Signaling Pathways', *Journal of Biological Chemistry*, 291(15), pp. 7809–20.

Hughes, S., Jagannath, A., Hickey, D., Gatti, S., Wood, M., Peirson, S. N., Foster, R. G. and Hankins, M. W. (2014) 'Using siRNA to define functional interactions between melanopsin and multiple G Protein partners', *Cellular and Molecular Life Sciences*, 72(1), pp. 165–179.

Inoshima, I., Inoshima, N., Wilke, G., Powers, M., Frank, K., Wang, Y. and Wardenburg, J. B. (2017) 'Identification of Phosphorylation Codes for Arrestin Recruitment by G protein-Coupled Receptors', *Cell*, 17(10), pp. 1310–1314.

Inoue, A., Raimondi, F., Kadji, F. M. N., Singh, G., Kishi, T., Uwamizu, A., Ono, Y., Shinjo, Y., Ishida, S., Arang, N., Kawakami, K., Gutkind, J. S., Aoki, J. and Russell, R. B. (2019) 'Illuminating G-Protein-Coupling Selectivity of GPCRs', *Cell*, 177(7), pp. 1933-1947.e25.

Inoue, K., del Carmen Marín, M., Tomida, S., Nakamura, R., Nakajima, Y., Olivucci, M. and Kandori, H. (2019) 'Red-shifting mutation of light-driven sodium-pump rhodopsin', *Nature Communications*, 10(1), pp. 1–11.

Irannejad, R., Tomshine, J. C., Tomshine, J. R., Chevalier, M., Mahoney, J. P., Steyaert, J., Rasmussen, S. G. F., Sunahara, R. K., El-Samad, H., Huang, B. and Von Zastrow, M. (2013) 'Conformational biosensors reveal GPCR signalling from endosomes', *Nature*, 495(7442), pp. 534–538.

Izquierdo-Serra, M., Trauner, D., Llobet, A. and Gorostiza, P. (2013) 'Optical modulation of neurotransmission using calcium photocurrents through the ion channel LiGluR', *Frontiers in Molecular Neuroscience*, 6(3), pp. 1–8.

Jagannath, A., Hughes, S., Abdelgany, A., Pothecary, C. A., Di Pretoro, S., Pires, S. S., Vachtsevanos, A., Pilorz, V., Brown, L. A., Hossbach, M., MacLaren, R. E., Halford, S., Gatti, S., Hankins, M. W., Wood, M. J. A., Foster, R. G. and Peirson, S. N. (2015) 'Isoforms of Melanopsin Mediate Different Behavioral Responses to Light', *Current Biology*, 25(18), pp. 2430–2434.

Jaiswal, P. B., Tung, J. K., Gross, R. E. and English, A. W. (2017) 'Motoneuron activity is required for enhancements in functional recovery after peripheral nerve injury in exercised female mice', *Journal of Neuroscience Research*, 98(3), pp. 448–457.

Janz, J. M. and Farrens, D. L. (2001) 'Engineering a Functional Blue-Wavelength-Shifted Rhodopsin Mutant', *Biochemistry*, 40(24), pp. 7219–7227.

Jensen, D. D., Lieu, TM., Halls, M. L., Veldhuis, N. A, Imlach, W. L., Mai, Q. N., Poole, D. P., Quach, T., Aurelio, L., Conner, J., Herenbrink, C. K., Barlow, N.,Simpson, J.S., Scanlon, M. J., Graham, B., McCluskey, A., Robinson, P. J., Escriou, V., Nassini, R., Materazzi, S., Geppetti, P., Hicks, G. A, Christie, M. J., Porter, C. J. H., Canals, M. and Bunnett, N. W (2017) 'Neurokinin 1 receptor signaling in endosomes mediates sustained nociception and is a viable therapeutic target for prolonged pain relief', *Science Translational Medicine*, 9(392), p. eaal3447.

Jimenez-Vargasa, N. N. et al. (2018) 'Neurokinin 1 receptor signaling in endosomes mediates sustained nociception and is a viable therapeutic target for prolonged pain relief', *PNAS*, 115(31), pp. E7438–E7447.

Johnston, Paul A., Dudgeon, D. D., Shinde, S. N., Shun, T. Y., Lazo, J. S., Strock, C. J., Giuliano, K. A., Taylor, D. L. and Johnston, Patricia A. (2010) 'Characterization and optimization of a novel protein-protein interaction biosensor high-content screening assay to identify disruptors of the interactions between p53 and hDM2', *Assay and Drug Development Technologies*, 8(4), pp. 437–458.

Jong, Y.-J. I., Harmon, S. K. and O'Malley, K. L. (2018) 'GPCR signalling from within the cell', *British Journal of Pharmacology*, 175, pp. 4026–4035.

Jong, Y. J. I., Kumar, V., Kingston, A. E., Romano, C. and O'Malley, K. L. (2005) 'Functional metabotropic glutamate receptors on nuclei from brain and primary cultured striatal neurons: Role of transporters in delivering ligand', *Journal of Biological Chemistry*, 280(34), pp. 30469–30480.

Kahlke, T. and Umbers, K. D. L. (2016) 'Bioluminescence', *Current Biology*, 26(8), pp. R313–R318.

Kandori, H., Shichida, Y. and Yoshizawa, T. (2001) 'Photoisomerization in Rhodopsin', *Biochemistry (Moscow)*, 66(11), pp. 1197–1209.

Kang, Y. et al. (2015) 'Crystal structure of rhodopsin bound to arrestin by femtosecond X-ray laser.', *Nature*, 523(7562), pp. 561–7.

Kang, Y. et al. (2018) 'Cryo-EM structure of human rhodopsin bound to an inhibitory G protein', *Nature*, 558(7711), pp. 553–558.

Karchin, R., Karplus, K. and Haussler, D. (2002) 'Classifying G-protein coupled

receptors with support vector machines.', *Bioinformatics*, 18(1), pp. 147–159.

Karnik, S. S., Gogonea, C., Patil, S., Saad, Y. and Takezako, T. (2003) 'Activation of G-protein-coupled receptors: a common molecular mechanism', *Trends in Endocrinology and Metabolism*, 14(9), pp. 431–437.

Karunarathne, W. K., Giri, L., Kalyanaraman, V. and Gautam, N. (2013) 'Optically triggering spatiotemporally confined GPCR activity in a cell and programming neurite initiation and extension', *PNAS*, 110(17), pp. E1565-74.

Keppler, A., Gendreizig, S., Gronemeyer, T., Pick, H., Vogel, H. and Johnsson, K. (2003) 'A general method for the covalent labeling of fusion proteins with small molecules *in vivo*', *Nature Biotechnology*, 21(1), pp. 86–9.

Keriel, A., Rene, C., Galer, C., Zabner, J. and Kremer, E. J. (2006) 'Canine Adenovirus Vectors for Lung-Directed Gene Transfer: Efficacy, Immune Response, and Duration of Transgene Expression Using Helper-Dependent Vectors', *Journal of Virology*, 80(3), pp. 1487–1496.

Khakh, B. S. and McCarthy, K. D. (2015) 'Astrocyte calcium signaling: From observations to functions and the challenges therein', *Cold Spring Harbor Perspectives in Biology*, 7(4), pp. 1–17.

Kilpatrick, L. E., Humphrys, L. J. and Holliday, N. D. (2015) 'A G Protein Coupled Receptor Dimer Imaging Assay Reveals Selectively Modified Pharmacology of Neuropeptide Y $Y_1/Y_5$ Receptor Heterodimers', *Molecular Pharmacology*, 87, pp. 718–732.

Kim, J. M., Hwa, J., Garriga, P., Reeves, P. J., RajBhandary, U. L. and Khorana, H. G. (2005) 'Light-driven activation of $\beta_2$-adrenergic receptor signaling by a chimeric rhodopsin containing the $\beta_2$-adrenergic receptor cytoplasmic loops', *Biochemistry*, 44(7), pp. 2284–2292.

Kim, S. S. (2016) 'Manipulation of P2X receptor activities by light stimulation', *Mediators of Inflammation*, 2016.

Kim, T. K. and Eberwine, J. H. (2010) 'Mammalian cell transfection: The present and the future', *Analytical and Bioanalytical Chemistry*, 397(8), pp. 3173–3178.

Kiser, P. D., Golczak, M., Maeda, A. and Palczewski, K. (2012) 'Key enzymes of the retinoid (visual) cycle in vertebrate retina', *Biochimica et Biophysica Acta*, 1821, pp. 137–151.

Klapoetke, N. C. et al. (2014) 'Independent optical excitation of distinct neural populations', *Nature Methods*, 11(3), pp. 338–346.

Kleinlogel, S., Feldbauer, K., Dempski, R. E., Fotis, H., Wood, P. G., Bamann, C. and Bamberg, E. (2011) 'Ultra light-sensitive and fast neuronal activation with the $Ca^{2+}$-permeable channelrhodopsin CatCh', *Nature Neuroscience*, 14(4), pp. 513–518.

von Kleist, L. et al. (2011) 'Role of the clathrin terminal domain in regulating coated pit dynamics revealed by small molecule inhibition', *Cell*, 146(3), pp. 471–484.

König, B., Arendt, A., McDowell, J. H., Kahler, M., Hargrave, P. A. and Hofmann, K. P. (1989) 'Three cytoplasmic loops of rhodopsin interact with transducin', *PNAS*, 86, pp. 6878–6882.

Koppel, I., Jaanson, K., Klasche, A., Tuvikene, J., Tiirik, T., Pärn, A. and Timmusk, T. (2018) 'Dopamine cross-reacts with adrenoreceptors in cortical astrocytes to induce BDNF expression, CREB signaling and morphological transformation', *Glia*, 66(1), pp. 206–216

Kotowski, S. J., Hopf, F. W., Seif, T., Bonci, A. and von Zastrow, M. (2011) 'Endocytosis Promotes Rapid Dopaminergic Signaling', *Neuron*, 71(2), pp. 278–290.

Kötter, K. and Klein, J. (1999) 'Adrenergic modulation of astroglial phospholipase D activity and cell proliferation.', *Brain research*, 830(1), pp. 138–45.

Koyanagi, M., Takano, K., Tsukamoto, H., Ohtsu, K., Tokunaga, F. and Terakita, A. (2008) 'Jellyfish vision starts with cAMP signaling mediated by opsin-$G_s$ cascade', *PNAS*, 105(40), pp. 15576–15580.

Koyanagi, M. and Terakita, A. (2014) 'Diversity of animal opsin-based pigments and their optogenetic potential', *Biochimica et Biophysica Acta*, 1837(5), pp. 710–716.

Kozak, M. (1987) 'At least six nucleotides preceding the AUG initiator codon enhance translation in mammalian cells', *Journal of Molecular Biology*, 196(4), pp. 947–950.

Krzyzaniak, M. A., Zumstein, M. T., Gerez, J. A., Picotti, P. and Helenius, A. (2013) 'Host Cell Entry of Respiratory Syncytial Virus Involves Macropinocytosis Followed by Proteolytic Activation of the F Protein', *PLoS Pathogens*, 9(4), pp. 1–19.

Kuga, N., Sasaki, T., Takahara, Y., Matsuki, N. and Ikegaya, Y. (2011) 'Large-scale calcium waves traveling through astrocytic networks *in vivo*.', *The Journal of Neuroscience*, 31(7), pp. 2607–14.

Kumar, P., Nagarajan, A. and Uchil, P. D. (2019) 'DNA Transfection Mediated by Cationic Lipid Reagents', *Cold Spring Harbor Protocols*, pp. 215–223.

Kurebayashi, N., Harkins, a B. and Baylor, S. M. (1993) 'Use of fura red as an intracellular calcium indicator in frog skeletal muscle fibers', *Biophysical Journal*, 64(6), pp. 1934–1960.

Kurita, M., Matsuoka, Y., Nakatsuka, K., Ono, D., Muto, N., Kaku, R. and Morimatsu, H. (2018) 'Norepinephrine-induced downregulation of GLT-1 mRNA in rat astrocytes', *Biochemical and Biophysical Research Communications*, 504(1), pp. 103–108.

Kurrasch-Orbaugh, D. M., Parrish, J. C., Watts, V. J. and Nichols, D. E. (2003) 'A complex signaling cascade links the serotonin$_{2A}$ receptor to phospholipase A2 activation: The involvement of MAP kinases', *Journal of Neurochemistry*, 86(4), pp. 980–991.

Lamb, T. D. (2009) 'Evolution of vertebrate retinal photoreception', *Philosophical Transactions of the Royal Society B*, 364(1531), pp. 2911–2924.

Lang, S. C., Bak, L. K., Waagepetersen, H. S., Schousboe, A. and Norenberg, M. (2016) 'Primary cultures of astrocytes: Their value in understanding astrocytes in health and disease', *Neurochemical Research*, 37(11), pp. 2569–2588.

Lattion, A. L., Diviani, D. and Cotecchia, S. (1994) 'Truncation of the receptor carboxyl terminus impairs agonist-dependent phosphorylation and desensitization

of the $\alpha_{1B}$-adrenergic receptor', *Journal of Biological Chemistry*, 269(36), pp. 22887–22893.

Lavis, L. D., Chao, T. Y. and Raines, R. T. (2011) 'Synthesis and utility of fluorogenic acetoxymethyl ethers', *Chemical Science*, 2(3), pp. 521–530.

Leroy, E., Balligand, T., Pecquet, C., Mouton, C., Colau, D., Shiau, A. K., Dusa, A. and Constantinescu, S. N. (2019) 'Differential effect of inhibitory strategies of the V617 mutant of JAK2 on cytokine receptor signaling', *Journal of Allergy and Clinical Immunology*, 144(1), pp. 224–235.

Li, D., Agulhon, C., Schmidt, E., Oheim, M. and Ropert, N. (2013) 'New tools for investigating astrocyte-to-neuron communication.', *Frontiers in Cellular Neuroscience*, 7(193).

Li, D., Hé, K., Oheim, M. and Ropert, N. (2009) 'FM dyes enter via a store-operated calcium channel and modify calcium signaling of cultured astrocytes', *PNAS December*, 22(51), pp. 21960–21965.

Li, D., Hérault, K., Isacoff, E. Y., Oheim, M. and Ropert, N. (2012) 'Optogenetic activation of LiGluR-expressing astrocytes evokes anion channel-mediated glutamate release', *Journal of Physiology*, 590(4), pp. 855–873.

Liang, X., Yao, Y., Lin, Y., Kong, L., Xiao, H., Shi, Y. and Yang, J. (2019) 'Panaxadiol inhibits synaptic dysfunction in Alzheimer's disease and targets the Fyn protein in APP/PS1 mice and APP-SH-SY5Y cells', *Life Sciences*.

Liang, Y. L., Khoshouei, M., Radjainia, M., Zhang, Y., Glukhova, A., Tarrasch, J., Thal, D. M., Furness, S. G. B., Christopoulos, G., Coudrat, T., Danev, R., Baumeister, W., Miller, L. J., Christopoulos, A., Kobilka, B. K., Wootten, D., Skiniotis, G. and Sexton, P. M. (2017) 'Phase-plate cryo-EM structure of a class B GPCR-G-protein complex', *Nature*, 546(7656), pp. 118–123.

Lima, S. Q. and Miesenböck, G. (2005) 'Remote control of behavior through genetically targeted photostimulation of neurons.', *Cell*, 121(1), pp. 141–52.

Lin, S. W., Kochendoerfer, G. G., Carroll, K. S., Wang, D., Mathies, R. A. and Sakmar, T. P. (1998) 'Mechanisms of Spectral Tuning in Blue Cone Visual Pigments', *The Journal of Biological Chemistry*, 273(38), pp. 24583–24591.

Liske, H., Qian, X., Anikeeva, P., Deisseroth, K. and Delp, S. (2013) 'Optical control of neuronal excitation and inhibition using a single opsin protein, ChR2.', *Scientific Reports*, 3(3110).

Lobingier, B. T. and von Zastrow, M. (2019) 'When trafficking and signaling mix: How subcellular location shapes G protein-coupled receptor activation of heterotrimeric G proteins', *Traffic*, 20(2), pp. 130–136.

Lock, J. T., Smith, I. F. and Parker, I. (2017) 'Comparison of $Ca^{2+}$ puffs evoked by extracellular agonists and photoreleased $IP_3$', *Cell Calcium*, 63, pp. 43–47.

Loening, A. M., Fenn, T. D., Wu, A. M. and Gambhir, S. S. (2006) 'Consensus guided mutagenesis of Renilla luciferase yields enhanced stability and light output', *Protein Engineering, Design and Selection*, 19(9), pp. 391–400.

Loh, J. M. S. and Proft, T. (2014) 'Comparison of firefly luciferase and NanoLuc luciferase for biophotonic labeling of group A Streptococcus', *Biotechnology Letters*,

36(4), pp. 829–834.

Loughrey, C. M., MacEachern, K. E., Cooper, J. and Smith, G. L. (2003) 'Measurement of the dissociation constant of Fluo-3 for $Ca^{2+}$ in isolated rabbit cardiomyocytes using $Ca^{2+}$ wave characteristics', *Cell Calcium*, 34(1), pp. 1–9.

Luttrell, L. M., Ferguson, S. S. G., Daaka, Y., Miller, W. E., Maudsley, S., Rocca, G. J. Della, Lin, F.-T., Kawakatsu, H., Owada, K., Luttrell, D. K., Caron, M. G. and Lefkowitz, R. J. (1999) 'β-Arrestin-Dependent Formation of $\beta_2$ Adrenergic Receptor-Src Protein Kinase Complexes', *Science*, 283(5402), pp. 655–661.

Luttrell, L. M. and Lefkowitz, R. J. (2002) 'The role of β-arrestins in the termination and transduction of G-protein-coupled receptor signals.', *Journal of Cell Science*, 115(3), pp. 455–465.

MacLaren, D. A. A., Browne, R. W., Shaw, J. K., Radhakrishnan, S. K., Khare, P., España, R. A. and Clark, S. D. (2016) 'Clozapine N-oxide administration produces behavioral effects in long-evans rats: Implications for designing DREADD experiments', *eNeuro*, 3(5).

Maeda, R., Hiroshima, M., Yamashita, T., Wada, A., Sako, Y., Shichida, Y. and Imamoto, Y. (2018) 'Shift in Conformational Equilibrium Induces Constitutive Activity of G-Protein-Coupled Receptor, Rhodopsin', *The Journal of Physical Chemistry B*, 122, pp. 4838–4843.

Magee, T. and Newman, C. (1992) 'The role of lipid anchors for small G proteins in membrane trafficking', *Trends in Cell Biology*, 2(11), pp. 318–323.

Mager, T., Wood, P. G. and Bamberg, E. (2017) 'Optogenetic Control of $Ca^{2+}$ and Voltage-Dependent Large Conductance (BK) Potassium Channels', *Journal of Molecular Biology*, 429(6), pp. 911–921.

Maguire, C. A., Deliolanis, N. C., Pike, L., Niers, J. M., Tjon-Kon-Fat, L. A., Sena-Esteves, M. and Tannous, B. A. (2009) 'Gaussia luciferase variant for high-throughput functional screening applications', *Analytical Chemistry*, 81(16), pp. 7102–7106.

Makowka, P., Bruegmann, T., Dusend, V., Malan, D., Beiert, T., Hesse, M., Fleischmann, B. K. and Sasse, P. (2019) 'Optogenetic stimulation of $G_s$-signaling in the heart with high spatio-temporal precision', *Nature Communications*, 10(1).

Mangmool, S. and Kurose, H. (2011) '$G_{i/o}$ protein-dependent and -independent actions of pertussis toxin (PTX)', *Toxins*, 3(7), pp. 884–899.

Marchant, N. J., Whitaker, L. R., Bossert, J. M., Harvey, B. K., Hope, B. T., Kaganovsky, K., Adhikary, S., Prisinzano, T. E., Vardy, E., Roth, B. L. and Shaham, Y. (2016) 'Behavioral and Physiological Effects of a Novel Kappa-Opioid Receptor-Based DREADD in Rats', *Neuropsychopharmacology*, 41(2), pp. 402–409.

Marchese, A., Paing, M. M., Temple, B. R. S. and Trejo, J. (2008) 'G Protein–Coupled Receptor Sorting to Endosomes and Lysosomes', *Annual Review of Pharmacology and Toxicology*, 48(1), pp. 601–629.

Marque, J. J. (1989) 'Using caged neurotransmitters.', *Nature*, 337(6207), pp. 583–4.

Marques, S. M. and Esteves Da Silva, J. C. G. (2009) 'Firefly bioluminescence: A

mechanistic approach of luciferase catalyzed reactions', *IUBMB Life*, 61(1), pp. 6–17.

Matsuyama, T., Yamashita, T., Imamoto, Y. and Shichida, Y. (2012) 'Photochemical properties of mammalian melanopsin', *Biochemistry*, 51(27), pp. 5454–5462.

Maurel, D., Comps-Agrar, L., Brock, C., Rives, M.-L., Bourrier, E., Ayoub, M. A., Bazin, H., Tinel, N., Durroux, T., Pre´zeau, L., Trinquet, E. and Pin, J.-P. (2008) 'Cell-surface protein-protein interaction analysis with time-resolved FRET and snap-tag technologies: application to G protein-coupled receptor oligomerization', *Nature Methods*, 5(6), pp. 561–567.

Mccluskey, A., Daniel, J. A., Hadzic, G., Chau, N., Clayton, E. L., Mariana, A., Whiting, A., Gorgani, N. N., Lloyd, J., Quan, A., Moshkanbaryans, L., Krishnan, S., Perera, S., Chircop, M., von Kleist, L., Mcgeachie, A. B., Howes, M. T., Parton, R. G., Campbell, M., Sakoff, J. A., Wang, X., Sun, J. Y., Robertson, M. J., Deane, F. M., Nguyen, T. H., Meunier, F. A., Cousin, M. A., Robinson, P. J. (2013) 'Building a better dynasore: The dyngo compounds potently inhibit dynamin and endocytosis', *Traffic*, 14(12), pp. 1272–1289.

Mcgregor, K. M., Bécamel, C., Marin, P. and Andrade, R. (2016) 'Using melanopsin to study G protein signaling in cortical neurons', *Journal of Neurophysiology*, 116, pp. 1082–1092.

McIntire, W. E. (2009) 'Structural determinants involved in the formation and activation of G protein βγ dimers', *Neurosignals*, 17(1), pp. 82–99.

Mederos, S., Hernández-Vivanco, A., Ramírez-Franco, J., Martín-Fernández, M., Navarrete, M., Yang, A., Boyden, E. S. and Perea, G. (2018) 'Melanopsin for precise optogenetic activation of astrocyte-neuron networks', *Glia*, 67, pp. 915–934.

Mellott, A. J., Forrest, M. L. and Detamore, M. S. (2013) 'Physical non-viral gene delivery methods for tissue engineering', *Annals of Biomedical Engineering*, 41(3), pp. 446–468.

Melyan, Z., Tarttelin, E. E., Bellingham, J., Lucas, R. J. and Hankins, M. W. (2005) 'Addition of human melanopsin renders mammalian cells photoresponsive', *Nature*, 433(7027), pp. 741–745.

Merriam, L. A., Baran, C. N., Girard, B. M., Hardwick, J. C., May, V. and Parsons, R. L. (2013) 'Pituitary adenylate cyclase 1 receptor internalization and endosomal signaling mediate the pituitary adenylate cyclase activating polypeptide-induced increase in guinea pig cardiac neuron excitability', *Journal of Neuroscience*, 33(10), pp. 4614–4622.

Miyazaki, K., Lisman, J. E. and Ross, W. N. (2019) 'Improvements in simultaneous sodium and calcium imaging', *Frontiers in Cellular Neuroscience*, 12(514), pp. 1–10.

Moaven, H., Koike, Y., Jao, C. C., Gurevich, V. V., Langen, R. and Chen, J. (2013) 'Visual arrestin interaction with clathrin adaptor AP-2 regulates photoreceptor survival in the vertebrate retina', *PNAS*, 110(23), pp. 9463–9468.

Morris, D. P., Price, R. R., Smith, M. P., Lei, B. and Schwinn, D. A. (2004) 'Cellular Trafficking of Human $\alpha_{1A}$-Adrenergic Receptors Is Continuous and Primarily Agonist-Independent', 66(4), pp. 843–854.

Mure, L. S., Rieux, C., Hattar, S. and Cooper, H. M. (2007) 'Melanopsin-dependent nonvisual responses: Evidence for photopigment bistability *in vivo*', *Journal of Biological Rhythms*, 22(5), pp. 411–424.

Mure, L. S. S., Hatori, M., Zhu, Q., Demas, J., Kim, I. M. M., Nayak, S. K. K. and Panda, S. (2016) 'Melanopsin-Encoded Response Properties of Intrinsically Photosensitive Retinal Ganglion Cells', *Neuron*, 90(5), pp. 1016–1027.

Murthy, K. S., Zhou, H., Huang, J. and Pentyala, S. N. (2004) 'Activation of PLC-1 by $G_{i/o}$-coupled receptor agonists', *Am J Physiol Cell Physiol*, 287, pp. 1679–1687.

Nagel, G., Ollig, D., Fuhrmann, M., Kateriya, S., Musti, A. M., Bamberg, E. and Hegemann, P. (2002) 'Channelrhodopsin-1: A light-gated proton channel in green algae', *Science*, 296(5577), pp. 2395–2398.

Nagel, G., Szellas, T., Huhn, W., Kateriya, S., Adeishvili, N., Berthold, P., Ollig, D., Hegemann, P. and Bamberg, E. (2003) 'Channelrhodopsin-2, a directly light-gated cation-selective membrane channel', *PNAS*, 100(24), pp. 13940–13945.

Nakajima, K. and Wess, J. (2012) 'Design and functional characterization of a novel, arrestin-biased designer G protein-coupled receptor', *Molecular pharmacology*, 82(4), pp. 575–582.

Nakamichi, H., Buss, V. and Okada, T. (2007) 'Photoisomerization mechanism of rhodopsin and 9-*cis*-rhodopsin revealed by X-ray crystallography', *Biophysical Journal*, 92(12).

Nash, C. A., Wei, W., Irannejad, R. and Smrcka, A. V (2019) 'Golgi localized $\beta_1$-adrenergic receptors stimulate Golgi PI4P hydrolysis by PLCε to regulate cardiac hypertrophy', *eLife*, 8, pp. 1–22.

Navarrete, M., Perea, G., Maglio, L., Pastor, J., García de Sola, R. and Araque, A. (2013) 'Astrocyte calcium signal and gliotransmission in human brain tissue.', *Cerebral Cortex*, 23(5), pp. 1240–6.

Nedergaard, M., Rodriguez, J. J. and Verkhratsky, A. (2010) 'Glial calcium and diseases of the nervous system', *Cell Calcium*, 47(2), pp. 140–149.

Nelson, C. D., Perry, S. J., Regier, D. S., Prescott, S. M., Topham, M. K. and Lefkowitz, R. J. (2007) 'Targeting of diacylglycerol degradation to M1 muscarinic receptors by β-arrestins', *Science*, 315(5812), pp. 663–666.

Nett, W. J., Oloff, S. H. and Mccarthy, K. D. (2002) 'Hippocampal astrocytes in situ exhibit calcium oscillations that occur independent of neuronal activity', *Journal of Neurophysiology*, 87(1), pp. 528–537.

Newman, L. A., Walker, M. T., Brown, R. L., Cronin, T. W. and Robinson, P. R. (2003) 'Melanopsin Forms a Functional Short-Wavelength Photopigment', *Biochemistry*, 42(44), pp. 12734–12738.

Norton, W. T. and Farooq, M. (1989) 'Astrocytes Cultured from Mature Brain Derive from Glial Precursor Cells', *The Journal of Neuroscience*, 9(3), pp. 769–775.

Oda, S., Tsuneoka, Y., Yoshida, S., Adachi-Akahane, S., Ito, M., Kuroda, M. and Funato, H. (2018) 'Immunolocalization of muscarinic M1 receptor in the rat medial prefrontal cortex', *Journal of Comparative Neurology*, 526(8), pp. 1329–1350.

Oh, E., Maejima, T., Liu, C., Deneris, E. and Herlitze, S. (2010) 'Substitution of 5-$HT_{1A}$ receptor signaling by a light-activated G protein-coupled receptor', *Journal of Biological Chemistry*, 285(40), pp. 30825–30836.

Oheim, M., van 't Hoff, M., Feltz, A., Zamaleeva, A., Mallet, J.-M. and Collot, M. (2014) 'New red-fluorescent calcium indicators for optogenetics, photoactivation and multi-color imaging', *BBA - Molecular Cell Research*, 1843(10), pp. 2284–2306.

Ohkura, M., Sasaki, T., Sadakari, J., Gengyo-Ando, K., Kagawa-Nagamura, Y., Kobayashi, C., Ikegaya, Y. and Nakai, J. (2012) 'Genetically Encoded Green Fluorescent $Ca^{2+}$ Indicators with Improved Detectability for Neuronal $Ca^{2+}$ Signals', *PLoS ONE*.

Oka, Y., Saraiva, L. R., Kwan, Y. Y. and Korsching, S. I. (2009) 'The fifth class of Gα proteins', *PNAS*, 106(5), pp. 1484–1489.

Olausson, B. E. S., Grossfield, A., Pitman, M. C., Brown, M. F., Feller, S. E. and Vogel, A. (2012) 'Molecular dynamics simulations reveal specific interactions of post-translational palmitoyl modifications with rhodopsin in membranes', *Journal of the American Chemical Society*, 134(9), pp. 4324–4331.

Omasits, U., Ahrens, C. H., Mu, S. and Wollscheid, B. (2014) 'Protter : interactive protein feature visualization and integration with experimental proteomic data', *Bioinformatics*, 30(6), pp. 884–886.

Ono, K., Suzuki, H., Higa, M., Tabata, K. and Sawada, M. (2014) 'Glutamate release from astrocyte cell-line GL261 via alterations in the intracellular ion environment', *Journal of Neural Transmission*, 121(3), pp. 245–257.

Ono, K., Suzuki, H., Yamamoto, R., Sahashi, H. and Takido, Y. (2017) 'Neurochemistry International Optogenetic control of cell differentiation in channelrhodopsin-2- expressing OS3 , a bipotential glial progenitor cell line', *Neurochemistry International*, 104, pp. 49–63.

Ozawa, T. (2006) 'Designing split reporter proteins for analytical tools', *Analytica Chimica Acta*, 556(1), pp. 58–68.

Ozawa, T., Kaihara, A., Sato, M., Tachihara, K. and Umezawa, Y. (2001) 'Split luciferase as an optical probe for detecting protein - Protein interactions in mammalian cells based on protein splicing', *Analytical Chemistry*, 73(11), pp. 2516–2521.

Pa ca, A. M., Sloan, S. A., Clarke, L. E., Tian, Y., Makinson, C. D., Huber, N., Kim, C. H., Park, J.-Y., O'Rourke, N., Nguyen, K. D., Smith, S. J., Huguenard, J. R., Geshwind, D. H., Barres, B. A. and Pa ca, S. P. (2015) 'Functional cortical neurons and astrocytes from human pluripotent stem cells in 3D culture', *Nature Methods*, 12(7), pp. 671–678.

Packer, A. M., Peterka, D. S., Hirtz, J. J., Prakash, R., Deisseroth, K. and Yuste, R. (2012) 'Two-photon optogenetics of dendritic spines and neural circuits in 3D', *Nature Methods*, 9(12), pp. 1202–1205.

Palczewski, K. (2006) 'G protein-coupled receptor rhodopsin.', *Annual Review of Biochemistry*, 75, pp. 743–67.

Palczewski, K., Kumasaka, T., Hori, T., Behnke, C. A., Motoshima, H., Fox, B. A.,

Trong, I. Le, Teller, D. C., Okada, T., Stenkamp, R. E., Yamamoto, M. and Miyano, M. (2000) 'Crystal Structure of Rhodopsin: A G Protein-Coupled Receptor', *Science*, 289, pp. 739–745.

Palygin, O., Lalo, U. and Pankratov, Y. (2011) 'Distinct pharmacological and functional properties of NMDA receptors in mouse cortical astrocytes', *British Journal of Pharmacology*, 163(8), pp. 1755–1766.

Paoletti, P., Ellis-Davies, G. C. R. and Mourot, A. (2019) 'Optical control of neuronal ion channels and receptors', *Nature Reviews Neuroscience*, 20, pp. 514–532.

Paredes, R. M., Etzler, J. C., Watts, L. T., Zheng, W. and Lechleiter, J. D. (2008) 'Chemical Calcium Indicators', *Methods*, 46(3), pp. 143–151.

Parekh, A. B. (2016) 'Advances in intracellular $Ca^{2+}$ signalling', *Journal of Physiology*, 594(11), pp. 2811–2812.

Park, P. S. (2014) 'Constitutively Active Rhodopsin and Retinal Disease', *Adv Pharmacol.*, 70, pp. 1–31.

Park, S. Y., Song, S.-H., Palmateer, B., Pal, A., Petersen, E. D., Shall, G. P., Welchko, R. M., Ibata, K., Miyawaki, A., Augustine, G. J. and Hochgeschwender, U. (2019) 'Novel luciferase-opsin combinations for improved luminopsins', *Journal of Neuroscience Research*, 98(3), pp. 410–421.

Paulmurugant, R. and Gambhir, S. S. (2003) 'Monitoring protein-protein interactions using split synthetic renilla luciferase protein-fragment-assisted complementation', *Analytical Chemistry*, 75(7), pp. 1584–1589.

Pauwels, P. J. and Colpaert, F. C. (2000) 'Disparate ligand-mediated $Ca^{2+}$ responses by wild-type, mutant $Ser^{200}$ Ala and $Ser^{204}$ Ala $\alpha_{2A}$-adrenoceptor : $G_{\alpha 15}$ fusion proteins: evidence for multiple ligand-activation binding sites', *British Journal of Pharmacology*, 130, pp. 1505–1512.

Perea, G. and Araque, A. (2007) 'Astrocytes potentiate transmitter release at single hippocampal synapses', *Science*, 317(5841), pp. 1083–1086.

Perez-Aso, M., Segura, V., Montó, F., Barettino, D., Noguera, M. A., Milligan, G. and D'Ocon, P. (2013) 'The three $\alpha_1$-adrenoceptor subtypes show different spatio-temporal mechanisms of internalization and ERK1/2 phosphorylation', *Biochimica et Biophysica Acta - Molecular Cell Research*, 1833(10), pp. 2322–2333.

Pérez-Garci, E., Larkum, M. E. and Nevian, T. (2013) 'Inhibition of dendritic $Ca^{2+}$ spikes by $GABA_B$ receptors in cortical pyramidal neurons is mediated by a direct $G_{i/o}$-$\beta\gamma$-subunit interaction with $Ca_v1$ channels', *Journal of Physiology*, 591(7), pp. 1599–1612.

Perry, S. J., Baillie, G. S., Kohout, T. A., McPhee, I., Magiera, M. M., Long Ang, K., Miller, W. E., McLean, A. J., Conti, M., Houslay, M. D. and Lefkowitz, R. J. (2002) 'Targeting of Cyclic AMP Degradation to $\beta_2$-Adrenergic Receptors by β-Arrestins', *Science*, 298, pp. 834–836.

Piascik, M. T. and Perez, D. M. (2001) '$\alpha_1$-Adrenergic receptors: New insights and directions', *Journal of Pharmacology and Experimental Therapeutics*, 298(2), pp. 403–410.

Pires, S. S., Hughes, S., Turton, M., Melyan, Z., Peirson, S. N., Zheng, L., Kosmaoglou, M., Bellingham, J., Cheetham, M. E., Lucas, R. J., Foster, R. G.,

Hankins, M. W. and Halford, S. (2009) 'Differential Expression of Two Distinct Functional Isoforms of Melanopsin (Opn4) in the Mammalian Retina', *Journal of Neuroscience*, 29(39), pp. 12332–12342.

Pologruto, T. A., Yasuda, R. and Svoboda, K. (2004) 'Monitoring Neural Activity and [$Ca^{2+}$] with Genetically Encoded Ca2+ Indicators', *Journal of Neuroscience*, 24(43), pp. 9572–9579.

Price, R. R., Morris, D. P., Biswas, G., Smith, M. P. and Schwinn, D. A. (2002) 'Acute agonist-mediated desensitization of the human $\alpha_{1a}$-adrenergic receptor is primarily independent of carboxyl terminus regulation: Implications for regulation of $\alpha_{1a}$AR splice variants', *The Journal of Biological Chemistry*, 277(11), pp. 9570–9579.

Proft, J. and Weiss, N. (2012) 'From opto-to radio-genetics: A switch in the wavelength', *Communicative and Integrative Biology*, 5(3), pp. 227–229.

Prole, D. L. and Taylor, C. W. (2016) 'Inositol 1,4,5-trisphosphate receptors and their protein partners as signalling hubs', *Journal of Physiology*, 594(11), pp. 2849–2866.

Pupo, A. and Minneman, K. (2002) 'Interaction of neuronal nitric oxide synthase with $\alpha_1$-adrenergic receptor subtypes in transfected HEK-293 cells', *BMC Pharmacol.*, 2(1), pp. 1–7.

Rajagopal, S. and Shenoy, S. K. (2018) 'GPCR desensitization: Acute and prolonged phases', *Cellular Signalling*, 41, pp. 9–16.

Rasmussen, S. G. F. et al. (2012) 'Crystal Structure of the $\beta_2$ Adrenergic Receptor-$G_s$ protein complex', *Nature*, 477(7366), pp. 549–555.

Rasmussen, S. G. F., Choi, H.-J., Rosenbaum, D. M., Kobilka, T. S., Thian, F. S., Edwards, P. C., Burghammer, M., Ratnala, V. R. P., Sanishvili, R., Fischetti, R. F., Schertler, G. F. X., Weis, W. I. and Kobilka, B. K. (2007) 'Crystal structure of the human $\beta_2$ adrenergic G-protein-coupled receptor', *Nature*, 450(7168), pp. 383–387.

Redfern, C. H., Coward, P., Degtyarev, M. Y., Lee, E. K., Kwa, A. T., Hennighausen, L., Bujard, H., Fishman, G. I. and Conklin, B. R. (1999) 'Conditional expression and signaling of a specifically designed $G_i$-coupled receptor in transgenic mice.', *Nature biotechnology*, 17(2), pp. 165–9.

Reiter, E., Ahn, S., Shukla, A. K. and Lefkowitz, R. J. (2012) 'Molecular Mechanism of β-Arrestin-Biased Agonism at Seven-Transmembrane Receptors', *Annu Rev Pharmacol Toxicol.*, 52, pp. 179–197.

Remy, I. and Michnick, S. W. (2006) 'A highly sensitive protein-protein interaction assay based on Gaussia luciferase', *Nature Methods*, 3(12), pp. 977–979.

Renault, R., Sukenik, N., Descroix, S., Malaquin, L., Viovy, J. L., Peyrin, J. M., Bottani, S., Monceau, P., Moses, E. and Vignes, M. (2015) 'Combining microfluidics, optogenetics and calcium imaging to study neuronal communication in vitro', *PLoS ONE*.

Reyes-Alcaraz, A., Lee, Y.-N., Yun, S., Hwang, J.-I. and Seong, J. Y. (2018) 'Conformational signatures in β-arrestin2 reveal natural biased agonism at a G-protein-coupled receptor', *Communications Biology*, 1(1).

Ricart-Ortega, M., Font, J. and Llebaria, A. (2019) 'GPCR photopharmacology',

*Molecular and Cellular Endocrinology*, 488, pp. 36–51.

Ronzitti, E., Conti, R., Zampini, V., Tanese, D., Foust, A. J., Klapoetke, N., Boyden, E. S., Papagiakoumou, E. and Emiliani, V. (2017) 'Submillisecond Optogenetic Control of Neuronal Firing with Two-Photon Holographic Photoactivation of Chronos', *The Journal of Neuroscience*, 37(44), pp. 10679–10689.

Rost, B. R., Schneider-Warme, F., Schmitz, D. and Hegemann, P. (2017) 'Optogenetic Tools for Subcellular Applications in Neuroscience', *Neuron*, 96(3), pp. 572–603.

Rusakov, D. A. (2015) 'Disentangling calcium-driven astrocyte physiology', *Nature Reviews Neuroscience*, 16(4), pp. 226–233.

Saari, J. C. (2012) 'Vitamin A Metabolism in Rod and Cone Visual Cycles', *Ann. Rev. Nutr.*, 32, pp. 125–45.

Salomon, M., Christie, J. M., Knieb, E., Lempert, U. and Briggs, W. R. (2000) 'Photochemical and Mutational Analysis of the FMN-Binding Domains of the Plant Blue Light Receptor, Phototropin', *Biochemistry*, 39, pp. 9401–9410.

Samways, D. S. K. and Henderson, G. (2006) 'Opioid elevation of intracellular free calcium: Possible mechanisms and physiological relevance', *Cellular Signalling*, 18(2), pp. 151–161.

Satoh, A. K. and Ready, D. F. (2005) 'Arrestin1 mediates light-dependent rhodopsin endocytosis and cell survival', *Current Biology*, 15(19), pp. 1722–1733.

Scarselli, M. and Donaldson, J. G. (2009) 'Constitutive internalization of G protein-coupled receptors and G proteins via clathrin-independent endocytosis', *Journal of Biological Chemistry*, 284(6), pp. 3577–3585.

Scearce-Levie, K., Lieberman, M. D., Elliott, H. H. and Conklin, B. R. (2005) 'Engineered G protein coupled receptors reveal independent regulation of internalization, desensitization and acute signaling', *BMC Biology*, 3.

Schneider, F., Gradmann, D. and Hegemann, P. (2013) 'Ion selectivity and competition in channelrhodopsins', *Biophysical Journal*, 105(1), pp. 91–100.

Schoenlein, R. W., Peteanu, L. A., Wang, S. Q., Mathies, R. A. and Shank, C. V (1993) 'Femtosecond Dynamics of *Cis-Trans* Isomerization in a Visual Pigment Analog: Isorhodopsin', *The Journal of Physical Chemistry*, 97, pp. 12087–12092.

Schrage, R. et al. (2015) 'The experimental power of FR900359 to study $G_q$-regulated biological processes.', *Nature communications*, 6(May), p. 10156.

Scott, K., Chamberland, S., Yang, H. H., Pan, M. M., Evans, S. W., Guan, S., Chavarha, M., Yang, Y., Salesse, C., Wu, H., Wu, J. C., Clandinin, T. R., Toth, K., Lin, M. Z. and St-Pierre, F. (2017) 'Fast two-photon imaging of subcellular voltage dynamics in neuronal tissue with genetically encoded indicators', *eLIFE*, 6(e25690).

Sekharan, S. and Morokuma, K. (2012) 'Why 11-*cis*-Retinal? Why not 7-*cis*, 9-*cis* or 13-*cis* Retinal in the Eye?', *Journal of the American Chemical Society*, 133(47), pp. 19052–19055.

Semack, A., Sandhu, M., Malik, R. U., Vaidehi, N. and Sivaramakrishnan, S. (2016) 'Structural elements in the $G_{\alpha s}$ and $G_{\beta q}$ C termini that mediate selective G Protein-

coupled Receptor (GPCR) signaling', *Journal of Biological Chemistry*, 291(34), pp. 17929–17940.

Sergin, I., Jong, Y. J. I., Harmon, S. K., Kumar, V. and O'Malley, K. L. (2017) 'Sequences within the C terminus of the metabotropic glutamate receptor 5 (mGluR5) are responsible for inner nuclear membrane localization', *Journal of Biological Chemistry*, 292(9), pp. 3637–3655.

Sexton, T. J. and Van Gelder, R. N. (2015) 'G-protein coupled receptor kinase 2 minimally regulates melanopsin activity in intrinsically photosensitive retinal ganglion cells', *PLoS ONE*, 10(6), pp. 1–12.

Sexton, T. J., Golczak, M., Palczewski, K. and Van Gelder, R. N. (2012) 'Melanopsin is highly resistant to light and chemical bleaching *in vivo*', *Journal of Biological Chemistry*, 287(25), pp. 20888–20897.

Shenoy, S. K., Drake, M. T., Nelson, C. D., Houtz, D. A., Xiao, K., Madabushi, S., Reiter, E., Premont, R. T., Lichtarge, O. and Lefkowitz, R. J. (2006) 'β-arrestin-dependent, G protein-independent ERK1/2 activation by the β2 adrenergic receptor', *Journal of Biological Chemistry*, 281(2), pp. 1261–1273.

Shichida, Y. and Matsuyama, T. (2009) 'Evolution of opsins and phototransduction', *Philosophical Transactions of the Royal Society B*, 364(1531), pp. 2881–2895.

Shigetomi, E., Bushong, E. A., Haustein, M. D., Tong, X., Jackson-Weaver, O., Kracun, S., Xu, J., Sofroniew, M. V., Ellisman, M. H. and Khakh, B. S. (2013) 'Imaging calcium microdomains within entire astrocyte territories and endfeet with GCaMPs expressed using adeno-associated viruses', *Journal of General Physiology*, 141(5), pp. 633–647.

Shigetomi, E., Hirayama, Y. J., Ikenaka, K., Tanaka, K. F. and Koizumi, S. (2018) 'Role of Purinergic Receptor P2Y1 in spatiotemporal $Ca^{2+}$ dynamics in astrocytes', *The Journal of Neuroscience*, 38(6), pp. 2625–17.

Shirzad-Wasei, N., Van Oostrum, J., Bovee-Geurts, P. H., Wasserman, M., Bosman, G. J. and Degrip, W. J. (2013) 'Large scale expression and purification of mouse melanopsin-L in the baculovirus expression system', *Protein Expression and Purification*, 91(2), pp. 134–146.

Shoham, S., O'Connor, D. H., Sarkisov, D. V and Wang, S. S.-H. (2005) 'Rapid neurotransmitter uncaging in spatially defined patterns.', *Nature methods*, 2(11), pp. 837–43.

Siehler, S. (2009) 'Regulation of RhoGEF proteins by $G_{12/13}$-coupled receptors', *British Journal of Pharmacology*, 158(1), pp. 41–49.

Siuda, Edward R., Copits, B. A., Schmidt, M. J., Baird, M. A., Al-Hasani, R., Planer, W. J., Funderburk, S. C., McCall, J. G., Gereau, R. W. and Bruchas, M. R. (2015) 'Spatiotemporal Control of Opioid Signaling and Behavior', *Neuron*, 86(4), pp. 923–935.

Siuda, Edward R, Mccall, J. G., Al-Hasani, R., Shin, G., Park, S. Il, Schmidt, M. J., Anderson, S. L., Planer, W. J., Rogers, J. A. and Bruchas, M. R. (2015) 'Optodynamic simulation of β-adrenergic receptor signalling', *Nature Communications*, 6, pp. 1–13.

Small, K. M., Brown, K. M., Forbes, S. L. and Liggett, S. B. (2001) 'Polymorphic Deletion of Three Intracellular Acidic Residues of the $\alpha_{2B}$-Adrenergic Receptor Decreases G Protein-coupled Receptor Kinase-mediated Phosphorylation and Desensitization', *Journal of Biological Chemistry*, 276(7), pp. 4917–4922.

Smyth, J. T., Hwang, S. Y., Tomita, T., DeHaven, W. I., Mercer, J. C. and Putney, J. W. (2010) 'Activation and regulation of store-operated calcium entry', *Journal of Cellular and Molecular Medicine*, 14(10), pp. 2337–2349.

Sojka, A. C., Brennan, K. M., Maizels, E. T. and Young, C. D. (2017) 'The Science Behind G Protein-Coupled Receptors (GPCRs) and Their Accurate Visual Representation in Scientific Research', *Journal of Biocommunication*, 41(1).

Song, D., Yang, Q., Lang, Y., Wen, Z., Xie, Z., Zheng, D., Yan, T., Deng, Y., Nakanishi, H., Quan, Z. and Qing, H. (2018) 'Manipulation of hippocampal CA3 firing via luminopsins modulates spatial and episodic short-term memory, especially working memory, but not long-term memory', *Neurobiology of Learning and Memory*, 155, pp. 435–445.

Song, X., Vishnivetskiy, S. A., Gross, O. P., Emelianoff, K., Chen, J., Gurevich, E. V, Burns, M. E. and Gurevich, V. V. (2009) 'Enhanced arrestin mutant facilitates photoresponse recovery and protects rhodopsin phosphorylation-deficient rod photoreceptors', *Current Biology*, 19(8), pp. 700–705.

Spiegel, A. M. (1987) 'Signal transduction by guanine nucleotide binding proteins', *Molecular and Cellular Endocrinology*, 49, pp. 1–16.

Spoida, K., Eickelbeck, D., Karapinar, R., Eckhardt, T., Mark, M. D., Jancke, D., Ehinger, B. V., König, P., Dalkara, D., Herlitze, S. and Masseck, O. A. (2016) 'Melanopsin Variants as Intrinsic Optogenetic on and off Switches for Transient versus Sustained Activation of G Protein Pathways', *Current Biology*, 26(9), pp. 1206–1212.

Spoida, K., Masseck, O. A., Deneris, E. S. and Herlitze, S. (2014) '$G_q$/5-$HT_{2C}$ receptor signals activate a local GABAergic inhibitory feedback circuit to modulate serotonergic firing and anxiety in mice', *PNAS,* 111(17), pp. 6479–6484.

Srinivasan, S., Vaisse, C. and Conklin, B. R. (2003) 'Engineering the Melanocortin-4 Receptor to Control $G_s$ Signalling in vivo', *Ann. N. Y. Acad. Sci.*, 994, pp. 225–232.

Sriram, K. and Insel, P. A. (2018) 'G protein-coupled receptors as targets for approved drugs: How many targets and how many drugs?', *Molecular Pharmacology*, 93(4), pp. 251–258.

Stanasila, L., Abuin, L., Dey, J. and Cotecchia, S. (2008) 'Different Internalization Properties of the $\alpha_{1A}$- and $\alpha_{1B}$-Adrenergic Receptor Subtypes : The Potential Role of Receptor Interaction with β-Arrestins and AP50', *Molecular pharmacology*, 74(3), pp. 562–573.

Stanley, S. A., Gagner, J. E., Damanpour, S., Yoshida, M., Dordick, J. S. and Friedman, J. M. (2012) 'Radio-Wave Heating of Iron Oxide Nanoparticles Can Regulate Plasma Glucose in Mice Sarah', *Science*, 336(6081), pp. 604–608.

Stierl, M., Stumpf, P., Udwari, D., Gueta, R., Hagedorn, R., Losi, A., Gärtner, W., Petereit, L., Efetova, M., Schwarzel, M., Oertner, T. G., Nagel, G. and Hegemann,

P. (2011) 'Light modulation of cellular cAMP by a small bacterial photoactivated adenylyl cyclase, bPAC, of the soil bacterium Beggiatoa', *Journal of Biological Chemistry*, 286(2), pp. 1181–1188.

Stojilkovic, S. S., Murano, T., Gonzalez-Iglesias, A. E., Andric, S. A., Popovic, M. A., Van Goor, F. and Tomić, M. (2009) 'Multiple roles of $G_{i/o}$ protein-coupled receptors in control of action potential secretion coupling in pituitary lactotrophs', *Annals of the New York Academy of Sciences*, 1152, pp. 174–186.

Storme, J., Cannaert, A., Van Craenenbroeck, K. and Stove, C. P. (2018) 'Molecular dissection of the human $A_3$ adenosine receptor coupling with β-arrestin2', *Biochemical Pharmacology*, 148, pp. 298–307.

Sugihara, H., Chen, N. and Sur, M. (2016) 'Cell-specific modulation of plasticity and cortical state by cholinergic inputs to the visual cortex', *Journal of Physiology Paris*, 110(1–2), pp. 37–43.

Svoboda, K. and Yasuda, R. (2006) 'Principles of Two-Photon Excitation Microscopy and Its Applications to Neuroscience', *Neuron*, 50(6), pp. 823–839.

Szekely, D., Brennan, S. C., Mun, H. C., Conigrave, A. D. and Kuchel, P. W. (2009) 'Effectors of the frequency of calcium oscillations in HEK-293 cells: Wavelet analysis and a computer model', *European Biophysics Journal*, 39(1), pp. 149–165.

Tan, L., Yan, W., McCorvy, J. D. and Cheng, J. (2018) 'Biased Ligands of G Protein-Coupled Receptors (GPCRs): Structure-Functional Selectivity Relationships (SFSRs) and Therapeutic Potential', *Journal of Medicinal Chemistry*, 61(22), pp. 9841–9878.

Tariqul Islam, A. F. M., Yue, H., Scavello, M., Haldeman, P., Rappel, W. J. and Charest, P. G. (2018) 'The cAMP-induced G protein subunits dissociation monitored in live *Dictyostelium* cells by BRET reveals two activation rates, a negative effect of caffeine and potential role of microtubules', *Cellular Signalling*, 48(February), pp. 25–37.

Tennigkeit, S. A., Karapinar, R., Rudack, T., Dreier, M.-A., Althoff, P., Eickelbeck, D., Surdin, T., Grömmke, M., Mark, M. D., Spoida, K., Lübben, M., Höweler, U., Herlitze, S. and Gerwert, K. (2019) 'Design of an ultra-fast G protein switch based on a mouse melanopsin variant', *ChemBioChem*.

Terakita, A. (2005) 'The opsins', *Genome Biology*, 6(3), p. 213.

Terakita, A., Kawano-Yamashita, E. and Koyanagi, M. (2012) 'Evolution and diversity of opsins', *Wiley Interdisciplinary Reviews: Membrane Transport and Signaling*, 1(1), pp. 104–111.

Tewson, P., Quinn, A. M. and Hughes, T. E. (2014) 'A multiplexed fluorescent assay for independent second messenger systems : Decoding GPCR activation in living cells', *J Biomol Screen*, 18(7), pp. 797–806.

Tewson, P., Westenberg, M., Zhao, Y., Campbell, R. E., Quinn, A. M. and Hughes, T. E. (2012) 'Simultaneous detection of $Ca^{2+}$ and diacylglycerol signaling in living cells', *PLoS ONE*, 7(8), pp. 1–6.

Thillaiappan, N. B., Chakraborty, P., Hasan, G. and Taylor, C. W. (2018) '$IP_3$ receptors and $Ca^{2+}$ entry', *Biochimica et Biophysica Acta - Molecular Cell Research*,

1866(7), pp. 1092–1100.

Thomas, P. and Smart, T. G. (2005) 'HEK293 cell line: A vehicle for the expression of recombinant proteins', *Journal of Pharmacological and Toxicological Methods*, 51, pp. 187–200.

Thomsen, A. R. B., Jensen, D. D., Hicks, G. A. and Bunnett, N. W. (2018) 'Therapeutic Targeting of Endosomal G-Protein-Coupled Receptors', *Trends in Pharmacological Sciences*, 39(10), pp. 879–891.

Thomsen, A. R. B., Plouffe, B., Cahill, T. J., Shukla, A. K., Tarrasch, J. T., Dosey, A. M., Kahsai, A. W., Strachan, R. T., Pani, B., Mahoney, J. P., Huang, L., Breton, B., Heydenreich, F. M., Sunahara, R. K., Skiniotis, G., Bouvier, M. and Lefkowitz, R. J. (2016) 'GPCR-G Protein-β-Arrestin Super-Complex Mediates Sustained G Protein Signaling', *Cell*, 166(4), pp. 907–919.

Tian, H., Sakmar, T. P. and Huber, T. (2017) 'Measurement of Slow Spontaneous Release of 11- *cis* -Retinal from Rhodopsin', *Biophysj*, 112(1), pp. 153–161.

Tobin, A. B., Butcher, A. J. and Kong, K. C. (2008) 'Location, location, location...site-specific GPCR phosphorylation offers a mechanism for cell-type-specific signalling', *Trends in Pharmacological Sciences*, 29(8), pp. 413–420.

Trentin, D., Hubbell, J. and Hall, H. (2005) 'Non-viral gene delivery for local and controlled DNA release', *Journal of Controlled Release*, 102, pp. 263–275.

Tsai, F. D., Lopes, M. S., Zhou, M., Court, H., Ponce, O., Fiordalisi, J. J., Gierut, J. J., Cox, A. D., Haigis, K. M. and Philips, M. R. (2015) 'K-Ras4A splice variant is widely expressed in cancer and uses a hybrid membrane-targeting motif', *PNAS*, 112(3), pp. 779–784.

Tsukamoto, H. and Terakita, A. (2010) 'Diversity and functional properties of bistable pigments', *Photochemical and Photobiological Sciences*, 9(11), pp. 1418–1425.

Tsunematsu, T., Tanaka, K. F., Yamanaka, A. and Koizumi, A. (2013) 'Ectopic expression of melanopsin in orexin/hypocretin neurons enables control of wakefulness of mice in vivo by blue light', *Neuroscience Research*, 75(1), pp. 23–28.

Tsvetanova, N. G., Irannejad, R. and Von Zastrow, M. (2015) 'G protein-coupled receptor (GPCR) signaling via heterotrimeric G proteins from endosomes', *Journal of Biological Chemistry*, pp. 6689–6696.

Tung, J. K., Gutekunst, C. A. and Gross, R. E. (2015) 'Inhibitory luminopsins: Genetically-encoded bioluminescent opsins for versatile, scalable, and hardware-independent optogenetic inhibition', *Scientific Reports*, 5.

Tung, J. K., Shiu, F. H., Ding, K. and Gross, R. E. (2018) 'Chemically activated luminopsins allow optogenetic inhibition of distributed nodes in an epileptic network for non-invasive and multi-site suppression of seizure activity', *Neurobiology of Disease*, 109, pp. 1–10.

Vardy, E. et al. (2015) 'A New DREADD Facilitates the Multiplexed Chemogenetic Interrogation of Behavior', *Neuron*, 86, pp. 936–946.

Venkatakrishnan, A. J., Deupi, X., Lebon, G., Heydenreich, F. M., Flock, T., Miljus, T., Balaji, S., Bouvier, M., Veprintsev, D. B., Tate, C. G., Schertler, G. F. X. and Babu, M. M. (2016) 'Diverse activation pathways in class A GPCRs converge near

the G-protein-coupling region', *Nature*, 536(7617), pp. 484–487.

Venkatakrishnan, A. J., Deupi, X., Lebon, G., Tate, C. G., Schertler, G. F. and Madan Babu, M. (2013) 'Molecular signatures of G-protein-coupled receptors', *Nature*, pp. 185–194.

Vogel, R., Mahalingam, M., Lüdeke, S., Huber, T., Siebert, F. and Sakmar, T. P. (2008) 'Functional Role of the "Ionic Lock"-An Interhelical Hydrogen-Bond Network in Family A Heptahelical Receptors', *Journal of Molecular Biology*, 380(4), pp. 648–655.

Volgraf, M., Gorostiza, P., Numano, R., Kramer, R. H., Isacoff, E. Y. and Trauner, D. (2006) 'Allosteric control of an ionotropic glutamate receptor with an optical switch', *Nature Chemical Biology*, 2(1), pp. 47–52.

Wacker, D., Wang, C., Katritch, V., Han, G. W., Huang, X. P., Vardy, E., McCorvy, J. D., Jiang, Y., Chu, M., Siu, F. Y., Liu, W., Xu, H. E., Cherezov, V., Roth, B. L. and Stevens, R. C. (2013) 'Structural features for functional selectivity at serotonin receptors', *Science*, 340(6132), pp. 615–619.

Wacker, D., Wang, S., McCorvy, J. D., Betz, R. M., Venkatakrishnan, A. J., Levit, A., Lansu, K., Schools, Z. L., Che, T., Nichols, D. E., Shoichet, B. K., Dror, R. O. and Roth, B. L. (2017) 'Crystal Structure of an LSD-Bound Human Serotonin Receptor', *Cell*, 168(3), pp. 377-389.e12.

Walker, J. R., Hall, M. P., Zimprich, C. A., Robers, M. B., Duellman, S. J., Machleidt, T., Rodriguez, J. and Zhou, W. (2017) 'Highly Potent Cell-Permeable and Impermeable NanoLuc Luciferase Inhibitors', *ACS Chemical Biology*, 12(4), pp. 1028–1037.

Walker, M. T., Brown, R. L., Cronin, T. W. and Robinson, P. R. (2008) 'Photochemistry of retinal chromophore in mouse melanopsin', *PNAS*, 105(26), pp. 8861–8865.

Wang, J. H., Nie, W. H., Shao, X. X., Li, H. Z., Hu, M. J., Liu, Y. L., Xu, Z. G. and Guo, Z. Y. (2019) 'Exploring electrostatic interactions of relaxin family peptide receptor 3 and 4 with ligands using a NanoBiT-based binding assay', *BBA - Biomembranes*, 1861(4), pp. 776–786.

Watson, S.-J., Brown, A. J. H. and Holliday, N. D. (2012) 'Differential signaling by splice variants of the human free fatty acid receptor GPR120.', *Molecular pharmacology*, 81(5), pp. 631–42.

Weick, J. P., Johnson, M. A., Skroch, S. P. and Williams, J. C. (2010) 'Functional control of transplantable human ESC-derived neurons via optogenetic targeting', *Stem Cells*, 28(11), pp. 2008–2016.

Welman, A., Burger, M. M. and Rg Hagmann, J. (2000) 'Structure and function of the C-terminal hypervariable region of K-Ras4B in plasma membrane targetting and transformation', *Oncogene*, 19, pp. 4582–4591.

Wennerberg, K., Rossman, K. L. and Der, C. J. (2005) 'The Ras superfamily at a glance', *Journal of Cell Science*, 118(5), pp. 843–846.

Weston, M., Kaserer, T., Wu, A., Mouravlev, A., Carpenter, J. C., Snowball, A., Knauss, S., von Schimmelmann, M., During, M. J., Lignani, G., Schorge, S., Young,

D., Kullmann, D. M. and Lieb, A. (2019) 'Olanzapine: A potent agonist at the hM4D($G_i$) DREADD amenable to clinical translation of chemogenetics', *Science Advances*, 5(eaaw1567).

Willox, A. K., Sahraoui, Y. M. E. and Royle, S. J. (2014) 'Non-specificity of Pitstop 2 in clathrin-mediated endocytosis', *Biology Open*, 3(5), pp. 326–331.

Wong, S. K. F. (2003) 'G protein selectivity is regulated by multiple intracellular regions of GPCRs', *NeuroSignals*, 12(1), pp. 1–12.

Wong, Y. H., Conklin, B. R. and Bourne, H. R. (1992) 'Gz-mediated hormonal inhibition of cyclic AMP accumulation', *Science*, 255(5042), pp. 339–342.

Wong, Y. H., Federman, A., Pace, A. M., Zachary, I., Evans, T., Pouysségur, J. and Bourne, H. R. (1991) 'Mutant α subunits of $G_{i2}$ inhibit cyclic AMP accumulation', *Nature*, 351(6321), pp. 63–65.

Wood, M. D., Murkitt, K. L., Rice, S. Q., Testa, T., Punia, P. K., Stammers, M., Jenkins, O., Elshourbagy, N. A., Shabon, U., Taylor, S. J., Gager, T. L., Minton, J., Hirst, W. D., Price, G. W. and Pangalos, M. (2000) 'The human $GABA_{B1b}$ and $GABA_{B2}$ heterodimeric recombinant receptor shows low sensitivity to phaclofen and saclofen', *British Journal of Pharmacology*, 131, pp. 1050–1054.

Wu, N., Hanson, S. M., Francis, D. J., Vishnivetskiy, S. A., Thibonnier, M., Klug, C. S., Shoham, M. and Gurevich, V. V. (2006) 'Arrestin Binding to Calmodulin: A Direct Interaction Between Two Ubiquitous Signaling Proteins', *Journal of Molecular Biology*, 364(5), pp. 955–963.

Wu, Y. I., Frey, D., Lungu, O. I., Jaehrig, A., Schlichting, I., Kuhlman, B. and Hahn, K. M. (2009) 'A genetically encoded photoactivatable Rac controls the motility of living cells', *Nature*, 461(7260), pp. 104–108.

van Wyk, M., Pielecka-Fortuna, J., Löwel, S. and Kleinlogel, S. (2015) 'Restoring the ON Switch in Blind Retinas: Opto-mGluR6, a Next-Generation, Cell-Tailored Optogenetic Tool', *PLoS Biology*, 13(5).

Xie, A. X., Petravicz, J. and McCarthy, K. D. (2015) 'Molecular approaches for manipulating astrocytic signaling in vivo', *Frontiers in Cellular Neuroscience*, 9(144).

Xu, Y., Hyun, Y. M., Lim, K., Lee, H., Cummings, R. J., Gerber, S. A., Bae, S., Cho, T. Y., Lord, E. M. and Kim, M. (2014) 'Optogenetic control of chemokine receptor signal and T-cell migration', *PNAS*, 111(17), pp. 6371–6376.

Yamamoto, S., Sippel, K. C., Berson, E. L. and Dryja, T. P. (1997) 'Defects in the rhodopsin kinase gene in the Oguchi form of stationary night blindness', *Nature Genetics*, 15, pp. 175–178.

Yan, E. C. Y., Kazmi, M. a, Ganim, Z., Hou, J.-M., Pan, D., Chang, B. S. W., Sakmar, T. P. and Mathies, R. a (2003) 'Retinal counterion switch in the photoactivation of the G protein-coupled receptor rhodopsin', *PNAS*, 100(16), pp. 9262–9267.

Yang, D., Zhang, Z.-J., Oldenburg, M., Ayala, M. and Zhang, S.-C. (2008) 'Human Embryonic Stem Cell-Derived Dopaminergic Neurons Reverse Functional Deficit in Parkinsonian Rats', *Stem Cells*, 26(1), pp. 55–63.

Yang, J., Cumberbatch, D., Centanni, S., Shi, S. Q., Winder, D., Webb, D. and

Johnson, C. H. (2016) 'Coupling optogenetic stimulation with NanoLuc-based luminescence (BRET) $Ca^{++}$ sensing', *Nature Communications*, 7(13268)

Yang, W., Carrillo-Reid, L., Bando, Y., Peterka, D. S. and Yuste, R. (2018) 'Simultaneous two-photon imaging and two-photon optogenetics of cortical circuits in three dimensions', *eLife*, 7(e32671).

Yarwood, R. E., Imlach, W. L., Lieu, T. M., Veldhuis, N. A., Jensen, D. D., Herenbrink, C. K., Aurelio, L., Cai, Z., Christie, M. J., Poole, D. P., Porter, C. J. H., McLean, P., Hicks, G. A., Geppetti, P., Halls, M. L., Canals, M. and Bunnett, N. W. (2017) 'Endosomal signaling of the receptor for calcitonin gene-related peptide mediates pain transmission', *PNAS*, 114(46), pp. 12309–12314.

Ye, H., Daoud-El Baba, M., Peng, R.-W. and Fussenegger, M. (2011) 'A synthetic optogenetic transcription device enhances blood-glucose homeostasis in mice.', *Science*, 332(6037), pp. 1565–8.

Zaccardi, G., Kelber, A., Sison-Mangus, M. P. and Briscoe, A. D. (2006) 'Color discrimination in the red range with only one long-wavelength sensitive opsin', *Journal of Experimental Biology*, 209(10), pp. 1944–1955.

Zeng, W., Mak, D.-O. D., Li, Q., Shin, D. M., Foskett, J. K. and Muallem, S. (2003) 'A New Mode of $Ca^{2+}$ Signaling by G Protein-Coupled Receptors: Gating of $IP_3$ Receptor $Ca^{2+}$ Release Channels by $G_{\beta\gamma}$', *Current Biology*, 13, pp. 872–876.

Zhang, B.-X., Zhang, W., Luo, J., Yeh, C.-K., Ma, X., Sprague, E. A., Swerdlow, R. H., Katz, M. S. and Lin, A. (2006) 'Polyunsaturated fatty acids mobilize intracellular $Ca^{2+}$ in NT2 human teratocarcinoma cells by causing release of $Ca^{2+}$ from mitochondria', *American Journal of Physiology-Cell Physiology*, 290, pp. C1321-33.

Zhang, F., Wang, L., Boyden, E. S. and Deisseroth, K. (2006) 'Channelrhodopsin-2 and optical control of excitable cells', *Nature Methods*, 3(10), pp. 785–792.

Zhang, J., Campbell, R. E., Ting, A. Y. and Tsien, R. Y. (2002) 'Creating new fluorescent probes for cell biology', *Nature Reviews Molecular Cell Biology*, 3(12), pp. 906–18.

Zhang, J. Y., Kowal, D. M., Nawoschik, S. P., Dunlop, J., Pausch, M. H. and Peri, R. (2010) 'Development of an improved $IP_1$ assay for the characterization of 5-$HT_{2C}$ receptor ligands', *Assay and Drug Development Technologies*, 8(1), pp. 106–113.

Zhang, Z., Ma, Z., Zou, W., Zhang, L., Li, Y., Zhang, J., Liu, M., Hou, W. and Ma, Y. (2019) 'N-myc downstream-regulated gene 2 controls astrocyte morphology via Rho-GTPase signaling', *Journal of Cellular Physiology*, 234(11), pp. 20847–20858.

Zhang, Y., Ying, J., Jiang, D., Chang, Z., Li, H., Zhang, G., Gong, S., Jiang, X. and Tao, J. (2015) 'Urotensin-II receptor stimulation of cardiac L-type $Ca^{2+}$ channels requires the βγ subunits of $G_{i/o}$-protein and phosphatidylinositol 3-kinase-dependent protein kinase Cβ1 isoform', *Journal of Biological Chemistry*, 290(13), pp. 8644–8655.

Zhao, G. Q., Zhang, Y., Hoon, M. A., Chandrashekar, J., Erlenbach, I., Ryba, N. J. P. and Zuker, C. S. (2003) 'The Receptors for Mammalian Sweet and Umami Taste', *Cell*, 115, pp. 255–266.

Zhou, X. E., Gao, X., Barty, A., Kang, Y., He, Y., Liu, W., Ishchenko, A., White,

T. A., Yefanov, O., Han, G. W., Xu, Q., de Waal, P. W., Suino-Powell, K. M., Boutet, S., Williams, G. J., Wang, M., Li, D., Caffrey, M., Chapman, H. N., Spence, J. C H, Fromme, P., Weierstall, U., Stevens, R. C., Cherezov, V., Melcher, K., Xu, H E. (2016) 'X-ray laser diffraction for structure determination of the rhodopsin-arrestin complex.', *Scientific Data*, 3(160021).

Zhou, Z., Tanaka, K. F., Matsunaga, S., Iseki, M., Watanabe, M., Matsuki, N., Ikegaya, Y. and Koyama, R. (2016) 'Photoactivated adenylyl cyclase (PAC) reveals novel mechanisms underlying cAMP-dependent axonal morphogenesis', *Scientific Reports*, 6(19679).

Zimmerman, B., Simaan, M., Lee, M. H., Luttrell, L. M. and Laporte, S. A. (2009) 'c-Src-mediated phosphorylation of AP-2 reveals a general mechanism for receptors internalizing through the clathrin pathway', *Cellular Signalling*, 21(1), pp. 103–110.

Zipfel, W. R., Williams, R. M. and Webb, W. W. (2003) 'Nonlinear magic: multiphoton microscopy in the biosciences.', *Nature Biotechnologyotechnology*, 21(11), pp. 1369–77.